Model predictive control of space heating system with building integrated energy-efficient technologies

By:

Zhichen Wei

A thesis submitted in partial fulfilment of the requirements for the degree of Doctor of Philosophy

The University of Nottingham
Faculty of Engineering
Department of Architecture and Built Environment,

Acknowledgement

I would like to express my gratitude firstly to Dr. John Calautit, who trusted to me this PhD role. He is a real inspiration of hardworking person, supervisor.

Secondly, I would like to thank Prof. Yupeng Wu, who supported me during the stages of my PhD, by guiding me and correcting me.

During the experimental part of my research in the University of Nottingham, Dr. Christopher Wood helped me to successfully complete my experimentation study for the case study pod.

Last but not least, I am deeply indebted to my family and friends, who have helped me and shared with me my worries, frustrations, and happiness.

Preface

Journal papers

1. Wei, Z., & Calautit, J. (2022). Investigation of the effect of the envelope on building thermal storage performance under model predictive control by dynamic pricing. *Smart Energy (Amsterdam)*, *6*, 100068. https://doi.org/10.1016/j.segy.2022.100068

2. Wei, Z., & Calautit, J. (2023). Predictive control of low-temperature heating system with passive thermal mass energy storage and photovoltaic system: Impact of occupancy patterns and climate change. *Energy (Oxford)*, *269*, 126791. https://doi.org/10.1016/j.energy.2023.126791

3. Wei, Z., & Calautit, J. Evaluation of model predictive control (MPC) of solar thermal heating system with thermal energy storage for buildings with highly variable occupancy levels. *Building simulation* (accept)

4. Wei, Z., & Calautit, J.Field experiment testing of a low-cost model predictive controller (MPC) for building heating systems and analysis of phase change material (PCM) integration. *Applied energy* (submit & with editor)

Conference papers

5. Zhichen wei; John Calautit; Paige Tien; Shuangyu Wei; Yupeng Wu "Investigation of the effect of envelope on building thermal storage performance under MPC strategy". SDEWES 2021, Dubrovnik

6. Zhichen wei; John Calautit; "Investigation of the effect of envelope on building heating energy flexibility under MPC control strategy". CUE 2021, Matsue, Japan

7. Zhichen wei; John Calautit; "Field experiment testing and demonstration of a low-cost MPC for building heating systems management". SDEWES 2023, Dubrovnik

Table of contents

List of Figures

List of Tables

Nomenclature

V_c	tank volume (m^3)
A	system matrix in state space model
a	slack variable
B	system matrix in state space model
C	thermal capacitance (J/K)
Cp	specific heat (J/kg°C)
D	system matrix in state space model
e	slack variable
E	white zero mean Gaussian noise
I	global solar radiation (W/m^2)
K	system matrix in state space model
k	time step
m	mass flow rate (kg/s)
N	prediction horizon
n	number of states
P	power demand (kWh)
q	weight of cost
Q	heat gain (W)
q	weighting factor
r	weight of cost
R	thermal resistance (K/W)
t	time step
T	Temperature (°C)
t	current time
u	input vector
x	system state vector
y	output vector
σ	disturbance matrix

Abbreviations

BAS	building automation system
COP	coefficient of performance
DR	demand response

UFH	underfloor heating
HEMS	home energy management system
HVAC	heating, ventilation and air-conditioning
ICT	information and communication technologies
IoT	Internet-of-Thing
MPC	model predictive control
PCM	phase change material
PID	proportional integral derivative
PV	photovoltaic
RC	resistance-capacitance
RES	renewable energy source
RPi	Raspberry Pi
ss	state space
STES	structural thermal energy storage

Subscripts

auxiliary	auxiliary heater
col	collector
d	discrete-time
fl	floor
in	indoor air
inlet	inlet of floor heating system
int	internal surface of wall
inter	internal heat gains
mean	mean point of heating pipe
o	outdoor
pp	pipeline
ra,inlet	inlet of radiator system
return	return water
tank	water storage tank
win	window

Abstract

With the increasing energy prices and growing concerns over energy security, an accelerated transition to net zero carbon built environment has never been more important. The UK's building sector is a major contributor to greenhouse gas emissions, primarily due to heating energy, 83% of which is derived from natural gas combustion. To enhance energy efficiency and reduce GHGs, advanced control strategies targeting peak energy shifting are vital. Many studies have shown the capabilities of advanced control strategies such as model predictive control (MPC) to achieve energy efficiency, balance with thermal comfort and indoor air quality. It has also shown its capability to provide demand flexibility, minimising peak load demands and maximising the production of renewable energy sources in buildings.

However, there remains a lack of research on the practicality of MPC for low-temperature heating systems, building-integrated energy-efficient systems, and assessing MPC under variable occupancies and future climates. Buildings with high occupancy variability, such as universities, where fluctuations occur throughout the day and across the year, can pose challenges in developing control strategies that aim to balance comfort and energy efficiency. While with changing climate conditions anticipated to modify building energy demands, especially in heating and cooling, the adaptability of MPC becomes vital.

This study seeks to evaluate the effectiveness of MPC for low-temperature heating systems, integrated with energy-efficient technologies, considering the challenges posed by variable occupancy and projected climate conditions. The proposed approach integrated price responsive MPC with low temperature heating system and passive structural thermal energy storage (STES) and active storage tank. Integration of the system with photovoltaic (PV) system and solar hot water are also explored. The system performance under future climate conditions is evaluated considering different design and operation conditions, including different thermal masses, occupancy patterns and internal heat gains, setpoint strategies and operation temperatures of the low-temperature heating system. Moreover, recognising the absence of affordable and easily implemented solutions in the sector, we proposed a cost-effective MPC approach using internet of things (IoT) and dynamic pricing.

The developed coupled model has undergone rigorous verification and validation using both numerical simulations and experimental data, demonstrating excellent agreement between the model predictions and observed outcomes. The study's findings indicate that the implementation of mediumweight thermal mass and a medium-temperature (45℃) under-floor heating inlet temperature enhances load shifting capabilities, considering a realistic occupancy profile and a high tolerance setpoint strategy during unoccupied periods.

The research also confirms the feasibility of implementing MPC to regulate phase change material (PCM) wallboard integrated into the building envelope, leading to electricity cost savings of up to 35%. Moreover, the introduction of rooftop photovoltaic (PV) electrical energy into the building energy supply network further improved energy shifting potential. Employing a solar hot water system for energy shifting resulted in more than half of the thermal energy cost savings compared to the original heating system. The result also showed that higher low-price energy usage and a lower heating energy usage could be achieved in future climate conditions. Finally, the experimental evaluation of the MPC showed that the proposed approach result in a 24% electricity cost reduction as compared to a conventional control strategy. This research provides significant insights into intelligent localised MPC control development for the built environment, offering a diverse array of energy-efficient technologies for building integration.

1. Introduction

Greenhouse gas emissions (GHGs) are recognised as the driving force behind global warming, leading to global policies such as The Paris Agreement, which seeks to limit global temperature rise to 1.5 °C above pre-industrial levels. In alignment with this, nations, including the United Kingdom, are striving to reduce carbon emissions through energy-efficient strategies, with the UK aiming for net zero emissions by 2050 [1]. The building sector in the UK is a significant contributor to national GHG emissions, largely due to its 83% dependence on natural gas for heating [2]. This heavy reliance on fossil fuels prompts the need for sustainable alternatives, as it not only has environmental repercussions but also financial ones.

According to the International Energy Association [3], the UK had the third highest electricity prices globally in 2019, a trend primarily driven by the increasing cost of natural gas [4]. Addressing the challenges of greenhouse gas emissions, there's an increasing focus on enhancing building energy efficiency using modern technologies and materials. This reduces energy demand for heating and cooling, thereby lessening fossil fuel reliance. In cold climates, a large percentage of the energy used in buildings is dedicated to indoor space heating, specifically during peak periods [5]. With the increasing energy prices and growing concerns over energy security, an accelerated transition to net zero carbon built environment has never been more important. There are many solutions that can be implemented to achieve this, including passive design optimisation, energy efficient control strategies, and integration of onsite renewable energy and storage.

Smart grid is considered as one of the solutions to building a low-carbon electricity future. The smart grid can help increase the efficiency of the power grid by providing bidirectional communication about the network state between the consumers and suppliers [6]. The existing power grid relies heavily on conventional fossil fuel-based electricity generation units [7]. Today's high volatility in fossil fuel prices, along with the increasing electricity demand, can lead to the increased chances of network congestion. The network congestion could decrease energy efficiency since the grid will be more efficient and experiences less line loss with the constant and stable energy supply condition [8]. Typically, the is an 8-10% electrical energy loss in the power transmission and distribution from power

generation plants to end-users. To minimise the energy loss and maintain system stability, energy management system (EMS) can be utilised to help reach the grid's optimal operation condition. EMS provides an optimal control strategy by performing optimal power flow analysis for constant monitoring basing on the data acquisition, which represents the current operating condition of the network. The optimal control strategies include the energy generation; as well as the way of the energy distribution [8-10]. The optimal operation profile is created based on the analysis of reliability and performance of the grid [11].

The optimal operation profile denotes to the demand profile matches the supply profile, which requires end-users changing consumption pattern in responding to time-dependent supply profile. The way that the electricity consumption pattern changes by end-users driven by incentive payment refer to Demand Response (DR). DR intends to change the load profile, i.e. timing, level of instantaneous demand, or total electricity consumption, to optimise the entire power system from generation to delivery to end use [12, 13]. The smart grid enables the DR strategy. With the help of the smart grid, different participants such as power supplier, delivers and consumers are involved and connected by the information and data communication network towards the win-win situation, i.e. energy production saving of the grid and cost-saving of consuming electricity for end uses [11].

One of the main targets of DR is to increase renewable energy source (RES) integration in smart grid. As renewable energy technologies such as photovoltaics (PV) systems become more affordable, the possibility of achieving net zero carbon buildings increases. However, the intermittency of solar power can lead to a mismatch between solar generation and energy demand. These issues of intermittency, fluctuation and unpredictability are hurdles to solar integration and are further intensified during peak load periods. At the same time, the building demand is influenced by various factors, including the weather, envelope, energy system and occupancy behaviour/patterns. Occupancy behaviour represents one of the major sources of uncertainty related to building energy use [14]. However, the harmonisation of renewable energy intermittency with the building's energy demands calls for an integrative solution. Thermal energy storage (TES) emerges as a complementary element to the predictive prowess of intelligent control, serving as a counterbalance to the variability of renewable energy sources. Exploiting time-

of-use tariff schemes, TES enhances demand-side flexibility and promotes the integration of a broader range of renewable technologies [11, 15].

While there are different types of TES that can be used to increase demand-side flexibility, the thermal heat capacity of a building envelope presents a potential for storing energy passively, and at the same time, it can be a cost-effective solution. Building thermal energy could be stored in advance by using the building envelope and structure itself, named structural thermal energy storage (STES) in this study, without the additional cost. In particular, STES can be coupled with heating, ventilation and air-conditioning (HVAC) systems in DR programs [16]. The thermal energy is charged or discharged automatically by the temperature difference between the indoor air and the envelope [17-19]. As a result, the energy system usage can be reduced at certain times for peak-time demand reduction [20, 21]. Phase change materials (PCMs) enhance the concept of structural thermal mass by providing additional thermal storage within the same volume of material [22]. Leveraging the inherent ability of certain materials to absorb and release thermal energy during phase transitions [23], these technologies hold potential to contribute to load shifting, peak demand reduction, and overall enhancement of energy efficiency. However, the system must still be operated within the limits of the thermal comfort requirements of the occupants. As a result, seeking an intelligent building energy system control to achieve both objectives of indoor comfort and energy saving is important.

Model predictive control (MPC) represents an advanced and adaptive approach to optimise the operation of building energy system dealing with multiple objectives. Unlike traditional control strategies, which react to current conditions, MPC uses predictive models to anticipate future requirements and make proactive adjustments. Incorporating a range of parameters such as weather forecasts, occupancy levels, energy prices, and system constraints [24, 25], it dynamically modulates HVAC operations to balance energy efficiency, cost-effectiveness, and occupant comfort. The robustness and accuracy of MPC have led to extensive research on its application for managing building power demand and implementing demand response controls [26]. However, the development of MPC in building sector is still costly and complex [27]. Finding a way for efficient introducing MPC into building energy system that is still urgent.

The Internet of Things (IoT) offers opportunities for developing low-cost MPC in building section. IoT has been reported as an easy-deployment and cheap platform for BES [28]. IoT generates valuable data that can be utilised for optimising energy consumption. Furthermore, the application of IoT to dynamic energy pricing systems could act as a potent driver for energy-efficient behaviour [29]. By digitalising dynamic pricing, consumers can gain real-time access to energy cost fluctuations, allowing them to adjust their energy consumption according to the price signals. IoT devices can provide the data necessary for the predictive models of the MPC [30], while the MPC, in turn, can optimise the building's energy usage based on real-time dynamic pricing information. Further, IoT-enabled real-time monitoring [31] can provide valuable data about the performance of PCMs [32], aiding in their control and maximising their potential for energy savings. IoT is widely applied in building sector through various technologies and communication ways [30]. Thus, the combination of IoT and MPC is worth to discover.

Given the substantial potential in building-integrated technologies helping DR towards increased energy efficiency and RES penetration and MPC's ability in controlling coupling building systems, there is need for the analysis of MPC for building heating systems integrated with energy-efficient technologies considering variable occupancy and future climates. Then, validate MPC's deployment in reality.

1.1 Aims and objectives

The adoption of energy-efficient technologies, such as programmable thermostats, low-carbon energy sources, improved HVAC systems, and high-performance windows, has played a crucial role in decreasing energy consumption [33]. The extent of energy savings in buildings is contingent upon the comprehensive utilisation of these technologies, spanning from the initial design to day-to-day operation. Numerous factors contribute to enhancing building energy efficiency, with significant emphasis on the in-depth exploration, both theoretically and experimentally, of heat transfer through building envelopes [34]. In recent years, there has been a growing focus on optimising the control of HVAC systems. This thesis sets out to propose innovative designs for building envelopes and

construction modules, aiming to reduce HVAC system costs through thermal energy shifting combined with intelligent Model Predictive Control (MPC) strategies. These strategies are designed to be compatible with various proposed designs.

Building thermal energy management is commonly achieved through the implementation of thermal storage systems. The exploration of thermal energy storage has been a longstanding subject of research, revealing its potential to positively impact a building's energy efficiency. This is achieved by contributing to an increased utilisation of renewable energy sources and/or by reducing overall energy demand and peak loads for HVAC systems. The storage of thermal energy encompasses both latent heat and sensitive heat storage methods [35]. Within sensitive heat storage technologies, there exists a distinction between active and passive storage approaches [36]. Notably, a majority of the existing reviews on this subject, as highlighted in the literature [37, 38], tend to focus on phase change materials utilised in latent heat storage.

The aim of this research project is to comprehensively evaluate the application of MPC for low-temperature heating systems integrated with energy-efficient technologies, while considering the challenges posed by variable occupancy and future climate conditions. The thesis aims to address the urgent need for energy-efficient solutions and the transition to a sustainable built environment, thereby contributing to the reduction of greenhouse gas emissions. It seeks to explore advanced control strategies, specifically MPC, to achieve energy efficiency while maintaining thermal comfort and indoor air quality in buildings.

This study aims to combine innovative designs of building envelopes and construction modules with intelligent HVAC control for energy shifting. The thesis covers passive storage and active storage technologies for sensible heat storage, as well as PCM latent heat storage technologies. The passive storage strategy involves utilizing building thermal mass, while the active storage applies mostly common water storage tanks with the assistance of collected solar thermal energy. Furthermore, PCM is expected to be integrated with building thermal mass for more significant energy storage. To achieve a more efficient HVAC system, the aforementioned storage systems will be coupled with an intelligent MPC strategy. Additionally, parametric analyses, such as heating system specifications, occupancy patterns, and climate change, will be conducted to fully assess the MPC

coupling with different storage systems for energy shifting. Finally, an IoT-based MPC experiment in a test pod will be conducted to examine the practicality of the proposed MPC.

The specific objectives of this thesis are as follows:

- Conduct an in-depth literature review to analyse the development and implementation of MPC models for low-temperature space heating systems, with a particular focus on dynamic pricing strategies.
- Perform a comprehensive sensitivity analysis to assess the impact of various factors, including occupancy patterns, future climate projections, different thermal masses, setpoint strategies, and operation temperatures of the low-temperature heating system on the MPC-controlled system's performance.
- Investigate the integration of the MPC-controlled low-temperature heating system with solar renewable technologies, aiming to enhance energy efficiency and promote the utilisation of renewable energy sources.
- Explore the feasibility of integrating the MPC-controlled system with passive thermal energy storage and Phase Change Material (PCM) wallboards to further optimise energy shifting capabilities and energy savings.
- Conduct field experiments to validate the proposed MPC model under real-world conditions, providing practical insights into the performance of the integrated low-temperature heating system with energy-efficient technologies.

By fulfilling these objectives, this research project aims to contribute valuable knowledge and practical recommendations for the effective implementation of MPC in low-temperature heating systems integrated with energy-efficient technologies.

1.2 Research methodology

This subsection presents the research methodology used for evaluating the results in line with the objectives of this thesis. The first analysis scenario focuses on the passive storage of building envelopes for sensible heat storage under an MPC control strategy with optional PV electrical energy usage. The second analysis scenario introduces an active thermal energy storage system for building coupling

with a solar thermal system under an MPC strategy. The third analysis develops an experimental MPC based on IoT technology. Furthermore, a novel passive storage system with PCM wallboard is simulated in the validated test pod with an MPC strategy.

The first analysis scenario is to evaluate the capability of a building integrated PV system in enhancing the performance of passive building energy storage technology under future climate scenarios (2030, 2050 and 2080). The use of MPC in controlling the low-temperature floor heating system in combination with the rooftop PV installation is explored (Fig 1-1). Other aspects, such as the impacts of occupancy patterns, system operating temperature and setpoint strategy are also investigated.

By doing so, a validated coupled model will be developed to simulate the performance of the price responsive MPC control strategy integrated with the STES, low-temperature heating and building-integrated PV system. The energy storage will be controlled by the proposed MPC control strategy, which automatically shifts energy under dynamic pricing of an applicable day-ahead electricity market i.e. from high-price energy to low-price periods and maximise the use of PV electrical energy.

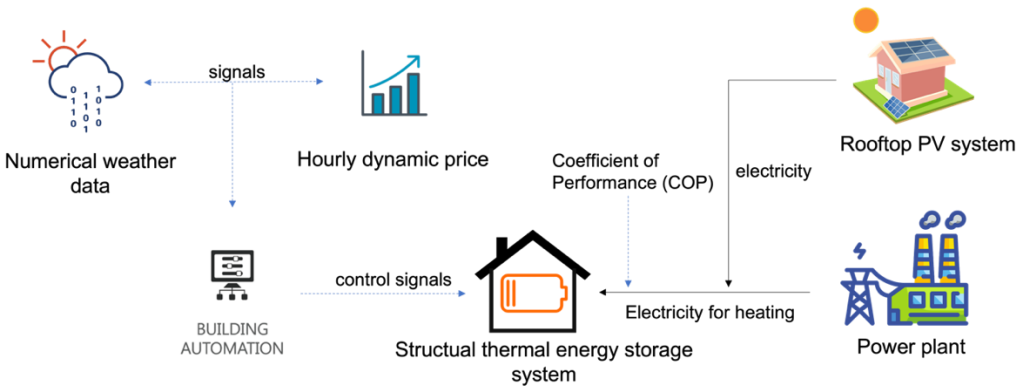

Fig. 1-1 STES with (a) energy fully charging from the grid (b) electrical energy partly charging from the rooftop PV panel

The second simulation model is developing for evaluating energy performance of a price responsive MPC integrated with a solar thermal heating system, active and passive thermal energy storage (TES) for buildings with high occupancy variability (Fig 1-2). The coupled system supplies the building heating energy through a low temperature under floor heating system. A case study lecture room

in the University building in Nottingham, UK, was employed for evaluating the feasibility of the proposed heating system controlled by MPC strategy during the heating season.

By doing so, a dynamic thermal representation of the building integrated with a solar hot water storage system through grey-box identification of a state-space model will be developed. The developed coupled model will undergo verification and validation process utilising both numerical simulations and experimental data. The developed MPC controller aims to improve the operation of the space heating system, lower the cost and maximise solar energy utilisation.

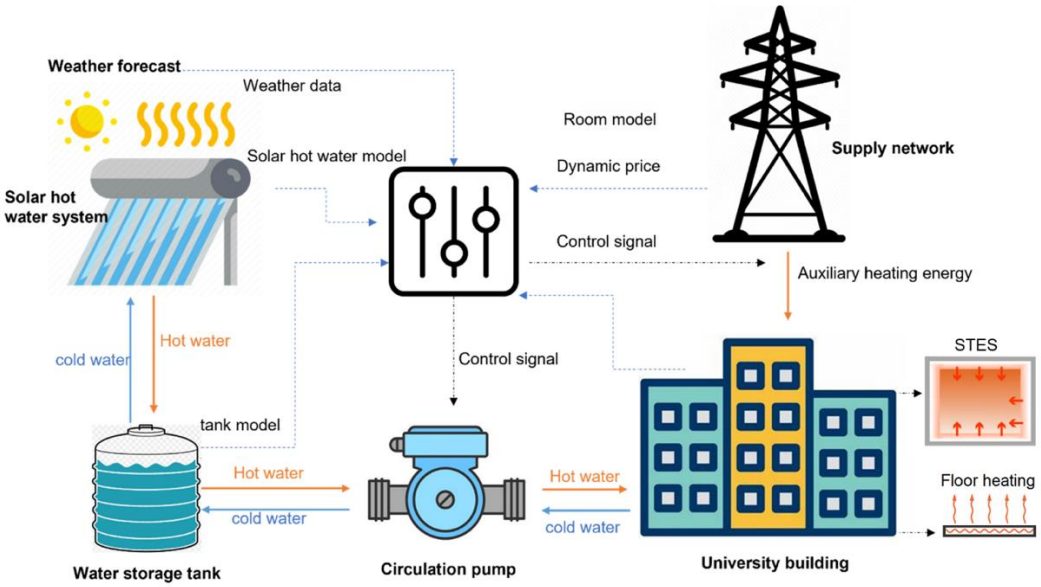

Fig. 1-2 Proposed price responsive model predictive control for a building-integrated solar thermal heating and passive/active storage system for a highly variable occupancy building

Finally, an experimental MPC was designed for efficient building energy management by optimising the operation of heating system. A cost-effective, easy-to-implement MPC will be developed, that is capable of leveraging IoT devices as a continuous, economic data source for its predictive models (Fig 1-3). The focus of this investigation will be how this interaction facilitates real-time and forecasted energy consumption optimisation, effectively integrating dynamic pricing strategies. Then, an integration of PCMs in validated MPC was simulated, investigating how MPCs can efficiently manage and capitalise on the thermal storage properties of PCM wallboards.

By doing so, a low-cost MPC will be created in MATLAB and deployed through a locally embedded Raspberry Pi (RPi) hardware via WiFi. The proposed MPC will be applied in a real-world setting - a test pod at the University of Nottingham, UK. This control system will maintain the indoor comfort levels by reacting to the hourly dynamic price of electricity, providing real-time indoor temperature feedback. Furthermore, a MPC in conjunction with PCMs will be developed bases on case study room. The developed coupled model will undergo verification and validation process utilising both numerical simulations and experimental data. The energy performance will be simulated through a co-simulation of TRNSYS and MATLAB

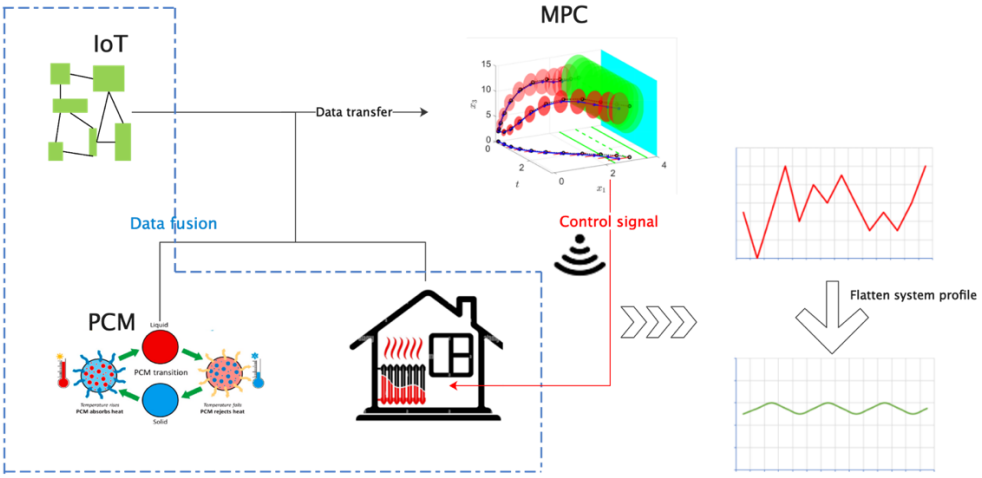

Fig. 1-3 IoT-based MPC strategy for building integrated with PCM wallboards

1.3 Thesis layout

The thesis is structured into seven chapters. The contents of them are summarised as followed:

Chapter 2 carries out literature review on developing MPC model for low temperature space heating system with dynamic pricing. Besides, this section also introduces various building integration systems towards an increased building energy efficiency, such as building RES, building storage systems, and PCM wallboards. It explores the potential of MPC for future energy shifting strategies, its practicality, and the need for cost reduction in its implementation. The importance of occupant-oriented system control and real-time clothing insulation feedback for enhancing energy efficiency in building energy systems is also discussed. Additionally, the chapter explores the integration of IoT to improve indoor thermal comfort and energy efficiency.

Chapter 3 introduces the state-space (ss) model that captures system dynamics for MPC implementation based on heat transfer processes and the validation method of ss model. Besides, the formulation of MPC in MATLAB using ss model is also detailed in this chapter. Later, the chapter also outlines the simulation platform by connecting TRNSYS to MATLAB for real-time feedback control and introduces the Kalman filter to aid co-simulation for real-time feedback MPC control. Finally, the chapter presents the test facility used for MPC experiment.

Chapter 4 investigates the heating energy storage performance of building thermal mass under different configurations, exploring aspects like thermal masses, setpoint strategies, occupancy profiles, and floor heating inlet temperatures. The goal is to achieve higher energy shifting performance and low-price energy usage, with insights into future integration of energy storage systems with RES.

Chapter 5 evaluates the performance of MPC in controlling buildings integrated with a solar hot water storage system. It presents the energy performance evaluation, comfort violations, and analysis of heating sources over time.

Chapter 6 designs an IoT-based MPC implementation in a case study room at the University of Nottingham. It presents the time-dependent control performance of the IoT-based MPC strategy and compares the measured indoor temperatures with simulated indoor temperatures using traditional on/off control in TRNSYS, aiming for higher energy shifting performance and low-price energy usage. Later, the energy usage performance of PCM wallboard integration bases on developed MPC model has also been evaluated in this chapter.

Chapter 7 summarises the conclusions drawn from the study and outlines future work that could enhance knowledge in MPC studies. Prospective points for further research are highlighted to advance the application of MPC in building energy systems.

2. Literature review

2.1 Introduction demand response strategy in building energy systems

In the context of building energy systems, the implementation of intelligent control necessitates the consideration of several crucial factors, such as building integrated systems, time-dependent energy requirements, and the dynamic electricity price prevailing in the market. To develop a practical MPC approach, it is imperative to thoroughly investigate the factors that could impact the control performance. This chapter conducts a comprehensive review of the key aspects that should be taken into account when designing an MPC-controlled building energy system. Section 3.2 delves into the details of DR programs and their widespread application across the globe. Section 3.3 outlines the significance of structural thermal energy storage (STES), which is extensively utilised in DR programs for efficient energy shifting. Section 3.4 underscores MPC's capabilities in energy shifting within DR programs, particularly in the control of various energy-efficient systems such as RES, TES, and underfloor heating (UFH) systems. Additionally, Section 3.5 evaluates studies conducted on the IoT in building system management, offering promising opportunities for deploying MPC in the building sector.

2.2 Demand response strategy in building energy systems

Given that buildings constitute the largest end-users of energy in the UK, it is crucial to address issues related to energy supply and demand. The chapter highlights the significance of mitigating energy loss due to mismatches between

demand and supply, particularly during peak periods, where backup generation costs escalate.

Figure 2-1 illustrates the daily peak curves for six European countries, revealing lower energy consumption during nighttime hours and a substantial reduction of load during night hours compared to daily peaks in the UK, indicating a notable gap between peak and valley loads. To ensure demand and supply alignment, energy flexibility becomes indispensable, especially during unexpected peak periods driven by extreme weather conditions. This flexibility is also advantageous for the seamless integration of intermittent renewable energy sources (RES). DR emerges as a primary approach to enhance energy flexibility and shape the system's load profile.

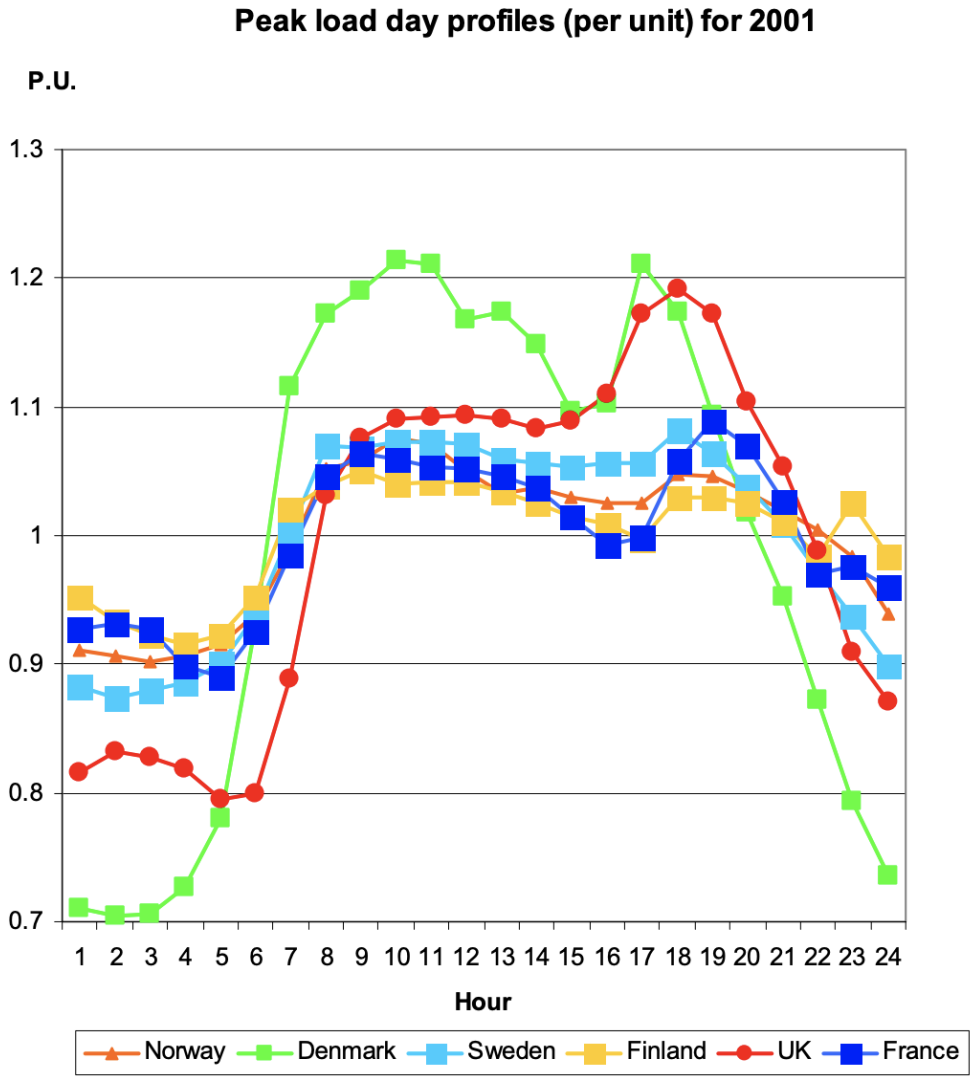

Fig. 2-1Peak day load profiles as per unit curves. [39]

In a DR strategy, end users adapt their energy consumption patterns in response to dynamic pricing [11, 12, 40-43]. Extensive research [44-60] has demonstrated the positive impact of DR on load shaping within the system and its potential for successful integration of renewable energy sources. Several studies have investigated DR's ability to reduce peak-period demand. For instance, Ashok [44] observed a significant decrease in peak-period demand, with off-peak energy consumption accounting for up to 62% of total energy consumption, showcasing DR's demand-shifting capacity. Likewise, Papadaskalopoulos et al. [45] simulated a peak-period demand reduction of approximately 14% through DR implementation in the operation system, while Ashok and Banerjee [46] demonstrated even more substantial peak demand reduction of up to 38% following the adoption of an optimised DR plan.

Furthermore, DR enables load shaping, enhancing the system's energy flexibility and providing a viable solution to address the intermittent nature of renewable energy sources within the power system. Studies by Falsafi et al. [54], Finn et al. [51], Keane et al. [57], and Moura and Almeida [58] have corroborated DR's ability to boost the utilisation of wind energy, increase system reliability with high wind energy penetration, and reduce non-guaranteed energy portions during peak times, effectively utilising renewable shares in the overall energy supply.

DR plans come in various programs, as depicted in Fig 2-2, which stimulate DR activities. These programs can be classified into two main categories: price-based (PB) DR and incentive-based (IB) DR. PBDR includes time-of-use (TOU) pricing, real-time pricing (RTP), and critical peak pricing (CPP). On the other hand, IBDR encompasses direct load control (DLC), interruptible/curtailable (IC) programs, emergency demand response programs (EDRP), demand bidding (DB), capacity market programs (CMP), and ancillary service markets (ASM).

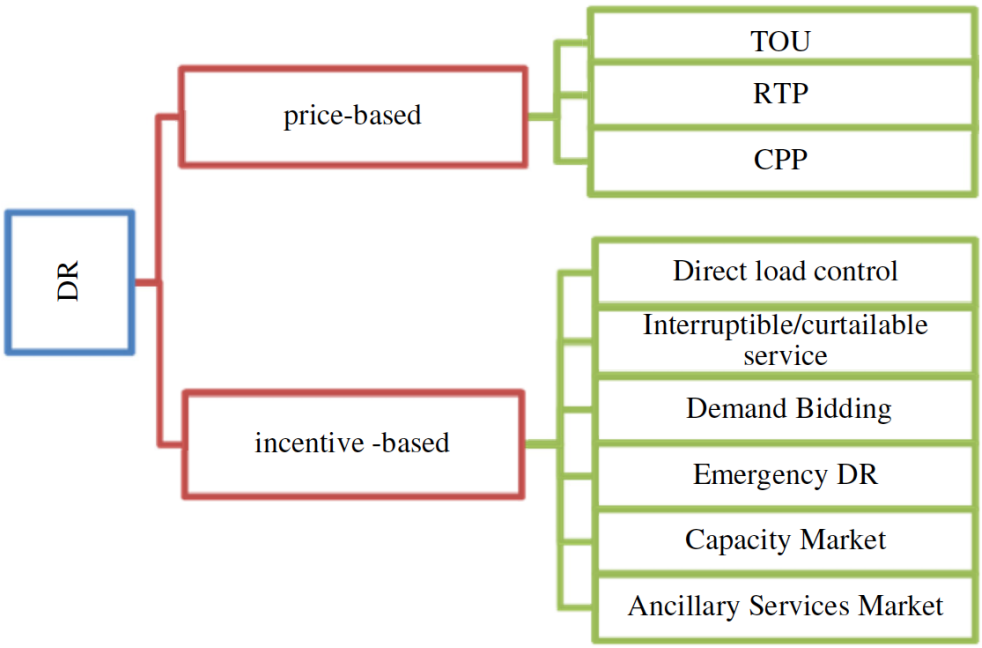

Fig. 2-2 Classification of demand response program. [54]

Price-Based Demand Response (PBDR) involves passing the price variation of the electricity market to customers, who then adjust their energy usage based on the economic penalties for on-peak consumption [41, 42, 61]. In PBDR, electricity tariffs are dynamically adjusted to flatten the demand curve, with higher prices during peak periods and lower prices during off-peak periods, prompting customers to modify their activities accordingly.

Time-of-Use (TOU) programs divide the day into several periods, each with different prices, leading to reduced demand during higher-priced periods. Studies by Nikzad et al. [53], Ashok and Banerjee [46], and Ashok [44] have confirmed the effectiveness of TOU tariffs in demand reduction without significantly impacting daily energy consumption. The determination of optimum TOU rates, based on the grid reliability index set by the operator, ensured that customers' required daily energy consumption remained unchanged [53].

Real-Time Pricing (RTP) involves charging different prices on an hourly or minutely basis, making it advantageous for responding to unexpected events in the supply side, such as renewable energy sources (RES). RTP has been observed to enable electricity demand to adjust to real-time wind resources, reducing the redispatching costs of wind resources and system load loss [59]. Similarly, De Jonghe et al. [49] demonstrated that applying RTP mitigated over-generation issues

during high wind generation periods, reducing the need for investment in peaking generation capacity and facilitating the integration of variable wind power.

Critical Peak Pricing (CPP) entails imposing particularly high rates for a limited number of critical hours on top of TOU rates or normal flat rates during unforeseen system events or periods of high wholesale electricity prices [62].

In Incentive-Based Demand Response (IBDR) programs, program sponsors take action for end-users, who are incentivised to participate. Load curtailment becomes mandatory whenever required by the system. Falsafi et al. [54] observed that in an ASM program, demand-side reserves were utilised to compensate for the unpredictable nature of wind. Additionally, load curtailment is usually pre-negotiated. In DLC programs, customers assign portions of their load to the utility for direct operational control, coordinating and organising controllable loads into groups for system dispatcher control, resulting in lower operational costs and significant peak reduction [52]. Similarly, in a DB program, customers submit price-sensitive bids, indicating their willingness to be curtailed for peak demand reduction, and adjust their activities based on their accepted bid on load reductions for the next day [47].

Demand response programs, combined with other technologies, form a typical approach to promoting flexibility. DR's role in load shaping is enhanced by its ability to store energy during off-peak times, providing additional flexibility. Studies by De Jonghe et al. [49] and Wang et al. [50] have demonstrated how DR increases the reserve for off-peak energy, enabling stored energy to be used during peak times, thus contributing to the system's energy flexibility. The practicality and widespread use of storage technology alongside DR for various objectives are confirmed by the articles reviewed in this section (Table 2-1), where "n.s." denotes "no specified."

Table 2-1 Summary of DR performance

Ref	DR program	Country	Storage applied	Key results
[53] 2012	TOU	n.s.	yes	The system operation cost has reduced about 4.1%
[52] 1995	DLC	n.s.	yes	System operation cost without any load interruption saving achieved 2.33%
[54] 2014	ASM	n.s.	n.s.	The air pollutants emission becomes 0.314 tons less than the case without DR
[46] 2003	TOU	India	n.s.	38% reduction of peak demand; customer cost saving is 5.9%
[49] 2012	RTP	Denmark	yes	Confirmed the DR on valley filling effects; contribute to a higher amount of wind energy schedule in power supply
[57] 2011	n.s.	Ireland	yes	Achieve 34.3% penetration of wind energy
[50] 2013	n.s.	n.s.	yes	Result in operation emission mitigation
[55] 2015	n.s.	China	yes	Reduce additional generating unit to save the cost for start-up in the peak times
[48] 2014	n.s.	Denmark	yes	Reduce the cost volatility by 7.74% and peak cost 14.35% in the electricity market
[51] 2012	n.s.	Ireland	yes	Demand on wind energy increase 15%; 13.8% financial generation cost saving of electricity;

[58] 2010	n.s.	Portugal	yes	Achieve 60% penetration of wind energy
[44] 2006	TOU	India	yes	Load shifting results in 62% off-peak energy consumption; 5.7% electricity bill reduction for end-users
[39] 2013	n.s.	United Kingdom	yes	Generation cost saving is 8%; demand peak reduction is 14%
[59] 2010	RTP	United States	yes	Social welfare increase is 6.6%
[56] 2006	RTP	n.s.	yes	Remarkably control the steepness of load curve
[47] 2009	DB	n.s.	yes	Confirm the DR's ability on valley filling effects
[60] 2011	RTP	United States	yes	20% saving of electricity cost for end-user without compromising users' comfort constraints

TOU= time-of-use, DLC= direct load control, ASM= ancillary services market, RTP= real time pricing, DB= demand bidding

Participating in DR programs offers economic benefits through leveraging dynamic pricing and DR incentives. The ability of DR to influence electricity prices was demonstrated in the study by Chua-Liang and Kirschen [47], wherein end-user load reductions generally led to a decrease in the market-clearing price, while load recoveries resulted in price increases. Given DR's potential to impact electricity prices, it becomes feasible to reduce cost volatility and peak costs in the electricity market. Notably, Feuerriegel and Neumann [48] observed reductions of up to 7.74% in cost volatility and 14.35% in peak costs. By curbing peak electricity consumption during high-priced periods and shifting it to lower-priced intervals [54], customers can realise considerable reductions in their operational costs through changes in consumption patterns. The study by Ashok and Banerjee [46] revealed a 5.9% saving in operating costs for customers under a DR plan, while Ashok's subsequent investigation [44] reported a 5.7% reduction in electricity bills for end-users. Similarly, Pengwei and Ning [60] achieved an approximately 20% decrease in electricity costs for end-users without compromising comfort. Although implementing energy storage in buildings entails additional investment compared to conventional systems, the potential cost savings from DR can serve as motivation for voluntary energy storage adoption by end-users, especially when the benefits outweigh the investment considerations.

DR's effectiveness has been explored in various countries through different DR programs, showcasing its ability to address energy challenges on a global scale. Additionally, most of the studies affirm the practicality of storage technology

during DR events, underscoring the value of end-users as crucial participants in DR initiatives. The subsequent section will provide a more detailed discussion of a specific type of storage technology employed in buildings, offering further insights into its implementation and advantages.

2.3 Structural thermal energy storage (STES)

Numerous case studies [11, 13, 17] frequently assess the viability of structural thermal energy storage (STES) for demand response (DR). These studies showcase the effectiveness of employing STES to shift peak heating demand, enhance the passive utilisation of renewable energy sources, leverage internal heat gains, and optimise advantages based on dynamic electricity prices [18, 19]. Thermal energy storage (TES) is often used in DR program to address the gap between supply and demand. TES could fill this gap and also take advantage of time-of-use tariff schemes [17, 63, 64], which further unlocks demand-side flexibility and allows the integration of more renewables. With an appropriate control strategy and local storage, buildings can work in synergy with the grid and be responsive to its requirements. Such a solution stores energy during off-peak periods and uses the stored energy during peak periods in response to dynamic electricity prices. This effectively shifts the thermal energy loads to daily off-peak hours.

Building thermal energy shifting eases the energy grid stress and contributes to optimal network operation [11, 15]. While there are different types of storage that can be used to achieve this, the thermal heat capacity of a building envelope presents a potential for storing energy passively, and at the same time, it can be a cost-effective solution. Building thermal energy could be stored in advance by using the building envelope and structure itself, named structural thermal energy storage (STES), without the additional cost.

High thermal inertia materials are commonly used for thermal energy storage for its capability to store a high amount of thermal energy [65]. In buildings, thermal mass stores heat during the daytime and release it back at night. The study of Zhu et al. [66] showed a lower heat flux through the massive wall system from the external around noontime than that through lightweight walls (Fig 2-3), which

indicated the ability of heavyweight walls to store more solar heat during peak times than that of lightweight walls.

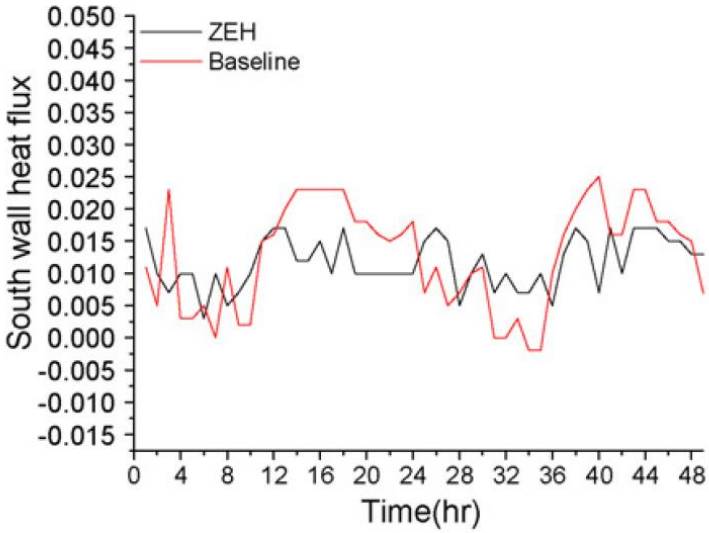

Fig. 2-3 Time-dependent heat flux in the cooling season of zero energy house (ZEH) (massive wall systems) and baseline (lightweight wall systems). [66]

The heat storage ability of thermal mass, especially for the massive wall system, contributes to a stable and comfortable indoor temperature. In the study of Zhu et al. [66], a more stable and more comfortable indoor temperature was achieved in the building with heavyweight walls than that of the building with lightweight walls. Similarly, in the study of Başaran [67], heat storage capacity of the building with heavyweight walls contributes to a stable inside temperature (change within 3℃ and stayed around 30℃) when there is a large outside temperature difference between day and night (42℃ in the afternoon and 22℃ at night). A comfortable indoor temperature due to the heat storage of high mass building was also achieved in the study of Ogoli [68]. In the study, when the maximum outdoor temperature was over 33℃, the maximum indoor temperature in the high mass building was 25.4℃, which was in the range of the comfort zone (Fig 2-4). Similarly, building thermal mass could store heat during winter and avoid an extremely cold inside temperature. In the study of Ip and Miller [69], heat released from the thermal mass of a building with the heavyweight constructions appeared to maintain a stable temperature of around 13℃ when the outdoor temperatures were extremely low.

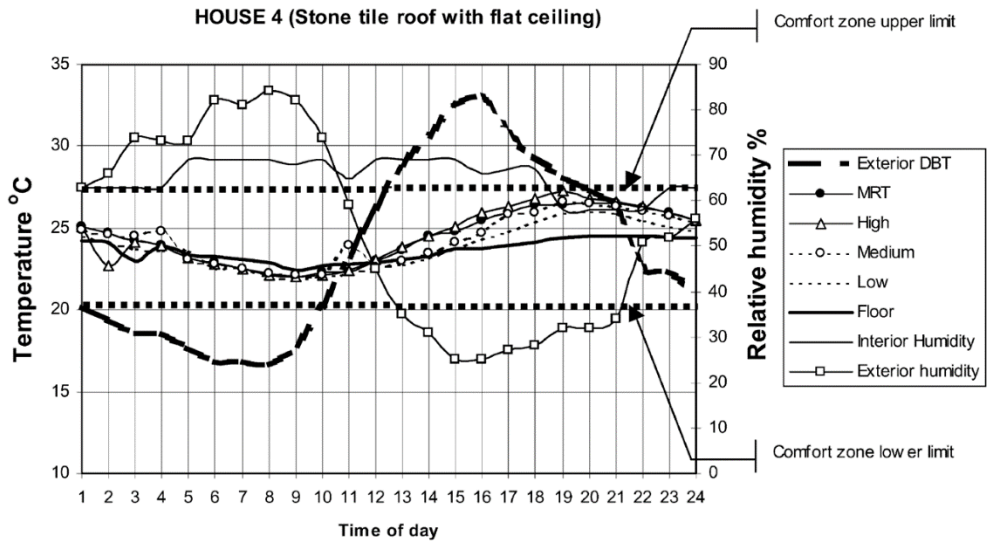

Fig. 2-4 Temperatures in the high mass building. [68]

In particular, STES can be coupled with heating, ventilation and air-conditioning (HVAC) systems in demand response (DR) programs [16]. The thermal energy is charged or discharged automatically by the temperature difference between the indoor air and the envelope [17-19]. As a result, the energy system usage can be reduced at certain times for peak-time demand reduction [20, 21]. However, the system must still be operated within the limits of the thermal comfort requirements of the occupants. An example of Sánchez Ramos et al. [70] confirmed the STES coupled with building energy system in DR for energy shifting is showed in Fig 2-5. They assessed a control system of demand management measures, which aimed at choosing the optimal strategy of pre-cooling/pre-heating/night ventilation for different types (various constructive characteristics) of residential when facing changes of electric tariffs. The results turned out that the maximum economic savings obtained after the implementation of the management system were 3.2% for heating and 8.5% for cooling. (PH is pre-heating, 0/1/2/3 means the number of operation hours, 20-25 corresponds to the set point temperature)

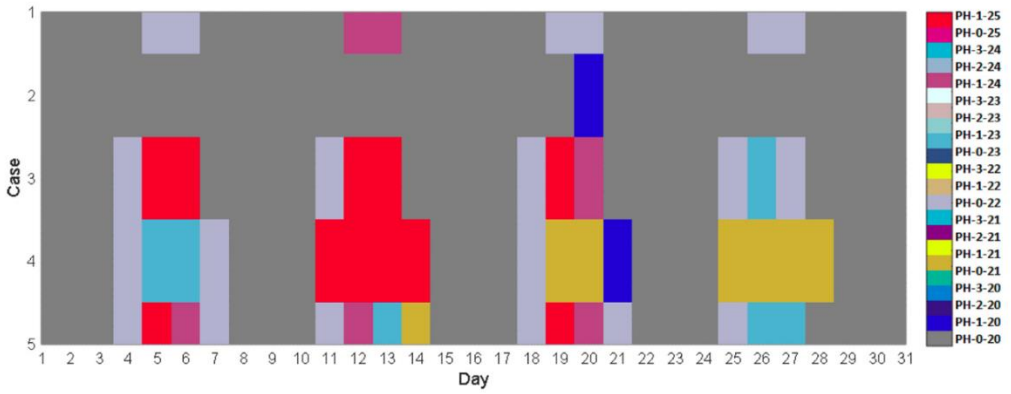

Fig. 2-5 Selection strategies for pre-heating for January. [70]

The storage capacity of building envelopes varies and studies [16, 66] showed that heavier thermal mass has a better thermal energy storage performance and can switch off the HVAC system for longer periods of time after fully charging [63]. The energy shifting performance of different envelopes are distinguished by the amount and the time of load shaping. Studies investigated the effect of envelopes in the DR program for better network stress relief. Le Dréau et al. [63] and Johra et al. [64] investigated the effects of envelopes on STES performance guided by dynamic price. They charged the building envelopes during low-price periods and discharged it during high-price periods. The results showed that the heavyweight envelope shifted more peak-time energy than the lightweight envelope (Fig 2-6). As a result, heavyweight thermal mass is preferable for STES in the application of dealing with network congestion. Reynders et al. [18] investigated the benefits of STES in the Belgian building stock and found that heating energy storage capacity could reach up to 12 kWh and 66 kWh for peak-time energy shifting in a day. Similarly, a Danish passive house demonstrated that nearly 90% of heating energy could be shifted to periods of low electricity prices by storing heating energy in the building's thermal mass over a year.

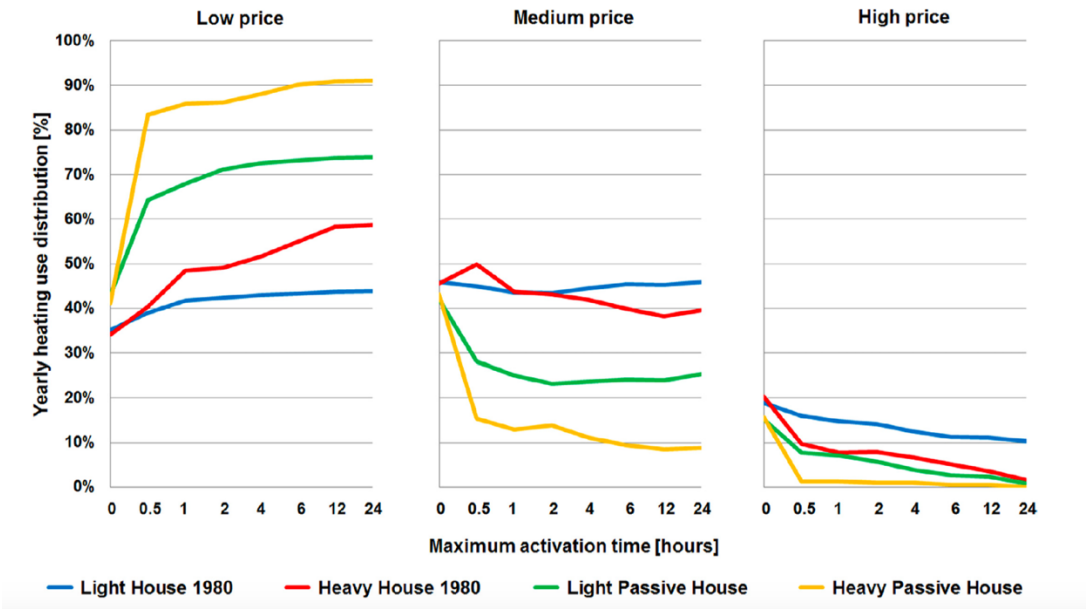

Fig. 2-6 Yearly heating use distribution variation for different STES in the study of Johra et al. [64]

A comparison of STES's energy flexibility for hot and cold climates [71] revealed that buildings across different climates could be optimally designed to implement energy control strategies for various seasons throughout the year. The results showed that the building in the hot climate gave higher power capacities but for a shorter time for maintaining the indoor thermal comfort. The building in the cold climate had lower capacity but for longer durations (Fig 2-7). Power capacity means that how much power can be delivered as flexible power; comfort capacity corresponds to the time it takes for the indoor temperature to reach the boundary of indoor comfort level.

In Fig 2-7 a, the power capacities of STES for the buildings in both cold climate (Netherlands) and hot climate (Texas) were varied based on seasons. Besides, STES for the buildings in the cold climate had the overall lower power capacity than that for the buildings in the hot climate. However, the results for winter showed that buildings in the Netherlands had higher power capacity during the winter. In Fig 2-7b, the comfort response also had seasonal variations of the buildings in both climate zones. The comfort response of buildings in the two climate zones showed the large difference during winter and summer. In general, buildings in the Netherlands had higher comfort response than buildings in Texas.

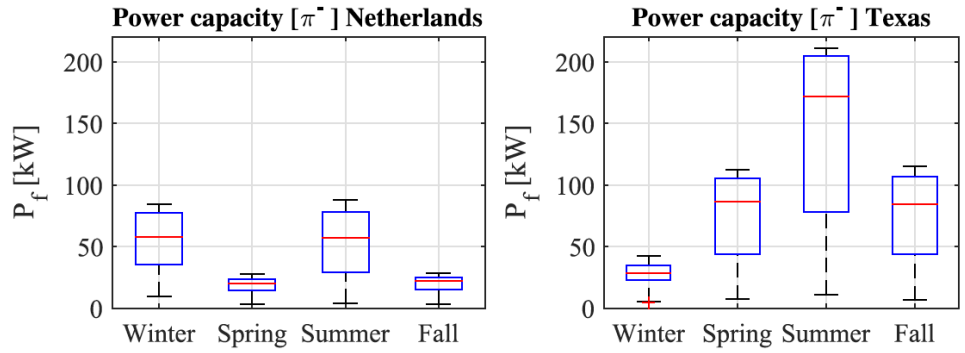

(a)

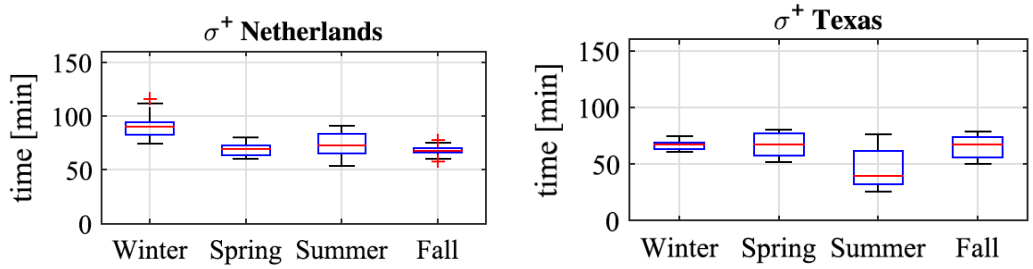

(b)

Fig. 2-7 (a) Power capacity (b) comfort capacity of the buildings in the Netherlands (cool humid) and the Texas (hot humid). [71]

Furthermore, STES can be fine-tuned to work in conjunction with advanced control strategies, accommodating heat transfer processes between building thermal mass and indoor air. For instance, Xue et al. [11] devised a building energy storage strategy that optimised interactions with a smart grid. Their building thermal mass storage model predicted power alteration potential, achieving energy storage efficiency of up to 41.61%. Similarly, Hu et al. [17] formulated an MPC strategy for STES that factored in weather conditions, occupancy, and dynamic electricity prices. This strategy, exhibiting superior energy shifting and maintenance of indoor thermal comfort, surpassed traditional on/off controllers in efficiency. Gi et al. [72] estimated that the thermal demand in 2050 would be 1.6-3.6 times that in 2010. Similarly, energy demand for buildings will rise by almost 50% between 2010 and 2050, based on the estimation of the International Energy Agency (IEA) [73]. Many works [15, 16, 18] have evaluated relevant solutions for decarbonisation and future climate change. It is predicted that climate change will affect the cooling and heating demand. The changes in daily peak supply periods would influence the performance of the storage technology.

Phase change materials (PCMs) enhance the concept of structural thermal mass by providing additional thermal storage within the same volume of material [22]. Leveraging the inherent ability of certain materials to absorb and release thermal energy during phase transitions [23], these technologies hold potential to contribute to load shifting, peak demand reduction, and overall enhancement of energy efficiency. MPCs, equipped with an understanding of the thermal characteristics of PCMs, can optimise the use of this enhanced thermal mass in synchronization with dynamic pricing signals, leading to efficient and cost-effective building heating systems [100].

Indeed, rather than resorting to traditional methods, such as the increase of building envelope layers for improved energy storage, research has given rise to PCM wallboards for optimised energy management. An illustration of this is the study by Kishore et al. [22], in which PCMs were deployed within the building envelope to evaluate load shaping (Fig 2-8). Their findings revealed that a wall integrated with PCM could yield an annual heat reduction of up to 72% and a 38% decrease in annual heat loss. A further case study by Wang et al. [101] implemented PCM wallboards within lightweight buildings situated in Shanghai, a city characterised by its hot summers and cold winters. Their simulations aimed to evaluate the potential impact of PCM wallboards on indoor thermal comfort. The results demonstrated a significant improvement in indoor comfort during both winter and summer periods, attributable to enhanced thermal energy storage by the envelope without necessitating additional thickness to the building structure.

Another exploration into the effectiveness of PCMs, conducted by Qu et al. [102], examined the factors influencing the energy performance of PCM wallboards concerning indoor thermal comfort and building energy savings. Their study underscored the potential for up to 34.8% energy savings and reduced indoor temperature fluctuation through the judicious selection of PCM wallboards based on local climate. Similarly, Wijesuriya et al. [103] examined the prospective energy savings of integrating PCMs into a building envelope. Under a future scenario where nearly 80% of the energy load is derived from renewable sources, their research indicated that the annual load flexibility facilitated by the integration of PCM could attain up to 33.6% in a lightweight residential building located in Baltimore, MD.

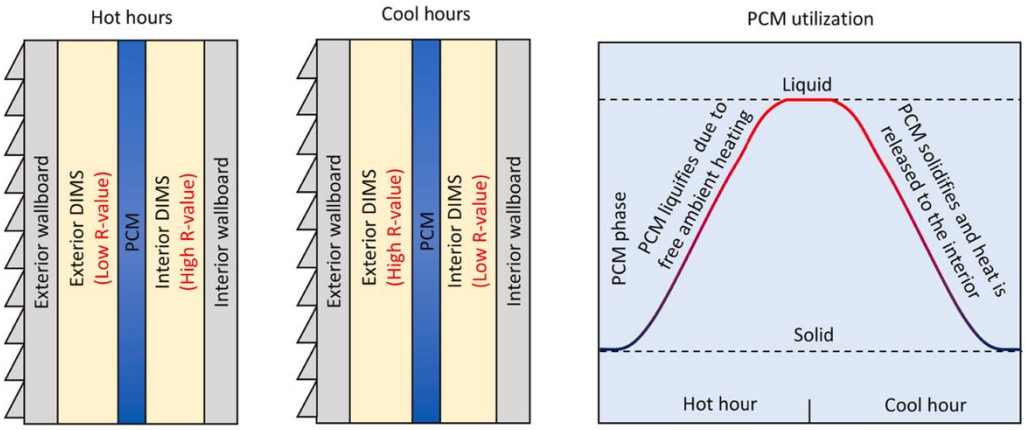

Fig. 2-8 PCM wallboard for heating energy storage. [22]

Although the STES is energy-efficient strategy in DR program, there is still lack of intelligent control for balance both building energy saving and indoor thermal comfort [17]. Especially for complex envelope with PCMs integration [100].

2.4 Model predictive control (MPC)

Continuously evolving are sophisticated control technologies in demand response (DR) and building HVAC systems. These advancements enable a spectrum of DR approaches, transitioning from manual to semi-automated and fully-automated systems [178]. As emphasized by Jingran et al.'s research [75], the inclusion of intelligence-based control strategies is crucial. With an increasing number of proposed modeling approaches and the aid of diverse modeling toolboxes, achieving accurate modeling for different building types is no longer a hindrance [179]. Model predictive control (MPC) has received much interest in the built environment field due to its potential for the optimal operation of building energy systems for multiple objectives [17]. MPC, an advanced method of process control, offers immense potential for managing heating, ventilation, and air conditioning (HVAC) systems efficiently. MPCs leverage mathematical models and predictive analytics to optimise control decisions, thereby reducing energy consumption and associated emissions. It offers a unique advantage in optimising energy consumption by not only reacting to current conditions but also anticipating future events. This includes the integration of dynamic pricing structures in energy markets. MPC has found widespread application as a predictive control strategy for energy shifting under dynamic pricing schemes in DR programs [74]. By

incorporating dynamic price signals into their predictive models, MPCs can schedule the operation of building heating systems during periods of lower energy prices, which not only minimises costs but also alleviates stress on the grid during peak demand periods (Fig 2-9).

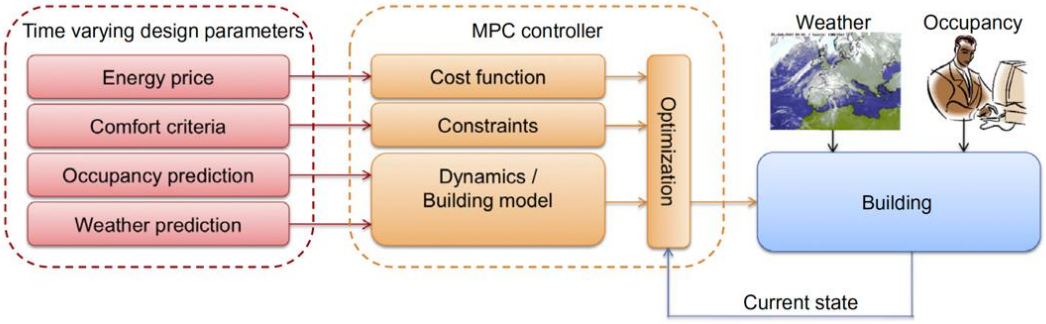

Fig. 2-9 Basic principle of model predictive control for buildings. [77]

Study of Ma et al. [75] included dynamic pricing in MPC objective functions to form an economic MPC by considering time-of-use rates. A trade-off can be observed between hours for precooling the indoor air to disconnect the energy usage during peak hours and an increased amount of total energy consumption. Finally, the result turned out that the proposed economic MPC successfully saved daily energy cost by energy shifting. Study of Hu et al. [17] applied hourly dynamic price into their MPC objective formulation. The result turned out that the energy flexibility of the building structure was realised by MPC firstly, and then controlled the indoor air for short preheating periods. Finally, the control strategy contributed up to 19% daily electricity cost saving.

In demonstrating the effectiveness of MPC, Michael et al. [76] conducted an experimental MPC for heating energy shifting guiding by dynamic heating price in a case study building. The result confirmed a flatten system load was achieved of MPC by increasing 45% low-price energy usage and reduced 82% high-price usage. Studies by Široký et al. [77] showed the ability of predictive control to reduce energy consumption by up to 28% in buildings using weather predictions. Khanmirza et al. [78] found that predictive control, when compared to the proportional integral derivative (PID) control strategy, lowered energy consumption by 2 kWh over a month in a residential building. On a larger scale, Rawlings et al. [79] proved that a predictive optimiser could autonomously operate

a central plant of HVAC systems for 25 buildings 90% of the time, decreasing operation costs by 10-15%. These studies underline the efficiency of MPC in realising economic benefits and enhancing indoor comfort levels in DR programs.

Despite these advancements, the widespread implementation of MPCs often faces hindrances due to their cost [80] and complexity [76], particularly in retrofitting existing buildings [27]. This reality underscores the potential impact of developing and testing a low-cost MPC, a development that could substantially enhance the energy efficiency of building heating systems.

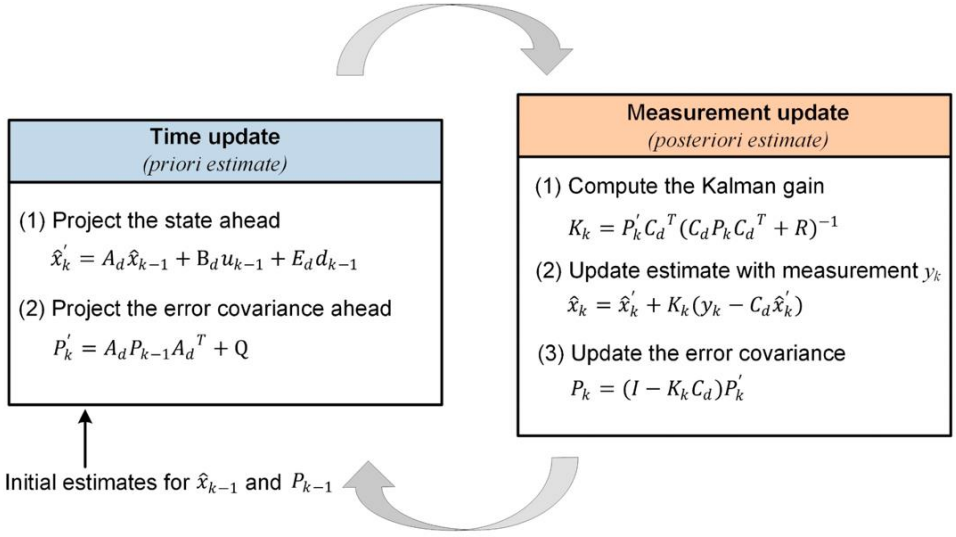

Fig. 2-10 Kalman filter cycle for current state estimation in MPC. [17]

Various factors such as weather, envelope, energy systems and occupancy behaviour/patterns have an impact on building energy demand [81]. Among these factors, occupancy pattern is one of the major sources of uncertainty related to building energy use [82]. MPC manages uncertainties related to occupancy patterns by incorporating predictive models that use historical data, current measurements, and forecast information in helping with Kalman filter (Fig 2-10). The controller leverages occupancy predictions, which may be obtained from various sources such as occupancy schedules [17], sensor data [83] or machine learning algorithms [84], and occupancy detection to anticipate changes in the building's thermal load. For instance, if the MPC anticipates a high occupancy in the building during a certain period of the day based on historical trends, it may preheat or precool the building to ensure the optimal indoor temperature at that specific time [17]. If the occupancy is lower than expected, the system will adjust its operations accordingly to save

energy while still maintaining comfort levels. This proactive management of HVAC systems allows for efficient energy use and comfort level optimisation, even in the face of occupancy uncertainties.In their study, Oldewurtel et al. [85] conducted an investigation into the effects of occupancy information on the performances of MPC. Homogeneous occupancy simulations revealed up to 34% potential savings for average vacancy and occupancy intervals of 5 and 10 days. In simulations with alternating occupancy, savings range around 50% compared to homogeneous occupancy scenarios. Ma et al. [86] addressed the uncertainties associated with occupancy forecasts by developing stochastic and robust MPC controllers.

MPC demonstrates its ability in controlling various building integrated energy-efficient system. The main two types highlighted by MPC are RES system and underfloor heating (UFH) system, which are facing problems under conventional control strategy limiting the developments of them.

2.5 MPC for RES penetration

The growing adoption of renewable energy sources (RES) has spurred a significant transformation in the strategies governing energy management and control in contemporary energy production systems [180]. Energy storage systems play pivotal roles in shaping this evolving energy landscape, effectively addressing discrepancies between demand and supply by implementing energy shifting, particularly in grids with high RES penetration. Achieving optimal energy flow management necessitates a control system that responds to external disturbances, aligning the supply with demand in real-time. Today, RES are increasingly being introduced into the energy supply system [87], which brings uncertainties in the amount of instantaneous energy supply. As a result, network congestion happens when the network load is high [88].

An optimal grid operation is required for congestion management, which manages to match the demand to the supply, such as by using DR which could be achieved by strategies such as the dynamic price [12, 13]. Many studies have integrated RES, such as PV systems, with energy storage and advanced control. In the study of Chapaloglou et al. [89], a photovoltaic (PV) system was integrated with

a storage system. In their TRNSYS simulation, the storage system could be controlled to discharge or charge depending on dynamic electricity pricing.

Similarly, in the study of Khordehgah et al. [90], a control system was proposed to charge the battery with power produced from the PV collector during the surplus supply periods based on the real-time load profile. By using such systems coupled with intelligent control, the study of Kemmler and Thomas [91] showed that up to 41% of the building's electricity consumption could be covered by the PV installation per year. The study by Toradmal et al. [92] simulated the performance of PV for powering the building heating energy system. They evaluated the thermal flexibility of a building to shift the heating system operation to the times of PV energy generation (Fig 2-11). The results showed that the building could offer significant thermal storage to improve the performance of onsite PV electricity utilisation. In the study of Langer and Volling [93], a simulation coupling of PV and the building heating showed that feed-in electricity from the grid was required for this type of coupling model for efficiently using PV surplus electrical energy.

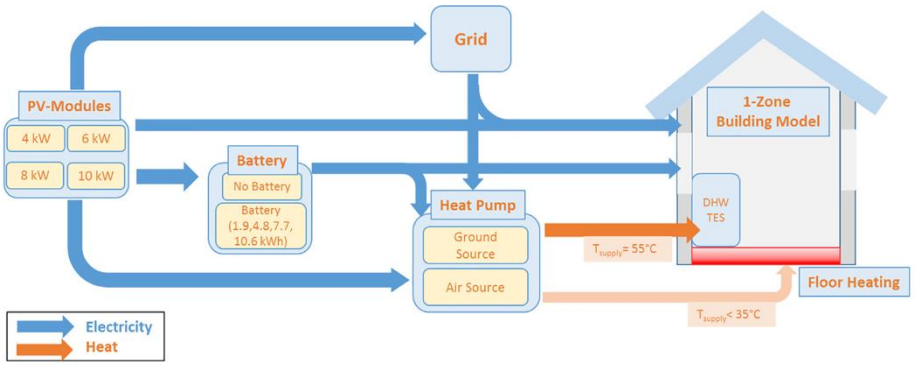

Fig. 2-11 Flow of energy within the system consisting of PV, battery, grid, heat pump and building. [92]

Various studies have demonstrated the potential of MPC in enabling demand flexibility, reducing peak load demands, and maximising the utilisation of renewable energy sources [94]. With the decreasing cost of renewable energy technologies such as solar energy systems, the goal of achieving net-zero carbon buildings has become more feasible. However, due to the intermittent nature of solar power, there can be a mismatch between energy demand and solar generation. This mismatch can be further exacerbated during peak load periods, resulting in issues such as intermittency, fluctuation, and unpredictability, which present

significant hurdles to the integration of solar energy [95]. The work [96] explored the use of MPC to optimise a hybrid heating system comprising an air-to-water heat pump and photovoltaic (PV) panels. The study demonstrated that the MPC strategy can adapt to different weather conditions and achieve significant financial savings with the right horizon and modeling. The research underscores the potential of MPC in maximising solar energy use in buildings, contributing to the design and implementation of energy-efficient heating systems. Currently, the study assessing MPC in building-integrated RES is still limited.

To further harmonise the intermittent nature of solar energy and the variable energy demand due to occupancy patterns, the integration of thermal energy storage (TES) becomes crucial. However, the harmonisation of renewable energy intermittency with the building's energy demands calls for an integrative solution. Thermal energy storage (TES) emerges as a complementary element to the predictive prowess of MPC, serving as a counterbalance to the variability of renewable energy sources (Fig 2-12). Exploiting time-of-use tariff schemes, TES enhances demand-side flexibility and promotes the integration of a broader range of renewable technologies.

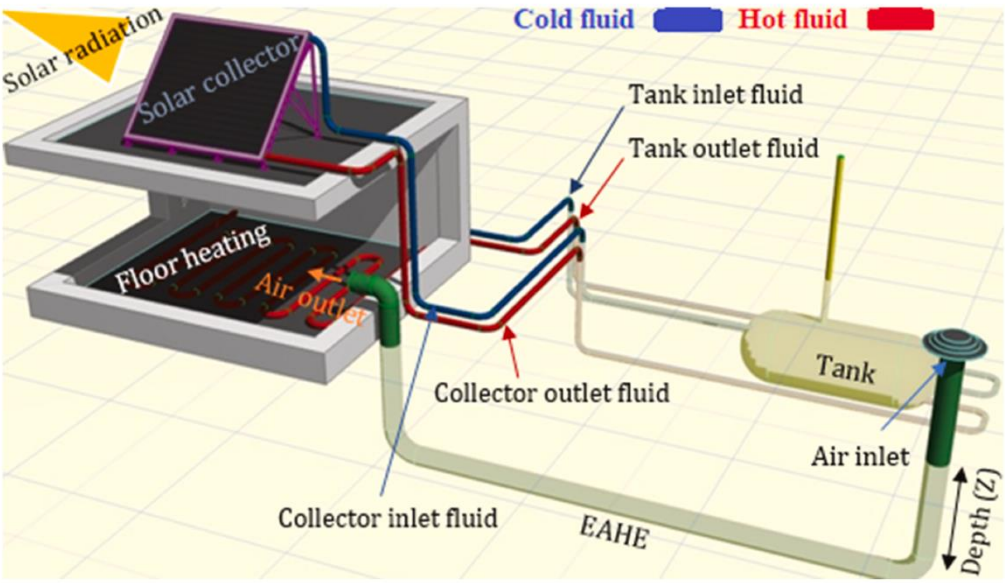

Fig. 2-12 Solar thermal system couple with building floor heating system through a storage tank. [97]

Since the RES providing building heating energy source often has the low temperature characteristic, it would be important to integrate RES with low temperature heating system avoiding further energy upgrade [97]. Underfloor

heating (UFH) system is a low temperature building heating system that can provide efficient heating energy in building.

2.6 MPC for controlling underfloor heating (UFH) system

Contemporary heating, ventilation, and air conditioning (HVAC) systems constitute a significant portion of overall building energy consumption, emerging as prominent electricity grid end-users [2]. Residential underfloor heating (UFH) systems leverage the substantial thermal inertia of structural thermal energy storage (STES) in buildings to execute preheating during off-peak or low-price hours, aligning with dynamic electricity pricing dynamics [105-107]. The inherent large time lag, often extending to several hours, between heat supply and the corresponding indoor air temperature response is a characteristic feature attributable to the extensive thermal inertia of the embedded concrete floor in UFH systems [17]. A UFH system is a good candidate for not only integrating with RES but also STES. For UFH coupling with STES for energy shifting, the system preheats the thermal mass, i.e., the floor element, and then uses it to heat the indoor air, resulting in a larger energy storage capacity compared to other heating systems, such as radiators, within the same charging time. In Reynder et al. [18] study, the UFH system provided almost twice the storage capacity of the radiator and was 20% more energy-efficient. The UFH system, which is a highly efficient heating system, utilises heating pipes containing hot water to heat the floor element, which in turn transfers the energy to the indoor air via convection [104]. Moreover, the floor heating system allows for lower temperature water circulation in the pipes due to the larger surface area for heat transfer. This characteristic improves the energy efficiency of the heating systems and enables the use of low-temperature energy sources, such as solar hot water. This system can operate using low-temperature heat sources with temperatures as low as 35 ºC [17], and it excels in maintaining uniform indoor temperatures. Zhou et al. [105] conducted a study on the UFH system's ability to control indoor temperature and found that it varied by less than 0.2 ºC for most periods of a 2-hour test.

Nevertheless, the substantial thermal inertia inherent to a pipe-embedded floor can induce a notable time lag between the supply of heat and the subsequent increase in indoor air temperature. This lag may extend over several hours,

contingent on factors such as pipe thickness, depth, and the thermal capacitance of the active floor. Conventional control mechanisms, such as the on-off controller and the proportional-integral (PI) controller, fall short of addressing this thermal lag and reacting promptly to abrupt load changes within the indoor space. As a solution, a predictive control strategy, capable of considering the delayed response of indoor temperature to environmental fluctuations, becomes pivotal in maintaining indoor comfort.

Study of Hu et al. [17] investigated the MPC controlling a UFH in energy shifting ability. The result turned out that compared to the conventional on-off controller, the MPC is able to use STES optimally shifted energy consumption from high-price periods to low-price periods and improved occupants' thermal comfort at the same time. As a result, the total electricity cost was reduced. Similarly, study of Široký et al [77] also confirmed MPC in controlling UFH system saved up to 28% energy cost with the weather forecast in a university building. Chen et al. [106] compared the energy performance of MPC and Proportional Integral Derivative (PID) in controlling a UFH system with an air-source heat pump. The results showed that the MPC controller is able to effectively reduce building energy consumption by around 15%. Meanwhile, the coefficient of performance (COP) was improved 24.5% by replacing PID controller with proposed MPC controller. Joe et al. [107] proposed an MPC used dynamic estimates for predicting zone loads and indoor temperature with the help of outdoor weather conditions and HVAC system models. The objective of their MPC is to minimise the energy cost of a UFH system while meeting thermal comfort requirements. The results showed a 10% energy savings when compared to a baseline feedback control.

MPC confirmed its ability in not only building energy system control but also building-integrated energy system control. However, the deployment of MPC in building still facing problems. One of the problems is the complex data extraction and data fusion prepared for MPC operation, which makes the MPC is costly and complex for its practical use [77].

2.7 Internet-of-thing (IoT) for MPC deployment

As a result of the declining costs of smart devices, the widespread availability of distributed sensors and data analytics tools, and the overall progress in information

and communication technologies (ICT), the adoption of Model Predictive Control (MPC) for optimizing energy efficiency and thermal comfort is becoming more immediate and cost-effective [181]. It is evident that the effectiveness of MPC relies on being associated with a suitable smart physical infrastructure capable of collecting and forwarding actual data from and to the field [182]. The Internet of Things (IoT) presents a viable solution by enabling the connection of sensors, actuators, and other objects to the Internet, facilitating seamless interaction [183]. IoT is increasingly being incorporated into building management systems, opening new horizons for energy efficiency. IoT devices facilitate real-time energy monitoring and control (Fig 2-13) [28], thereby generating valuable data that can be utilised for optimising energy consumption. Furthermore, the application of IoT to dynamic energy pricing systems could act as a potent driver for energy-efficient behaviour [29]. By digitalising dynamic pricing, consumers can gain real-time access to energy cost fluctuations, allowing them to adjust their energy consumption according to the price signals. IoT devices can provide the data necessary for the predictive models of the MPC [30], while the MPC, in turn, can optimise the building's energy usage based on real-time dynamic pricing information. Further, IoT-enabled real-time monitoring [31] can provide valuable data about the performance of PCMs [32], aiding in their control and maximising their potential for energy savings.

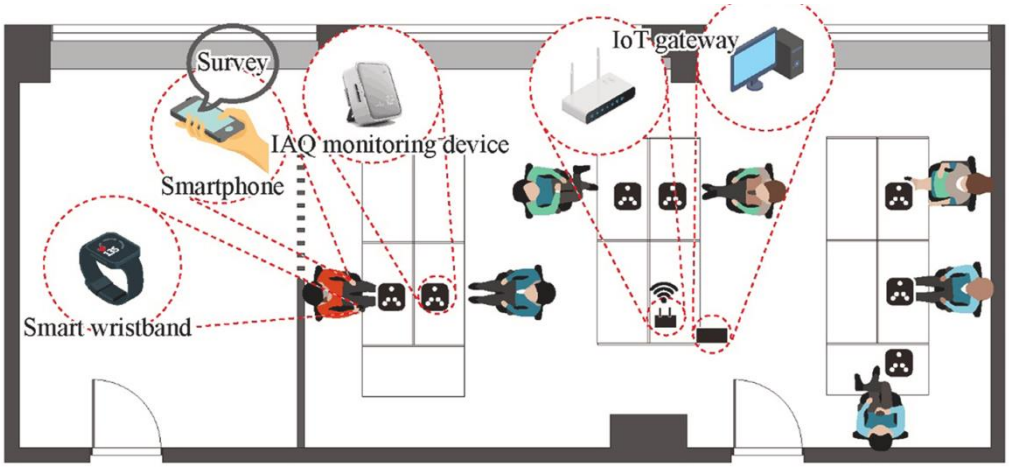

Fig. 2-13 IoT helps automatically building data collection. [28]

IoT integrated with building information system or in helped with automation in architecture, engineering, and construction (AEC) industry that have been evaluated by studies. Study of Jeoung et al. [28] proposed a peer-to-peer network to collect distributed indoor data regarding indoor thermal comfort bases on IoT technology. This blockchain framework successfully transferred data to a single PC for data-driven room model training for later use in building management system (BMS). Furthermore, study of huang et al. [30] highlighted the benefit of data fusion of building information modelling (BIM) and IoT system for efficient data process flow to meet different control targets in the AEC industry. Similarly, Fredriksson et al. [108] developed an IoT-based monitoring system to capture real-time disturbances in construction work and updated to decision making system for automatically planning corrected. This increased the reliability and practicality of the supervisory automation process in building sector.

The research by Acha et al. [109] identified an avenue for augmenting building energy efficiency: digitalising dynamic pricing to motivate consumers to capitalise on low-price energy. To achieve this, IoT was brought into the building sector [84], enabling two-way communication between the smart grid and end-users. The advent of IoT has enabled numerous embedded devices in the building sector, resulting in effective monitoring and intelligent control of building energy. Bases on the available IoT techniques, Li et al. [110] successfully implemented an event-driven optimisation method that activated the control system of HVAC only when the sensing data was below the event threshold defined by the control system. The reduced awake times of the sensors resulted in a significant reduction of the sensor power consumption.

The integration of IoT into building energy systems has amplified the application of cross-domain technologies, enabling digitalised energy chains, automated distribution, and maximised interaction between energy producers and consumers. The integration of IoT technology with MPCs could potentially yield a low-cost solution to efficient energy management. IoT devices can serve as an inexpensive and continuous data source for the predictive models employed in MPCs. Through the efficient collection and analysis of this real-time data, MPCs can be optimised to adjust energy usage based on current and predicted energy prices, effectively integrating dynamic pricing strategies. Thus, IoT technology could significantly lower the cost barriers associated with MPCs, making these advanced controllers a

more accessible option for a wide range of buildings. While the individual merits of MPCs and IoT devices are increasingly recognised, the empirical understanding of their integrated application within building heating systems is comparatively limited, which open for various combinations of IoT systems for monitoring, data extraction and control implementation. As such, the current research endeavours to bridge this knowledge gap by conducting a field experiment to test a low-cost MPC for building heating systems. Our study aims to shed light on the feasibility, scalability, and potential of these novel technologies.

2.8 Research gaps

The developments of practical MPCs for building energy management required both scenario analysis and experiment conduction considering future intelligent technologies. The literature has confirmed the practicality of MPC in wide condition with different targets in building sector and highlighted the potential systems and technologies can be applied in synergy with MPC for building energy shifting. The research gaps are identified thereafter:

2.8.1 Effect of different thermal mass and occupancy variability in building energy performance under MPC

A limited number of studies [63, 64] that assessed the effect of the envelope on energy shifting performance under dynamic pricing. Both showed that heavyweight thermal mass can shift more high-price energy to the low-price periods. However, in their study, the control strategy set varied temperature setpoints to trigger the preheating effects in a low-price period. Thus, there would be offsets caused by delay effects when heating switches, especially with the UFH system. As a result, this kind of control strategy might result in overheating, especially for lightweight houses with indoor temperature fluctuating more quickly than heavyweight houses. Moreover, Buildings with high occupancy variability, such as universities, where fluctuations occur throughout the day and across the year, can pose challenges in developing control strategies that aim to balance comfort and energy efficiency. This situation becomes even more complex when such buildings are integrated with renewable energy technologies, due to the inherently intermittent nature of these energy source. To promote widespread integration of renewable energy sources in such buildings, the adoption of advanced control strategies such as model predictive

control (MPC) is imperative. Furthermore, the variable nature of occupancy patterns must be considered in MPC's design. Studies investigate the influence of occupancy pattern influencing the building energy shifting performance under MPC is still limited.

2.8.2 Scenario analysis of MPC under climate change and RES system with UFH system

Most studies haven't considered the building's response in the control strategy orin the case when there is no need for charging during peak periods. Besides, comfort violation is unavoidable when the setpoint energy shifting is controlled by a simple thermostat controller [19]. This will be further explored in the present study. Currently, no study has investigated the impact of future climate conditions on STES performance, particularly low-temperature heating energy storage. Furthermore, the increased uptake of solar energy systems in the future could aid the energy shifting capabilities of such an energy storage system. Meanwhile, Various works [111, 112] have shown the importance of incorporating occupancy information to enhance the effectiveness of MPC. This incorporation allows MPC to more accurately forecast the building's energy demand, consequently adjusting its charging and discharging schedules to maximise energy savings without sacrificing occupant comfort. However, prior studies such as those conducted by Torreglosa et al. [113] and Bartolucci et al. [114], while proposing MPC strategies for controlling the charge and discharge cycles of storage tanks coupled with renewable energy systems (RES), have not considered the building thermal mass storage and the indoor temperature's response. Therefore, the synergistic effect of combining active and passive storage within such systems remains an open area for investigation. The amount of stored energy is larger in a floor heating system than in other heating systems, such as the radiator, under the same charging time. There are limited number of studies on the use of MPC in controlling the low-temperature floor heating system in combination with the RES. Other research gaps, such as system operating temperature and setpoint strategy that hasn't been analysed in previous studies will be investigated.

2.8.3 PCM wallboard controlled under MPC strategy

Moreover, while PCMs are recognised for their thermal energy storage capabilities, research on their integration into building systems and how this can be optimised using MPCs is still emerging. There are two studies currently aim for

evaluating the energy cost saving performance of PCM wallboards under MPC strategy for building sector. Study of Yang et al. [100] proposed a MPC framework in MATLAB for price-responsive control of PCM-wallboard-enhanced space heating system by eliminating nonlinearity between specific heat capacity and temperature of PCM wallboards. The simulation result reported a significant (i.e., more than 60%) heating electricity cost was achieved. Study of Gracia et al. [94] used python to simulate the energy performance of PCM wallboard under MPC control strategy. By inputting the weather forecast to the proposed MPC, PCM wallboard provided a significant thermal benefit (i.e., around 30%) for the space heating system. However, current studies haven't simulated a completely feedback control for building with PCM wallboard integration. Thus, lack of insights for energy shifting performance of intelligent unsupervised controlling of PCM wallboards. There is a need for further studies exploring how MPCs can leverage the thermal characteristics of PCMs for load shifting, peak demand reduction, and overall enhancement of energy efficiency. To fill this gap, this study proposed a PCM simulation bases on an experimental validated unsupervised IoT-based MPC control strategy.

2.8.4 Low-cost MPC design

Currently, there are limited field experimental studies assessing the technical and energy performance aspects of MPC implementation in buildings. Study of Bünning et al. [115] controlled indoor air temperature through existing actuators of building heating/cooling grid by inputting control signal solved by MPC via OPC-UA software clients. They successfully saved between 26% and 49% of heating and cooling energy, compared to the building's baseline hysteresis controller. Study of Knudsen et al. [76] adjusted the supply water temperature for space heating system determined by a MPC in a living lab. The sensing data from the existing sensors were sent back through cRIO real-time controllers. The control strategy was solved by MATLAB. Finally, the updated heating system setpoint was adjusted by LabVIEW. The results confirmed the MPC shifted energy consumption from high-price periods to low-price periods. Similarly, Yang et al. [27] realised an indoor climate control by a MPC strategy through various data exchange by interaction with existing building control system. Finally, both an increased indoor thermal comfort and electricity cost saving were achieved under proposed MPC strategy.

Study of Široký et al. [77] and study of Sturzenegger et al. [80] also showed the improved indoor thermal comfort and building energy efficiency by integrating MPC into the building energy management system and exerted control signal to actuators later. However, the current MPC experiment should always be included in existing BMS. This increased the cost for MPC experiment compared with other lightweight experiment. Later, reviewed experimental MPC required interaction between different environments that reported to be a large power consumption [110]. Furthermore, potential execution errors and memory fragmentation might be occurred through intermittently data exchange. For this purpose, this study proposed an indoor MPC control strategy bases on peer-to-peer data exchange in help with IoT technologies, targeting for a lightweight and compatible MPC intelligent control.

2.8.5 Summary

This chapter provides a comprehensive overview of studies aimed at enhancing building energy efficiency through DR programs, focusing on diverse aspects, including materials and technologies. MPC emerges as a suitable strategy for optimising building energy efficiency by enabling energy shifting through a broad range of system integrations and applicable technologies. Notably, MPC facilitates the integration of various systems such as the UFH system, renewable energy storage system, and PCM wallboard system, effectively supporting building energy shifting efforts. However, research gaps have been identified, particularly concerning the analysis of MPC's performance under the influence of climate change. Furthermore, to achieve widespread adoption, continuous efforts are required to enhance the integration of various systems and technologies within the framework of MPC. Table 2-2 provides a comprehensive summary of the most influential studies on intelligent building control, underscoring their contributions to energy shifting through the implementation of novel systems and technologies. Those studies provide insights for methods/simulation model of this thesis.

Table 2-2 Summary of most influential research findings on building intelligent control for energy shifting

Reference	Technology	Objective	Results description	Insights
Xue et al. [11]	STES	Heating energy shifting	The energy storage of STES for a commercial building reached 41.6%	Proposed a platform for STES simulation
Hu et al. [17]	MPC and UFH	Heating energy shifting	MPC controlled UFH achieved daily heating energy cost saving up to 14%	Highlighted a co-simulation platform for MPC controlling STES under UFH system
Yang et al. [100]	MPC and PCM	Heating energy shifting	MPC controlled PCM wallboard shifted 80% peak heating loads to off-peak times	Introduced a validated PCM model for MPC
Široký et al.[77]	Experimental MPC	Heating energy saving	Almost 30% heating energy was saved by the proposed experimental MPC in a University case study room	Introduced a practical MPC implementation on building heating system
Tarragona et al. [96]	MPC and PV	Heating energy saving	MPC controlled a space heating system coupling with PV system saved 58% energy cost	Created a model for building integrated RES technologies under MPC
Martín-Garín et al. [116]	IoT-based sensing system	Design automatically sensing system	The information obtained from the sensors is collected and stored in a flash memory card, and simultaneously is sent via WiFi to the cloud. This data is stored in an online spreadsheet, which permits us to access the information in real time.	Introduced real-time data collection and data fusion through low-cost IoT technologies, which is useful for data preparation in MPC.

3. Methodology

This chapter introduces the basic information about the MPC, includes its formulation and simulation platform. Later, the test facility used for MPC experiment and general procedure has been introduced in this chapter.

3.1 State space (ss) model

MPC strategy of building thermal energy system requires a numerical room representation so that the future indoor temperatures could be compared under different control trajectories. Resistance-Capacitance (RC) room model can predict the future indoor temperature by responding to the weather condition and thermal energy feed. The room under consideration can be conceptualised as a collection of first-order systems, where the temperatures of indoor air, walls, floor, and ceiling represent the states of these systems. The heat transfer between nodes within the room can be characterised using thermal RC concepts [77]. By employing time-series governing equations that describe heat transmission between nodes, we can calculate the current temperatures of each node. Indoor temperature can be calculated from the previous time's temperature and the current time's heat exchange. This network of first-order systems can be further leveraged for MPC by formulating a state-space (ss) model.

This thesis employed gray-box identification, a technique that aims to identify system properties by capturing physical connections between states [117], to estimate the model through machine learning methods using input/output data. ss model typically provides a fast approach to identifying a discrete-time model of the continuous-time system [77]. In the present study, a linear, time-invariant state space model was formulated to predict the temperatures of nodes.

$$x_{k+1} = Ax_k + Bu_k + K\sigma_k \qquad \text{eq 3-1}$$

$$y_k = Dx_k + \sigma_k \qquad \text{eq 3-2}$$

A, B, D and K are the system matrices, which have to be identified. x_k are system states u_k are input variables, y_k are the output variables. σ_k is an unknown noise, e.g. zero mean Gaussian white noise. In this study, σ_k is assumed to be zero. System identification aims to minimise the error between measured data and output

of the simplified RC representation with a limited searching magnitude by giving the initial values of system matrices (based on construction properties). The identification process used a cost function for minimising errors [117].

This study assumed a reasonable original state for each temperature node. Since not all states are measurable in reality, a Kalman filter was used to estimate unmeasurable states and filter the noises in each cycle. Leveraging a dual-pronged approach, which involves updating measurements and error covariance simultaneously, the Kalman filter has the capacity to estimate the current state at each starting point of the optimisation process [17].

3.2 Kalman filter

For each time step, the proposed MPC strategy would identify the optimal control trajectories in the prediction horizon, only the first control strategy was taken and fed to the building model. Then, the predicted temperatures by the state-space model in the previous time step were corrected with the simulated temperatures after the current-time control signal was applied. The correction was done by the Kalman filter [118]:

Predicted sate in previous time step:	$\bar{x}_k = Ax\_e_{k-1} + Bu_k + Ed_k$	eq 3-3
Error covariance:	$\bar{p}_k = A * p_k * A' + G * Q * G'$	eq 3-4
Kalman filter gain:	$K_k = \bar{p}_k * C'/(C * \bar{p}_k * C' + R)$	eq 3-5
Update state estimation from predicted value with m:	$x\_e_k = \bar{x}_k + K_k * (y_k - C * \bar{x}_k)$	eq 3-6
Covariance of predicted state estimation error:	$p_{k+1} = (G - K_k * C) * \bar{p}_k$	eq 3-7

Where $\bar{x}$ is the predicted state by state-space model. x_e is the updated current state by both the predicted state and measured state. y denotes the measurement used to update the current state. $\bar{p}$ is the error covariance. K is the Kalman filter gain. $A\ B\ C\ E\ G$ are the system matrices. The above Kalman filter equations apply the measurement noise covariance R and process noise covariance Q to update the current state $x\_e_{(k)}$ through both the measured state y_k and the predicted state $\bar{x}_k$. R is smaller than G, which means the measured values are more reliable than the

predicted values and vice versa. In this study, R is set to 1 and Q is set to 50 to trust the simulating data more than the predicted data.

3.3 MPC formulation

The MPC strategy carries out future control based on constraints and system dynamics for a minimal cost [77]. In this study, the heating system was controlled by MPC based on pre-set temperature constraints and shift the energy to low price periods. The formulation of MPC is:

$$min \sum_{k=0}^{N-1} (u_k, y_k) \quad \text{eq 3-8}$$

k means the current time step. N means the prediction horizon. u and y stand for manipulating variables and system states. The solver compared different trajectories. Then, it chooses one with minimal cost in the prediction horizon. Besides, MPC strategy can include the Kalman filter, which corrects the predicted system states with real-time measured system states to increase the prediction accuracy. As a result, a more reliable control trajectory is solved by MPC.

Once ss model is obtained, the MPC strategy is formulated by defining the objective function, incorporating the identified ss model, and establishing relevant constraints. The primary aims of MPC approach in this thesis are to minimise heating energy consumption while ensuring indoor thermal comfort. To achieve this, we introduced indoor thermal comfort as a constraint, penalising any deviations from the desired comfort levels within the objective function. The structure of our objective function was designed as quadratic forms, allowing us to appropriately weigh each term. Notably, we assigned significant weight to the comfort violation term, underscoring the paramount importance of precise comfort control.

$$J = min \sum_{k=0}^{N-1} a_k^T \, q \, a_k + b_k^T \, r \, b_k \quad \text{eq 3-9}$$

With the constraints:

$$y_{r,k} - y_k - a_k \leq 0, a_k \geq 0 \quad \text{eq 3-10}$$

$$y^k = C(A_d x^{k-1} + B_d u^k) \quad \text{eq 3-11}$$

In this study, the prediction horizon N is set to 24 with a time interval of 30 minutes. Weighting factors q and r are used to quantify the importance of each term, where a_k represents comfort violation, and b_k represents thermal energy cost.

3.4 Computation of MPC in MATLAB

The system matrix is identified in MATLAB with the initial guess from wall's material, including layers' conductivity and capacity [17]. The initial ss model *m* is:

$$m = idss(A, B, C, D) \quad \text{eq 3-12}$$

Where *idss* is the function to create a state space model with identifiable parameters. The data captured collected is used to identify the ss model, and the time step is 30 mins (i.e., 1800s). The data object is:

$$data = iddata(output, input, 1800) \quad \text{eq 3-13}$$

Data is a *"iddata"* object, which can store the input data, output data and the time step. Then, the system matrix is adjusted in MATLAB with *ssest* function, which aims to minimise the error between the measured data and the identified data by identifying the system matrix start from the initial values.

$$m = ssest(data, m) \quad \text{eq 3-14}$$

Where *ssest* is the state space model estimation command.

Later, the MPC was developed in MATLAB through the optimisation toolbox [119]. MPC have manipulating variables, which are identified in the optimisation and are solved for each time step in the prediction horizon by inputting time-dependent parameters. Thus, we set the control signal as the manipulating variable. The algorithm of the MPC includes the relationship between variables by setting the constraints. In this study, the indoor temperature inferred from the numerical room model was set as a constraint.

$$constraints = [x\{k+1\} == a * x\{k\} + b * w\{k\} + e * disturbance(k)] \quad \text{eq 3-15}$$

Where *a*, *b* and *e* are the system matrices, *x* is the temperature states, *w* is the heating water temperature, disturbance includes the outdoor temperature, internal heat gains and solar radiation etc., and *k* is the current time step. Besides, MPC can

limit the temperature by including the comfort violation in the cost function. The comfort violation is:

$$constraints = [constraints,\ T_{min}(k+1) - e\{k+1\} \leq c * x\{k+1\} \leq T_{max}(k+1) + e\{k+1\} \quad \text{eq 3-16}$$

Where T_{min} *and* T_{max} are the temperature bounds, and e is the comfort violation.

The limitation of the comfort violation in the cost function with denoted weights q is:

$$e\{k+1\}' * q * e\{k+1\} \quad \text{eq 3-17}$$

The cost function of multi-objectives with denoted weights can give priority to the most important objective. In this study, a larger weight of temperature violation gives priority to indoor comfort. The two conflicting objectives were summarised in the cost function. The cost function is:

$$Objective = \left(uheating\{k\} * price(k)\right)' * r * \left(uheating\{k\} * price(k)\right) + e\{k+1\}' * q * e\{k+1\} \quad \text{eq 3-18}$$

where r is the weight for limiting the heating cost, *price* is the day ahead hourly price, *uheating* is the amount of heating energy.

Comfort violation is calculated based on the current time heating system status by setting the constraints. Finally, we could infer unknown parameters based on the known parameters. In each loop, current time parameters are inputs for calculating the control signal with minimal cost. The current time parameters include:

$$parameter = \{x\{1\}, price, disturbance,\ T_{min},\ T_{max}\} \quad \text{eq 3-19}$$

Where $x\{1\}$ is the current state proposed to be updated by the Kalman filter and measure temperature from TRNSYS.

The MPC calculates the optimal trajectory of the control signal by the denoted solver (e.g., gurobi solver [120]) based on the current time input.

$$ops = sdpsetting('solver','gurobi') \quad \text{eq 3-20}$$

$$control = optimizer(constraints, objective, ops, parameter) \quad \text{eq 3-21}$$

Finally, the algorithm can be stored as an optimiser to return the control signal with time-dependent inputs.

$$solved\ control\ signal\ = control\ \{input(k)\} \quad \text{eq 3-22}$$

3.5 Co-simulation of TRNSYS and MATLAB modelling MPC feedback control

TRNSYS [121] is a well-known software for building dynamics simulation by white-box. In TRNSYS, each type represents a single sub-system. Then, users create linkage between variables of Types for data exchange. TRNSYS is widely used for simulating indoor HVAC system, RES and thermal storage systems.

In order to perform feedback control, a MATLAB engine for solving real-time control strategy. TRNSYS can call MATLAB in each time step and feed the results back to the simulation (Fig 3-1a). At the start of the simulation, state-space models, Kalman filter, MPC model and predicting disturbance were loaded in MATLAB and were prepared for use in the calculation. After TRSNYS calculates the room model temperatures, TRNSYS feeds the room or/and pipe temperatures to MATLAB for the Kalman filter. Then, MPC model can obtain the control strategy. At the end of each time step in TRNSYS, MATLAB is called by Type 155 for the control signal of the next time step. Besides, there is a step increment (eq 3-22) in MATLAB to match the time step with TRNSYS. The co-simulator runs by sharing time information at each time step in the simulation to ensure synchronization between these two platforms (Fig 3-1b).

$$nStep = nStep + 1 \qquad \text{eq 3-23}$$

$$nStep\ means\ the\ current\ time\ step$$

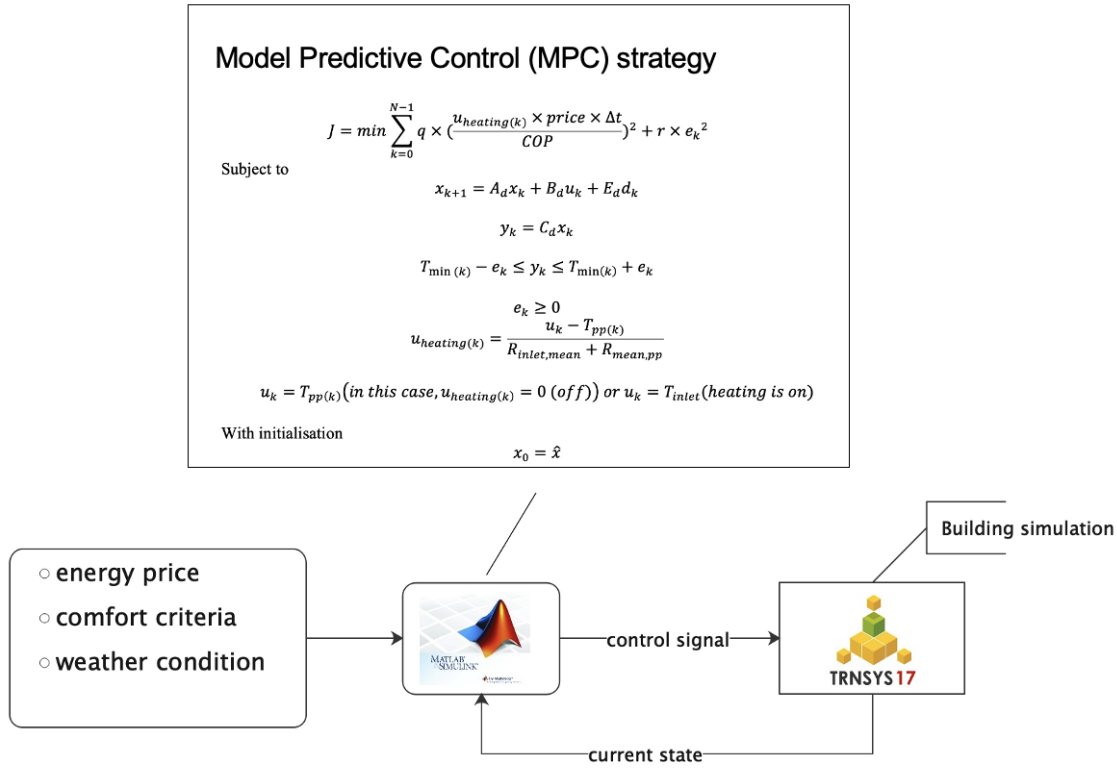

(a)

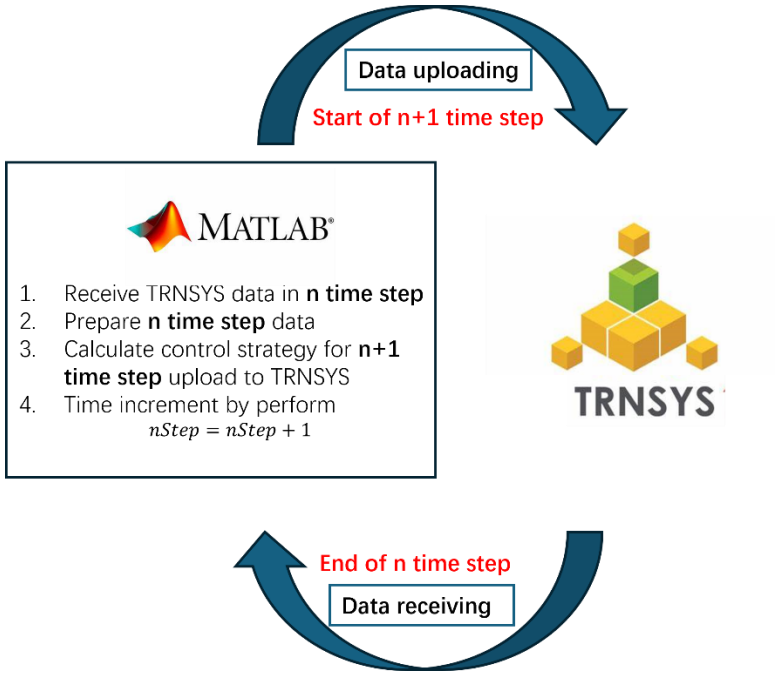

(b)

Fig. 3-1 (a) Co-simulation of MATLAB and TRNSYS (b) time information sharing between two plarforms

First case study building used a simple room in Chapter 4.2, resembling a standard living space in a residential apartment. The room utilized floor heating to warm the indoor air. This case study aimed to explore the capacity for energy shifting, focusing on various building and heating system attributes. To supplement energy needs and minimise consumption during peak hours, a rooftop PV system was integrated. Additionally, simulations were conducted to assess how future climate changes might impact the heating energy flexibility of the case study building.

Next, to assess the effectiveness of MPC in a building with a highly variable occupancy pattern in Chapter 5.2, we employed the Marmont lecture room located at the University of Nottingham, UK, as our designated case study space. This facility is primarily intended for the instruction of architecture and engineering students. The occupancy pattern in these areas can experience significant fluctuations throughout the day, driven by the diverse schedules of the students.

To examine the feasibility of the suggested MPC strategy , we employed a test pod situated within the University building in Nottingham in Chapter 6.1. The rationale behind selecting this test pod lies in its uncomplicated construction material and external-facing façade on all sides, making it an ideal setting for testing the practical implementation of MPC, as highlighted in [80].

3.6 Test facility of MPC experiment

This subsection introduces the test facility of an MPC experiment conducted in a test pod located in the University building in Nottingham and individual function in MPC deployment.

(a)

(b)

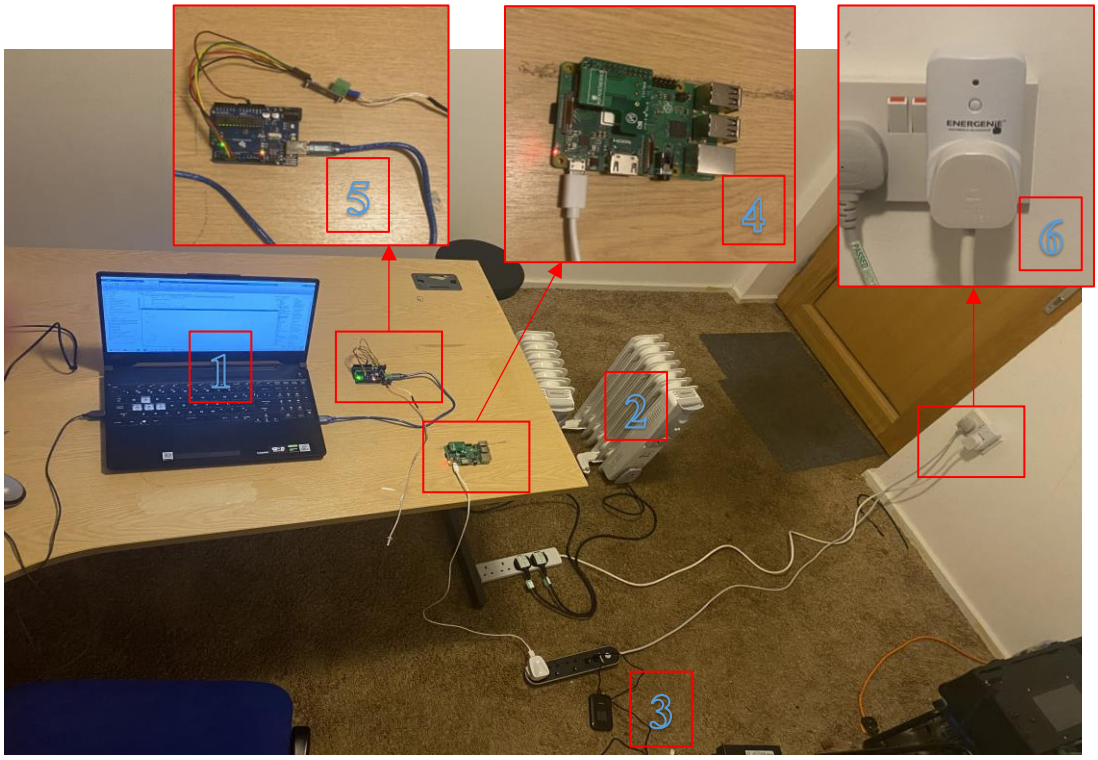

1. Control laptop
2. Radiator
3. WiFi router
4. Raspberry Pi with add-on board
5. Arduino with K type thermocouple
6. Smart plug

(c)

Fig. 3-2 (a) Local weather station (b) external view of the test pod (c)internal view of the test pod

The experimental room in this study, denoted as a test pod (as depicted in Fig 3-2 b), is situated at the University Park campus of the University of Nottingham, UK. This test pod, constructed predominantly of wood, embodies the principles of passive house design, possessing a volumetric capacity of 22 cubic meters, an envelope surface area of 48 square meters, and an air leakage rate of 1.7 [122]. The construction of the walls, 145mm in thickness, yields an overall U-value of 0.51 W/m^2K. This rectangular pod, with dimensions measuring 3.15m in length, 3.94m in width, and 2.91m in height, is oriented in a north-west direction. On its south-eastern façade, a double-glazed window of 0.79 square meters is installed.

To maintain thermal comfort within the pod, two radiators, each with a capacity of 1.5 kW, are utilised (as presented in Fig 3-2c). The maximum surface allowed temperature of radiators is 65°C. Within this test pod, a comprehensive measurement system is deployed for the purposes of monitoring the indoor temperature, logging external meteorological conditions, and recording the energy consumption. An ECOWITT weather station [123] (as shown in Fig 3-2a) is situated outside the test pod for local meteorological data collection. Furthermore, a smart meter is installed to aggregate the power consumption of both radiators (illustrated in Fig 3-2c). These pieces of equipment transfer the collected data to a cloud-based server via a WiFi connection.

For indoor temperature monitoring, a real-time sensor system based on Arduino technology is employed. An analog-to-digital converter, the Max 6675 module, is used in conjunction with a K-type thermocouple to sense the indoor temperature. The Arduino platform then acts as an intermediary, processing the data from the Max 6675 module and transmitting them to the serial port of a PC via a USB serial adapter. The precise pin connections between the Max 6675 module and the Arduino system are described in Table 3-1. This low-cost, compact, and compatible sensing system has been implemented successfully in similar studies [124, 125].

In order to verify that the K thermocouple temperature sensor is working properly, it is calibrated using the built-in indoor temperature sensor of gateway of the ecowitt weather station [123] placed near the K thermocouple for two days with indoor temperature range from 10 to 30 as seen in Fig 3-3. The built-in temperature sensor then logged the real-time temperature via WiFi to cloud. The sampling interval was of 30 minutes and the data was collected for four days from 19th

December to 23rd December. The plot shows the match of results of two sensors with root mean square error (RMSE) was 0.97 ℃. This adheres to the specifications provided in the Max 6675 user manual [126].

Table 3-1 Connection between Arduino and MAX 6675

Arduino	MAX6675
Ground	Ground
VCC	5V
SO (serial output)	Pin 4
CS (chip select)	Pin 5
SCK (serial clock pin)	Pin 6

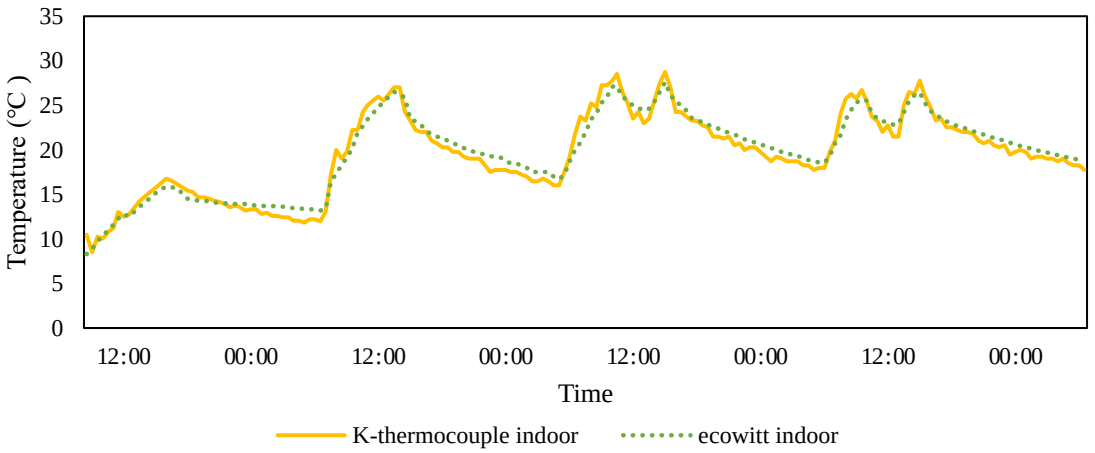

Fig. 3-3 Comparison of two sensors

A Raspberry Pi (RPi) 3 module is utilised as the control system for this investigation, chosen for its cost-effectiveness, compatibility, and ease of interfacing [127]. In this study, the RPi is tasked with transmitting signals to a WiFi-enabled smart plug (see Fig 3-2 c), facilitated by an interfaced add-on board. The RPi receives command instructions from a PC via a wireless connection, processing the information into a format that is recognisable by the smart plug. A MATLAB engine [128] operating on the PC is used in this study for control signal processing and communication with the RPi. Simultaneously, MATLAB retrieves real-time indoor temperature data from the sensor system through the PC's serial port, employing the "read" and "serialport" functions.

3.7 Summary

This chapter gives general backgrounds to form MPC simulation platform and experiment in this thesis. The detailed MPC formulations target at different objectives in controlling different building and building-integrated systems are presented in chapter 4-6. The detailed experiment arrangement and performance analysis is presented in chapter 6.

4. MPC controlled UFH system with STES and PV system: impact of occupancy patterns and climate change

Energy distributor sets the dynamic price for maximising the renewable energy efficiency by matching the demand to real-time energy supply [87]. In this chapter, the building fabric stores energy to shift the peak load to off-peak times. The control strategy considers the building's response under current weather condition and maximise the low-price electricity usage. As a result, a reduction of electricity cost along with an increased supply energy efficiency is achievable by the designed information exchange platform (Fig 4-1).

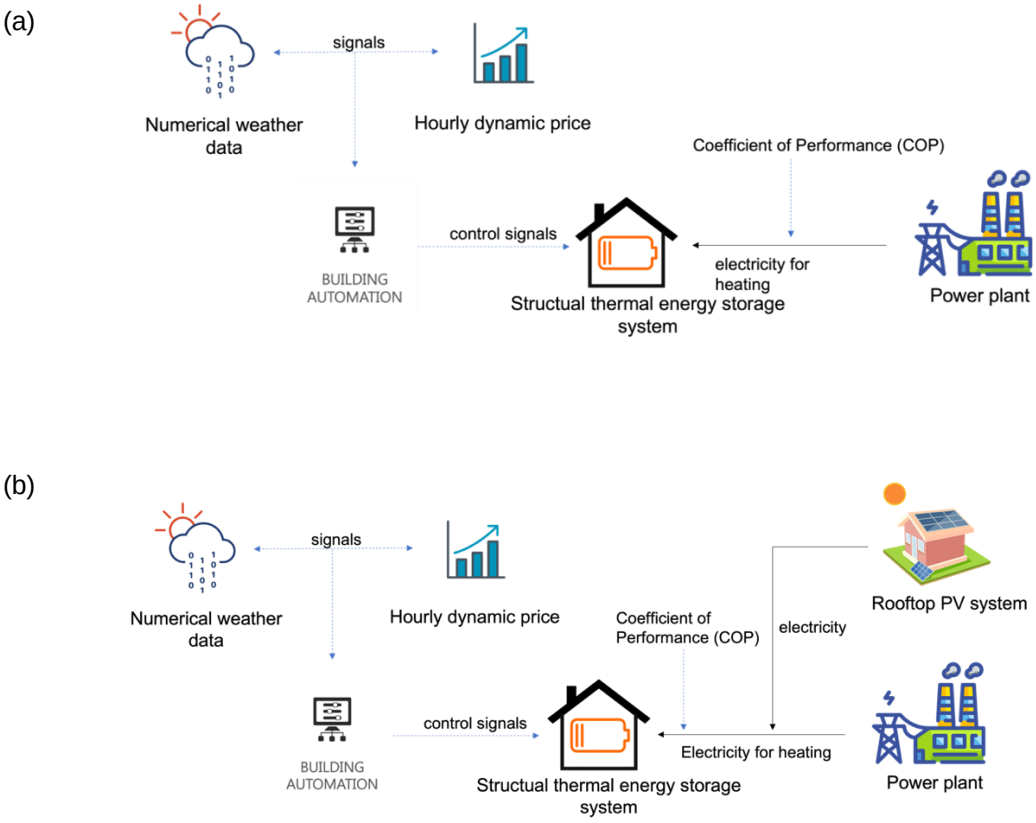

Fig. 4-1 STES with (a) energy fully charging from the grid (b) electrical energy partly charging from the rooftop PV panel

This chapter will introduce the R-C model for simulating room dynamics for indoor temperature prediction. Then, the MPC objective equations for maximising low-price energy usage and rooftop PV energy usage, along with Kalman filter for MPC functions, are discussed. Control strategy based on the energy supply.

4.1 Model predictive control scheme for maximising heating energy storage

The MPC strategy carries out future control based on constraints and system dynamics for a minimal cost [17]. The heating system was controlled by MPC based on pre-set temperature constraints and shift the energy use to low price periods. The formulation of MPC is:

eq 4-1

$$min \sum_{k=0}^{N-1} (u_k, y_k)$$

k means the current time step. N means the prediction horizon. u and y stand for manipulating variables and system states. The solver compared different trajectories. Then, it chooses one with minimal cost in the prediction horizon. Besides, MPC strategy can include the Kalman filter [118], which corrects the predicted system states with real-time measured system states to increase the prediction accuracy. As a result, a more reliable control trajectory is solved by MPC. Two optimisation problems were formed to investigate the effect of the envelope on STES performance. The optimisation aims to maximise the solar energy and low-price energy usage for heavyweight, mediumweight and lightweight thermal masses.

4.2 Dynamic model of the simulated room with a low-temperature floor heating system

In this model, it is assumed that there is no internal masses, such as internal walls and internal wall, partitions and furniture. The room RC model includes the heat loss and heat transfer from node to node (Fig 4-2a) [17].

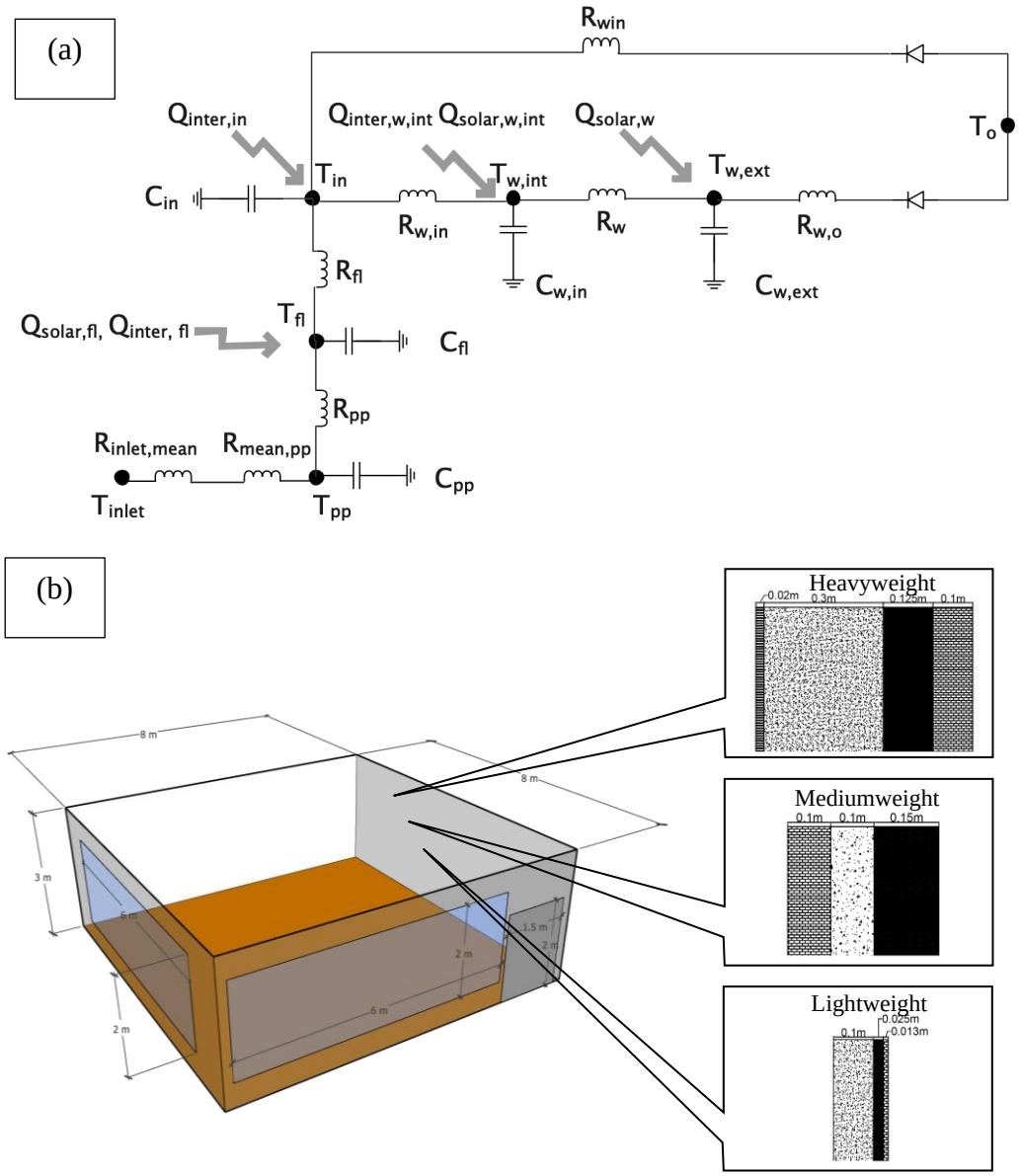

Fig. 4-2 (a) Room resistance-capacitance model (b) 3D model of the simulated room with dimensions in meters

Each temperature node represents a state for heat transfer. Three nodes were used for walls, including the external wall ($T_{w,ext}$), internal wall ($T_{w,int}$) and floor element (T_{fl}). One node for indoor air (T_{in}) and one node for floor heating system temperature (T_{pp}). The heating sources are solar radiation Q_{solar} to all inside surfaces and heating energy $Q_{heating}$ to the pipeline. The continuous-time heat transfer equations of different temperature nodes are:

$$\frac{dT_{w,ext}}{dt} = \frac{T_o - T_{w,ext}}{R_{w,o}C_w} + \frac{T_{w,int} - T_{w,ext}}{R_w C_w} + \frac{Q_{solar,w}}{C_w} \quad \text{eq 4-2}$$

$$\frac{dT_{w,int}}{dt} = \frac{T_{w,ext} - T_{w,int}}{R_w C_w} + \frac{T_{in} - T_{w,int}}{R_{w,in} C_w} + \frac{Q_{inter,w,int}}{C_w} + \frac{Q_{solar,w,int}}{C_w} \quad \text{eq 4-3}$$

$$\frac{dT_{in}}{dt} = \frac{T_{w,int} - T_{in}}{R_{w,in} C_{in}} + \frac{T_o - T_{in}}{R_{win} C_{in}} + \frac{T_{fl} - T_{in}}{R_{fl,in} C_{in}} + \frac{Q_{inter,in}}{C_{in}} \quad \text{eq 4-4}$$

$$\frac{dT_{fl}}{dt} = \frac{T_{in} - T_{fl}}{R_{fl,in} C_{fl}} + \frac{T_{pp} - T_{fl}}{R_{pp,fl} C_{fl}} + \frac{Q_{solar,fl}}{C_{fl}} + \frac{Q_{inter,fl}}{C_{fl}} \quad \text{eq 4-5}$$

$$\frac{dT_{pp}}{dt} = \frac{T_{fl} - T_{pp}}{R_{pp,fl} C_{pp}} + \frac{Q_{heating}}{C_{pp}} \quad \text{eq 4-6}$$

$$Q_{heating} = \frac{T_{inlet} - T_{pp}}{R_{inlet,mean} + R_{mean,pp}} \quad \text{eq 4-7}$$

$$\frac{dT_{pp}}{dt} = \frac{T_{fl} - T_{pp}}{R_{pp,fl} C_{pp}} + \frac{T_{inlet} - T_{pp}}{(R_{inlet,mean} + R_{mean,pp}) C_{pp}} \quad \text{eq 4-8}$$

The indoor temperature and pipe temperature can then be calculated from a state-space representation:

$$\frac{dx(t)}{dt} = Ax(t) + Bu(t) \quad \text{eq 4-9}$$

$$y(t) = Cx(t) \quad \text{eq 4-10}$$

The state vector x is:

$$[T_{w,ext} \quad T_{w,int} \quad T_{in} \quad T_{fl} \quad T_{pp}]^T$$

The output vector y is:

$$\begin{bmatrix} T_{in} \\ T_{pp} \end{bmatrix}$$

And input vector u

$$[T_o \quad I_{solar} \quad Q_{inter} \quad T_{inlet}]^T$$

With system matrices $A\ B\ C$ are:

A

$$\begin{pmatrix} \frac{-1}{R_{w,o}C_w} + \frac{-1}{R_w C_w} & \frac{1}{R_w C_w} & 0 & 0 & 0 \\ \frac{1}{R_w C_w} & \frac{-1}{R_w C_w} + \frac{-1}{R_{w,in} C_w} & \frac{1}{R_{w,in} C_w} & 0 & 0 \\ 0 & \frac{1}{R_{w,in} C_{in}} & \frac{-1}{R_{w,in} C_{in}} + \frac{-1}{R_{win} C_{in}} + \frac{-1}{R_{fl,in} C_{in}} & \frac{1}{R_{fl,in} C_{in}} & 0 \\ 0 & 0 & \frac{1}{R_{fl,in} C_{fl}} & \frac{-1}{R_{fl,in} C_{fl}} + \frac{-1}{R_{pp,fl} C_{fl}} & \frac{1}{R_{pp,fl} C_{fl}} \\ 0 & 0 & 0 & \frac{1}{R_{pp,fl} C_{pp}} & \frac{-1}{R_{pp,fl} C_{pp}} + \frac{-1}{(R_{inlet,mean} + R_{mean,pp}) C_{pp}} \end{pmatrix}$$

B

$$\begin{pmatrix} \frac{1}{R_{w,o}C_w} & \frac{\int_{solar,w} \times A_w}{C_w} & 0 & 0 \\ 0 & \frac{\int_{solar,int,w} \times A_{win}}{C_w} & \frac{\int_{inter,w,int}}{C_w} & 0 \\ \frac{1}{R_{win}C_{in}} & 0 & \frac{\int_{inter,in}}{C_{in}} & 0 \\ 0 & \frac{\int_{solar,fl} \times A_{win}}{C_{fl}} & \frac{\int_{inter,fl1}}{C_{fl}} & 0 \\ 0 & 0 & 0 & \frac{1}{(R_{inlet,mean} + R_{mean,pp})C_{pp}} \end{pmatrix}$$

C

$$\begin{bmatrix} 0 & 0 & 1 & 0 & 0 \\ 0 & 0 & 0 & 0 & 1 \end{bmatrix}$$

The system matrices A and B were identified by *ssest* function [3] in MATLAB [118] with known input and output data.

4.3 Dynamic price model

The continuous-time state space model ((9)(10)) was turned into the discrete-time model ((12)(13)) with input vector u is T_{inlet} and disturbance vector d is $[T_o \quad I_{solar}]^T$. Then, predicted indoor temperature by state-space model was used in the MPC strategy to trace the future temperature constraints. By introducing the dynamic price [17], which encourages energy usage during off-peak times, a cost function is formed to evaluate the energy shifting ability of envelopes with different thermal mass.

$$J = min \sum_{k=0}^{N-1} q \times (\frac{u_{heating(k)} \times price \times \Delta t}{COP})^2 + r \times {e_k}^2 \quad \text{eq 4-11}$$

Subject to

$$x_{k+1} = A_d x_k + B_d u_k + E_d d_k \quad \text{eq 4-12}$$

$$y_k = C_d x_k \quad \text{eq 4-13}$$

$$T_{\min(k)} - e_k \leq y_k \leq T_{\min(k)} + e_k \quad \text{eq 4-14}$$

$$e_k \geq 0 \quad \text{eq 4-15}$$

$$u_{heating(k)} = \frac{u_k - T_{pp(k)}}{R_{inlet,mean} + R_{mean,pp}} \quad \text{eq 4-16}$$

$$u_k = T_{pp(k)}\big(in\ this\ case, u_{heating(k)} = 0\ (off)\big)\ or\ u_k = T_{inlet}(heating\ is\ on) \quad \text{eq 4-17}$$

q and r are the weights in the cost function. r is set for a larger value to give priority to limit the indoor temperature going beyond the temperature constraints [77]. COP is the coefficient of performance, which is used to identify the amount of thermal energy produced from electrical energy. COP is set to a constant [11] (i.e., 3). N is the prediction horizon, set to 12 h with 30 minutes for each time step.

4.4 Solar electrical energy usage model

To investigate the increased energy flexibility offered by envelopes with the help of rooftop PV panel, a rooftop solar electrical energy usage model was simulated. In this case, solar electrical energy would be generated by photovoltaic (PV) panels during the daylight period. Then, the available electrical energy ($surplus\_energy(k)$) assumes to be the primary energy supply source of the simulated room. The cost function for maximising rooftop solar electrical energy usage is:

$$J = min \sum_{k=0}^{N-1} q \times ((\frac{u_{heating(k)}}{COP} - surplus\_energy(k)) \times price \times \Delta t)^2 + r \times {e_k}^2 \quad \text{eq 4-18}$$

Subject to

$$x_{k+1} = A_d x_k + B_d u_k + E_d d_k \quad \text{eq 4-19}$$

$$y_k = C_d x_k \quad \text{eq 4-20}$$

$$T_{\min(k)} - e_k \le y_k \le T_{\min(k)} + e_k \quad \text{eq 4-21}$$

$$e_k \ge 0 \quad \text{eq 4-22}$$

$$u_{heating(k)} = \frac{u_k - T_{pp(k)}}{R_{inlet,mean} + R_{mean,pp}} \quad \text{eq 4-23}$$

$$u_k = T_{pp(k)}\big(in\ this\ case, u_{heating(k)} = 0\ (off)\big)\ or\ u_k = T_{inlet}(heating\ is\ on) \quad \text{eq 4-24}$$

4.5 Building energy simulation (BES) model

4.5.1 Case study building model

The building room model is shown in Fig 4-2b. It is a simple room model with the dimension of $8 \times 8 \times 3$ m3. An underfloor heating system was used for maintaining indoor thermal comfort [17]. There are two windows, one located on the south wall and another window located on the east wall. The window-to-wall ratio is 0.5 [11]. The convective heat transfer coefficient between wall internal surface and indoor air is 11W/ (m2 ◦C), air infiltration parameter is 0.26 h^{-1} according to the similar types of case study building in Lu et al [146]. The time constant of the building thermal masses are 6.74hrs for lightweight thermal mass, 14.80hrs for mediumweight thermal mass and 18.15hrs for heavyweight thermal mass. These values are obtained based on the building's internal heat capacity and overall heat transmittance, according to the method by Xue et al. [11]. The total building surface area involved in the heat exchange process is 200 m^2. The energy shifting ability of the STES is determined by the amount of energy charge/discharge through the heat transfer between the indoor air and building construction.

The building is located in London, UK, which typically requires heating from October to May. London has high heating demand, with around 5750 heating degree hours (HDH) in December for its climate zones [129], which is larger than the mean yearly HDH of Sydney [130] and similar to the cities in cold climate zones in China [131] and Athens, Greece [132]. UK household accounts for up to 40% of UK greenhouse gas emissions [133], and the heating energy demand is responsible for a significant portion of this. Hence, using optimal heating control strategies to provide demand flexibility, minimise peak load demands and maximise the production of renewable energy sources could go a long way in reducing the residential sector's emissions. Unlocking the energy shifting potential in the residential sector requires an understanding of the energy storage potentials and constraints by thermal mass in specific typologies. In this study, the selected single-family semi-detached house represents a typical house in the UK and accounts for a quarter of houses in the UK [133]. This dwelling type keeps increasing year by year. To simplify, a zone of a single-family semi-detached house was created (Fig 4-2b) to simulate the effect of the envelope on energy flexibility. Three weights of thermal mass were compared (Fig 4-2b & Table 4-1) [11]. Finally, the energy

shifting of envelopes with different weights was investigated. The control strategy was proposed based on previous MPC strategy [17].

Table 4-1Walls' properties of the building of different weights from inside to outside [11]

Heavy weighted wall	**Medium weighted wall**	**Light weighted wall**
20mm gypsum	100mm brick	100mm dense concrete
300mm dense concrete	100mm low-density concrete	25mm insulation layer
125mm insulation layer	150mm insulation layer	13mm finish layer
100mm brick		
Overall u-value: 0.30 (W/m^2 K)	**Overall u-value:** 0.25 (W/m^2 K)	**Overall u-value:** 1.11 (W/m^2 K)

4.6 Future weather data generation

Future weather data was obtained from Meteonorm [134]. The future weather data was predicted following the RCP 4.5 scenario (Fig 4-3). RCP means Representative Concentration Pathways. RCP 4.5 means the scenario aims at limiting the radiation at 4.5 W/m^2 in the year 2100. The scenario includes the long-term strategy, including limiting the greenhouse gas [135]. Following the scenario, the future weather could be predicted [136]. In this study, RCP 4.5 scenario was used to predict the future climate, including global radiation, ambient temperature and relative humidity, of 2030, 2050 and 2080 by Meteonorm software [134].

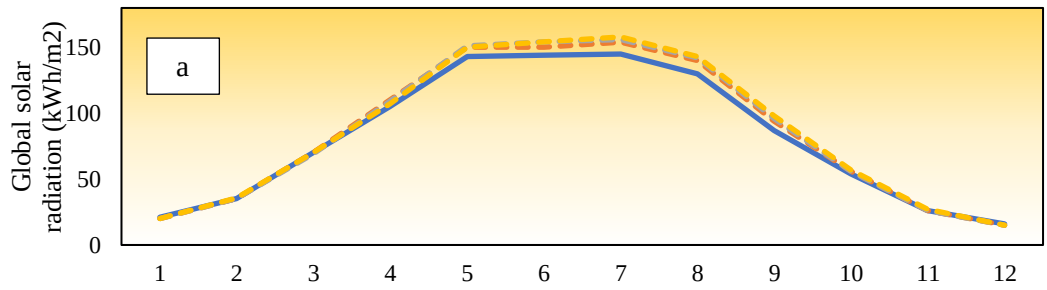

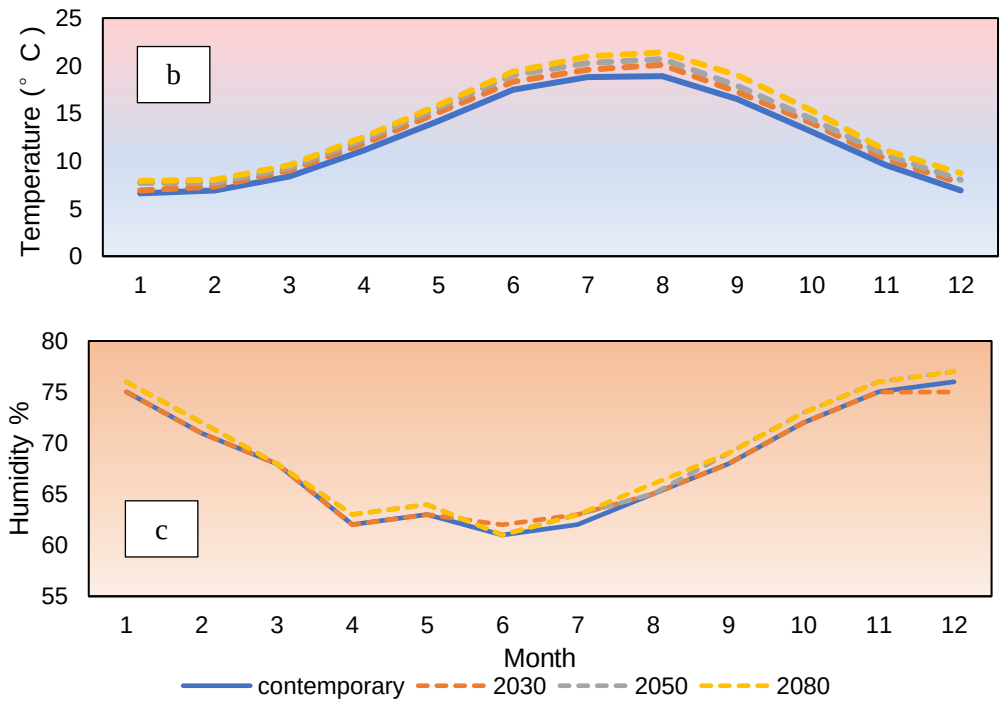

Fig. 4-3 Current and future predicted weather data for London, UK: (a) global radiation, (b) outdoor temperature (c) relative humidity

The simulation was carried out for a typical winter period to compare the performance of the STES with the floor heating system. The average temperatures for simulation periods of contemporary, 2030, 2050 and 2080 are 8.07 °C, 9.01 °C, 9.08 °C and 9.58 °C. The average daily global solar radiation for simulation periods of contemporary, 2030, 2050 and 2080 are 1175.86 W/m^2, 986.43 W/m^2, 1175.29 W/m^2 and 1429.43 W/m^2.

4.6.1 Internal heat gains

Since occupancy contributes to the building energy use and its modelling uncertainty, its impact on the predicted results was evaluated by comparing different configurations of occupancy profiles and occupant-related loads (Fig 4-4). In this case, the setpoint strategies were proposed based on a typical occupancy in a residential building. A working family household occupancy pattern almost accounts for 1/3 of the family population in the UK [137]. The pattern of working family household occupancy usually has a regular daily pattern (members are absent during the day) throughout the week [137]. The internal heat gains include 4 people (working couples with 2 children). The weekly schedule is shown in Fig 4-4, which shows that occupants stay in the house for a weekend and away from the house from 9:00 am to 16:00 pm during weekdays.

The internal heat gains for people were obtained according to CIBSE Guide A [138], including convective (46 W), and radiative (69 W) gains for each occupant. Fluorescent-triphosphor lightings were assumed to be installed with a max 10 W/m^2 power density with 30% radiative gains [138]. Electric equipment was assumed with a max 10 W/m^2 power density with 14% radiative heat dissipation [138]. Weekday lighting and equipment profile was generated according to Dott et al. [139] and Simson et al. [140]. Lights are switched on during the early morning and the periods starting from the time that members come back home from offices and schools (i.e., 16:00) until 22:00 and reach their max usage from 18:00 pm to 22:00 pm. Equipment assumes to reach its minimal capacity when people are off and have a max capacity during early morning and from 18:00 pm to 22:00 pm. For the weekend, the peak times of lights and equipment were assumed to be the same as on weekdays. For the weekend, people assumes to be stay at home for whole day with lightings turned on from morning to night. (decreased to a usual value for the remaining periods). proposed weekly internal heat gains (Fig 4-4b-c) was used for simulation. Then, a constant internal heat gain was used for comparison. There are fixed lighting, people and equipment values based on a fixed weekly schedule (Fig 4-4a). The total internal heat gains were equal to the proposed realistic internal heat gains for the whole simulation period. Thus, the fixed internal heat gain model applied a fixed setpoint strategy (low bound 22℃ and high bound is 25℃) was applied for the fixed internal heat gain model.

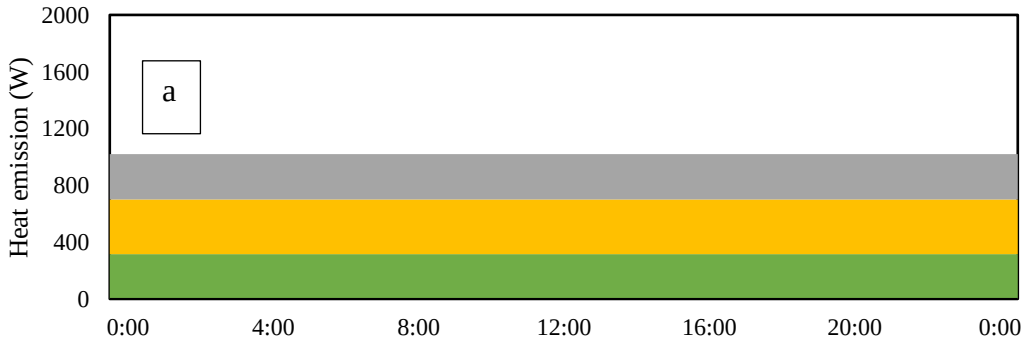

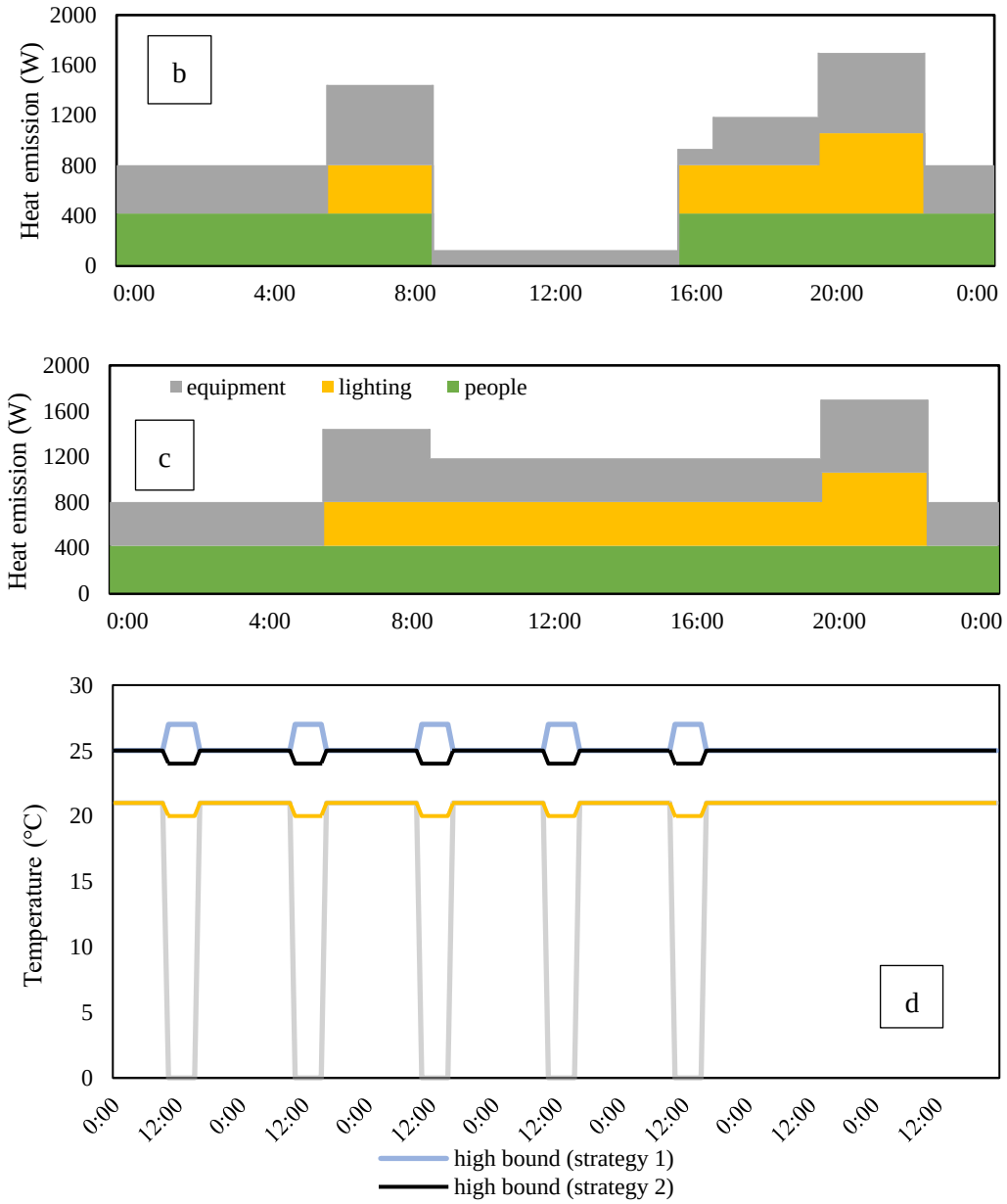

Fig. 4-4 Constant internal heat gains profiles (a) typical daily UK residential building internal heat gains profiles during (b) weekdays (c) weekends [139] and (d) Week schedule floor heating setpoint

Relatively, a higher setpoint (2℃ higher) [64] of the upper bound of floor heating system for preheating [8] of thermal mass and benefits of low-price energy for storage (strategy 1). The results of storage of strategy 1 would be compared with a normal setpoint strategy (strategy 2) that lower (1℃ lower) bounds for unoccupied periods [11] (Fig 4-4d).

4.6.2 UFH inlet temperatures

Underfloor heating systems typically require lower energy to run than other conventional space heating systems, e.g., radiator heating and warm-air heating

[141]. UFH requires low temperature heat source, while traditional convection heating needs to raise the water temperature to higher levels [142]. UFH systems have been evaluated by an experimental study [143] on assisting solar energy integration for energy-saving (up to 30.55%) compared with the conventional central heating system because of the benefit of a low-temperature heat source for UFH [142]. In this chapter, the performance of different thermal masses was compared on STES integrated with a low-temperature heating system. This chapter will evaluate the STES performances under different UFH inlet temperatures. UFH inlet temperature was set between 35-55℃ for utilisation of low-temperature energy sources [17].

4.6.3 Electricity prices

The UK electricity spot price from the "Nord Pool" [144] from November 23 Monday to 7 Dec 2021was applied (Fig 4-5). The electricity spot price is a good indicator of the demand shifting towards a higher supply efficiency because the dynamic price considers renewable energy sources (RES) availability and the energy demand [11]. The limits for the prices were: *price ≤ 16.7 GBP pence/kWh)* for low price (appears 20% time of simulation time), *16.7 GBP pence/kWh < price ≤ 25 GBP pence/kWh* for medium price (appears 65% time of simulation time), *price > 25 GBP pence/kWh* for high price (appears 15% time of simulation time).

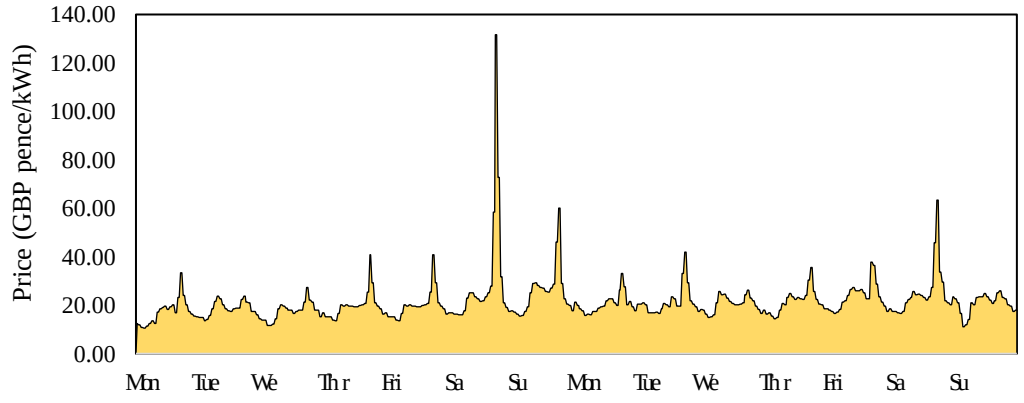

Fig. 4-5 Daily dynamic price from November 23 [68]

4.6.4 Electrical energy generation from a rooftop PV system

To further evaluate the energy shifting ability and impact on the energy cost of the STES integrated with RES, PV system was installed on the roof of the building model. The rooftop PV was set based on the utilisation factor (UF), which is the ratio of PV area to total roof area [20]. UF indicates the availability of the PV area

and is estimated based on the rooftop characteristics. In this study, a UF for the rooftop PV installation was assumed by proper design of the roof's hurdles, e.g., staircase, water tanks and open-air sitting space. The UF was chosen to represent a high value (i.e., 0.45) for a residential building [75]. The PV panel was simulated in TRNSYS (Fig 4-6) using Type 103 (photovoltaic). The PV panel is modeled based on a monocrystalline solar panel. The array is assumed to be connected to the load side through a maximum power point tracker (MPPT). Thus, the power output from the PV panel to building is maximised under nonlinear electrical characteristics of PV panel [145]. This model type in TRNSYS calculates the power output based on the current-voltage characteristics of the model, based on the incident solar radiation and temperature at the reference open-circuit condition. The parameters settings of the PV panel are detailed in Table 4-2.

Table 4-2 Parameter settings of the PV panel in TRNSYS [121]

Component	Type	Descriptions	Value
Solar collector	103	Module short-circuit current	6.5 A
		Module open-circuit voltage	21.6 V
		Reference temperature	25 ℃
		Reference insolation	1000 W/m^2
		Module voltage at max power point	17 V
		Module current at max power point	5.9 A
		Temperature coefficient of short-circuit current	0.02 A/K
		Temperature coefficient of open-circuit voltage	-0.079 V/K
		Module temperature at nominal operating cell temperature (NOCT)	40 ℃

Coupling electricity and heat sector is one of the most applicable solutions for building energy shifting through the equipment such as heat pump, electric heater [92]. The STES is using as PV electrical energy storage. The energy flexibility of STES is activated for shifting the heating energy usage to times of PV-generation

by the objective for maximum onsite PV-electrical utilisation. Then, the excess solar power provides part of space heating needs in the simulation period.

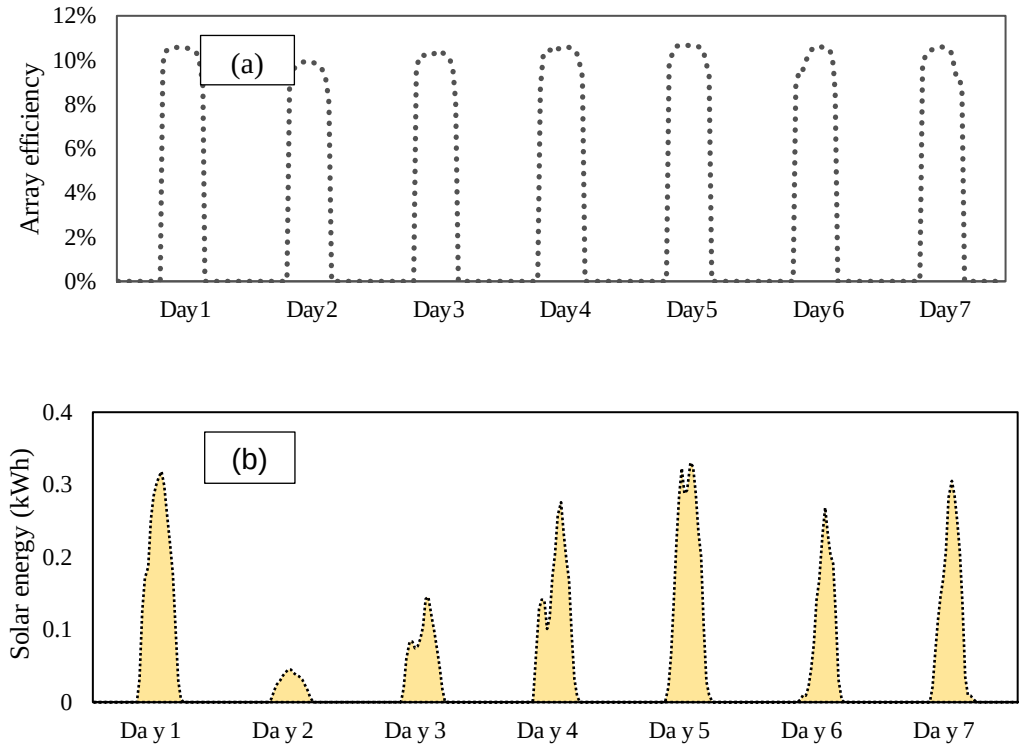

Fig. 4-6 (a) Array efficiency of the PV panel (b) generated solar electrical energy for the selected week by the rooftop PV system.

4.7 BES and MPC model validation, state space model verification

Three stages of model validation and verification were carried out. The building energy simulation (BES) model developed in TRNSYS was initially validated with the work of Lu et al. [146]. After inputting the collected weather data (ambient temperature, outdoor relative humidity, solar radiation on horizontal, etc.) and building construction materials (layer by layer), the simulated temperature had a similar patter and response as the measured temperatures for six continuous days (Fig 4-7a). Ref [23] suggests that the primary indicators for determining the thermal characteristics of a building construction are the daily indoor temperature range and its change trend. Validation of TRNSYS simulation for construction elements can be achieved through a comparison with 4 to 7 days of measurement data [23, 146]. The alignment of simulated results with experimental findings over the same time frame suggests that the building model implemented in TRNSYS is reasonably accurate and reliable. Overall, the minimum percentage of difference is 0%, the

maximum percentage of difference is 11.06% with the minimum predictive temperature error is 0℃, and the maximum predictive temperature error of 1.18 ℃. The validation indicated the reliability of the TRNSYS model. Then, the material was changed to the proposed heavyweight, mediumweight and lightweight thermal masses for the simulation and extended the room volume for a more stable indoor temperature and larger heating capacity of the underfloor heating system.

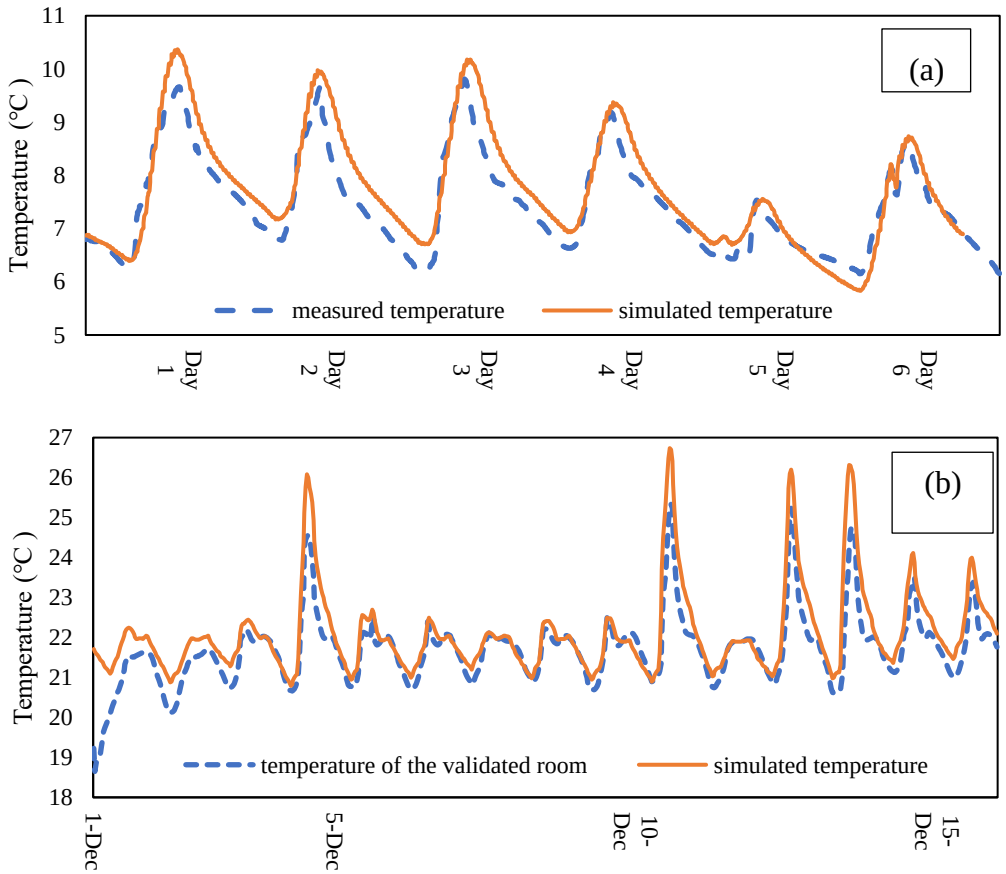

Fig. 4-7 (a) Validated indoor temperature with Lu et al. [140], (b) Validated indoor temperature with Hu et al. [17].

Furthermore, the proposed MPC strategy with the work of Hu et al. [17] was validated by simulating a similar building model incorporating an MPC method. The indoor temperature in the simulated room has been compared with the indoor temperature of the validated room model under the same conditions (Fig 4-7b). The minimum percentage of difference is 0%, The maximum percentage of difference is 13.47% with minimum predictive temperature error is 0 ℃ and maximum predictive temperature error of 2.55 ℃, which indicates accurate modelling of the MPC method and heat storage of the thermal mass. As can be seen, the indoor temperature controlled by MPC contributed to a much stable indoor environment

(in terms of the air temperature) when compared with an on/off control (Fig 4-8a). Furthermore, with some energy compensation, MPC shows its good performance on energy shifting from peak times to off-peak times by STES. Overall, MPC shifted around half of the energy (48.34%) to off-peak times when the on/off controller uses 100% peak-time energy (Fig 4-8b), which was consistent with the findings of Hu et al. with an error of 4.17% [17].

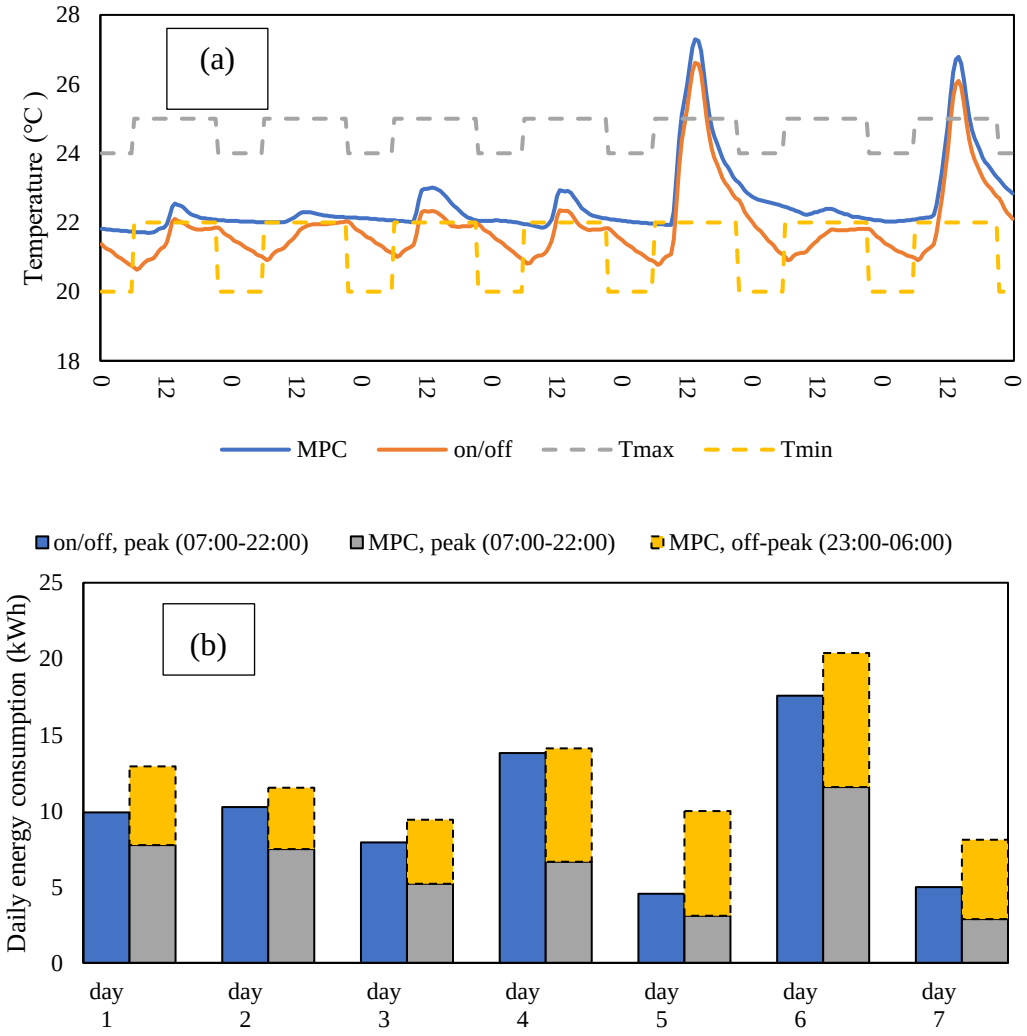

Fig. 4-8 (a) Indoor temperature controlled by different control strategies, (b) energy consumption by electricity price.

The room temperature and pipe temperature were outputted from TRNSYS. 500 data points of both room and pipe temperature were used to train the state space model. Another 500 data points were generated for verification. The identification and verification results are shown in Table 4-3.

Table 4-3 Fit percentage of identification and verification

	Parameters	Heavy weighted house	Medium weighted house	Light weighted house
Identification	T_{in}	75.8 fit%	83.3 fit%	84.3 fit%
	T_{pp}	93.1 fit%	81.2 fit%	90.6 fit%
Verification	T_{in}	75.6 fit%	77.5 fit%	81.8 fit%
	T_{pp}	88.8 fit%	78.3 fit%	89.8 fit%

Fit %: the percentage of the model outputting temperatures matching the experimental outputting temperatures [119]

$$best\ fit = (1 - \frac{|y - \hat{y}|}{|y - \bar{y}|}) \times 100 \quad \text{eq 4-25}$$

There is a large number of data points for model identification and validation. The identification accuracy was close to the validation accuracy with high Fit% (Table 4-3), which indicated that this numerical model could reproduce the simulated temperatures with known inputs.

4.8 Results and Discussion

This section presents the heating energy storage performance by building thermal mass under different configurations. The aspects, including different thermal masses, setpoint strategies, occupancy profile and floor heating inlet temperatures, were investigated towards a higher energy shifting performance and low-price energy usage. Finally, a chosen configuration was simulated under future climate conditions and a rooftop PV system provided insights for developing future STES systems integrated with RES.

In the initial stage, three thermal masses are compared to identify a more energy-efficient option for a specific type of thermal mass. This particular thermal mass

plays a crucial role in establishing an improved setpoint strategy. Subsequently a case study utilised the well-suited thermal mass and setpoint strategy is conducted, to determine the optimal inlet temperature for the Underfloor Heating (UFH) system and corresponding occupancy pattern. Finally, the identified optimal configuration, which offers the highest energy flexibility, is employed to evaluate the performance of Seasonal Thermal Energy Storage (STES) under Model Predictive Control (MPC), considering future climate conditions and the installation of a rooftop PV system.

4.8.1 Comparison between different thermal masses

Firstly, the floor heating energy storage performances are investigated of different thermal masses. For comparison, the results for a typical winter period (23rd November – 2nd December) were evaluated. The daily setpoint strategy, i.e., (21 ℃ - 25 ℃) for daytime (20 ℃ - 24 ℃) for night-time, are same for simulated periods [17]. The initial inlet temperature of the floor heating system was set to 50 ℃.

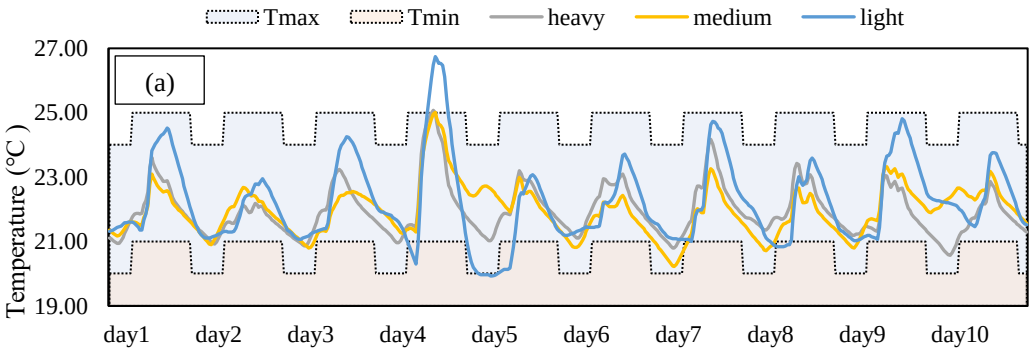

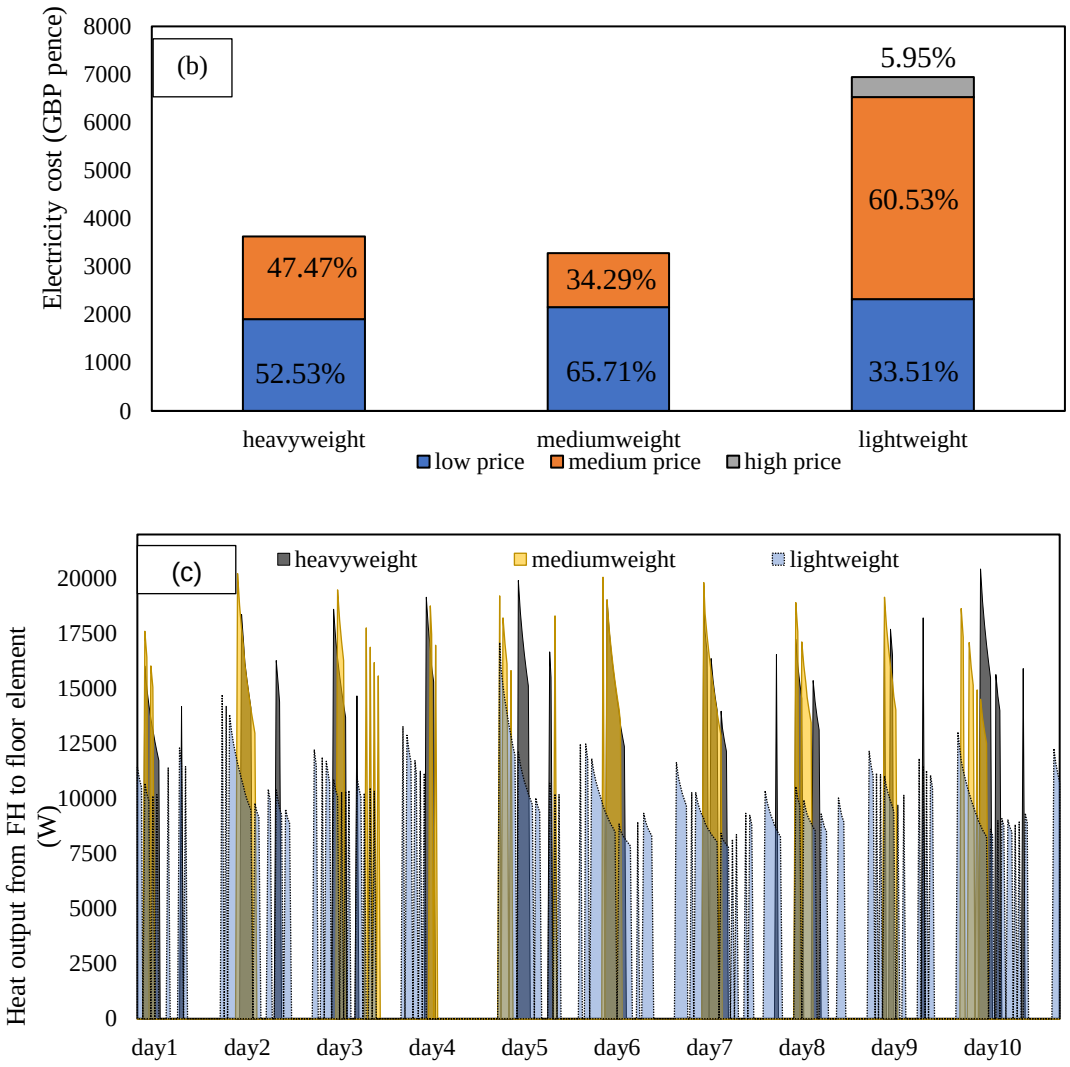

Fig. 4-9 (a) Indoor temperatures controlled by MPC control strategy, (b) energy consumption of three thermal masses, (c) heat charged from the UFH system to the floor element, and (d) energy consumption.

Fig 4-9a shows that the indoor temperature trajectory meets the indoor constraints under the MPC control strategy. The percentage of time the indoor temperature going beyond the temperature bounds was 0.32% for the heavyweight building, 0.48% for the mediumweight and 0.48% for the lightweight building, which had a higher comfort violation as compared with mediumweight and heavyweight buildings. The findings are as expected and reasonable because the low insulation of the building tends to result in a higher indoor temperature variation because of the low thermal capacitance of the thermal mass [67, 69].

In terms of how this affects the energy cost (Fig 4-9b), the average electricity price used by a heavyweight building was 16.75 GBP pence/kWh, 16.15 GBP

pence/kWh for mediumweight and 18.5 GBP pence/kWh for lightweight. It should be noted that the average dynamic price is for the specific simulation period. Under the proposed MPC control strategy, the average electricity price used by the mediumweight building was lower than the current electricity price standing for 87% periods, and they were 65% and 81% for the lightweight and heavyweight buildings. The average consumed electricity price of heavyweight and mediumweight buildings were lower than that of lightweight building. Besides, the mediumweight building had a lower average electricity price than the heavyweight building. As a result, the mediumweight building consumed more low-price energy than the heavyweight and lightweight buildings (Fig 4-9c).

Furthermore, the mediumweight building also had the shortest average daily charging time (heavyweight: 4.15 hrs; mediumweight: 3.75 hrs; lightweight: 11.75 hrs) among the three buildings with different thermal masses. Looking at the amount of energy charge (Fig 4-9), the mediumweight has the highest average heat charge based on the simulated periods (heavyweight: 15.67 kW; mediumweight: 16.26 kW; lightweight: 10.21 kW). Consequently, with similar average heating energy requirements (heavyweight: 126.06 kW daily average; mediumweight: 122.48 kW daily average), mediumweight could shorten the daily heating charging times. The results are consistent with the study of Xue et al.[11]. Their results showed that with the same precooling periods for light, medium, and heavy-weight buildings, medium-weight buildings shifted most of their their energy to off-peak times with the highest storage efficiency. The heavy weighted envelope requires a longer charging time than the medium weighted envelope [147]. Thus, the heavyweight building offers less energy flexibility under stochastic hourly dynamic price than the mediumweight building, which has relatively big thermal capacitance and medium time constant [148].

4.8.2 Comparison of the impact of setpoints, UFH inlet temperatures and occupancy patterns.

For comparison, the simulation results of the typical winter weeks of the mediumweight building were used for the analysis. The comfort violations for the two strategies were 0.56% for strategy 1 and 2.44% for strategy 2 during occupied periods (Fig 4-10a). Strategy 1 had a more satisfactory indoor temperature trajectory in line with the setpoints. Low-price energy usage strategy 1 had a 3% increase (from 41.64% to 44.96%) compared to strategy 2, while the total electricity

cost for the two strategies is similar (around 5450 GBP pence for two weeks). Thus, under the MPC control strategy, the strategy with a higher tolerance of indoor temperature during unoccupied periods used a higher proportion of low-price energy based on similar total electricity cost.

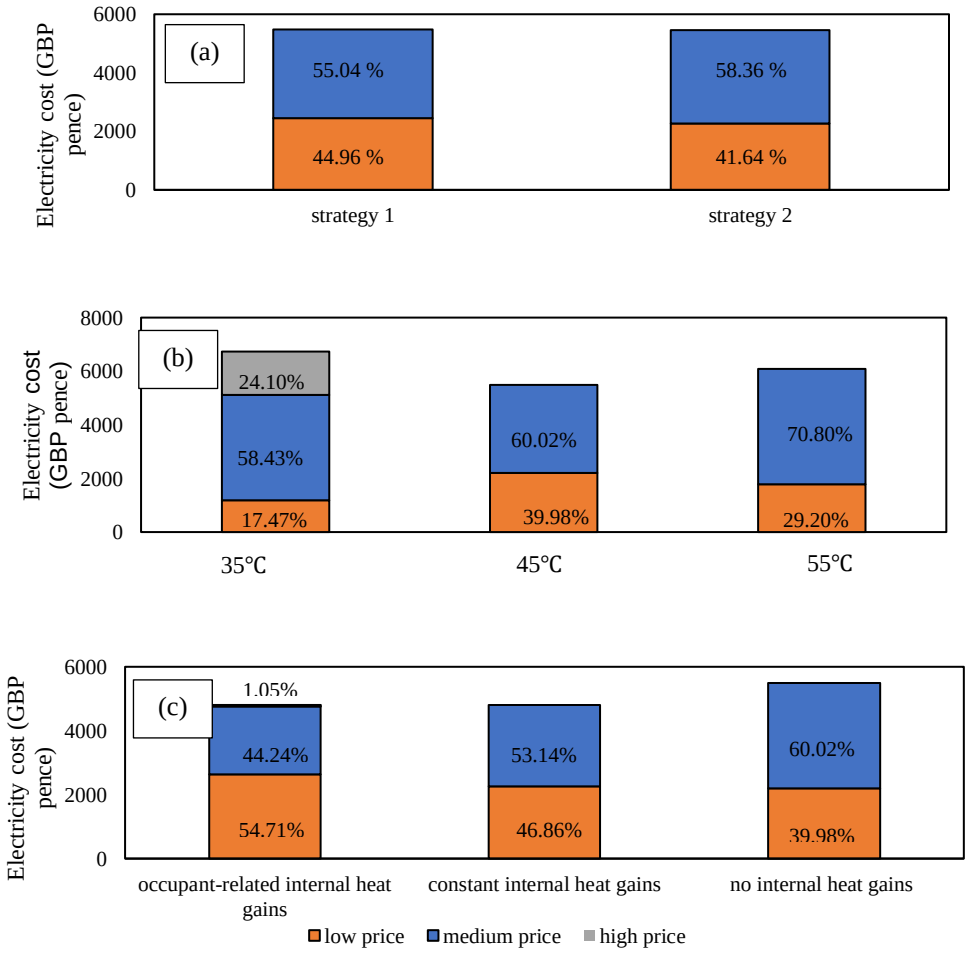

Fig. 4-10 (a) Electricity price usage of setpoint strategy 1 and strategy, (b) electricity price usage of different UFH inlet temperatures, (c) electricity usage by price for the room with realistic, constant and no internal heat gains

Then the impact of the floor heating system's operation on the energy shifting performance was evaluated. Inlet temperatures were set to 35℃, 45℃ and 55℃. For this evaluation, the energy shifting ability of mediumweight thermal mass under different UFH inlet temperatures were compared (Fig 4-10b). This will assess the performance of STES with dynamic pricing based MPC, under different UFH inlet temperatures. Low price energy usage, and thermal mass under 45℃ (39.98%) UFH inlet temperature outperformed 35℃ (17.47%) and 55℃ (29.20%). This showed

that the low UFH inlet temperature (e.g., 35℃) offered less energy flexibility for high price energy shifting because the heating system was required to turn on frequently (average 23.5 hours daily with 13.84% comfort violation) based on relatively low heat flux. 45℃ UFH inlet temperature could satisfy the indoor comfort requirement with 0.15% comfort violation and an average 6.5 hrs daily turn-on time that offers more energy flexibility than a larger heat flux (i.e., 55℃), which allows a shorter average daily charging time (i.e., 4.0 hrs).

For the evaluation of the impact of occupancy patterns on the STES performance, an UFH inlet temperature of 45℃ was set for its high energy shifting ability. As mentioned in the previous section, typical residential building occupancy heat gains profiles were simulated to assess its contribution to the energy flexibility offered by STES. The results were also compared with constant internal heat gains and no internal heat gains in order to assess its importance when evaluating such systems. Simulations were taken for a mediumweight building set with the three configurations. The comfort violation was 0.6% for building with realistic occupant-related internal heat gains, 0.74% for building with constant internal heat gains and 0.15% for building without internal heat gains. The average price used by the building with realistic internal heat gains was 16.3 GBP pence/kWh. They were 16.5 and 16.8 GBP pence/kWh for the buildings with constant internal heat gains and no internal heat gains. Fig 4-10c shows that when the building applies the occupant-related setpoint strategy of the heating system, the low-price usage ability outperformed the building with constant internal heat gains and constant setpoint strategy based on a similar total electricity cost. Besides, A lower electricity price used by the building with internal heat gains indicates that the internal heat gains charged the thermal mass and contributed to the energy flexibility offered by the proposed STES system. The result showed that a building with internal heat gains was responsible for 10% of the heating energy consumption and 690 GBP pence for the simulated period. The result confirms that the internal heat gains could save electricity costs under MPC strategy with no comfort violations. Internal heat gains' contribution to heating energy saving was also confirmed by study [39,40]. While the impact of occupancy on the residential case study was not significant, it should be further evaluated for buildings or spaces with higher occupancy and internal heat gains.

4.8.3 Effect of future climate conditions on STES performance

This section aims to evaluate how the changing climate conditions in the future would affect the storage performance of STES. Four simulations were carried out to compare the storage performances during contemporary, 2030, 2050 and 2080 periods. The result (Fig 4-11) provides insight into the influence of climate change on STES performance by comparing the energy shifting ability of contemporary and future years. The mediumweight building was chosen for the simulation of the residential building under different climate conditions. Simulation results during the typical winter week periods (23rd November – 7th December) were compared and the realistic weekly internal heat gains' profile was applied. UFH inlet temperature was set to 45℃ for a high energy shifting performance.

The proposed MPC controller controlled the indoor temperatures well in the temperature bounds with comfort violations for contemporary, 2030, 2050 and 2080 were at 0.60%, 0.00%, 0.00% and 0.45%. The total energy usage for contemporary, 2030, 2050 and 2080 were 281 kWh, 279 kWh, 263 kWh and 243 kWh. The results of energy demand based on price usage intervals are shown in Fig 4-11which highlights that the predicted future weather conditions would lead to heating energy reduction and an increased in low-price energy usage because of the increased ambient temperature based on similar average daily solar radiation. Future energy storage system calls for the introduction of integrated storage technologies because of the increased application of RES in the supply system [151]. Thus, an increased STES performance for heating periods under climate change would be one of the main considerations in the integration of energy storage system. While the heating energy results are as expected, the influence of the changing outdoor conditions on the energy shifting and energy use price usage should be evaluated for other types of buildings with different characteristics and operations.

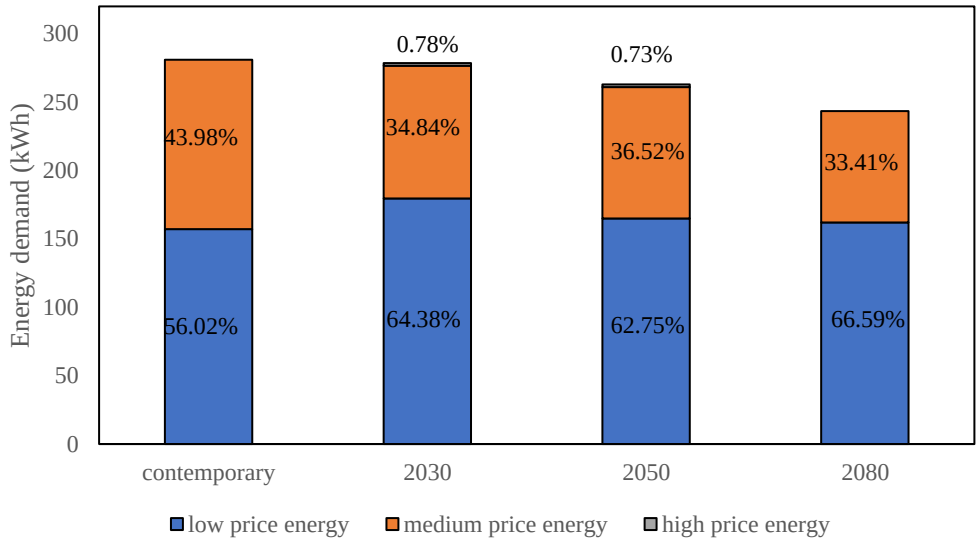

Fig. 4-11 Dynamic price usage by mediumweight building of contemporary and future years for the evaluated period.

This thesis models climate change based on the RCP 4.5 scenario. There are other RCP 2.6 and RCP 8.5 scenarios in general [136]. RCP 2.6 represents a more efficient, low-carbon trajectory for future climate change, resulting in a lower average temperature. Conversely, RCP 8.5 signifies less emphasis on low-carbon pathways in the coming decades, leading to a higher average temperature. In the specific case study building, the anticipated average temperature differences from RCP 2.6 to RCP 4.5 and from RCP 8.5 to RCP 4.5 in future years are -0.9℃ and 1.4 ℃, respectively [134]. As indicated by [71], when the ambient average temperature ranges are smaller than 7℃ within two climate conditions, the energy flexibility of the same building construction varies within 4%. Therefore, it is anticipated that the effective reduction of high-priced energy usage under the MPC control strategy will fluctuate within this 4% range among different climate change scenarios.

4.8.4 Rooftop solar PV system integration with STES and MPC

The mediumweight building was chosen to evaluate the contribution of the rooftop PV system to the energy flexibility offered by STES system. The integrated model simulation results were compared for the typical winter week periods. The impact of the addition of the rooftop PV system on the heating energy flexibility was evaluated. The system was based on an UFH system with 45 ℃ inlet temperature. The result highlights the potential of using rooftop PV panels for

energy conservation in the case of high penetration of RES in the future. The comfort violation was 0.30% for both cases. The average electricity price used by the building without a PV panel.

was 16.5 GBP pence/kWh, it is 16.05 GBP pence/kWh for the building with rooftop PV installed. Simulation results (Fig 4-12) show that the rooftop PV panel could contribute to the increased low-price energy usage under the proposed MPC control strategy. Then, a lower average electricity price.

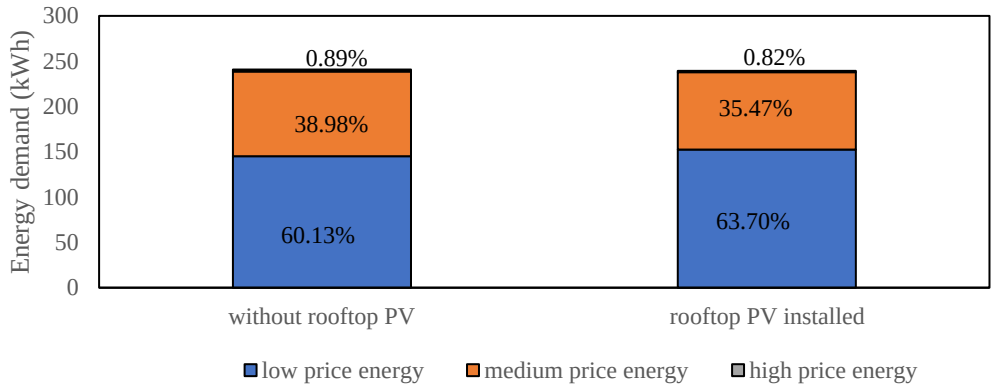

Fig. 4-12 Electricity energy usage by the buildings without PV and with PV installed for the evaluated period.

For two week simulation, a total of 22.79 kWh PV electrical energy was generated by the installed PV panel. 1.34 kWh real-time PV electrical energy could be used for a floor heating system and covers 29.50 GBP pence electricity cost. Because the usage of PV energy was real-time, a wastage of solar energy during heating system turn-off times occurs. Thus, if an active storage system is included, the energy shifting ability could be increased. With a better design of energy storage units, PV penetration in the supply could reach 5% [151]. In this scenario, 11.98 kWh among 239.60 kWh for the two-week heating energy demand of the building with a rooftop PV system installed stands for the PV energy penetration in the residential microgrid [153]. Investment costs of RES have been dropping, and the RES penetration in the supply could lower the spot prices [154]. If the supply price of the PV penetration energy with the average low price 15.00 GBP pence/kWh and the covering energy was average medium price 20.60 GBP pence/kWh previously, the energy cost saving would be 66.30 GBP pence for the simulated period of the building with rooftop PV panel installed.

4.9 Summary

This chapter investigated the impact of building configuration and operation on a low-temperature heating energy storage performance. The configurations explored included the building thermal mass, under-floor heating inlet temperature, heating setpoint strategy, occupancy patterns and internal heat gains. A coupled modelling approach was introduced, which simulated a building with STES and a price responsive model predictive control (MPC). The model was verified/validated against numerical and experimental data, and good agreement was observed between the results. The result confirmed that mediumweight thermal mass and a medium-temperature (45℃) under-floor heating inlet temperature provided a higher energy shifting ability under a price-responsive MPC control strategy.

Besides, the building model, which employed a realistic occupancy profile for a residential building and a high tolerance setpoint strategy during unoccupied periods showed that a higher thermal energy storage performance could be achieved by the building's thermal mass. Finally, the present study further addressed the research gap by evaluating the performance of passive building energy storage technology under future climate conditions (2030, 2050 and 2080). Based on the simulated case study and conditions, the result showed that higher low-price energy usage and lower heating energy usage could be achieved in future climate conditions.

This chapter also evaluated the capability of a building integrated PV system to enhance the performance of passive building energy storage technology. The results confirmed that an increase in the energy shifting ability could be achieved with the addition of the solar PV system. The results also showed the importance of various design parameters and operation conditions when designing such a system.

While the results presented here showed the promising performance of the integrated system, more work is required to fully evaluate the system. The limitations of this model are the simplifications on the building model, internal heat source content and heat transfer process. Firstly, this work simulated a single-zone building model. For those buildings with multiple zones, the heat transfer process of one zone usually takes into consideration of heat transfer between nearby zones see [155]. Besides, RCP 4.5 is a stabilisation scenario that makes assumptions about climate policies based on the introduction of global greenhouse gas emissions prices. The climate change details are modeled with sophisticated land-use and land-cover models. Thus, the limitation of using this climate change scenario would be any

variations that might occur due to different climate policies, land-use, and land-cover models applied

Secondly, the roof area of the simulated room assumes to be flat and equal to the floor area. In reality, the roof will be angled in most detached house. Thus, the design of PV should be title to an angle basing on the slope of the roof. The output PV power and the amount of incident solar radiation in a titled surface would be different from a flat surface due to a different slope of the PV array see [150].

Thirdly, a constant schedule of occupancy profile is assumed in weekday. In reality, the occupancy profiles are mostly stochastic especially for the start periods of occupancy see [84]. The mismatch between stochastic occupancy profile and regular occupancy profile used by MPC strategy might influence a bit of prediction accuracy of the MPC control strategy.

Fourthly, a constant mass flow rate was assumed in the heating pipe always larger than a certain level (i.e., 13 kg/ (h m2)) so that the water temperature change along the downstream direction (z direction) won't be affected by overall thermal transmittance from the heating water to the indoor air. For the case of a lower mass flow rate (less than 13 kg/ (h m2)), the water temperature in the pipe won't change linearly, and exponentially instead [17], which has not been considered in this study. In future works, a more comprehensive model is required to be developed and validated with full scale experimental data. Full integration with the grid should also be explored. While the impact of occupancy on the residential case study was not significant, it should be further evaluated for buildings or spaces with higher occupancy and internal heat gains. The influence of the changing outdoor conditions on energy shifting and energy use price usage should be evaluated for other types of buildings with different characteristics and operations.

5. MPC of solar thermal heating system with thermal energy storage for buildings with highly variable occupancy levels

This chapter aims to address the aforementioned gaps by developing and evaluating a price responsive MPC integrated with a solar thermal heating system, active and passive thermal energy storage (TES) for buildings with high occupancy variability (Fig. 5-1). The coupled system supplies the building heating energy through a low temperature under floor heating system. A case study lecture room in the University building in Nottingham, UK, will be employed for evaluating the feasibility of the proposed heating system controlled by MPC strategy during the heating season. This chapter will develop a dynamic thermal representation of the building through grey-box identification of a state-space model. The developed coupled model will undergo verification and validation process utilising both numerical simulations and experimental data. The developed MPC controller aims to improve the operation of the space heating system, lower the cost and maximise solar energy utilisation.

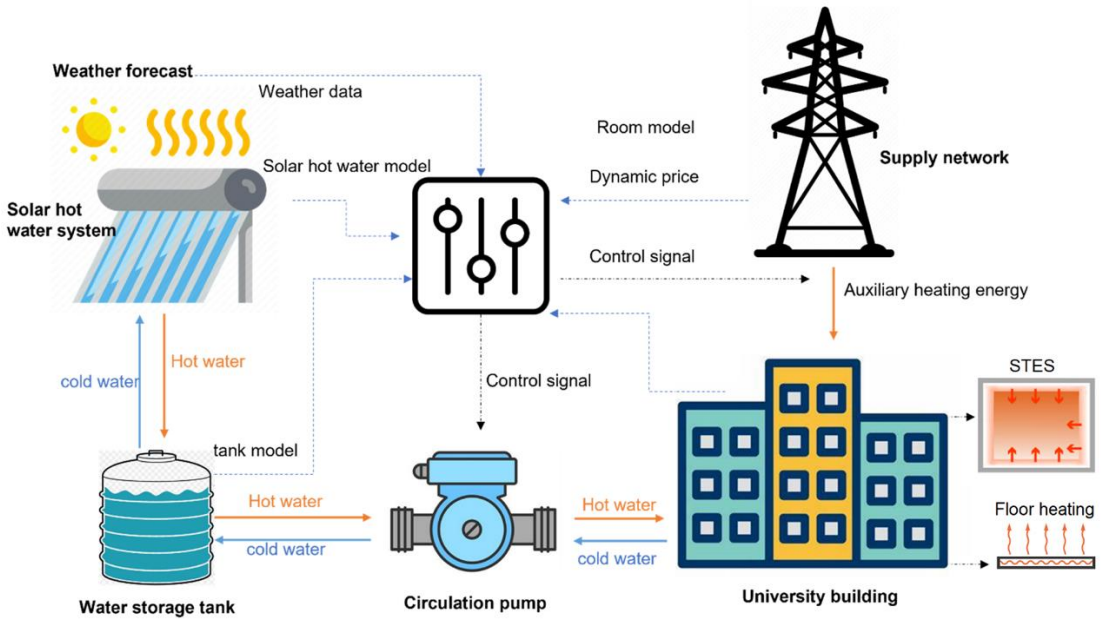

Fig. 5-1 Proposed price responsive model predictive control for a building-integrated solar thermal heating and passive/active storage system for a highly variable occupancy building

5.1 Method

This section outlines the methodology employed to simulate the suggested building-integrated solar energy system using the MPC strategy. Initially, a numerical state-space model is proposed for the room, along with models for the storage tank and solar hot water system. Subsequently, an MPC control strategy is designed based on the state-space models to maximise the utilisation of solar thermal energy. Finally, the simulation platform is introduced to provide real-time indoor temperature feedback and implement the control strategy.

5.1.1 RC representation for the gray-box models

5.1.1.1 Building room model

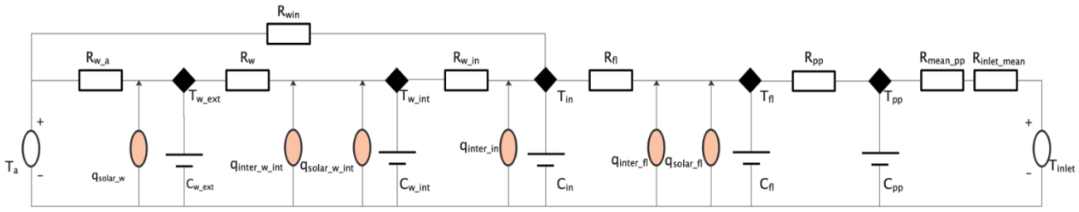

Fig. 5-2 Room R-C model with UFH system and storage tank [17]

The Resistance-Capacitance (RC) room model is a commonly used method for representing indoor heat transfer. This model consists of a network of first-order systems, where the temperature nodes for both the walls and indoor air serve as the system states [77]. To illustrate, consider an example of the RC representation for indoor air:

$$\frac{dT_{in}}{dt} = \frac{T_{w\_int} - T_{in}}{R_{w\_in}C_{in}} + \frac{T_o - T_{in}}{R_{win}C_{in}} + \frac{T_{fl} - T_{in}}{R_{fl\_in}C_{in}} + \frac{Q_{inter\_in}}{C_{in}} \qquad \text{eq 5-1}$$

This chapter employed gray-box identification, a technique that aims to identify system properties by capturing physical connections between states, to identify room model properties using the proposed R-C model (see Fig. 5-2). To estimate the model through machine learning methods using input/output data, a state space model was utilised. This model typically provides a fast approach to identifying a discrete-time model of the continuous-time system [77]. A linear, time-invariant state space model was formulated to predict the temperatures of nodes.

$$x_{k+1} = Ax_k + Bu_k + K\sigma_k \qquad \text{eq 5-2}$$

$$y_k = Dx_k + \sigma_k \qquad \text{eq 5-3}$$

A, B, D and K are the system matrices, which have to be identified. $x_k \epsilon R^5$ are system states include temperatures of the external node of the external wall T_{w_ext}, internal node of external wall T_{w_int}, node of indoor air T_{in}, node of floor T_{fl} and node of floor heating pipe T_{pp}. $u_k \epsilon R^4$ are input variables, including ambient temperature T_a, global solar radiation I_{solar}, internal heat gain q_{inter} and UFH inlet temperature T_{inlet}. $y_k \epsilon R^2$ are the output variables, including indoor temperature T_{in}, pipe temperature T_{pp}. σ_k is an unknown noise, e.g. zero mean Gaussian white noise. In this study, σ_k is assumed to be zero. System identification aims to minimise the error between measured data and output of the simplified RC representation with a limited searching magnitude by giving the initial values of system matrices (based on construction properties). The identification process used a cost function for minimising errors [117]. One example is the MATLAB system identification toolbox [119].

A reasonable original state was assumed for each temperature node. Since not all states are measurable in reality, a Kalman filter was used to estimate unmeasurable states and filter the noises in each cycle. Leveraging a dual-pronged approach, which involves updating measurements and error covariance simultaneously, the Kalman filter has the capacity to estimate the current state at each starting point of the optimisation process [17].

5.1.1.2 Storage tank and solar thermal collector model

A TRNSYS model (Fig 5-3) was developed to simulate a solar thermal system that supplies heat to a domestic floor heating system with a storage tank. The model uses Type 15, which employs a TMY hourly weather file of Nottingham, UK, obtained from Meteonorm [134]. Type 15 is responsible for reading data at regular time intervals from an external weather data file, interpolating the data (including solar radiation for tilted surfaces) at time steps of less than one hour, and making it available to other TRNSYS components. The information on global radiation, solar radiation for the tilted surface of the collector, and ambient temperature are then fed to Type 1, which represents the solar thermal collector. A pump (Type 114) circulates the water of the thermal storage tank (Type 158) to the solar thermal collector to collect the heat from the sun and heat the water in the hot water storage tank. There is another pump that circulates the water in the building UFH system to the storage tank. Type 155 connects TRNSYS to MATLAB. MPC simulated in

MATLAB would give signals for each pump and the amount of auxiliary heating required for the tank at each time step.

On the other side of the storage tank, hot water is supplied to the building's floor heating system (Type 56), and two streams exchange heat in the storage tank. The outlet 1 fluid of the storage tank is the return water to the solar thermal collector, while the outlet 2 fluid of the storage tank is the floor heating system inlet water. Additionally, auxiliary heat input is provided to the storage tank in case of insufficient heat supplied to the floor heating system when the temperature of outlet 2 of the storage tank does not meet the setpoint temperature of 45 degrees Celsius. The design parameters of the system in TRNSYS are listed in Table 5-1.

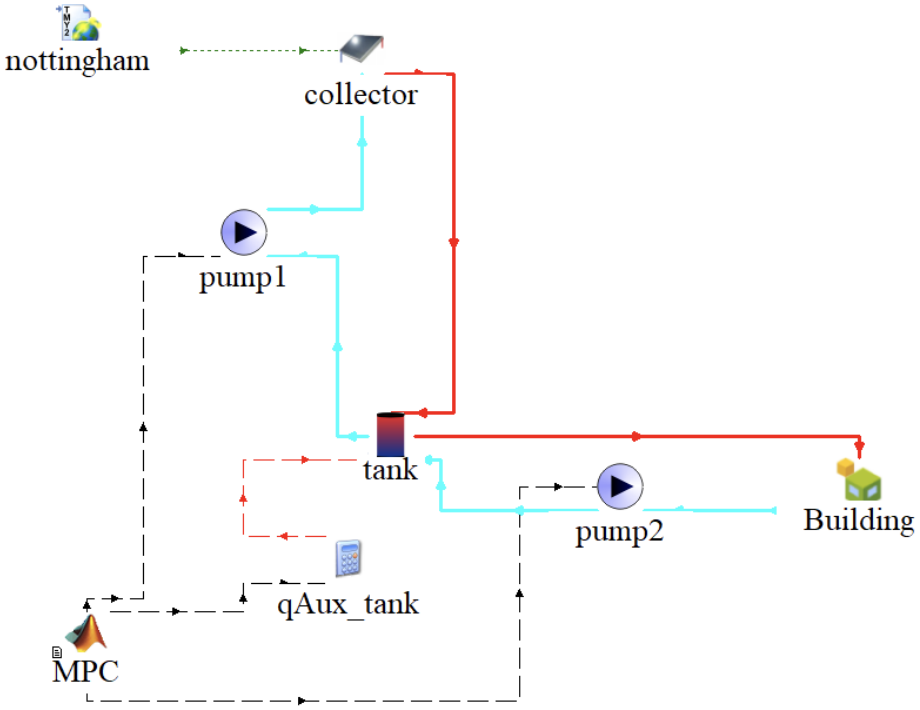

Fig. 5-3 TRNSYS model for thermal storage tank integrated with the solar thermal system and UFH.

Table 5-1Design parameters of the system in TRNSYS [121]

Component	Type	Descriptions	Value
Solar collector	1	Collector area	4 m^2
		Fluid specific heat	4.19 kJ/kg.K
		Intercept efficiency (a1)	0.723
		Efficiency slope (a2)	3.818kJ/hr.m^2.K
		Efficiency curvature (a3)	0 kJ/hr.m^2.K^2
Storage tank	158	Tank volume	0.5 m^3
		Tank height	1.8 m
		Number of tank nodes	1
		Loss efficiency	0
		Fluid specific heat	4.19 kJ/kg.K
		Fluid density	1000 kg/ m^3
Auxiliary control	106	Temperature dead band	2 ℃
		Setpoint temperature	45 ℃

In the event that solar radiation impinges upon a solar thermal collector, the efficiency of solar heat transfer is contingent upon the temperature differential between the inlet water and the ambient temperature. The overall thermal efficiency of the solar collector is determined through the utilisation of the Hottel-Whillier equation, which takes into account the difference between the amount of absorbed solar radiation and the corresponding thermal loss:

$$n = a1 - a2 \times \frac{(Ti - To)}{Isolar} - a3 \times \frac{(Ti - To)^2}{Isolar} \qquad \text{eq 5-4}$$

In TRNSYS, the number of tank nodes is specified for designating the level of stratification for the storage tank [121]. Each of the tank nodes is assumed to be isothermal, and the TRNSYS then calculate the heat transfer pass through each node by:

$$\frac{dT_{tank,j}}{dt} = \frac{Q_{in,tank,j} - Q_{out,tank,j}}{C_{tank,j}} \qquad \text{eq 5-5}$$

To simplify, the storage tank is modeled with only one node, which denotes a fully mixed tank [121] and heat loss to the environment is assumed to be negligible. The rationale behind not considering thermal stratification during the modelling

process of the storage tank stems from a desire to maintain model simplicity and computational efficiency. For future work or studies with an increased emphasis on granular thermal dynamics, modelling the thermal stratification in the hot water storage tank could provide additional insights into the system's performance and potential optimisations. The model of the storage tank was expressed in the form of the equation governing the temperature of the tank node as follows:

$$\frac{dT_{tank}}{dt} = \frac{\dot{m}_{solar}c\left(T_{solar_{outlet}} - T_{tank}\right) + \dot{m}_{return}c\left(T_{building\_return} - T_{tank}\right) + Q_{auxiliary}}{C_{tank}} \quad \text{eq 5-6}$$

$\dot{m}_{solar}$ and $\dot{m}_{return}$ are the mass flow rates of the solar outlet water and UFH system return water. Then, a state space model is created to identify the real-time tank node temperature by the temperature of the outlet of the solar collector ($T_{solar_{outlet}}$), the temperature of the return water of the UFH system ($T_{building\_return}$) and the amount of auxiliary heat ($Q_{auxiliary}$). The temperature variation of the node in the tank is dependent on the heat transfer occurring between the two streams flowing inside, and the auxiliary heat is supplied. Then the state space model of the storage tank would be identified by the data output from TRNSYS.

The auxiliary heating energy serves as a standby heating source to supply the UFH system. If the heating energy from the storage tank is insufficient to meet the building's heating demand, an auxiliary heating pump equipped with a building with a constant coefficient of performance (COP) of 3 [17] is employed to raise the temperature of the water from the storage tank to 45 degrees Celsius. The energy consumption of the auxiliary heating is:

$$P_{sys} = \frac{Q_{est}}{COP_{sys}} \quad \text{eq 5-7}$$

Where Q_{est} is the heating load of a system. COP_{sys} is the overall COP of the heat pump. P_{sys} is the power demand for the system.

5.1.2 MPC strategy

The aim of the proposed MPC control strategy is to minimise the usage of auxiliary heating energy sourced from the grid. Typically, an external hot water storage tank receives solar thermal energy from a solar thermal collector. In instances where there is insufficient heat supply to the case study room, additional

heating energy is provided by an auxiliary heater to heat the inlet hot water of the UFH system to reach 45℃ while considering real-time wholesale market electricity prices [144]. The economic cost function is presented below:

$$J = min \sum_{k=0}^{N-1} q \times (\frac{auxiliary_{(k)}}{COP} \Delta t \cdot price)^2 + r \times {e_k}^2 \quad \text{eq 5-8}$$

Subject to

$$x_{k+1} = A_d x_k + B_d u_k + E_d d_k \quad \text{eq 5-9}$$

$$y_k = D_d x_k \quad \text{eq 5-10}$$

$$T_{\min\,(k)} - e_k \leq y_k \leq T_{\min(k)} + e_k \quad \text{eq 5-11}$$

$$e_k \geq 0 \quad \text{eq 5-12}$$

$$u_{heating(k)} = \frac{u_k - T_{pp(k)}}{R_{inlet,mean} + R_{mean,pp}} \quad \text{eq 5-13}$$

$$u_k = Tank_{\,(k)}(auxiliary\ heating\ is\ off)\ or\ u_k = 45\ (auxiliary\ heating\ is\ on) \quad \text{eq 5-14}$$

Δt is the time interval and N is the prediction horizon, which means the number of the time step predicted in advance. q and r mean the weights of cost. A large weight means the cost is more important than other costs. k means the current time step and J denotes the total electricity cost of the thermal energy demand of the building.

In the development of MPC programming, the objective function was structured as quadratic forms. This approach stems from the study of Široký et al. [77] indicates that minor deviations in comfort levels can lead to significant penalisation in the total cost, thereby highlighting the importance of precision in comfort control.

5.1.3 Co-simulation of TRNSYS and MATLAB with room model

The co-simulation of TRNSYS and MATLAB is commonly employed to simulate the MPC applied in buildings [17]. The building's dynamics are computed using Type 56 of TRNSYS [121], while MATLAB offers several toolboxes that could be utilised to simulate MPC strategies. In this study, the Yalmip toolbox [158] was used for MPC construction, and the Gurobi solver [120] was utilised to determine the control signal. Additionally, a real-time adaptation algorithm, specifically the Kalman filter [118], was employed to correct the state-space model prediction during the co-simulation process. The building model was initially

developed in SketchUp and then integrated with TRNSYS through the TRNSYS3d plug-in [121].

5.2 Case study

5.2.1 Description of the case study building

The Marmont lecture room, situated on the first floor of the Marmont Centre at the University Park Campus, University of Nottingham, UK (as depicted in Fig 5-4b and 5-4c), was utilised as the case study room. This building is primarily designed to facilitate the teaching of architecture and engineering students. This building includes a variety of spaces conducive to multifaceted academic activities. The teaching spaces comprise a lecture room and a seminar room, each can accommodate up to 38 students. The occupancy pattern of these spaces can fluctuate substantially throughout the course of a day, influenced by the students' varying schedules. Both the lecture and seminar rooms are equipped with large, operable windows, which not only provide natural light but also serve as a means for ventilating the spaces.

The lecture room is heated by a central heating system, which includes a boiler and radiators. Located strategically within the building, the boiler supplies a stable source of heat during the colder months. The heating is typically required from October to May. The heated water is distributed via a network of pipes connected to a series of radiators positioned below the windows across the lecture room. This positioning not only ensures optimal heat distribution but also effectively counteracts the cold downdraughts from the windows. Individual control valves on each radiator allow for adjustments in heat output, offering a level of room-specific temperature control. However, the overall control strategy for the central heating system is an on/off mechanism, which, although simple, can sometimes lead to less efficient heating performance compared to more advanced control strategies like proportional-integral-derivative (PID) control or MPC. In the modelling phase of this study, it's important to note that certain factors were not considered to maintain simplicity. For instance, the potential impact of the window opening on the indoor temperature and the effect of varying radiator heat outputs via individual control valves were disregarded. In the case of the latter, it was assumed that these valves were in a fully open state.

The 3D model of the room was developed using SketchUp, with dimensions of 12.75 meters in length, 7.6 meters in width, and heights of 2.71 meters and 4.26 meters. The windows are located on the south-east and north-west facing walls, with a window-to-wall ratio of 0.22 and 0.08, respectively. Air infiltration sets 0.6 h^{-1} according to the similar construction used with the commercial building used for TRNSYS simulation in study of Xue et al [11].

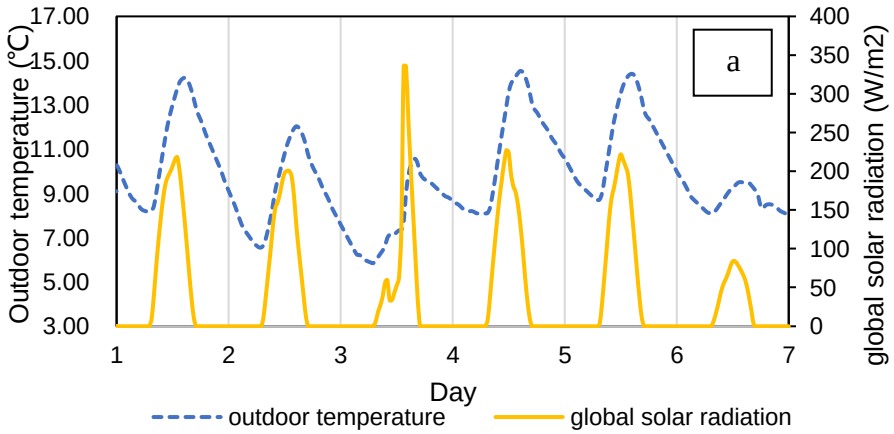

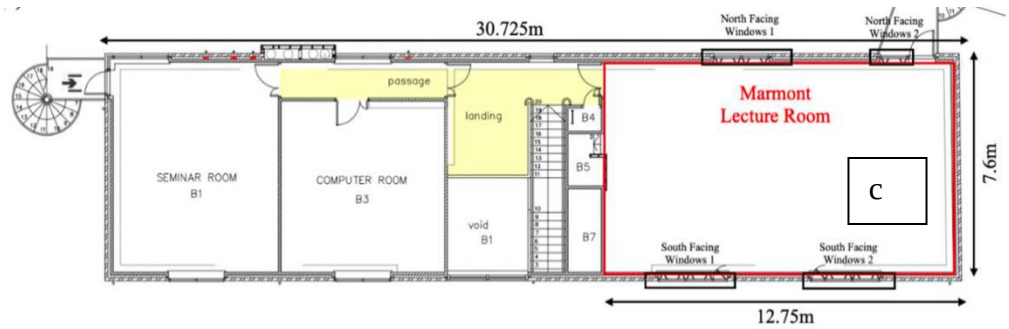

Fig. 5-4 (a) Outdoor temperature and global solar radiation of the simulation periods (b) front view of the Marmont centre building (c) floor plan of the first floor with the lecture room

The construction was based on the real structure, and Table 5-2 presents the materials utilised, ordered from outside to inside. The properties and overall U-values of the wall, roof, and floor are listed in Table 5-2. The room was constructed using lightweight materials, and the window U-value was assumed to be 1.1 W/m2K.

Table 5-2 Properties of materials in the case study room

	Material	Conductivity (w/m K)	Density (kg/m^3)	Specific heat (J/kg K)	Overall U-value (W/m^2 K)
Wall	100mm brick	0.84	1700	800	1.133
	100mm insulation	0.2	1000	1700	
	100mm concrete	1.13	2000	1000	
	225mm mild steel	45	7800	480	
Roof	0.9mm aluminum sheet	230	2700	880	0.259
	25mm Plywood	0.15	700	1420	
	150mm Softwood rafters	0.047	250	1300	
	67mm insulation	0.2	1000	1700	
Floor	95mm sand/cement	0.72	1860	840	2.301
	150mm concrete	1.13	2000	1000	
	heating pipes	30 pipes			

The case study building has a solar thermal collector installed on the roof. Utilisation factor (UF), which is the ratio of collector area to total area (i.e.,98.89 m2), sets to 0.5 based on the real installation (Fig 5-4b).

5.2.2 Occupancy and equipment profiles

The case study room is a lecture room that can accommodate up to 38 students, as illustrated in Fig 5-5. In this study, typical occupancy profile and occupant-related heat gains was defined for one week during the autumn semester based on the timetabled classes/activities and the knowledge of the usage of the space. For simplification purposes, natural ventilation was assumed not employed in the simulations. The indoor lighting consists of 8 luminaires and 1 side light, while the indoor equipment includes 15 laptops, 1 projector, 1 computer, and 1 monitor. Students attend the lecture room based on class schedules, and their arrival and departure times are highly variable. The usage of equipment in the case study room depends on the types of classes. The occupancy profile during a typical autumn semester week is shown in Fig 5-5(b), and the lighting and equipment usage profile is presented in Fig 5-5(c).

On Day 1, a typical lecture day, the maximum number of students present was 32, and 18 electric equipment (15 laptops, 1 projector, 1 monitor, and 1 computer) were occasionally used. On Day 2, there were two lectures with a break, and 25 students attended class with a maximum of 21 electric equipment being used. Day 3 was a group workshop with 20 students and 13 electric equipment. Day 4 was a seminar with 30 students and 23 electric equipment. Day 5 was another group workshop with 20 students and 14 electric equipment. On Tuesday, there was a break during noon, and the number of occupants was significantly reduced. Furthermore, few students would stay in the room for a while after class.

The internal heat gains due to occupants were estimated based on the guidelines provided by CIBSE Guide A [138], which included convective [138] and radiative (69 W) gains for each occupant. LED luminaires were assumed to be installed with a maximum power of 10 W per light, with 30% radiative gains [138]. Electric equipment was assumed to have a maximum power of 10 W per piece of equipment, with 20% radiative heat dissipation [138].

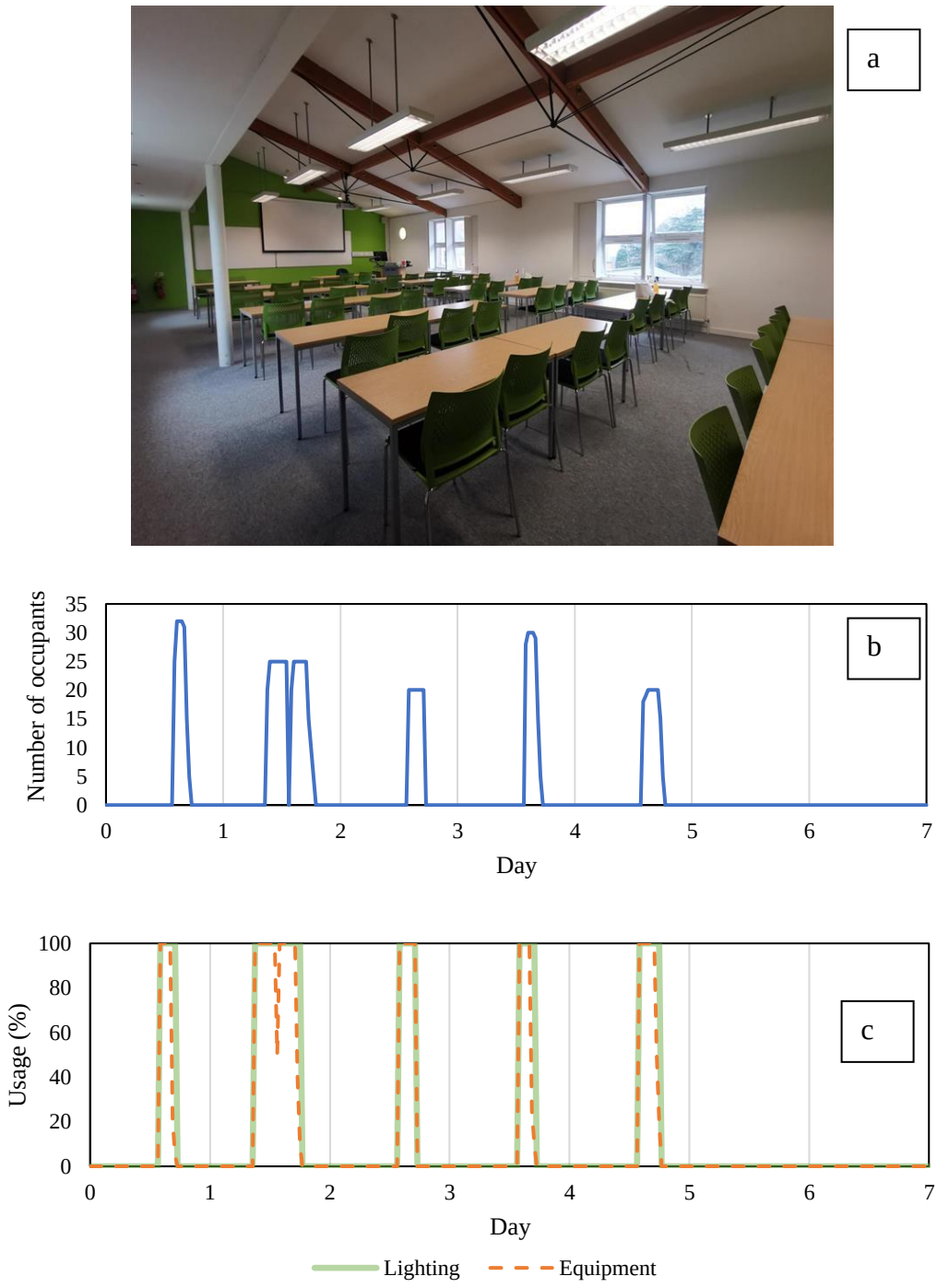

Fig. 5-5 (a) Lecture room (b) occupancy profile and (c) lighting and equipment usage

5.2.3 Setpoint and control strategy

The energy efficiency of the building in this case study was critically assessed by employing two distinct set-point strategies. The first strategy, referred to as the reference case (Strategy 1), strictly maintains an indoor temperature of 22°C during lecture periods, implementing an on/off controller to permit free-floating half an

hour prior to and subsequent to class hours [11]. Fig 5-6 visualises the set-point strategy for the observation week. In contrast, Strategy 2 leverages a structural thermal energy storage (STES) control strategy. This strategy optimises the building's structural capability to store energy during periods of low-price, until the indoor temperature escalates to 25℃, a value considered the upper limit of indoor comfort [17] as depicted in Fig 5-6.

The MPC control strategy maintains the lower temperature bound consistent with the reference strategy, but it introduces an early start-up. The weather prediction data used in the MPC strategy was sourced from Meteonorm [134], specifically for Nottingham, UK. Moreover, to enable the STES storage effect, a day-ahead dynamic price of electricity was used, procured from the UK power market of Nord Pool [144] from 29th October to 4th November 2022 accounting for daily and hourly variations.

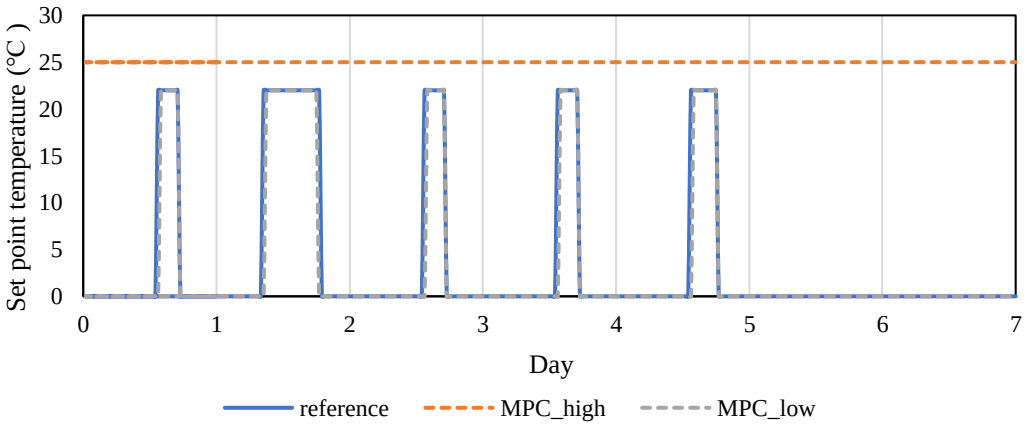

Fig. 5-6 Control strategies evaluated for the case study building

This research conducts a comparative analysis of three control strategies for the floor heating system. The first scenario employs a conventional on/off controller to manage the floor heating system. In the second scenario, an MPC to control the floor heating system was leveraged. The third scenario expands upon the second, wherein the floor heating system is integrated with a solar hot water system, with an MPC strategy orchestrating both systems. The case study revolves around a room currently warmed by central heating radiators. An integral part of this analysis includes assessing the potential electricity cost savings realised by transitioning to the proposed solar hot water heating system, in comparison to the existing heating setup.

5.3 Results and discussion

5.3.1 State-space model verification

The state-space model was identified and validated using different datasets. The comparison was made for results (indoor temperature T_{in} and floor temperature T_{pp}) by inputting the same values of input variables $[T_o \quad I_{solar} \quad Q_{inter} \quad T_{inlet}]$. Each dataset contains 500 data points. Table 5-3 presents the results of system matrix identification and identification accuracy. The values of R_{inlet_mean} and R_{mean_pp} in this study were found to be 0.00040 K/W and 0.00056 K/W.

A

$$\begin{pmatrix} \frac{-1}{R_{w,o}C_w}+\frac{-1}{R_wC_w} & \frac{1}{R_wC_w} & 0 & 0 & 0 \\ \frac{1}{R_wC_w} & \frac{-1}{R_wC_w}+\frac{-1}{R_{w,in}C_w} & \frac{1}{R_{w,in}C_w} & 0 & 0 \\ 0 & \frac{1}{R_{w,in}C_{in}} & \frac{-1}{R_{w,in}C_{in}}+\frac{-1}{R_{win}C_{in}}+\frac{-1}{R_{fl,in}C_{in}} & \frac{1}{R_{fl,in}C_{in}} & 0 \\ 0 & 0 & \frac{1}{R_{fl,in}C_{fl}} & \frac{-1}{R_{fl,in}C_{fl}}+\frac{-1}{R_{pp,fl}C_{fl}} & \frac{1}{R_{pp,fl}C_{fl}} \\ 0 & 0 & 0 & \frac{1}{R_{pp,fl}C_{pp}} & \frac{-1}{R_{pp,fl}C_{pp}}+\frac{-1}{(R_{inlet,mean}+R_{mean,pp})C_{pp}} \end{pmatrix}$$

B

$$\begin{pmatrix} \frac{1}{R_{w,o}C_w} & \frac{\int_{solar,w}\times A_w}{C_w} & 0 \\ 0 & \frac{\int_{solar,int,w}\times A_{win}}{C_w} & 0 \\ \frac{1}{R_{win}C_{in}} & 0 & 0 \\ 0 & \frac{\int_{solar,fl}\times A_{win}}{C_{fl}} & 0 \\ 0 & 0 & \frac{1}{(R_{inlet,mean}+R_{mean,pp})C_{pp}} \end{pmatrix}$$

C

$$\begin{bmatrix} 0 & 0 & 1 & 0 & 0 \\ 0 & 0 & 0 & 0 & 1 \end{bmatrix}$$

5.3.2 Room model verification

The state-space model identification was accomplished using the output data from a TRNSYS simulation. 1500 data sets was generated for model identification and 1000 for model verification, with a 30-minute time interval starting from November 4th. This data was acquired with the indoor temperature managed by an on/off controller. The identification accuracy was similar to the verification accuracy, as shown in Table 5-3, which showed a high Fit% value. This outcome

substantiates that the numerical model was capable of accurately replicating simulated temperatures given known input parameters.

Table 5-3 Fit percentage of identification and verification

	Parameters	Fit %
Identification	T_{in}	75.6 fit%
	T_{pp}	83.2 fit%
Verification	T_{in}	73.6 fit%
	T_{pp}	78.8 fit%

Fit %: the percentage of the model outputting temperatures matching the experimental outputting temperatures.

$$best\ fit = (1 - \frac{|y - \hat{y}|}{|y - \bar{y}|}) \times 100 \quad \text{eq 5-15}$$

The TRNSYS model's validity was further confirmed by the case study room's measured indoor temperature, gathered every 5 minutes over two days (2nd December - 4th December), post the disconnection of heating on the preceding Friday night. The indoor temperature was measured using a K-type thermocouple and data logger TC-08 thermocouple data logger with an accuracy of ±0.5 °C [158]. The months of November and December were chosen for the simulation due to their representative climatic conditions. December typically experiences the lowest ambient temperature, leading to peak heating energy consumption throughout the year. Solar radiation also tends to be at lower levels during this period. Consequently, the performance of the proposed system under these conditions offers valuable insights for evaluating the feasibility of similar systems.

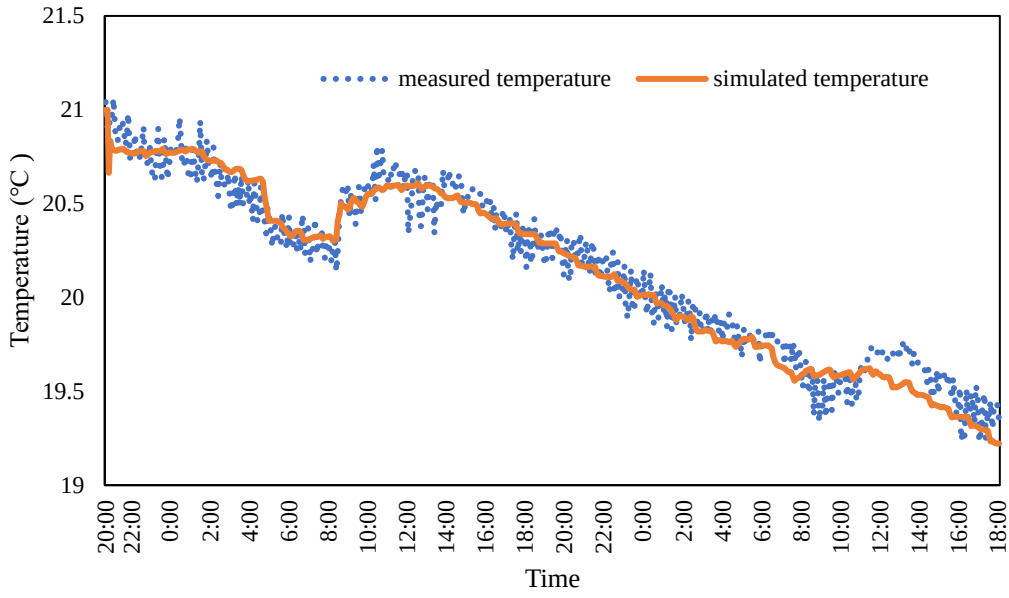

Fig. 5-7 Measured and simulated indoor temperature

The results, as depicted in Fig 5-7, demonstrate that the simulated data offers satisfactory accuracy in predicting indoor temperature, with a cross-validation root mean square error (CVRMSE) of 0.0052. The TRNSYS model's time interval was then adjusted from 5 minutes to 30 minutes to form a model suitable for MPC usage. This is because the control strategy for a typical room usually takes between half an hour to an hour [17]. Thus, the prediction interval should match the control interval.

5.3.3 Storage tank model verification

The state-space model for the storage tank was validated utilising MATLAB's system identification function, ssest. To identify system parameters, 1000 data points were employed, while the verification of the identified model necessitated 2000 data points, these points were collated starting from November 4th at 5-minute intervals. The tank model would further adjust the time interval from 5 minutes to 30 minutes to match the trigger of the control strategy. The model displayed commendable congruity between input and output data at both the identification and verification stages, as evidenced by a CVRMSE of 0.01 (illustrated in Fig 5-8). A comparative analysis of the tank temperature output from the state space model and TRNSYS is detailed in Fig 5-8.

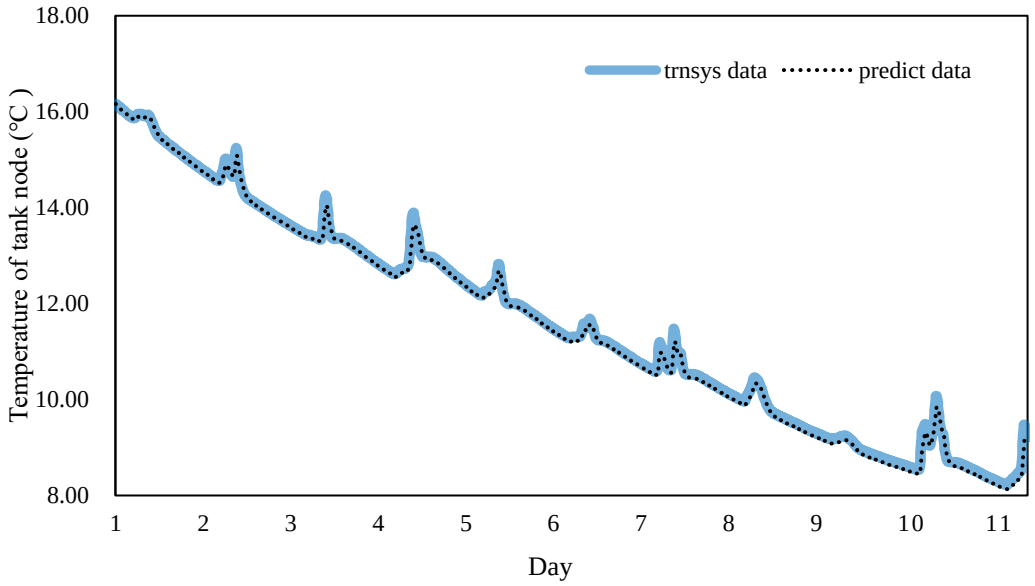

Fig. 5-8 Predicted tank temperatures by the TRNSYS and state space model.

5.3.4 Evaluation of the indoor temperature control

Two types of controllers, namely on/off and MPC, were utilised to achieve indoor temperature control, independent of any integrated solar hot water system. The results of these control strategies are depicted in Fig 5-9(a) and 5-9(b), respectively. The simulation period ranges from November 7th to November 13th, covering both weekdays and weekends.

The application of an on/off controller led to considerable indoor temperature fluctuations over the course of the day, attributable to drastic variations in both outdoor temperature and indoor occupancy patterns. This resulted in significant comfort violations, rendering the on/off controller as less effective for ensuring indoor thermal comfort. On the other hand, the substitution of the on/off controller with an MPC controller facilitated the adoption of a preheating strategy for the UFH system, as demonstrated in Fig 5-9(b) (where '1' signifies 'on', and '0' denotes 'off').

Subsequently, the indoor temperature was successfully maintained within the desired bounds. This was made possible as the MPC controller took into account occupant-related internal heat gains and anticipated the distribution of heating energy to the indoor air, thereby sustaining a comfortable indoor temperature. This was realised by incorporating predefined occupancy profiles and occupant-related heat gains into the MPC controller to solve for the prospective control strategy. For the purpose of this study, it is important to note that a pre-specified occupancy

pattern was opted, simplifying the model for clarity and ease of understanding. This choice was made to allow for a more straightforward exploration of the primary variables under consideration, including energy consumption, cost effectiveness, and thermal comfort.

As discussed in the introduction, forecasting occupancy patterns typically employs on-site models that leverage statistical and machine learning methodologies. There have been previous studies that developed stochastic and robust MPCs designed to handle the uncertainties associated with occupancy forecasts [159]. However, in this chapter, such complexities are not delved into. In practical application scenarios, information regarding occupancy can be either preset according to customary patterns or gathered through intelligent devices such as smartphones or Internet of Things devices. This data can then be fed into the MPC for more accurate and efficient climate control in the building. Nonetheless, for the scope of the current investigation, a pre-determined occupancy pattern have been purposefully maintained.

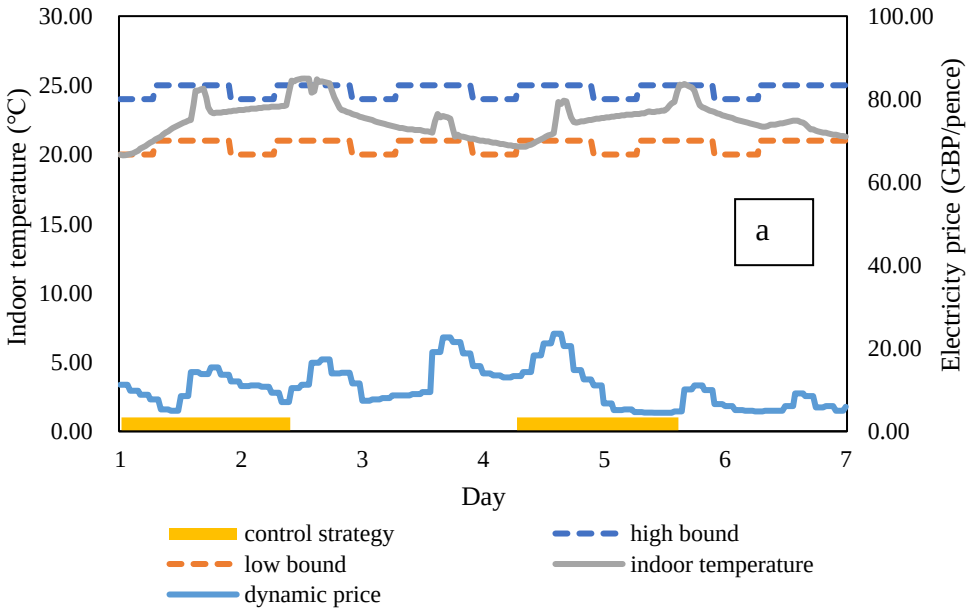

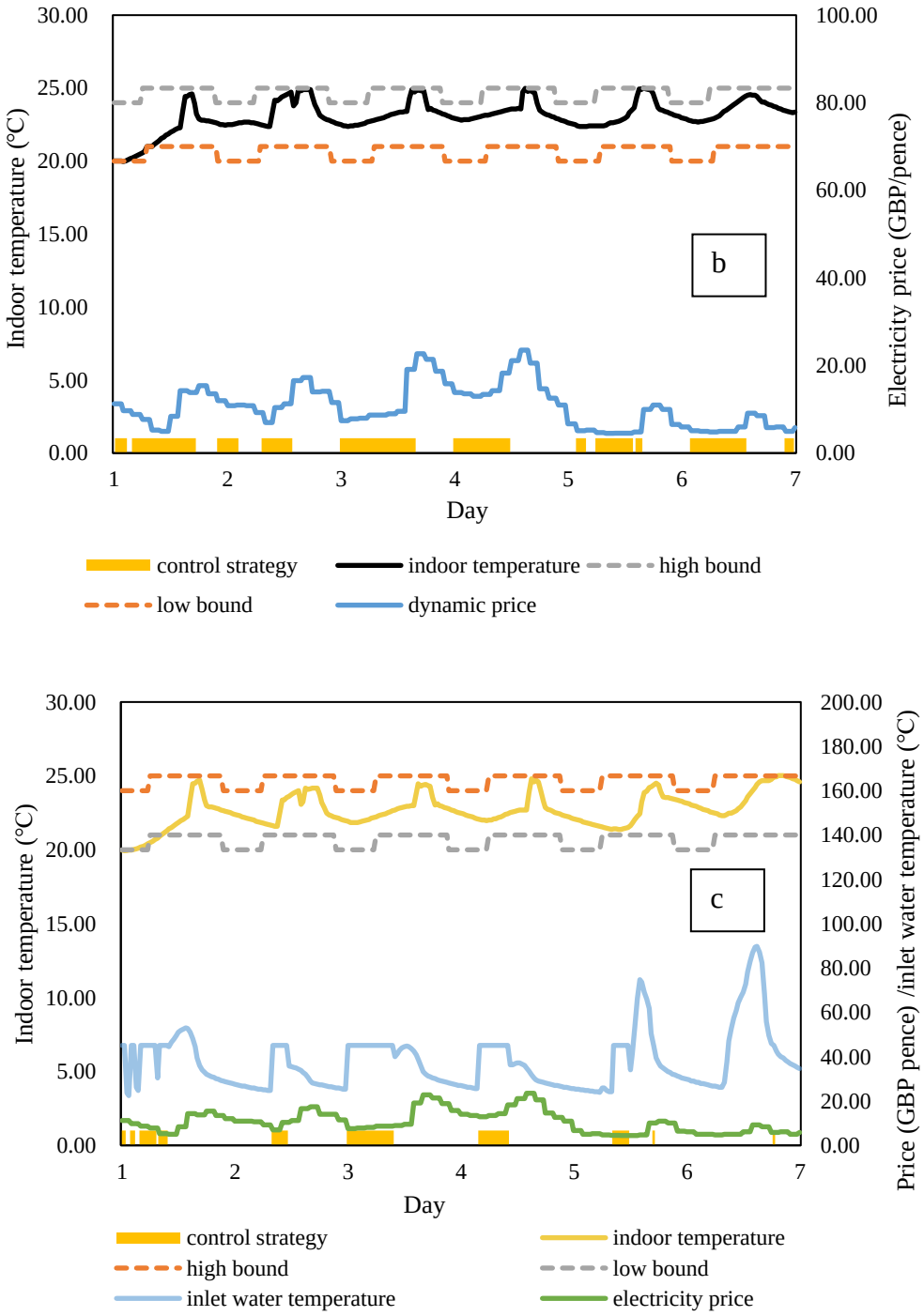

Fig. 5-9 Indoor temperature controlled by (a) on/off controller**,** (b) reference MPC controller**,** (c) proposed MPC by considering solar thermal energy.

As depicted in Fig 5-10, the occupant-related internal heat gains vary according to time, and the control strategy is carefully formulated by the MPC. It was previously established that the MPC is capable of keeping the indoor temperature consistently within the stipulated bounds, as shown in Fig 5-10(c). Furthermore, the MPC displays the capacity to accurately forecast daily occupancy patterns,

subsequently selecting a timely initiation of the heating system prior to the arrival of students.

The MPC also discerns instances of preheating prior to the day's peak times, thus orchestrating a consumption of electricity energy that primarily falls within the lower to medium price range. This chapter also provides an illustrative representation of how the MPC regulates indoor temperature in response to fluctuating occupant presence within the day. For instance, a break occurring at noon on Tuesday is associated with a sudden decrease in occupant numbers. The MPC, recognising this abrupt drop in internal heat gains, opts for a preemptive increase in indoor temperature before the break, effectively exploiting the low-price energy available at that time. The MPC demonstrates a preference for utilising low-cost energy during the nighttime and morning hours to preheat the room, whilst disconnecting the heating system in the afternoon when electricity prices tend to peak.

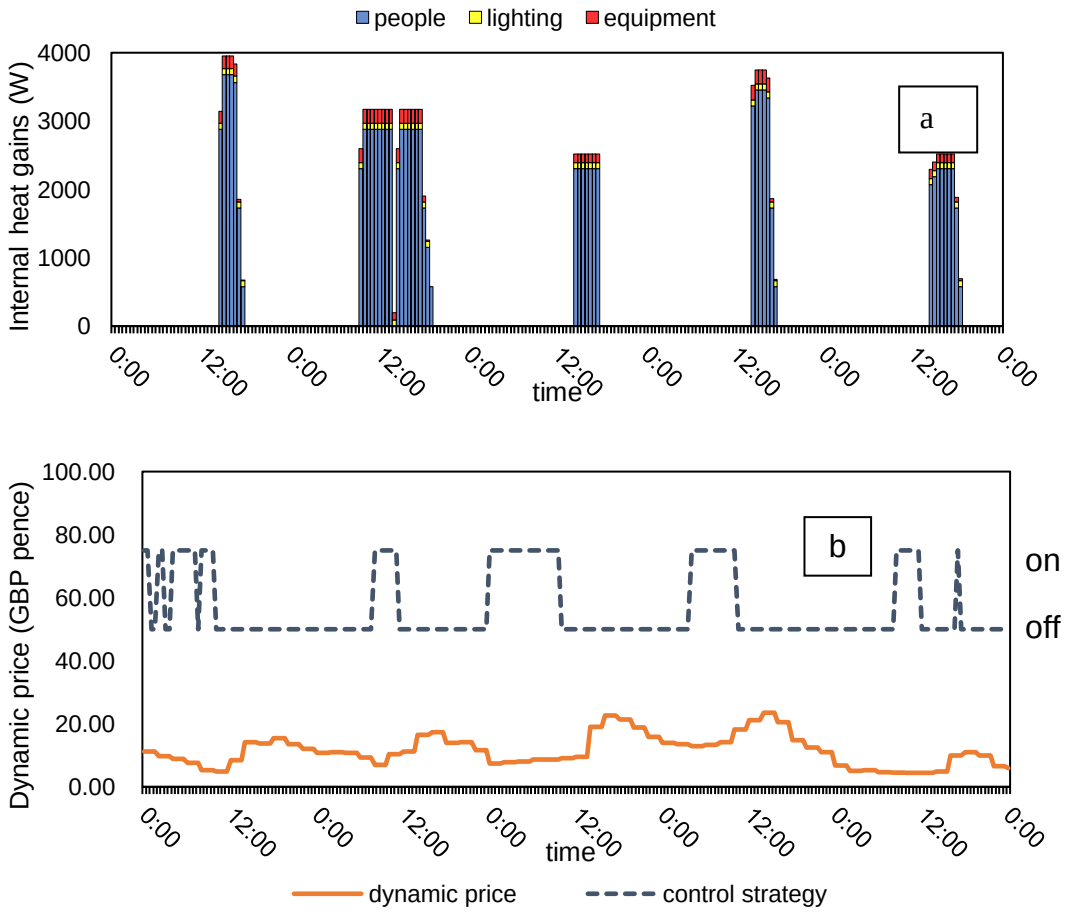

Fig. 5-10 (a) Internal heat gains and (b) control strategy based on the prediction of internal heat gains.

5.3.5 Energy performance and thermal comfort violations

The MPC-regulated under floor heating system operated for 13 hours more compared to the on/off controller, consuming 725 kWh of electricity compared to the on/off controller's 560 kWh. However, the electricity costs for both remained comparable (Table 5-4), attributable to the MPC's capacity to capitalise on low-cost energy. This finding echoes the outcomes of earlier studies [17], which demonstrated the MPC's predilection for charging during periods of lower prices and initiating early startup before occupancy. The proposed MPC sought to leverage the advantages of low-cost energy, storing the heat within the building's structure and discharging heat during periods of higher prices.

Table 5-4 Energy performance of different control strategies

	Total heating hours (hrs)	Electricity cost (GBP pence)
On/off	131.00	6160
MPC	161.00	6299
MPC with solar hot water	64.00	3035

In the integration of the solar hot water system with the MPC, the primary objective is to favor the usage of solar thermal energy and minimise electricity costs. As depicted in Fig 5-10(c), the inlet water temperature of the floor heating system aligns with the outlet temperature of the hot water storage tank when solar thermal energy is utilised. In the absence of solar thermal energy, the inlet temperature is adjusted to 45 degrees, complemented by auxiliary heat sourced from the supply network. The proposed MPC control strategy guarantees that the indoor temperature remains completely within the stipulated temperature bounds. Moreover, the introduction of an active water storage tank contributes significantly to reducing the switch-on hours to half of those in the reference case where no solar hot water system exists, as indicated in Table 5-4. As a result, the total electricity cost during the simulation period decreases substantially to half of the reference case. This outcome is attributed to the enhanced solar thermal storage capacity made possible by the integration of an active hot water tank.

Thermal comfort was evaluated based on the integral of room temperature comfort range violations over time, quantified in terms of kelvin hours (Kh) (Fig 5-11). The total Kh for the on/off, reference MPC, and MPC with the solar hot water system are 7.78℃, 0.03℃, and 0.17℃, respectively. Overall, the reference MPC,

despite consuming marginally more control energy, delivered considerably enhanced thermal comfort.

The reference MPC, which only leverages STES for energy storage and disregards the integration of the solar hot water system, necessitated greater energy use. This was offset by capitalising on low-to-medium priced energy, reducing comfort violations compared to the conventional on/off control strategy. Despite the increase in total energy consumption with the reference MPC control, a net improvement in overall comfort was observed, a finding that aligns with the study conducted by Sturzenegger et al. [80].

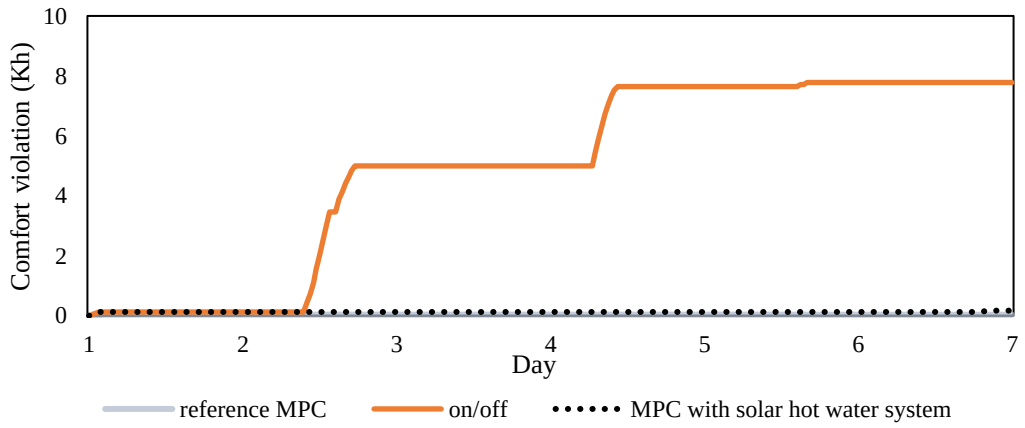

Fig. 5-11 Cumulative comfort violation for each strategy

5.3.6 Energy cost based on electricity price

At present, the lecture room's heating needs are serviced by six continuously operational radiators. The indoor thermostat manages the ambient temperature, maintaining it between 20℃ and 24℃. Fig 5-12 offers a comparison of energy consumption between the existing heating approach and the modified strategy incorporating both a floor heating system and a solar thermal system. Under the conventional system, the accumulated electricity cost over the period amounts to 6956 GBP pence. However, this figure was 3035 GBP pence lower when implementing the solar hot water and floor heating system under an MPC strategy. During the simulation period, electricity prices fluctuated between 4 GBP pence and 23 GBP pence. Three pricing tiers have been categorised: low-price energy (4 GBP pence to 10 GBP pence), medium-price energy (10 GBP pence to 16 GBP pence), and high-price energy (16 GBP pence to 23 GBP pence). Fig 5-12 illustrates the energy consumption of both systems. The system incorporating solar hot water

exhibited increased usage (58%) of low-to-medium price energy as compared to the conventional system (33%). Conversely, the conventional system largely relied (67%) on high-price energy.

The low usage during low-price periods for the MPC with solar energy heating and active/passive storage, in contrast to a conventional on/off system, can be primarily attributed to several reasons. The MPC integrated with a solar energy heating system seeks to maximise the usage of freely available solar energy. This naturally harvested energy source can often meet a substantial portion of the heating demand, reducing the need for additional electricity even during periods of low-cost energy. Furthermore, the presence of active and passive storage mechanisms within these advanced systems enables the storage of excess harvested solar energy during periods of high solar yield. This stored energy can then be utilised during periods of high demand or when solar radiation is insufficient or non-existent, reducing the need for additional, low-cost electrical energy during these times. As the MPC system is capable of predicting demand, it can efficiently manage and distribute the stored energy, minimising the need for extra energy during low-price periods. In contrast, the conventional on/off systems lack these capabilities. It cannot harvest, store, or efficiently manage solar energy. Moreover, it does not have demand forecasting capabilities, and its operation is not linked to energy price fluctuations. As a result, it consumes more energy overall and has higher usage during low-price periods.

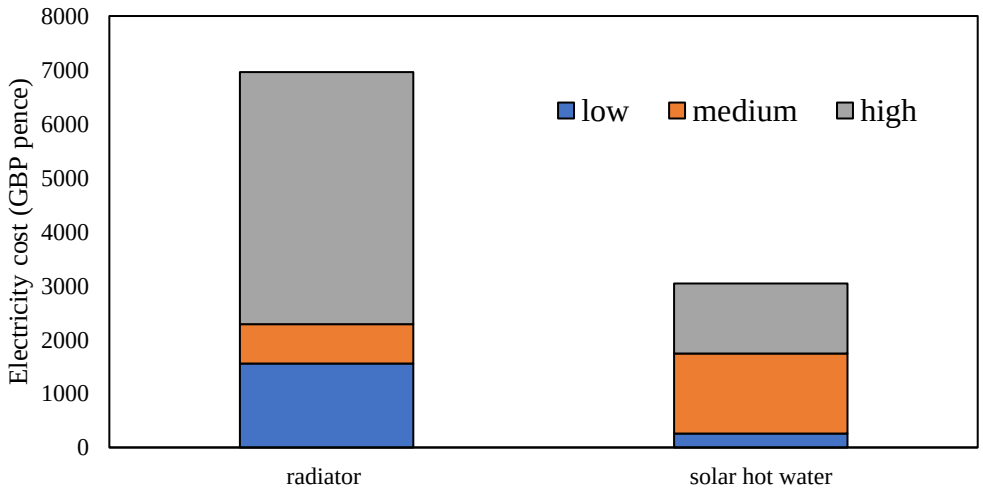

Fig. 5-12 Electricity cost based on electricity price for original system and the proposed solar hot water system (MPC).

5.3.7 Analysis of heating energy source

The heating source's composition for the building heating system is depicted in the stacked bar graph in Fig 5-13. Under conditions of low solar radiation, auxiliary heating usage increases. It is discernible that under the control of the MPC, the auxiliary heating drawn from the grid was predominantly used during the hours from midnight to early morning, coinciding with periods of relatively low electricity prices. However, with sufficient solar radiation, the heating energy harnessed directly from the storage tank adequately covers daily energy consumption, further aided by energy shifting through STES. Coupled with active and passive storage systems, the MPC successfully moved most of the heating demand to periods of ample solar radiation availability. The MPC's ability to maximise solar energy usage during daytime, when electricity prices are at their peak, takes advantage of a peak load shifting strategy. Subsequently, the MPC predicts demand for the following 12 hours, determining the solar energy to be stored via both passive and active storage techniques, further shifting demand away from nighttime peak hours (i.e., 18:00 ~22:00) to midnight. Overall, the solar hot water system supplied 63% of the heating energy to the case study room, primarily during periods with high solar radiation availability. This result validates the effectiveness of the MPC in augmenting RES integration into residential micro-grids by predicting both the building's load and system's response under varying weather conditions, in alignment with the studies of Torreglosa et al. [113] and Bartolucci et al. [114].

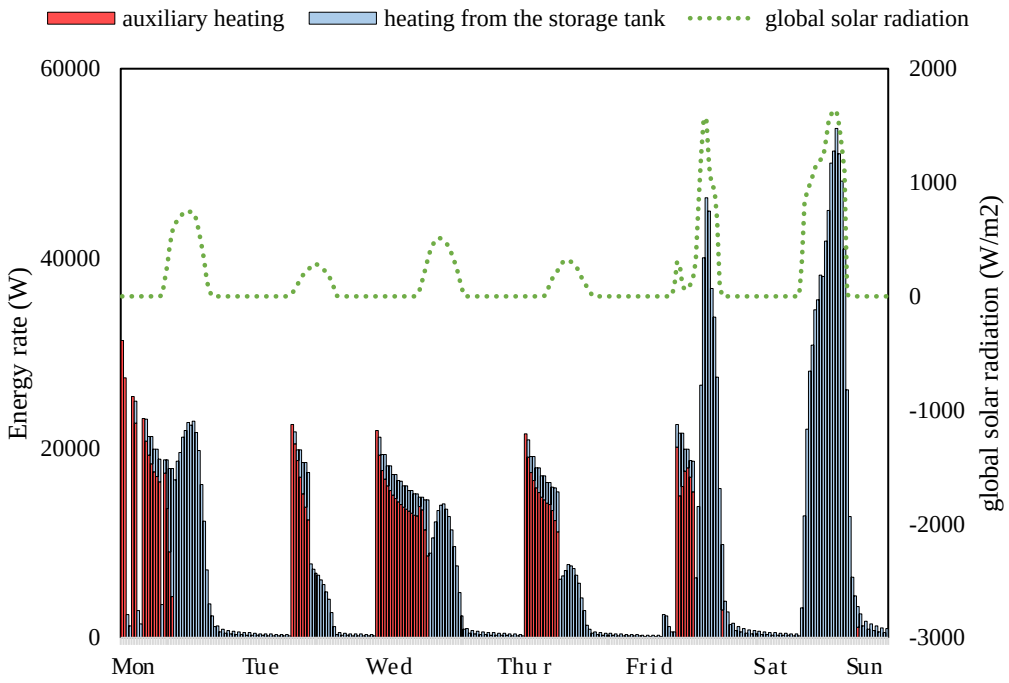

Fig. 5-13 Heating energy source for the integrated solar hot water system

5.3.8 Limitations and application scope

The simulation conducted offers insightful perspectives into the application of a price-responsive MPC strategy for solar thermal heating systems with thermal energy storage in buildings exhibiting high occupancy variability. However, the interpretation of these findings must acknowledge certain limitations. The geographical focus of the study, Nottingham, UK, might pose a constraint on the broader generalisability of the findings, particularly concerning areas with different climates and solar energy conditions. Furthermore, the university-specific context may restrict the broader application of the proposed strategy to buildings with differing occupancy patterns. Also, conclusions about cost savings are inherently tied to the locality's specific energy price structures and solar energy availability, possibly affecting the economic viability of the proposed system in different settings.

Despite these limitations, the proposed MPC strategy maintains utility across diverse contexts. Even in regions with static electricity prices, the multifaceted capability of MPC to regulate energy use based on anticipated occupancy, weather forecasts, and the expected performance of integrated renewable energy systems allows for the optimisation of comfort and efficiency. As grid structures evolve and

renewable energy integration amplifies, MPC's benefits, such as mitigating grid stress through peak demand reduction, could become more pertinent.

Furthermore, the effectiveness of MPC extends to regions with lower solar energy availability, thanks to its fundamental mechanism of leveraging future condition predictions to optimise system control. Here, while solar energy utilisation could diminish, integration of other renewable energy sources into the MPC framework can maintain consistent benefits such as improved comfort, adaptiveness to occupancy patterns, and potential energy demand reductions.

Lastly, although the developed model underwent a robust validation process using numerical simulations and experimental data, its broad applicability might encounter unanticipated operational complexities. Future research endeavors could concentrate on addressing these limitations, further enhancing the model's universal applicability across various buildings, climates, and energy scenarios.

5.4 Summary

This chapter investigated a price responsive MPC strategy for a solar thermal heating system with thermal energy storage (TES) for buildings with high occupancy variability. The TES system, comprising a hot water storage tank and the building's thermal mass was integrated with a rooftop solar hot water system. The primary objective of the MPC controller was to enhance the performance of the renewable energy-based space heating system, reduce costs, and optimise the utilisation of solar energy resources. This is achieved by forecasting the system's responses under varied weather conditions and integrating dynamic pricing. The developed grey-box state space model has undergone verification and validation process, utilising both numerical simulations and experimental data. A case study university building located in Nottingham, UK was employed to assess the viability of implementing the heating system controlled by the MPC strategy, leading to the following key conclusions:

The implementation of MPC in managing an integrated solar hot water and under floor heating system demonstrated a significant reduction in energy costs, with savings reaching up to 50% compared to a reference case.

The MPC control strategy, paired with an active water storage system, managed to reduce the switch-on hours by half of the reference case. This, coupled with the

exploitation of solar thermal storage, reduced total electricity costs during the simulation period by half compared to the reference case.

Utilising the solar thermal energy, the integrated MPC system managed to maintain the indoor temperature within the desired temperature bounds, thereby minimising electrical costs and optimising the use of freely available energy.

Despite periods of low solar radiation, the MPC's prediction capabilities, including early pre-heating before room occupancy, ensured that the indoor temperature was maintained at a comfortable level, achieving zero violations of the temperature bounds.

The system controlled by MPC presented a 58% utilisation of low to medium-priced energy, a significant improvement from the conventional system, which showed only a 33% utilisation in the same price range.

With an integral focus on leveraging low-price energy and active thermal storage, the MPC-controlled system resulted in substantial thermal comfort improvements, reducing the total time-integral of room temperature comfort range violations (measured in Kelvin hours) to a minimal 0.03°C, compared to 7.78°C for the on/off controller.

Overall, this chapter proves the viability of an integrated solar hot water system with an MPC control strategy as a promising approach to enhancing the energy efficiency and thermal comfort of building heating systems, making it an attractive solution in the face of fluctuating energy prices and varying occupancy patterns. However, for comprehensive realisation of this integrated system, additional research is necessitated. Future work should focus on empirical validation of this integrated storage model and consider the water stratification within the storage tank.

The results opens numerous avenues for future research in the realm of optimising energy management systems and elevating building thermal comfort. One such opportunity lies in the exploration of integrating additional renewable energy sources. Working synergistically with the existing solar system, these could further diminish reliance on grid electricity and bolster the overall sustainability of the system.

Moving from the pre-defined occupancy patterns used in this model, an interesting prospect is to enhance the realism and accuracy of system control by

incorporating predictive models of occupancy. These models could be founded on real-time data harvested from smart devices or Internet of Things technologies.

The development of the existing MPC algorithm presents another promising area of research. The algorithm could be refined or expanded to account for a broader spectrum of environmental conditions and building features. The implementation of machine learning or artificial intelligence techniques could also augment the prediction and control performance of the system.

A more robust approach to handling uncertainties, such as solar radiation forecasts and occupancy profiles, could be the development of robust and stochastic MPC controllers. Such systems would bolster performance under uncertain conditions.

Another important perspective is the economic feasibility of such an energy management system. Future studies should scrutinise the life-cycle costs, including installation, operation, and maintenance, and juxtapose them against potential energy savings. Real-world implementation also merits attention: conducting field studies and experimental validations can elucidate the practical applicability and efficacy of the proposed system, bringing to light potential challenges and solutions for practical implementation.

Finally, understanding the scalability of the proposed system in larger settings like office buildings, industrial complexes, or residential communities is paramount. Each of these different settings may present unique challenges and opportunities for energy management. Pursuing these recommendations will undoubtedly drive forward the boundaries of current knowledge and contribute substantially to the development of more sustainable, efficient, and comfortable building energy systems.

6. Experimental evaluation of low-cost MPC and analysis of PCM integration

Collectively, this chapter will contribute to the field by providing insights into the feasibility, scalability, and potential of these innovative integrations. The primary aim of this chapter is to develop a cost-effective, easy-to-implement MPC that is capable of leveraging IoT devices as a continuous, economic data source for its predictive models. The focus of this investigation will be how this interaction facilitates real-time and forecasted energy consumption optimisation, effectively integrating dynamic pricing strategies. To substantiate this research, the designed MPC, created in MATLAB and deployed through a locally embedded Raspberry Pi (RPi) hardware via WiFi, will be applied in a real-world setting - a test pod at the University of Nottingham, UK. This control system will maintain the indoor comfort levels by reacting to the hourly dynamic price of electricity, providing real-time indoor temperature feedback. Furthermore, the integration of this low-cost MPC with PCMs, investigating how MPCs can efficiently manage and capitalise on the thermal storage properties of PCM wallboards was explored (Fig 6-1). Lastly, to validate the feasibility and energy performance of the MPC in conjunction with PCMs, energy performance will be simulated through a co-simulation of TRNSYS and MATLAB, incorporating the proposed control strategy.

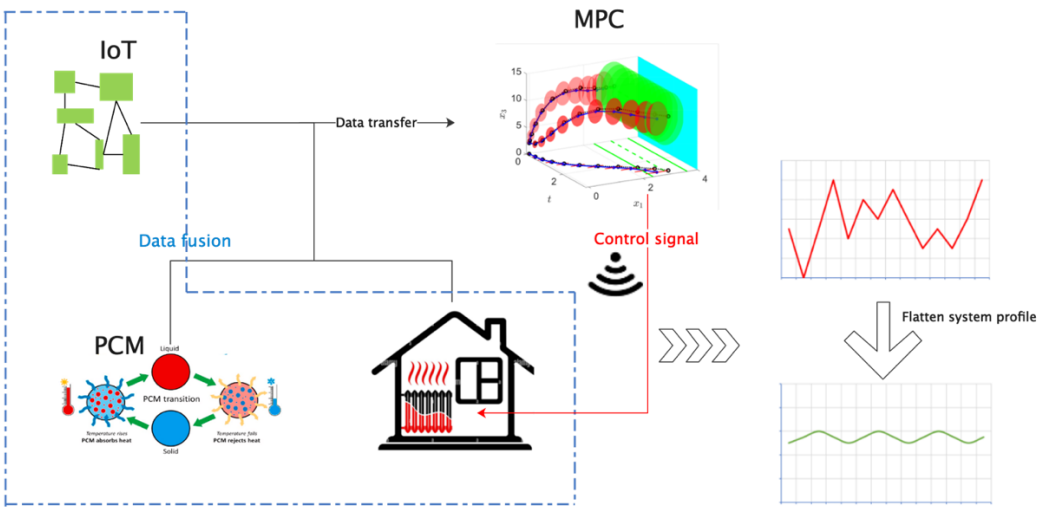

Fig. 6-1 IoT-based MPC strategy for building integrated with PCM wallboards.

6.1 Method

This section outlines the methodology employed to create an unsupervised MPC system. Initially, a numerical state-space model is proposed for the case study room, along with model validations with measured data for several days. Monitoring and IoT technologies are presented in this section along with connections of them for data extraction and control strategy implementation. A case study lecture room in the University building in Nottingham, UK, which was introduced in chapter 3, will be employed for evaluating the feasibility of the proposed low-cost MPC strategy. Furthermore, a platform of PCM-wallboard controlled under validated MPC strategy was proposed aims to address the aforementioned gaps through software co-simulation. The model development underwent numerical model, TRNSYS model and finally connecting to MPC model in MATLAB. The numerical model of PCM was designed for eliminating nonlinearity in this study for easy integration in MPC.

6.1.1 Experiment arrangement and simulation platform

The test facility has been introduced in chapter 3. This section provides description of the experiment procedure and simulations conducted in the study, as illustrated in Figure 6-2. The data collection phase extended over a period of three days, specifically from 09.12.2022 to 12.12.2022, with data being collected at 5-minute intervals. The collected data encompassed various parameters, including local weather data, indoor temperature, radiator schedule, and power consumption. The primary objective of this data collection was for model validation, which is elucidated in detail in Section 6.1.4. The specifics of the weather data collection process are outlined in appendix A1.

Subsequently, two distinct models were developed for simulating the indoor temperature's response within the test pod. Firstly, a TRNSYS model was constructed, and secondly, a numerical model was employed. The initial performance analysis involved a comparison between the experimental MPC conducted over an eight-day period (16.12.2022 to 23.12.2022) and a simulated TRNSYS on/off controller. This comparison was based on indoor thermal comfort and heating energy usage metrics.

In the following step, the chapter explored the integration of a PCM wallboard into the pod's envelope. The subsequent performance analysis aimed to evaluate the

potential enhancement in energy performance resulting from the integration of the PCM wallboard under the proposed MPC strategy. The experimental details pertaining to the MPC experiment and the specifics of the TRNSYS simulations are elaborated in the subsequent paragraphs.

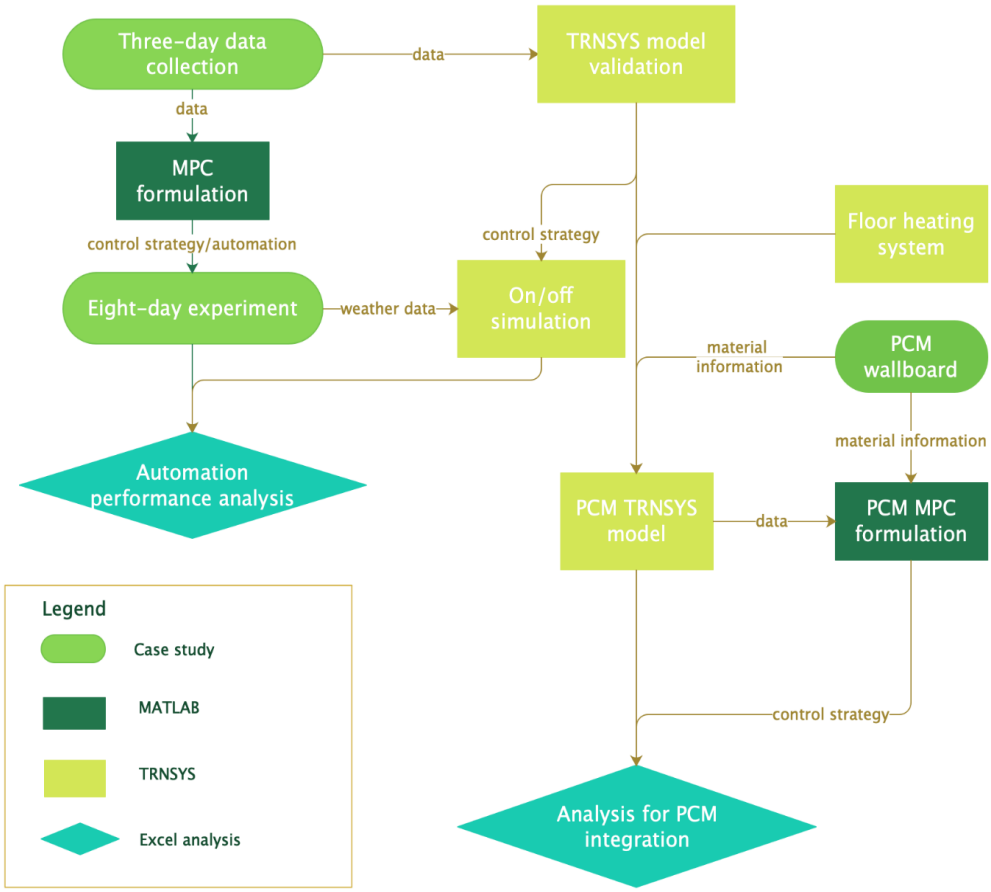

Fig. 6-2 Flowchart of the proposed method in this study

6.1.2 MPC automation

In the unsupervised scheme, an MPC strategy was employed to make control decisions for two radiators every half an hour. The main objective was to minimise electricity costs while ensuring indoor thermal comfort, taking into account dynamic pricing and future weather conditions. The detailed MPC algorithm is presented in Section 6.1.5.

To initiate the control strategy calculation, the current indoor temperature was first extracted and used to correct the predicted indoor temperature within the model integrated into the proposed MPC strategy (as depicted in Fig 6-3). Concurrently, MATLAB was utilised to extract online 12-hour weather forecast data from the official website of the UK Met Office [160] through the application of regular

expression function 'regexp' [161]. This allowed us to match the relevant keywords pertaining to weather data. Additionally, MATLAB acquired the current electricity price, which was downloaded the previous day from an open-access day-ahead electricity wholesale market [144] from 16th December 2022 to 23rd December 2022.

Considering the need for data update preparation, control signal calculation, and the establishment of a connection with the remote controller, the "ticking" and "timing" function in MATLAB was employed to accurately loop the MPC at the commencement of each half an hour. Upon MPC solving the control signal, it constructed either an on or off signal by generating a group of 1/0 combinations, which were then transmitted to the GPIO pins in the Raspberry Pi (RPi) for effectively controlling the radiators.

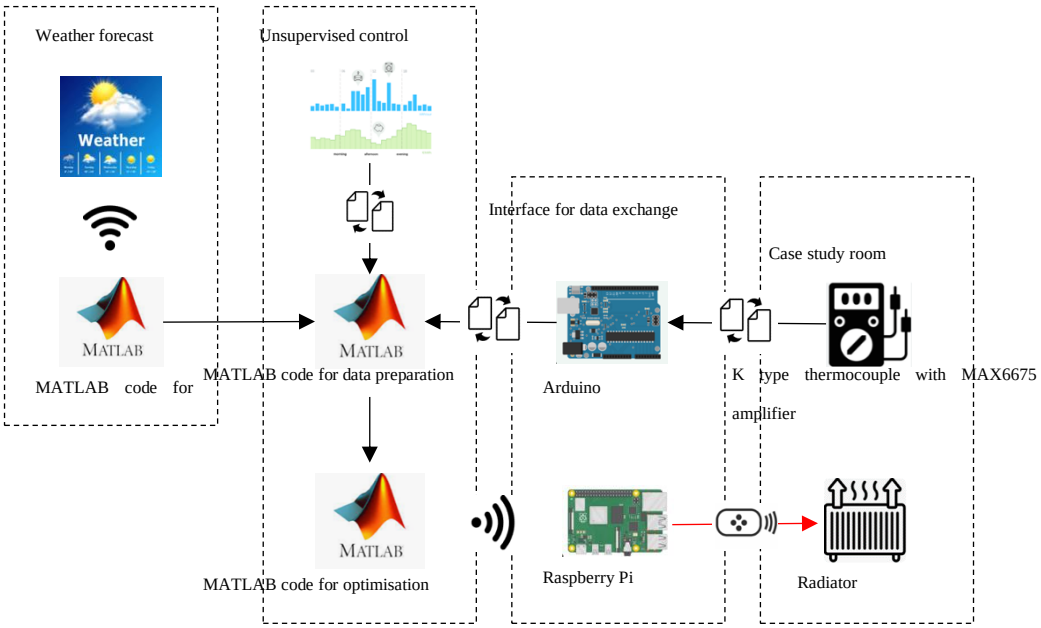

Fig. 6-3 The proposed MPC strategy employed in the case study room.

6.1.3 Co-simulation of TRNSYS and MATLAB

In this chapter, TRNSYS [121], a widely recognised software based on white-box approaches, was employed for the dynamic simulation of building behavior. Specifically, a validated TRNSYS model was applied to simulate the indoor temperature of the test pod under various scenarios. A comprehensive description of the TRNSYS model can be found in Section 6.1.4.

For the control strategy, a Type in TRNSYS, namely Type 155 was used, to invoke MATLAB at each simulation time step in order to generate the control signal.

At the end of each time step, TRNSYS provided the current room temperature to MATLAB. Subsequently, the Kalman filter updated the current error covariance and Kalman filter gain by utilising the indoor temperature information. This information was then used to solve the current state for MPC optimisation. At the beginning of the next time step, TRNSYS would call MATLAB to obtain the recently computed control signal. Meanwhile, a step increment was implemented in MATLAB to synchronise the time step with TRNSYS.

Typically, MPC necessitates a predictive model, constraints, and an objective function [77]. These components was then formulated as a mixed integer linear programming problem. To achieve this, the Yalmip toolbox, a robust optimisation tool designed to model and solve problems occurring in systems and control theory, was used effectively running within the MATLAB environment [128]. To solve the mixed integer linear programming problem, Gurobi external solver [120] was used.

By incorporating these tools and techniques, an efficient and effective MPC for the experiment was constructed, enabling the algorithm to optimise the control of the indoor temperature in the test pod under varying conditions and scenarios.

6.1.4 TRNSYS modelling

6.1.4.1 Original model for pod with radiators

Three TRNSYS types to simulate the case study room. Type 1231 was utilised to model the radiator, with the inlet water temperature set at a constant 65 degrees and a flow rate typically set to 15 kg/(hm2) [17] To process the weather data collected from the local weather station and transmit it to the building model (Type 56), Type 9, Type 16, Type 33, and Type 69 were used. Additionally, a thermostat (Type 106) was assumed to control the radiator by sensing the indoor temperature and applying predefined setpoints. The detailed TRNSYS model is presented in Fig A2 in appendix A2.

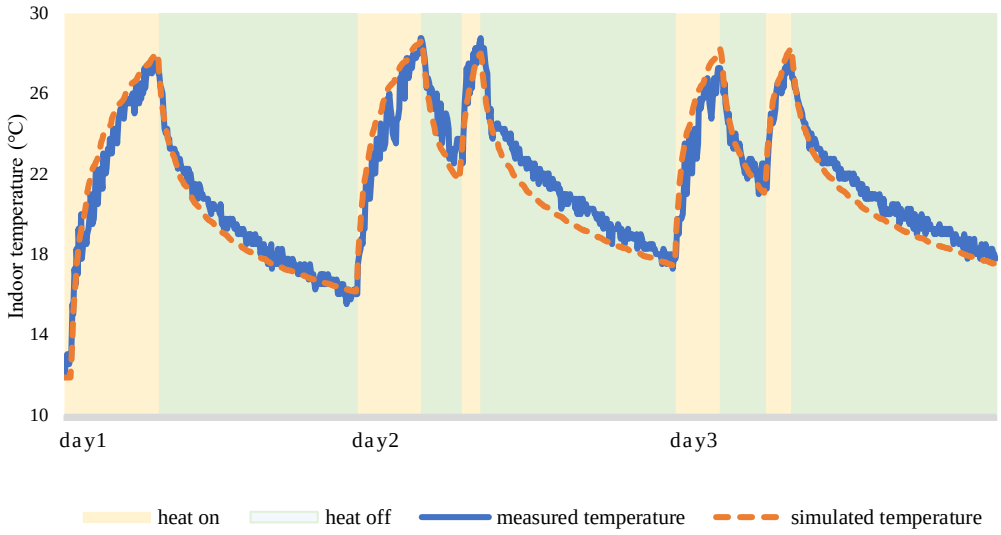

Fig. 6-4 Comparison between measured data and TRNSYS simulated data.

The validation process for the original pod heating system was conducted. The measured data collected over the first three days were utilised to validate two specific scenarios (Figure 6-4). The data with the heating turned on were used to validate the TRNSYS room model, while the data with the heating turned off were employed to validate the radiator system. The validation of the TRNSYS model exhibited a good agreement with the measured data collected from the test pod. The root mean square error (RMSE) between the TRNSYS simulated data and the measured data was calculated to be 0.86℃, confirming the accuracy and reliability of the simulation results.

6.1.4.2 Pod system with PCM wallboard under UFH system

Subsequently, PCM wallboards were introduced to the south, east, west, and roof walls, while replacing the original radiator system with an UFH system. This is motivated by several factors. UFH offers enhanced thermal comfort through uniform heat distribution and improved energy efficiency due to lower operating temperatures. Lastly, UFH aligns well with the use of PCM wallboards, as the even heat distribution could promote efficient heat absorption and release, thereby improving the overall performance of the integrated system. A heating pump equipped with a building with a constant coefficient of performance (COP) of 3 [11] is employed to raise the temperature of the inlet water of UFH system to set-point. The energy consumption of the heating system is:

$$P_{sys} = \frac{Q_{est}}{COP_{sys}} \quad \text{eq 6-1}$$

Where Q_{est} is the heating load of a system. COP_{sys} is the overall COP of the heat pump. P_{sys} is the power demand for the system.

The PCM layers assumes adding to the walls except the floor construction and the north wall, which have heating pipes and windows located. The PCM layer was mainly located on inside surface behind a 45 mm plywood panel with thickness is 25mm (Fig 6-5). Type 1270 was used. Four Type1270s were applied in this study to simulate PCM wallboard integration in west, east, south walls and roof. The detailed TRNSYS platform is showed in Section A6. The component in TRNSYS used to model the PCM layers (Type 1270) assumes that the temperature of the PCM material keeps unchanged with constant specific heat capacity for its solid and liquid states. The theory of the PCM material in TRNSYS is [121]: additional weather data for Nottingham from Meteonorm [134] were derived using TRNSYS Type 109. In the building model (Type 56), an active layer, typically utilized to simulate UFH systems, was established with an inlet temperature of 45 degrees and a flow rate of 15 kg/(hm2). The air leakage rate, as determined by Zheng's test on the same test pod [122], was found to be 4.2 h-1. In the simulation, a constant assumed infiltration rate of 0.27 h-1, similar to that of case study 1 in chapter 4.5, was utilized based on the linear regression relationship between infiltration and leakage with a constant air leakage-infiltration rate ratio of 18 outlined in reference [168].

The utilisation of Phase Change Materials (PCMs) in building components holds the potential to enhance human thermal comfort by minimising the frequency of fluctuations in internal air temperature. Consequently, the indoor air temperature can closely align with the desired temperature for an extended duration. The choice of integrated PCM material should be based on melting temperatures that align with the thermal comfort zone recommended by guidelines, such as ASHRAE, which typically ranges between 20 and 27 degrees Celsius [138]. Numerous organic materials have undergone extensive research as low-temperature PCMs due to their minimal super-cooling and phase segregation characteristics.

Existing literature indicates that certain solid-liquid organic PCMs, including paraffins, fatty acids, and polyethylene glycol (PEG), meet the specified requirements [169]. Among the widely utilized solid-liquid organic PCMs are

Capric acid, PEG 600, Dodecanol, and Heptadecane. These PCMs can be seamlessly integrated into common building construction materials such as plaster, concrete blocks, and gypsum board. They share similar advantages in terms of integration into the building layer, including high latent heat capacity, appropriate phase change temperature, non-corrosivity, nontoxicity, good thermal/chemical stability, low vapor pressure, and minimal supercooling [170](Table 6-1).

Table 6-1 performance of PCMs for building thermal energy storage

	Capric acid [169]	PEG 600 [171]	Dodecanol [169]	Heptadecane [169]
Class	Fatty acid	Organic polymer	Fatty alcohol	Paraffin
Thermal conductivity $W\ m^{-1}K^{-1}$	0.15	0.19	0.17	0.14
Laten heat of fusion $kJ/\ kg$	190	127	215	216
Melting point ℃	31	20-25	23	23
Density kg/m^3	890	1126	831	777
Cost ($/kg)	85.8	72.8	100	485

In this study, PEG 600 was chosen for thermal energy storage due to its large range of the melting temperatures with suitable ranges for thermal comfort in buildings, low cost and it has a better availability than others [162]. The specific heat capacity curve, illustrating the effective performance of the chosen PCM wallboard and the properties associated with this PCM material, is detailed in Section A 3. The PCM wallboard employed in this investigation has a melting temperature of 22.5°C [172]. Consequently, the temperature range for computing the average thermal capacity was established from 19°C to 24°C. This specific range was deliberately selected to comprehensively capture the PCM's behavior during its phase change process. Encompassing the PCM's phase change temperature, it accurately reflects the thermal storage and release characteristics of the material. The chosen temperature range holds significance not only for its alignment with the indoor temperature setpoints aimed at ensuring thermal comfort

within the building but also for its correlation with the temperature fluctuations observed in the test pod, as indicated by the experimental data.

The PCM layers were assumed to be added to the walls, excluding the floor construction and the north wall, where heating pipes and windows were situated. The PCM layer was primarily placed on the inner surface behind a 45mm plywood panel, with a thickness of 25mm, as illustrated in Fig. 6-5. Type 1270 was employed to simulate the PCM layers.

In this chapter, four Type 1270s were utilised to simulate the integration of PCM wallboards in the west, east, south walls, and the roof. The intricate TRNSYS platform is detailed in appendix A4. The component in TRNSYS used to model the PCM layers (Type 1270) presumes that the temperature of the PCM material remains constant, with a steady specific heat capacity in its solid and liquid states. The theoretical underpinnings of the PCM material in TRNSYS are discussed in reference [134].

Solid state

$$T_{t+1} = T_t + \frac{Q_1 + Q_2}{m_{PCM} Cp_{solid}} \quad \text{eq 6-2}$$

Liquid state

$$T_{t+1} = T_t + \frac{Q_1 + Q_2}{m_{PCM} Cp_{liquid}} \quad \text{eq 6-3}$$

Q_1 and Q_2 are the energy going from two sides of the PCM layers, i.e., adjacent wall layers, Cp_{solid} and Cp_{liquid} are the heat capacity of the solid and liquid states.

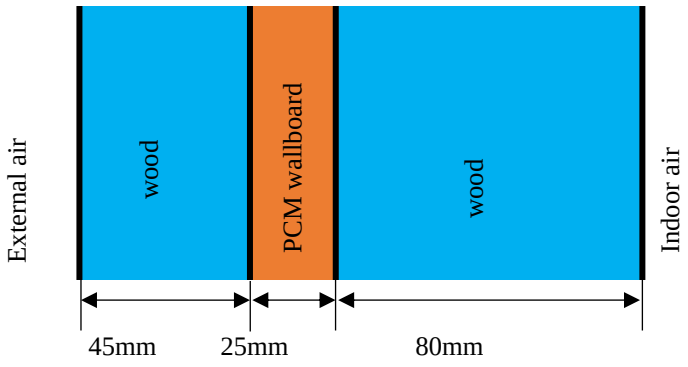

Fig. 6-5 PCM wallboard integration into the building wall [162]

The validation of the TRNSYS Type for PCM was conducted using the Polyethylene glycol 600 experiment from Ahmad et al.'s study [162]. By inputting the same weather conditions, the indoor temperature obtained from the TRNSYS simulation was compared with their experimental results. The detailed wall layers of the test cell were presented in appendix A5. The comparison of indoor temperatures confirmed a root mean square error (RMSE) of 1.73°C. Moreover, when comparing it with the original test pod, the integration of PCM resulted in a reduction of indoor temperature fluctuations from 45°C to 25°C. This finding is consistent with the validated case study. Further validation details can be found in appendix A5.

6.1.5 MPC system

6.1.5.1 RC representation of the room model

In building room RC model, the temperature nodes encompass indoor air, floor, roof, internal surface of walls, and external surface of walls. The detailed RC representation is elucidated in appendix A6.

For the room integrated with a PCM wallboard, the average effective specific heat capacity method was applied proposed by Yang et al. [100]. Generally, the correlation between the effective specific heat capacity and the temperature of the PCM wallboard is nonlinear. However, Yang et al. [100] addressed this issue by employing an averaged effective specific heat capacity over a common temperature range (e.g., 19 - 24 degrees) to mitigate the nonlinearity in the PCM numerical model. Consequently, the RC representation of the PCM wallboard can be expressed as follows:

$$\frac{dT_{pcm}}{dt} = \frac{T_{w,ext} - T_{pcm}}{R_{pcm,ext}C_{eff,ave}} + \frac{T_{w,int} - T_{pcm}}{R_{pcm,int}C_{eff,ave}} \quad \text{eq 6-4}$$

T_{pcm} is the temperature of the PCM wallboard node, $T_{w,ext}$ and $T_{w,int}$ are the temperature of external wall surface and internal wall surface. $R_{pcm,ext}, R_{pcm,int}$ are the thermal resistance between PCM wall layer and external wall, internal wall layers. $C_{eff,ave}$ denotes to the average thermal capacity of PCM wallboard. Please note that the detailed expression and derivation of the RC representation for the PCM wallboard are provided in appendix A7. With the RC representation showed in Fig 6-6a. The whole RC model of room integrated with PCM wallboard is shown in appendix A7.

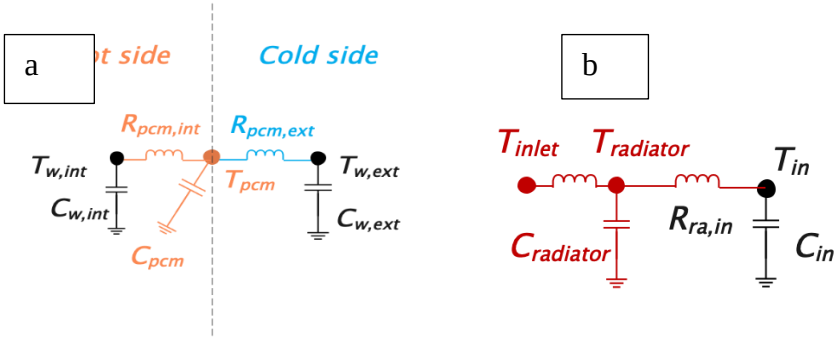

Fig. 6-6 (a) PCM wallboard RC representation (b) RC representation of radiator system

6.1.5.2 RC representation of the room heating system

To accurately model the radiator system, a virtual inlet point in the radiator model is created to account for the hysteresis of the system (Fig. 6-6b). The radiator was numerically represented as a single-node grey-box model, where the node temperature is influenced by the indoor temperature, mass flow rate, and fluid inlet temperature [163]. Subsequently, the radiator node was integrated into the room state-space model identification using Equation 4, where $T_{ra}, T_{in}, T_{inlet,ra}$ denote the temperatures of the radiator node, indoor air node, and virtual inlet water node, respectively. The thermal resistances between the radiator and indoor air $R_{ra,in}$ and between the inlet water and radiator $R_{inlet,ra}$, as well as the thermal capacitance of the radiator C_{ra}, were considered in the model. The complete RC model of the indoor air heated by radiators is presented in appendix A6.

$$\frac{dT_{ra}}{dt} = \frac{T_{in} - T_{ra}}{R_{ra,in}C_{ra}} + \frac{T_{inlet,ra} - T_{ra}}{R_{inlet,ra}C_{ra}} \qquad \text{eq 6-5}$$

In the UFH heating system, a simplified approach was adopted where the entire pipe plane is represented as a single lumped node that receives heat from the inlet hot water [17]. Subsequently, the heat gradually transfers from the pipeline to the floor element, and this process is mathematically described by equation 6-5. $T_{pp}, T_{fl}, T_{inlet}$ represent the temperatures of floor, pipeline and inlet water. $R_{pp,fl}, R_{inlet,mean}, R_{mean,pp}$ are the thermal resistance of pipeline surface and floor element, inlet water and mean point of pipeline, mean point of pipeline and pipe surface. Furthermore, C_{pp} is the thermal capacitance of the heating pipes. The complete RC model of the indoor air heated by the UFH system can be found in

appendix A7, providing a comprehensive representation of the interconnected relationships and heat transfer dynamics within the system.

$$\frac{dT_{pp}}{dt} = \frac{T_{fl} - T_{pp}}{R_{pp,fl}C_{pp}} + \frac{T_{inlet} - T_{pp}}{(R_{inlet,mean} + R_{mean,pp})C_{pp}} \quad \text{eq 6-6}$$

6.1.5.3 Optimisation algorithm

The governing equations then can be represented by the states, inputs, disturbances and system matrix of state space (ss) model.

$$\dot{x}(t) = Ax(t) + Bu(t) + w(t) \quad \text{eq 6-7}$$

A, B are system matrices. x is the system state. u is the system input. $A \epsilon R^{m\times n}$, $B \epsilon R^{n\times m}$, $u(t) \epsilon R^{m}$. $w(t) \epsilon R^{n} \sim \mathcal{N}(0, \Sigma)$ is the process noise. In this study, the number of states n is 5 ($T_{w,ext}$ $T_{w,int}$ T_{in} T_{fl} T_{ra}) for original radiator system and is 6 ($T_{w,ext}$ T_{pcm} $T_{w,int}$ T_{in} T_{fl} T_{pp}) for PCM and UFH system. The number of inputs m is 3. The input vector includes outdoor temperature T_o, global solar radiation I_{solar} and the inlet fluid temperature of the radiators/UFH system $T_{ra,inlet}/T_{inlet}$. Later, a discrete-time model was formed of the continuous-time system for prediction of future states in prediction horizon N (eq. 6-7):

$$x^k = [A_d \;\; B_d]\begin{bmatrix} X^{k-1} \\ u^{k-1} \end{bmatrix} + E^{k-1} \quad \text{eq 6-8}$$

Where, E is white zero mean Gaussian noise. Because of the Kalman filter integration, E equals to 0 was assumed. k is the current time step. After that, the indoor temperature can be extracted from states through equation (6-6)-(6-8) by introducing another system matrix C equals to $[0 \;\; 0 \;\; 1 \;\; 0 \;\; 0]$ or $[0 \;\; 0 \;\; 0 \;\; 1 \;\; 0 \;\; 0]$ depending on which system is used.

$$y^k = Cx^k \quad \text{eq 6-9}$$

In which y represents the final ss system output. Once state-space (ss) model was obtained, the MPC strategy was formulated by defining the objective function, incorporating the identified ss model, and establishing relevant constraints. The primary aims of the MPC approach were to minimise heating energy consumption while ensuring indoor thermal comfort. To achieve this, indoor thermal comfort set as a constraint, penalising any deviations from the desired comfort levels within the objective function. The structure of objective function was designed as quadratic forms, allowing objective function to appropriately weigh each term. Notably, significant weight was signed to the comfort violation term, underscoring the paramount importance of precise comfort control.

$$J = min \sum_{k=0}^{N-1} a_k^T \, q \, a_k + b_k^T \, r \, b_k \qquad \text{eq 6-10}$$

With the constraints:

$$y_{r,k} - y_k - a_k \leq 0, a_k \geq 0 \qquad \text{eq 6-11}$$

$$y^k = C(A_d x^{k-1} + B_d u^k) \qquad \text{eq 6-12}$$

In this study, the prediction horizon N is set to 24 with a time interval of 30 minutes. weighting factors are q and r to quantify the importance of each term, where a_k represents comfort violation, and b_k represents heating energy cost. Table 6-1 provides a concise summary of the various modules utilised in the MPCs of this investigation.

Table 6-2 Summary of different modules of proposed MPC

Modules		Descriptions
Objective function		Equation (6-10)
Constraints		Equation (6-11)-(6-12)
Original pod model	Building	Equation A1–A5 in appendix A.6
	Radiator	Equation (6-5)
PCM wallboard model	Building	Equation A6–A11 in appendix A.7
	PCM wallboard	Equation (6-4)
	Floor heating system	Equation (6-6)
State estimator	Kalman filter	Described in chapter 3
Dynamic pricing		Described in section 6.1.2
Disturbances		MPC inputs, described in section 6.1.5

6.2 State space model validation

To establish the system models, ss model was created combining room's thermal characteristics with a sufficient amount of measured data. For model identification, a two-day dataset was utilised, while another day's data was reserved for validation purposes. "ssest" function was employed in MATLAB to identify the state-space (ss) model. The validation dataset yielded a percentage fitness [119] of 77%, indicating a satisfactory match between the identified model and the validation data.

Furthermore, a comparison between the measured indoor temperature and the ss-estimated indoor temperature was conducted, using the "compare" function in MATLAB. As shown in Fig 6-7, the results exhibited a RMSE of 0.89 ℃, confirming the accuracy and reliability of the identified ss model's predictions.

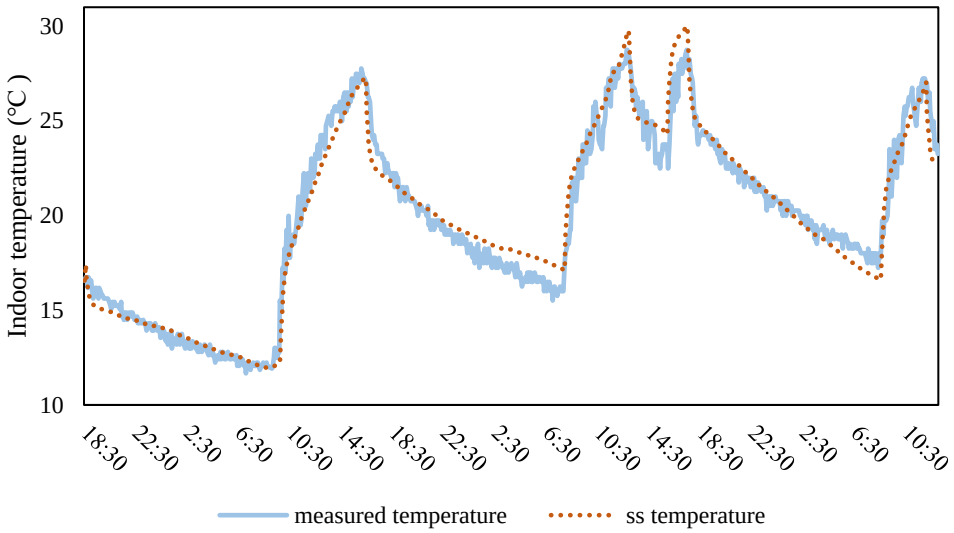

Fig. 6-7 Indoor temperature comparison between ss model and measurement

The state-space model employed for the PCM system was trained using TRNSYS output data. The training dataset consisted of 1500 data points collected at 30-minute intervals from 1st October. For validation, a separate dataset was used containing 1000 data points collected at the same 30-minute intervals from 1st November.

To assess the performance of the ss model, the indoor temperature predicted was compared by the model with the corresponding TRNSYS output data, as depicted in Fig 6-8. The value of R-Square [27], which signifies the proportion of output that can be explained by the inputs in the ss model, was found to be 0.792. Moreover, the model demonstrated good accuracy, with 92% of the predictions falling within a range of ±1℃ from the actual temperature readings. This high level of accuracy and goodness-of-fit in the model's predictions validates its effectiveness in simulating the PCM system's indoor temperature dynamics.

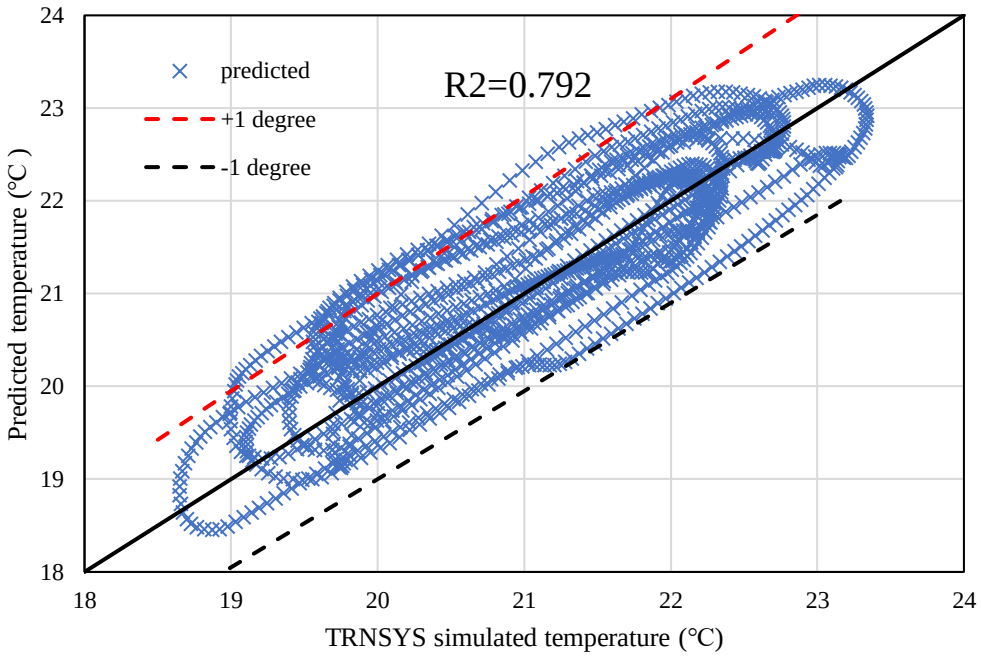

Fig. 6-8 Validation of PCM room model with TRNSYS data

6.3 Results and discussion

This section showcases the time-dependent control performance of the IoT-based MPC strategy implemented in the case study pod. The measured indoor temperature achieved through the proposed MPC was compared with the simulated indoor temperature obtained using the traditional on/off control strategy in TRNSYS. This comparison was conducted to evaluate the MPC's effectiveness in achieving higher energy shifting performance and optimising low-price energy usage. Additionally, the energy usage performance of the PCM system controlled by the low-cost MPC was presented, simulated through co-simulation of TRNSYS and MATLAB. This performance was compared with that of the PCM system controlled by a conventional on/off control strategy. Furthermore, the hourly energy shifting performance and indoor comfort violation under both control strategies was evaluated to gain insights into their respective efficacy.

6.3.1 Feasibility and cost-effectiveness of the proposed MPC strategy: computation time and resource analysis

To assess the feasibility of the proposed MPC strategy, a single loop of the MPC implementation was conducted in the case study room. Fig 6-9 illustrates the computation time for each process involved in implementing the proposed MPC.

An example of the MATLAB command window on a PC with Intel Core i5-10300H 2.5GHz for one control signal implementation is provided in appendix A8 Fig A9. The total computation time amounts to approximately 3.6 seconds, significantly shorter than both the prediction interval and the control interval of 30 minutes. This indicates that the proposed MPC is well-equipped to meet its objectives.

A more detailed evaluation of the CPU time allows for the distinction of six different consumption phases. The first two phases have relatively shorter CPU consumption times, averaging 0.16 seconds. In these phases, the calculation process and online data extraction have not yet commenced, with only data from the PC's serial portal being read by the MATLAB engine and initialisation being performed. In the third phase, the calculation still hasn't started, and the entire CPU usage is dedicated to extracting online weather forecasts for the following hours and the day-ahead dynamic price. This phase takes 0.28 seconds. Subsequently, after all preparations are completed, the MPC calculates the control signal responsible for the next half-hour and sends it via WiFi. These two phases last for 3.01 seconds. Finally, the Kalman filter efficiently corrects the current state based on the measured temperature feedback.

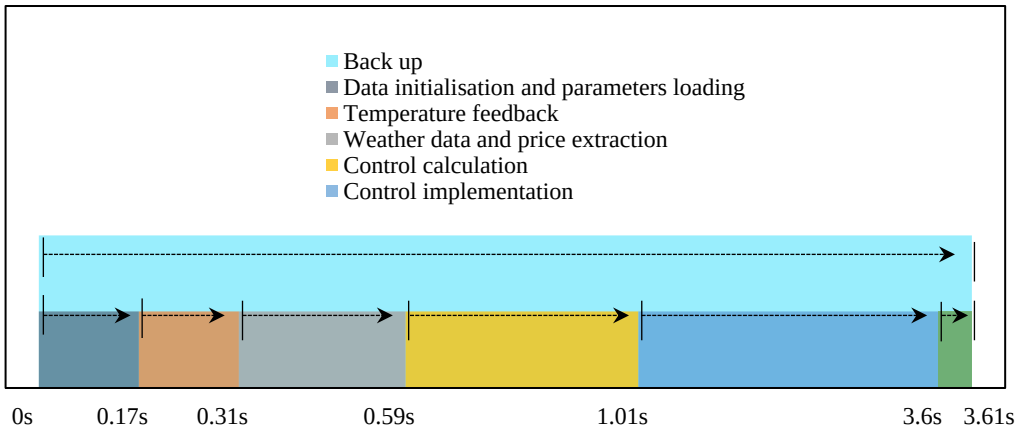

Fig. 6-9 CPU used time by MATLAB for each process

Based on the measurements, the primary CPU consumption arises from the calculation and implementation of the control signal based on the collected data. Traditionally, data storage in control systems faces limitations in capacity, necessitating periodic data saving and resetting [116]. However, IoT technology offers a solution by enabling data extraction and overwriting in each loop, with

online data transmission for storage and exchange. Moreover, the lightweight nature of the proposed control strategy prevents connection loss between elements.

Cost is another crucial consideration for widespread adoption of IoT-based control systems in the building sector. Typically, intelligent control systems come with high capital costs due to the scale of their implementation [116]. According to Jáñez et al.'s study [164], the capital cost for typical information and communication technologies (ICT) for a single house ranges from £260 to £860, depending on the number of devices installed. In this study, MATLAB R2017b with MATLAB support package for RPi was used, Raspberry Pi 3 Model B+, a smart plug with RPi add-on board, and an Arduino R3 board with a MAX6675 K-Type thermocouple. The total cost for the system is £110, and this includes the control system. Notably, most available ICT options do not account for intelligent control systems [164]. Furthermore, proposed system easily accommodates further integration of smart sensors, such as humidity and atmospheric pressure, or additional smart elements, like microcontrollers, microSD cards, and OLED screens [116]. These additional components do not significantly increase the overall cost, making the system even more cost-effective as its complexity expands.

6.3.2 Efficiency and cost-effectiveness of the MPC strategy

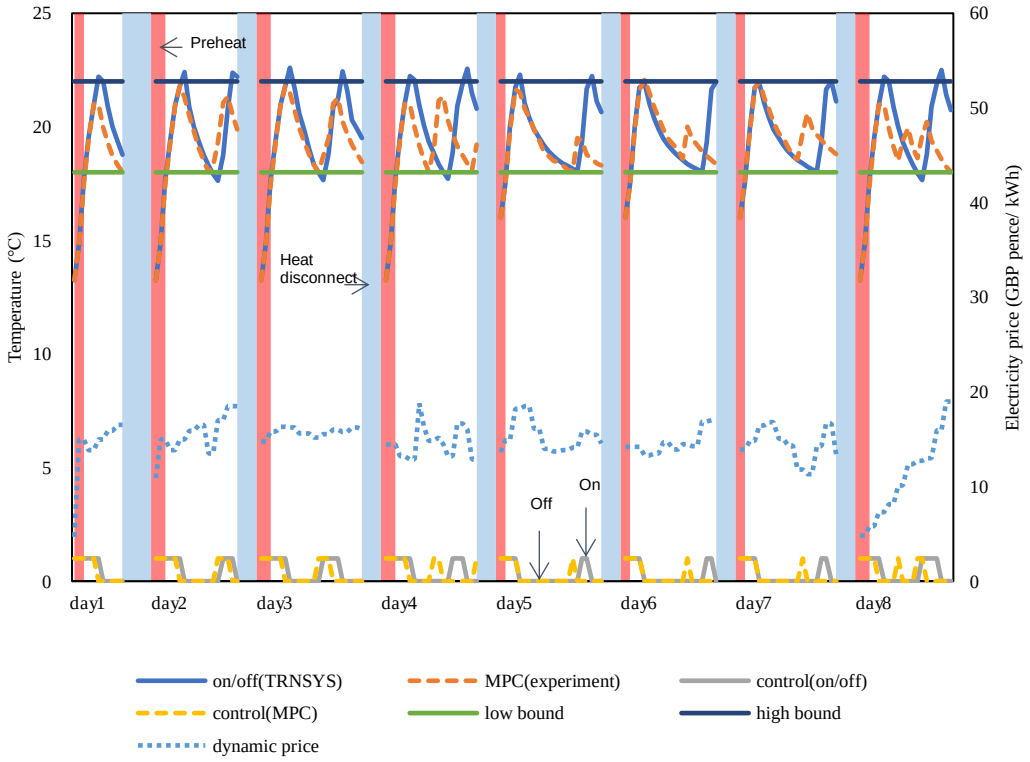

Fig. 6-10 Energy performance of proposed MPC and on/off (TRNSYS)

To assess thermal comfort violations, cross-validation root mean square error (CVRMSE) was used for both the MPC and conventional on/off controller. The CVRMSE is 0.006 for the on/off controller and 0 for the MPC, considering the indoor temperature's lower bound during preheating. The passive nature of the case study room, with high thermal inertia, results in stable indoor temperature even under the on/off controller. However, the MPC strategy effectively avoids comfort violations by making predictions several hours ahead and preheating the room before the temperature drops below the setpoint. For example, on day 4 (Fig. 6-10), the MPC anticipates the temperature drop and turns on the heating at noon, while the on/off controller only activates at the setpoint temperature. This capability of the MPC aligns with findings from other studies [93, 104] even in lightweight constructions where the on/off controller exhibits significant comfort violations [98].

The proposed MPC strategy is designed as a price-responsive control approach, aiming to optimise energy usage by shifting consumption to low-price periods and avoiding peak-time energy consumption. Throughout the simulation periods, the average electricity price is recorded as 14.5 GBP pence/kWh. In comparison, the traditional on/off controller uses the average price of 14.4 GBP pence/kWh for room heating. The MPC controller, on the other hand, effectively reduces the electricity price to 13 GBP pence/kWh, saving 1.4 GBP pence/kWh in energy costs when compared to the on/off controller.

The MPC demonstrates a preference for utilising relatively low-price energy, as illustrated in the following examples. On day 1, the MPC predicts the indoor response for the upcoming hours and identifies optimal turn-on hours for the heating system to avoid additional energy usage while maintaining indoor thermal comfort until the daily heat disconnecting time. Over the course of days 1 to 8, the MPC strategically selects morning or early afternoon periods for electricity usage, rather than utilising high-price electricity in the late afternoon, as the on/off controller does.

The overall heating hours for the on/off controller amount to 61 hours, whereas the MPC controller reduces this to 51 hours. As a result, the total electricity cost for the on/off controller is 1284 GBP pence for the simulation periods, while the MPC controller reduces this cost to 1038 GBP pence. This substantial reduction in

electricity cost confirms the successful energy-efficient performance of the proposed MPC strategy in this study.

6.3.3 Comparative analysis of indoor temperature control: conventional vs. MPC with PCM integration

This section presents an analysis of indoor temperature control under three different scenarios: conventional on/off controller, conventional MPC controller, PCM layers integrated in the building envelope under on/off controller, and PCM layers integrated in the building envelope under the proposed Model Predictive Control (MPC) approach. The simulations were conducted over a 20-day period, and the statistical room air temperature distributions for each scenario are depicted in Fig 6-11. The average indoor temperatures for the original setup, conventional MPC, PCM integration under on/off control, and PCM integration under MPC were found to be 21.18℃, 20.86℃, 20.99℃, and 20.81℃, respectively, with corresponding standard deviations of 1.19℃, 0.37℃, 1.16℃, and 0.39℃ (Fig 6-11a).

Notably, the proposed MPC approach demonstrated a higher level of precision in maintaining indoor air temperature within a narrower range compared to the two conventional controls. This improved thermal comfort performance can be attributed to the MPC's predictive optimisation capability, which effectively kept the room air temperature within the indoor setpoints throughout the simulation period, unlike the other two controls that resulted in high comfort violations (Fig 6-11b).

Furthermore, the cases of MPC exhibited lower average indoor temperatures than the other two scenarios. This deliberate maintenance of a lower room air temperature is a strategic measure to reduce electricity consumption, thereby minimising electricity costs as per the MPC's objective. This finding aligns with similar studies by Yang et al. [100].

The proposed MPC approach demonstrated enhanced indoor temperature control with narrower fluctuations and reduced comfort violations compared to conventional on/off controllers, even with PCM integration in the building envelope. The MPC's ability to optimise energy usage based on predictive models contributes to its enhanced thermal comfort performance and cost-efficiency.

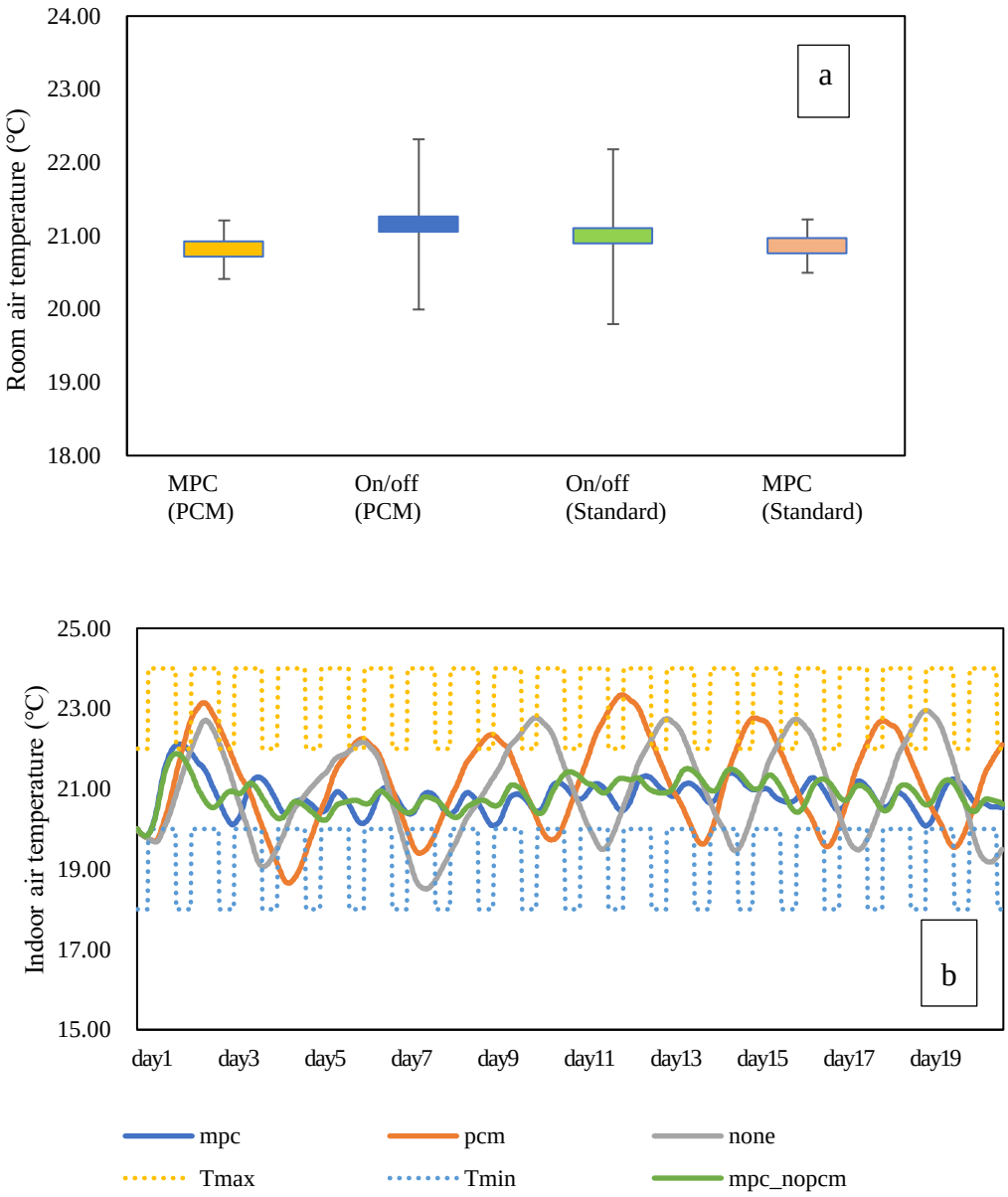

Fig. 6-11 (a) Average room air temperature with error bar (b) hourly room air temperature for three scenarios

6.3.4 Impact of PCM wallboard integration on energy costs and efficiency in building envelopes

The integration of PCM wallboard into the building envelope has shown promising results in reducing electricity costs, even under conventional control strategies. The increased thermal energy storage capacity provided by the PCM layers leads to improved energy performance in lightweight buildings [165]. This study further confirms the significant energy savings achieved by PCM integration, even in passive houses (Fig. 6-12b). Moreover, by replacing the conventional on/off

controller with the proposed Model Predictive Control (MPC) approach, additional energy cost savings were realised.

The optimised operation of energy shifting is depicted in Fig. 6-12a, comparing the building with PCM wallboard integrated under conventional on/off control and the price-responsive MPC control. Leveraging its predictive nature, the MPC controller strategically activates the heating system during low-price hours to meet room heat consumption when electricity prices are high. Fig. 6-12(a) highlights some preheating hours, illustrating the strong correlation between electricity prices and the availability of renewable energy sources in the global electricity market. The results indicate that the proposed MPC efficiently charges thermal energy into the building envelope during periods of excess power generation and disconnects the heating system during renewable energy shortages. This energy shifting benefit through preheating has also been demonstrated in the study by Golmohamadi et al. [166].

(a)

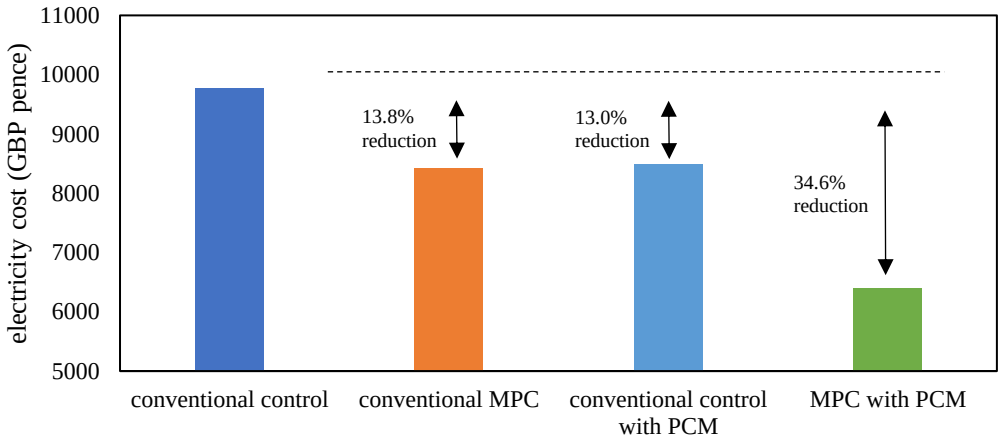

(b)

Fig. 6-12 (a) Heating consumption of UFH system in price responsive and non-responsive states (b) total electricity consumed by heat pump for four cases

It is essential to consider different transition temperatures of PCM materials, as they significantly impact indoor thermal comfort and thermal demand. Hysteresis and subcooling effects affect the energy storage and release characteristics of PCM materials, especially during rapid temperature changes or extreme weather conditions. A parametric analysis of PCMs can identify the optimal type, melting temperature, latent heat capacity, thickness, and configuration for specific buildings and climate conditions, maximising the thermal benefits and demand response potential of the integrated system. For instance, Jayalath et al. [23] analysed PCM materials with different transition temperatures in various outdoor temperature conditions for two climates (Sydney and Melbourne). The study found an optimal transition temperature of 23 degrees, which maximised indoor comfort periods in both climates for the same type of free-running residential building. Furthermore, the study highlighted those different materials offered distinct energy savings, depending on the preference for reducing either building heating load or cooling load. Similar results have been observed in other studies [165].

In this simulation, the PCM's transition temperature was set at 25℃, effectively achieving energy savings and maintaining indoor comfort during a simulation period with outdoor temperature variations ranging from -2℃ to 14℃, with an average outdoor temperature of 5.7℃. This information suggests that with the proposed strategy and specific PCM materials, which can vary in thickness and melting temperature, feasible retrofitting options such as BioPCMs [167] can be

explored, enabling optimal control strategies tailored to different renovation objectives under varying climates.

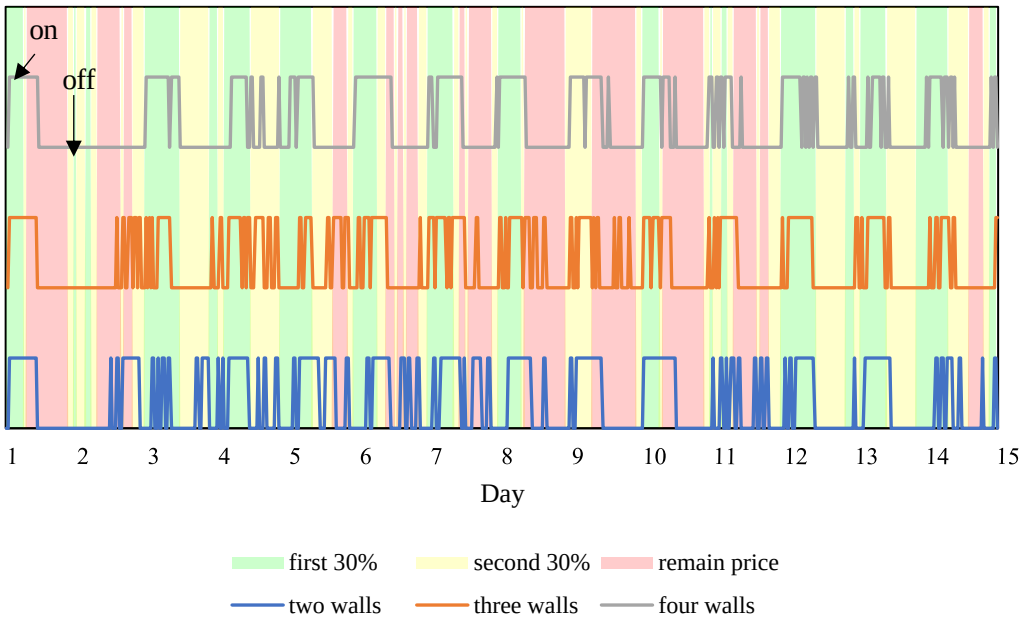

Fig. 6-13 Heating system schedules under different PCM amount integration

Subsequent to the initial integration of PCM wallboards into all four walls of the building, further experiments were conducted, gradually reducing PCM integration to three walls and eventually two walls. The outcomes of these scenarios are presented in Fig. 6-13. The electricity prices were categorised into three segments: the first 30% representing relatively low prices, the second 30% indicating medium prices, and the remaining 40% reflecting relatively high prices. Analysing the impact on energy costs, the average electricity price used for rooms with two PCM wallboards integration was 28.4 GBP pence/kWh, while for three PCM wallboards integration, it was 27.3 GBP pence/kWh, and for four PCM wallboards integration, it reduced to 25.8 GBP pence/kWh. It is essential to note that these average dynamic prices are specific to the simulation period. The average consumed electricity price decreased with an increase in the number of PCM wallboard integrations. Examining the timing of heating system switch-on (Fig. 6-13), the building with four PCM wallboards exhibited the lowest likelihood of consuming high-priced energy. This can be attributed to the higher energy storage capacity of the building envelope resulting from increased PCM integration. Consequently, it utilised low/medium electricity priced energy to charge the building construction during most periods with high electricity prices. These results align with findings from the

study by Yang et al. [100], which demonstrated that an increased PCM wallboard thermal storage capacity enhanced electricity cost savings for space heating systems due to the higher energy flexibility offered by increased PCM amounts.

PCM integration has shown the potential to enhance the thermal performance of building envelopes without necessitating significant structural modifications or expansion. In this study, the UFH system was applied, which is inherently energy-efficient. The addition of PCMs further improved energy performance by providing thermal storage capabilities. Leveraging the proposed predictive control strategy, energy consumption can be shifted from peak to off-peak periods by utilising the thermal storage capacity of PCMs within the UFH system. Overall, the integration of a 25mm PCM wallboard in the building envelope resulted in a remarkable 35% thermal energy cost reduction compared to the reference case. This indicates the complementary nature of these technologies and their potential synergistic effects. Furthermore, the findings showed that such renovations outperformed a similar system in previous study [98], where an additional 150mm construction in a lightweight building contributed to approximately 50% thermal energy cost reduction, and further thickness failed to yield significant cost savings. The current study's results emphasise not only the additional thermal energy cost savings achievable with PCM wallboard integration in a passive house but also the cost-effectiveness of a narrower PCM wallboard thickness compared to traditional building envelope materials. Consequently, PCM wallboard integration holds significant promise as a crucial strategy for future building renovations.

Future work should explore the impact of PCM wallboard integration in other types of buildings and in different climatic conditions to assess the generalisability of the findings. Also, while this study examined the effects of integrating PCM wallboards into all, three, and two walls, further research should investigate scenarios where only one wall or none of the walls is integrated with PCM wallboards, providing a more comprehensive understanding of its effects on energy consumption and cost savings. Also, a detailed cost-benefit analysis considering the cost of PCM wallboards and their installation would provide more realistic insights into the economic viability of this technology. Moreover, while the model used a particular type of PCM, it would be interesting to investigate the effects of different PCMs with various phase change temperatures, thermal conductivities, and thermal storage capacities. It would also be beneficial to study the long-term performance

and durability of PCM wallboards, including their potential degradation over time and the impact on energy savings. Finally, integration with other renewable energy sources, like solar panels, can be considered to optimise the overall building energy performance, making the building even more sustainable and resilient against future energy price fluctuations.

6.4 Summary

This chapter has established a novel monitoring and control framework through the integration of a MPC system with IoT technology. Designed to precisely monitor environmental conditions within buildings and subsequently relay control signals to the building's heating system, this system has demonstrated considerable promise in improving energy efficiency and cost-effectiveness. The system was tested through a series of simulations and practical experiments in a passive house standard pod at the University of Nottingham, yielding results that confirm both the lightweight and cost-effective nature of this intelligent control system. The inclusion of PCM wallboards within the building envelope was explored as an additional variable within the study. This model validates the viability of integrating the MPC system with PCM wallboards, despite the increased complexity this presents.The critical insights gained from results can be synthesised into the following key conclusions:

• The proposed MPC system demonstrated the ability to maintain indoor temperature control, reacting within mere seconds to real-time temperature feedback.

• The capital expenditure for implementing the MPC was found to be approximately half that of conventional ICT devices, presenting a cost-effective solution for building management.

• The MPC system predicted temperature trends hours in advance and adjusting controls to avoid comfort violations.

• Substantial cost savings were realised through the strategic use of the MPC system. By shifting energy usage from peak periods to off-peak periods, based on real-world wholesale electricity market data, a 20% reduction in electricity costs was achieved over an eight-day experimental period.

• In a scenario where conventional control systems could not maintain indoor thermal comfort, the proposed MPC system, integrated with PCM wallboards, proved to be a feasible and effective solution. Under the control of the proposed MPC strategy, the building integrated with PCM wallboards demonstrated electricity cost saving of 35%.

The result underscores the viability of an IoT-based MPC strategy as an effective and innovative approach to enhancing energy efficiency and thermal comfort in building heating systems. This presents a compelling alternative to the traditionally high-cost intelligent control systems employed in the building sector. However, to further evolve this IoT-based MPC strategy, more research is necessitated.

Future work should focus on broadening the scope of MPC experimentation across diverse types of heating systems. This line of research opens up a multitude of avenues, all aimed at optimising energy management systems and elevating building thermal comfort based on IoT technology.

One such promising path involves exploring the integration of additional monitoring sensors, such as computer vision sensors. When working in harmony with the existing intelligent data fusion system, these could further enhance the overall sustainability and effectiveness of the residential smart grid.

In addition, the application of MPC in controlling PCM wallboards reveals another exciting area of research. The MPC system acknowledges the storage features and capacities of PCM wallboards, providing a more robust approach to handle uncertainties in building construction, particularly when PCM is involved.

The results suggest that the proposed MPC could be further refined or expanded to accommodate a wider variety of building materials. Moving forward, it is critical to understand the scalability of the proposed system across an extensive range of PCM wallboards. Each variant of PCM wallboards may pose unique challenges and offer distinct opportunities for energy management. Investigating these potential paths will undoubtedly push the boundaries of short-term energy storage (STES) in the building sector. Furthermore, such exploration is set to make substantial contributions towards the development of cost-effective and lightweight intelligent building energy control systems. This area of study, integrating modern control strategies with emerging material technology, holds the key to unlocking new levels of efficiency in the built environment.

In this study, the CPU time required for the proposed MPC implementation was 3.6 seconds. To further minimize this duration, additional equipment and software may be introduced. An illustrative study [76] utilized cRIO real-time controllers and LabVIEW software. In this setup, LabVIEW handled the logging of sensor data and updating the thermostat setpoint, calculated from MPC in MATLAB. The cRIO real-time controllers managed data acquisition. To enable remote access, an IoT platform could transmit information via WiFi from the microcontroller through a router to the cloud [116]. LabVIEW was scheduled to invoke MATLAB at every control interval to execute the MPC calculation with updated sensor data and weather forecasts (Fig 6-14). This approach led to a more focused CPU utilization on MPC calculations, thereby reducing the CPU time to 0.42 seconds. However, the introduction of additional embedded equipment is costly, significantly higher than our low-cost system.

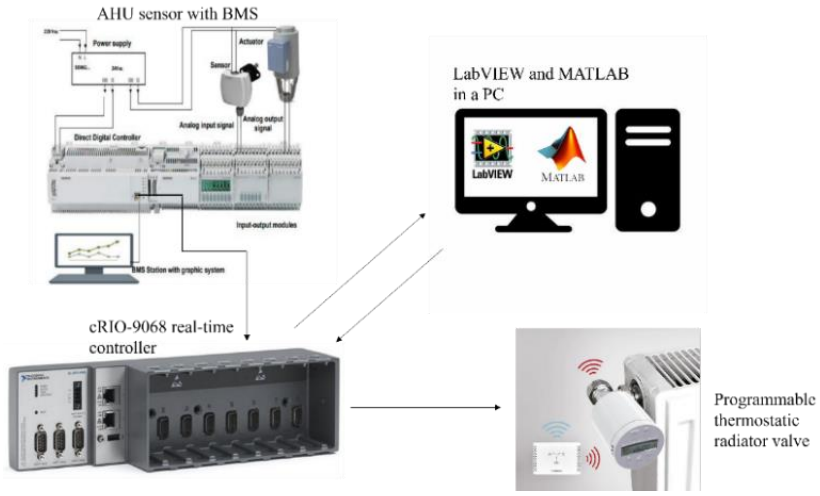

Fig. 6-14 intelligent MPC applied on existing BMS

7. Conclusion and future works

7.1 Conclusion

The present work provided a computational method and comprehensive experimental to assess MPC in controlling different building-integrated systems for thermal energy shifting and provide a low-cost design of building intelligent MPC control strategy. The main conclusions of thesis are presented thereafter, numerically linked to the defined objective of Chapter 1:

1. The first part of thesis investigated the impact of building configuration and operation on a low-temperature heating energy storage performance. The configurations explored included the building thermal mass, under-floor heating inlet temperature, heating setpoint strategy, occupancy patterns and internal heat gains. A coupled modelling approach was introduced, which simulated a building with STES and a price responsive model predictive control (MPC). The model was verified/validated against numerical and experimental data, and good agreement was observed between the results.

   The result firstly confirmed the ability of MPC in controlling low temperature UFH system in both increased indoor thermal comfort and energy saving. Later, the scenarios analysis indicates that the MPC's performance would varies under different building system characteristics. Mediumweight thermal mass and a medium-temperature (45\degc) under-floor heating inlet temperature provided a higher energy shifting ability under a price-responsive MPC control strategy. Besides, a high tolerance setpoint strategy during unoccupied periods showed that a higher thermal energy storage performance could be achieved by the building's thermal mass. Finally, based on the simulated case study and conditions under future scenario, the result showed that higher low-price energy usage and lower heating energy usage could be achieved in future climate conditions.

   In the simulation of MPC controlling energy system for building with highly variable occupancy, the results confirmed that the MPC displays the capacity to accurately forecast daily occupancy patterns, subsequently selecting a timely initiation of the heating system prior to the arrival of students. The MPC is able to regulate indoor temperature in response to fluctuating occupant presence within the day by discerning instances of preheating prior to the day's peak times, thus orchestrating a consumption of electricity energy that primarily falls within the lower to medium price range.

2. Regarding MPC controlling the integration of the building system with solar renewable technologies. The simulation of the capability of a building integrated PV system to enhance the performance of passive building energy storage technology showed that an increase in the energy shifting ability could be achieved with the addition of the solar PV system.

The simulation results of a price responsive MPC strategy for a solar thermal heating system with thermal energy storage (TES) shows that the implementation of MPC in managing an integrated solar hot water and under floor heating system demonstrated a significant reduction in energy costs, with savings reaching up to 50% compared to a reference case. The system controlled by MPC presented a 58% utilisation of low to medium-priced energy, a significant improvement from the conventional system, which showed only a 33% utilisation in the same price range. Finally, the MPC control strategy, paired with an active water storage system, managed to reduce the switch-on hours by half of the reference case. This, coupled with the exploitation of solar thermal storage, reduced total electricity costs during the simulation period by half compared to the reference case.

The simulation results prove the viability of an integrated solar system with an MPC control strategy as a promising approach to enhancing the energy efficiency and thermal comfort of building heating systems, making it an attractive solution in the face of fluctuating energy prices and varying occupancy patterns. In another aspect, the results open numerous avenues for future research in the realm of optimising energy management systems and elevating building thermal comfort.

3. The simulation of MPC controlled building with PCM wallboard integration was conducted through co-simulation of TRNSYS and MATLAB. The simulation results compared with the performance of PCM controlled by a conventional on/off control strategy. The hourly energy shifting performance along with indoor comfort violation were assessed under two control strategies.

   The results confirmed the proposed MPC is feasible in controlling PCM wallboard integrated in building envelope in the case of conventional control cannot maintain indoor thermal comfort. Besides, the building integrated with PCM wallboard could save around 35% electricity cost under proposed MPC control strategy.

   The development of the proposed MPC on controlling PCM wallboard present another promising area of the research. MPC realised the storage feature and capacity of PCM wallboard, which becomes a more robust

approach to handling uncertainties on building construction, especially for PCM. The result indicated the proposed MPC could be refined or expanded to account for a broader spectrum of building materials.

4. An IoT-based MPC strategy was experimentally conducted in a case study pod. The proposed system was simulated in a passive pod at the University of Nottingham and obtained the results both from experiments and simulations. The measured indoor temperature of the proposed MPC and the simulated indoor temperature by traditional on/off control strategy simulated in TRNSYS was compared towards a higher energy shifting performance and low-price energy usage.

   The comparison between two strategies confirmed the proposed MPC is able to control the indoor temperature in short seconds with real-time temperature feedback. Besides, the capital cost for the MPC was proven to be half of that of usual ICT device. Overall, the proposed MPC avoid the indoor comfort violation by the prediction of indoor temperature in few hours ahead. The electricity cost saving has been confirmed for using the MPC through energy shifting from peak periods to off-peak periods bases on a real-world electricity wholesale market. The total saving reached 20% for eight-day experiment.

   Results prove the viability of an IoT-based MPC strategy as a promising approach to enhance the energy efficiency and thermal comfort of building heating systems, making it an attractive solution in the face of costly intelligent control system in building sector.

7.2 Contribution to knowledge

This thesis evaluates the impacts of occupancy, thermal mass, water temperature, setpoint strategy and climate change for building energy performance under MPC controlled UFH system. These aspects haven't been analysed in previous studies. Besides, the results of this study point out the potential of energy storage by building thermal mass without any active storage installation. The findings help the

government that plan to renovate the building structure for a more efficient energy supply.

Besides, advanced building-integrated solar energy systems were developed. The first coupled system triggers the STES storage by a proposed MPC control strategy, which automatically shift the high-price energy to low-price periods and give priority of self-supply PV electrical energy by preheating the building structure. The second coupled system consist of a solar hot water system and an active water storage tank was proposed to supply the building heating energy through floor heating (UFH) system. These help identify to what extent the self-supply renewable energy source in saving building thermal energy and energy shifting.

There is a significant gap in the existing body of research regarding the practical, field implementation of MPC strategies in the building sector, particularly those that are cost-effective and easily deployable. This thesis addresses these research gaps by proposing a low-cost IoT-based MPC strategy for a heating system and demonstrating its effectiveness using a real-world case study in a passive house standard pod at the University of Nottingham, UK.

The simulation of PCM wallboard integration under MPC control strategy highlights potential of PCM wallboards to enhance the energy efficiency of buildings, showcasing how these materials can complement intelligent control strategies. The results of PCM simulation and validated MPC strategy create a benchmark for future research on integrating smart control strategies with innovative construction materials to optimise building energy performance.

7.3 Recommendation for future works

In future works, a more comprehensive model is required to be developed and validated with full scale experimental data. Full integration with the grid should also be explored. The influence of the changing outdoor conditions on energy shifting and energy use price usage should be evaluated for other more types of buildings with different characteristics and operations.

The validation periods for the models presented in this thesis were constrained by limited data availability and limited access to the facility. In future work, a more extensive, long-term monitoring approach will be employed to ensure the robustness and applicability of the proposed strategy within the built environment,

as exemplified by [77]. Besides, Future work should focus on empirical validation of the integrated storage model and consider the water stratification within the storage tank. A more robust approach to handling uncertainties, such as solar radiation forecasts and occupancy profiles, could be the development of robust and stochastic MPC controllers. Such systems would bolster performance under uncertain conditions. Moreover, the economic feasibility of such an energy management system. Future studies should scrutinise the life-cycle costs, including installation, operation, and maintenance, and juxtapose them against potential energy savings. Real-world implementation also merits attention: conducting field studies and experimental validations can elucidate the practical applicability and efficacy of the proposed system, bringing to light potential challenges and solutions for practical implementation. Understanding the scalability of the proposed system in larger settings like office buildings, industrial complexes, or residential communities is paramount. Each of these different settings may present unique challenges and opportunities for energy management.

The development of the proposed MPC on controlling PCM wallboard present another promising area of the research. MPC realised the storage feature and capacity of PCM wallboard, which becomes a more robust approach to handling uncertainties on building construction, especially for PCM. The result indicated the proposed MPC could be refined or expanded to account for a broader spectrum of building materials. In the future, understanding the scalability of the proposed system in wide range of PCM wallboards is paramount. Each of these different PCM wallboards may present unique challenges and opportunities for energy management. Pursuing these ideas will undoubtedly drive forward the boundaries of STES in building sector and contribute substantially to the development of low-cost and lightweight intelligent building energy control system.

For comprehensive development of the IoT-based MPC strategy, additional research in necessitated. Future work should focus on expend the experiment MPC on vary types of heating system and consider an inferring method for weather prediction from real-time measured weather data. The results open numerous avenues for future research in the realm of optimising energy management systems and elevating building thermal comfort bases on IoT technology. One such opportunity lies in the exploration of integrating additional monitoring sensors, e.g., computer vision sensors. Working synergistically with the existing intelligent data

fusion system, these could further bolster the overall sustainability of the residential smart grid.

Furthermore, an intelligent feedback control not only bases on real-time indoor temperature, but also comfort-based conditions of occupancy is expected to develop. The initial study conducted was confirmed that the real-time comfort information collection contributes to a significant amount of thermal energy saving. The study was showed in appendix B.

Appendix A

A1. Weather data collection

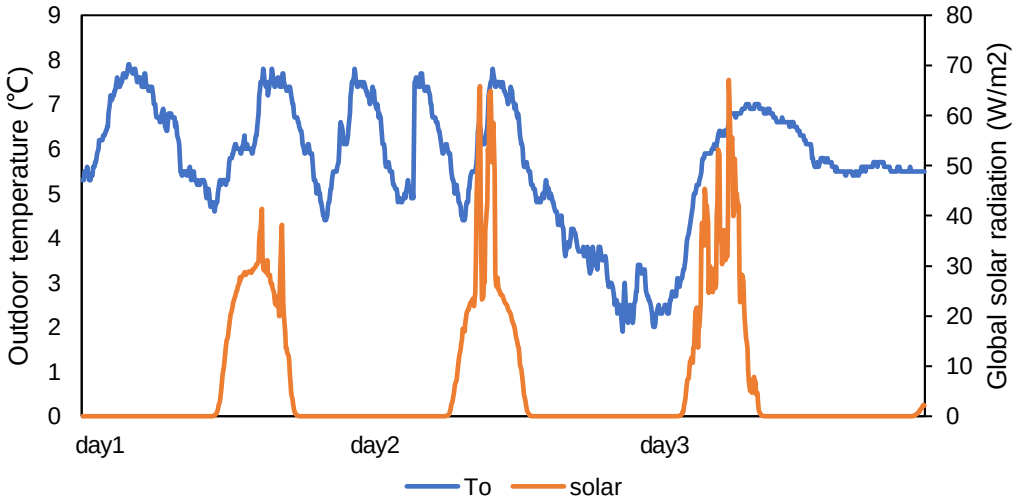

Fig A1. Local weather condition for three days

A2. TRNSYS model of original pod system

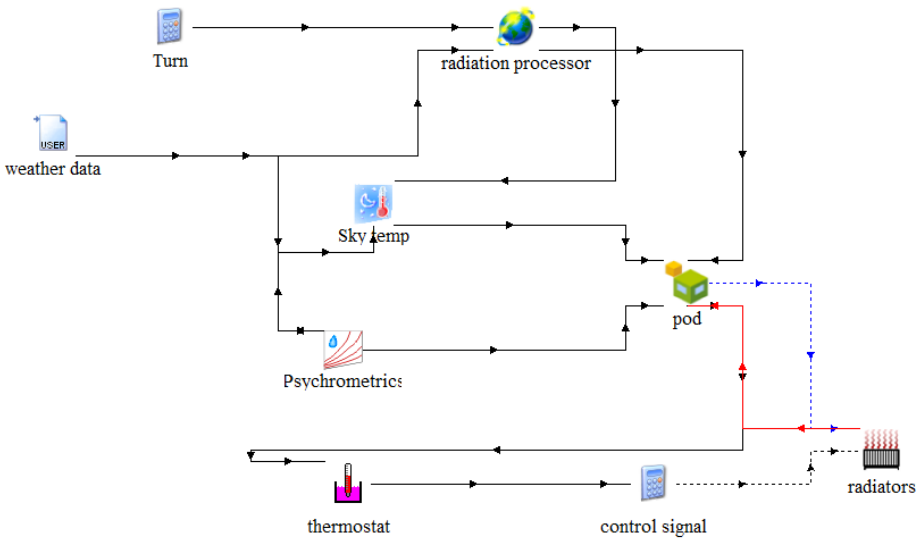

Fig A2. TRNSYS simulation of the test pod

A3. Properties of PCM wallboard

Table A1. Physical properties of PEG 600 [141]

Molar mass	570-630 (g mol^{-1})
Density at 20 ℃	1128 (kg m^{-3})
Melting temperature	21-25 (℃)
Liquid specific heat capacity	2490 (J kg^{-1} K^{-1})
Latent heat of fusion	148 (kJ kg^{-1})

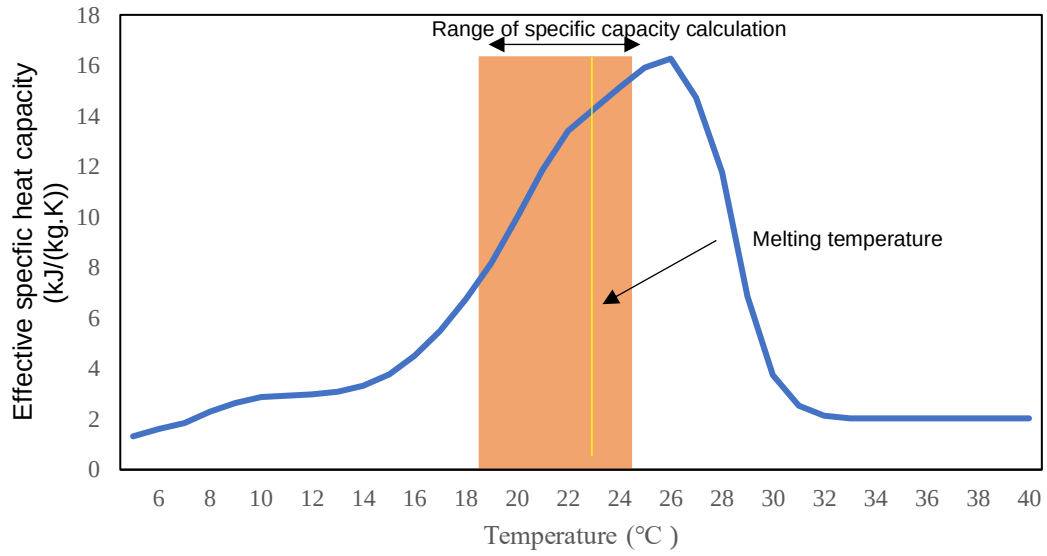

Fig A3. Effective specific heat capacity against temperature

A4. TRNSYS model for PCM system

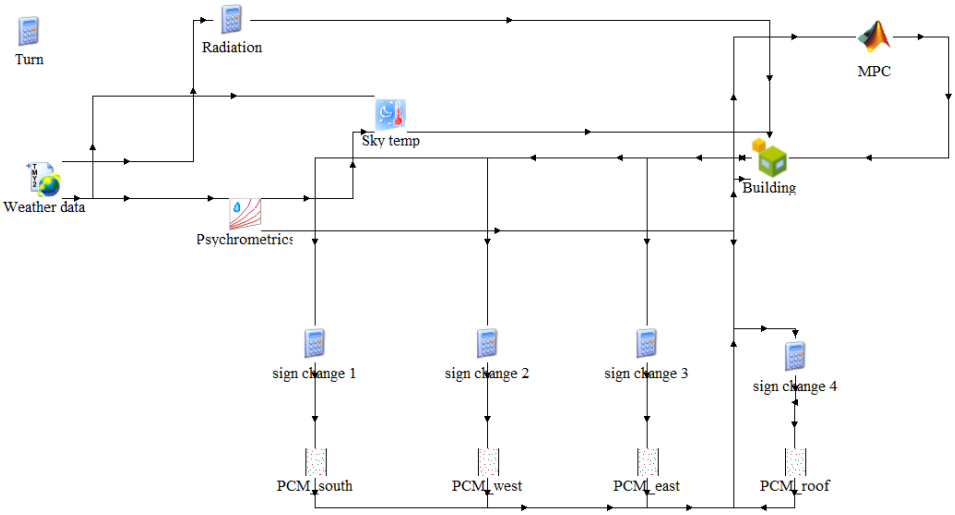

Fig A4. Co-simulation of MATLAB and TRNSYS of pod with PCM wallboards

A5. External view and wall layer of the test cell of validated case study

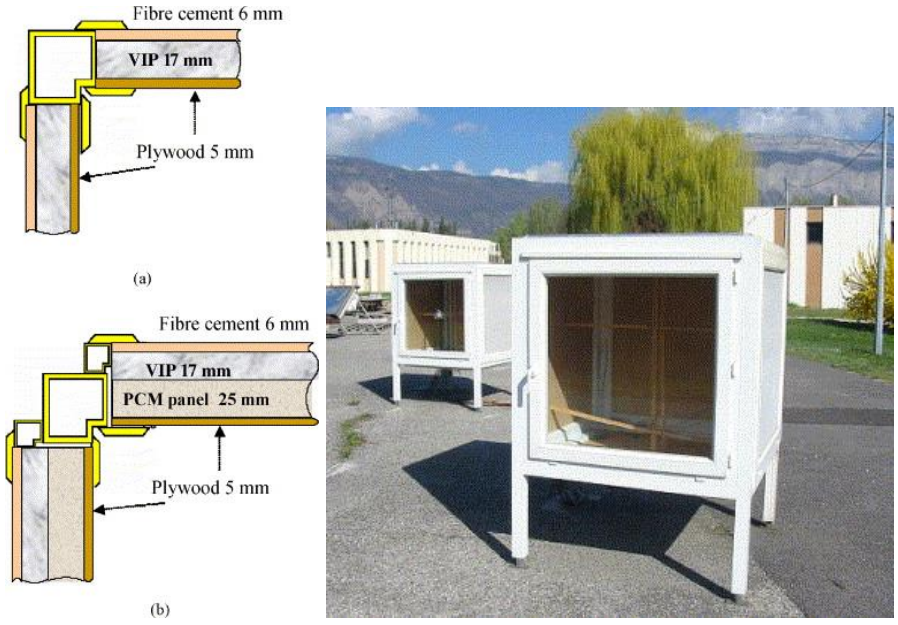

Fig A5. Cross-section of the wallboards: (a) test-cell without PCM and (b) test-cell with PCM and (c) exterior view of test-cell [141]

The validation process involved comparing the simulated indoor temperature from TRNSYS with the experimental results obtained in the study conducted by Ahmad et al. [141]. For the case study, a test-cell (depicted in Fig A5) was utilised, featuring one glazed wall facing south and other surfaces constructed with fibre cement, plywood, and vacuum insulation panels (VIPs). To enhance the building's thermal performance, polyethylene glycol 600 (PCM) layers were incorporated into the five opaque surfaces. The location of the test-cell was in Grenoble, France. The study of Ahmad et al. [141] provided comprehensive details of the materials used, weather data, and PCM layers, which were incorporated into the TRNSYS simulation.

The simulation was conducted over a four-day period, spanning from the 18th to the 21st of September. The results from the simulations without PCM layers demonstrated that the indoor temperature of the test-cell could reach as high as 60°C during noon due to substantial solar radiation (Fig A6a). However, in the evening, the indoor temperature drastically dropped to below 15°C (Fig A6b). In contrast, when PCM layers were integrated into the test-cell, the amplitude of indoor temperature fluctuations became smaller, ranging from 20°C to 45°C, which verified the heat storage capacity of the PCM walls. The comparison between the simulated indoor temperatures by TRNSYS and the experimental data for both scenarios, with and without PCM layers, revealed good agreement. The root mean square errors (RMSE) were computed to be 1.73°C and 1.53°C for the respective cases, indicating a relatively small discrepancy between the simulated and experimental indoor temperatures. This validation process confirms the accuracy of the TRNSYS simulation in predicting the indoor temperature behavior with and without PCM layers in the test-cell.

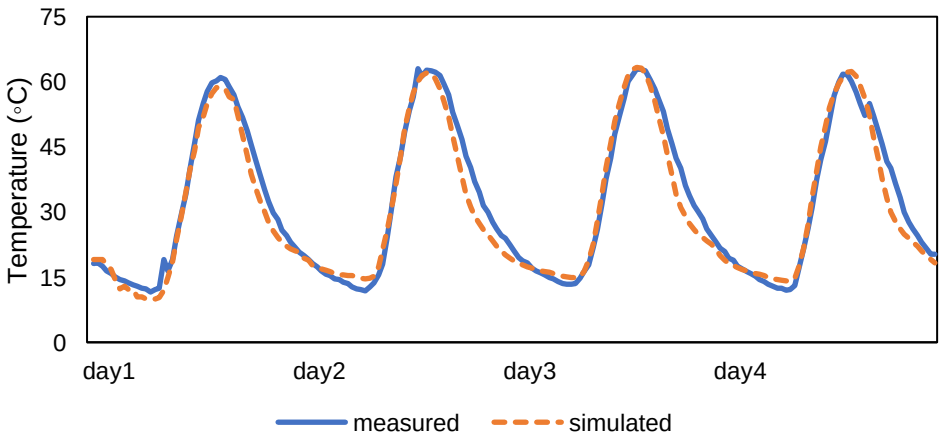

(a)

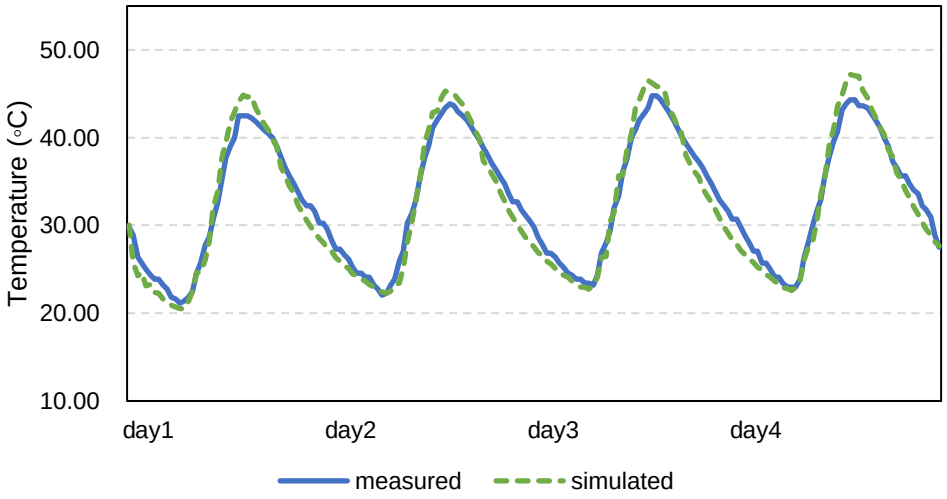

(b)

Fig A6. Indoor temperature (a) without PCM (b) with PCM

A6. RC representation of the room and governing equations

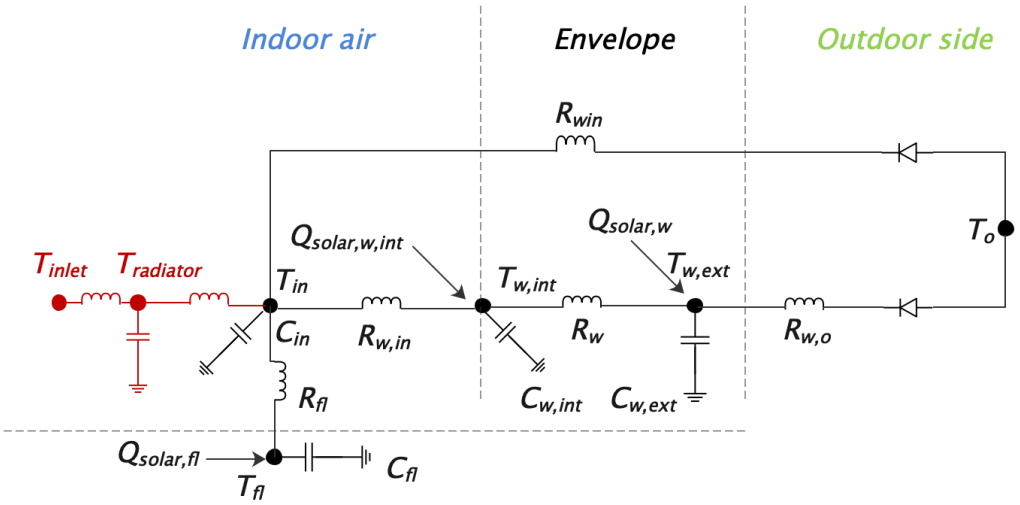

Fig A7. RC model of pod with radiators

$$\frac{dT_{w,ext}}{dt} = \frac{T_o - T_{w,ext}}{R_{w,o}C_w} + \frac{T_{w,int} - T_{w,ext}}{R_w C_w} + \frac{Q_{solar,w}}{C_w} \quad \text{A1}$$

$$\frac{dT_{w,int}}{dt} = \frac{T_{w,ext} - T_{w,int}}{R_w C_w} + \frac{T_{in} - T_{w,int}}{R_{w,in} C_w} + \frac{Q_{solar,w,int}}{C_w} \quad \text{A2}$$

$$\frac{dT_{in}}{dt} = \frac{T_{w,int} - T_{in}}{R_{w,in} C_{in}} + \frac{T_o - T_{in}}{R_{win} C_{in}} + \frac{T_{fl} - T_{in}}{R_{fl,in} C_{in}} + \frac{T_{ra} - T_{in}}{R_{ra,in} C_{in}} \quad \text{A3}$$

$$\frac{dT_{fl}}{dt} = \frac{T_{in} - T_{fl}}{R_{fl,in} C_{fl}} + \frac{Q_{solar,fl}}{C_{fl}} \quad \text{A4}$$

$$\frac{dT_{ra}}{dt} = \frac{T_{in} - T_{ra}}{R_{ra,in} C_{ra}} + \frac{T_{inlet,ra} - T_{ra}}{R_{inlet,ra} C_{ra}} \quad \text{A5}$$

A7. RC model of PCM system

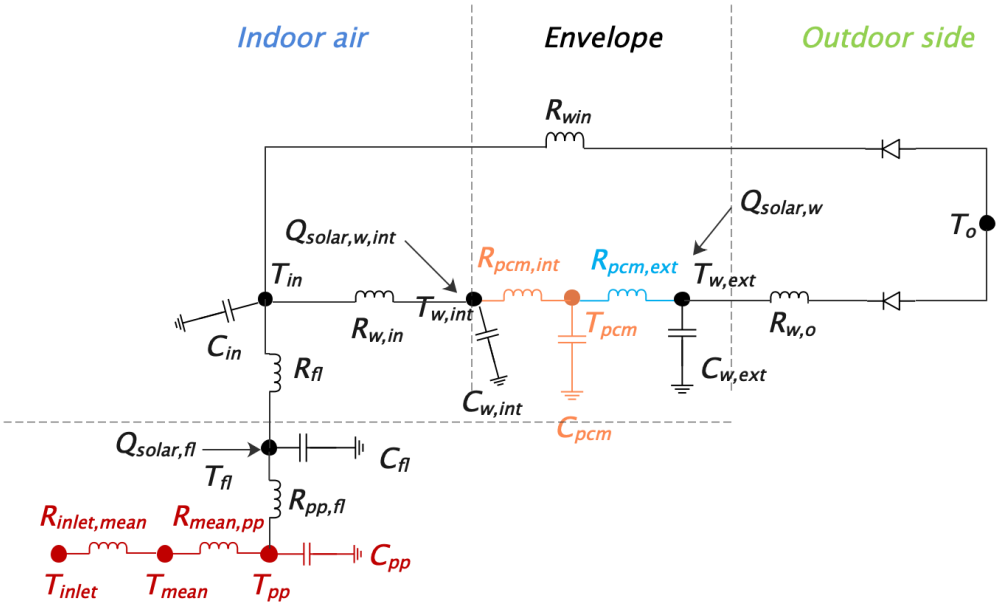

Fig A8. room RC model with PCM wallboard and UFH system

$$\frac{dT_{w,ext}}{dt} = \frac{T_o - T_{w,ext}}{R_{w,o} C_w} + \frac{T_{pcm} - T_{w,ext}}{R_{pcm,ext} C_w} + \frac{Q_{solar,w}}{C_w} \quad \text{A6}$$

$$\frac{dT_{pcm}}{dt} = \frac{T_{w,ext} - T_{pcm}}{R_{pcm,ext}C_{eff,ave}} + \frac{T_{w,int} - T_{pcm}}{R_{pcm,int}C_{eff,ave}} \quad \text{A7}$$

$$\frac{dT_{w,int}}{dt} = \frac{T_{w,ext} - T_{w,int}}{R_w C_w} + \frac{T_{pcm} - T_{w,int}}{R_{pcm,int}C_w} + \frac{Q_{solar,w,int}}{C_w} \quad \text{A8}$$

$$\frac{dT_{in}}{dt} = \frac{T_{w,int} - T_{in}}{R_{w,in}C_{in}} + \frac{T_o - T_{in}}{R_{win}C_{in}} + \frac{T_{fl} - T_{in}}{R_{fl,in}C_{in}} \quad \text{A9}$$

$$\frac{dT_{fl}}{dt} = \frac{T_{in} - T_{fl}}{R_{fl,in}C_{fl}} + \frac{T_{pp} - T_{fl}}{R_{pp,fl}C_{fl}} + \frac{Q_{solar,fl}}{C_{fl}} \quad \text{A10}$$

$$\frac{dT_{pp}}{dt} = \frac{T_{fl} - T_{pp}}{R_{pp,fl}C_{pp}} + \frac{Q_{heating}}{C_{pp}} \quad \text{A11}$$

A8. An example of MATLAB command window during MPC implementation

```
ans =

    '08:17:22'

temperature =

   16.5000

controller =

     1

x_ =

  -24.6354
   11.4555
   21.1397
    2.2958
   56.2727
```

```
ans =

    '10:17:19'

temperature =

   21.2500

controller =

     0

x_ =

  -25.3773
   13.6551
   20.1774
    1.3144
   20.4585
```

Fig A9. An example in MATLAB command window

Appendix B

Real-time clothing insulation level prediction based on model transfer learning and computer vision for PMV-based heating system optimisation through piecewise linearisation

Abstract

Achieving a balance between energy efficiency and thermal comfort is a pivotal aspect of sustainable building design. Traditional control methods typically maintain indoor air temperature within predetermined limits, disregarding variable factors like occupancy activity and clothing levels, which significantly influence thermal comfort perception. Conversely, comfort-based control strategies present an opportunity to automate heating systems, dynamically responding to variations in thermal comfort. To achieve this, real-time information on activity levels and clothing insulation (and its adjustment) is indispensable for accurate estimation of thermal comfort. In this study, we explore the potential of a novel detection approach capable of predicting clothing insulation in real-time and utilising this information to optimise the operation of building energy systems. By doing so, the proposed method facilitates the delivery of indoor conditions tailored to individual user requirements, effectively reducing energy wastage and promoting sustainability. The development of a 2stage computer vision-based framework for occupancy detection and clothing insulation prediction forms the core of this approach. Leveraging deep learning network algorithms, this framework successfully performs detection and recognition tasks, even with limited training data, enabling real-time predictions of both light and heavy clothing. To address the nonlinearity of traditional predicted mean vote (PMV) models, we applied a piecewise linearisation approach to our PMV-based optimal control strategy. Through initial experimental field tests conducted in a case study university building, we evaluate the detection method's performance. The results demonstrate the framework's proficiency in predicting clothing insulation levels and generating real-time profiles. We further analyse the impact of our proposed approach on thermal comfort and energy performance through scenario-based modeling and simulations. The initial results showcase the potential of integrating our method with PMV-based controls to enhance thermal comfort and overcome the limitations of pre-defined schedules. However, while our study highlights the feasibility of predicting clothing insulation levels for multiple occupants engaged in diverse indoor activities, we acknowledge the need for further refinement to enhance detection accuracy and seamless integration with building energy systems.

Keywords: Artificial intelligence; building energy; computer vision; clothing insulation; real-time comfort-based control

Highlights

- YOLO & GoogLeNet algorithms ensure accurate occupant clothing insulation prediction.
- Case study validates successful detection in a lecture room in university building.
- Detection approach successfully handles multiple occupants' clothing variations during different activities.
- Scenario-based simulations demonstrate energy savings and optimise thermal comfort.
- Lightweight CPU usage and fast response times ensure practical implementation.

Graphical abstract

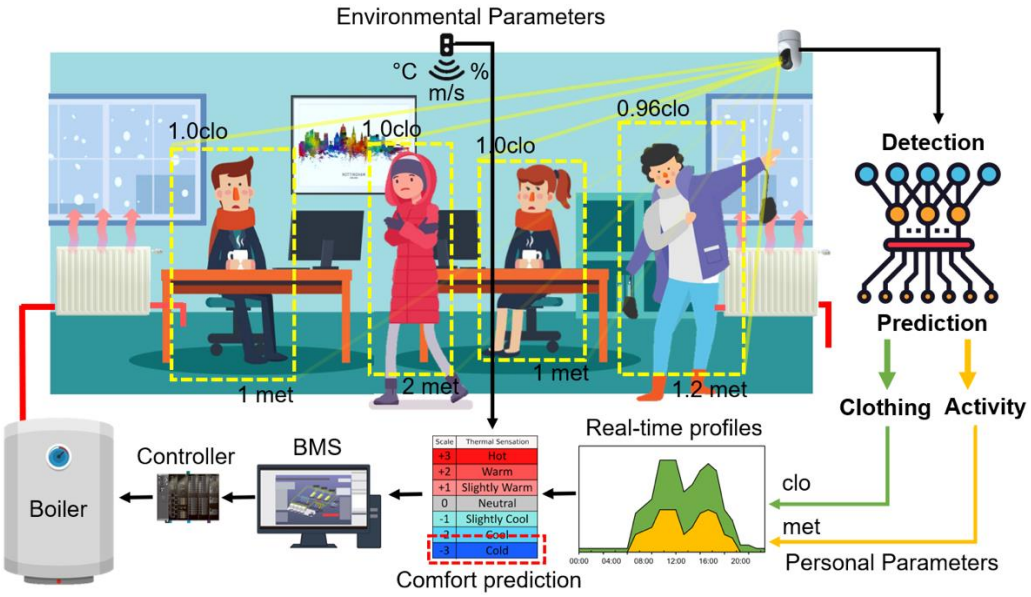

Nomenclature

Symbols

$\overline{t_r}$	mean radiant temperature (℃)
f_{cl}	clothing surface area factor
h_c	convective heat transfer coefficient ($\mathrm{W}/(\mathrm{m}^2 \cdot K)$)
h_r	relative humidity (%)
I_{cl}	clothing insulation ($m^2 \cdot K \cdot W^{-1}$)
P_a	water vapour partial pressure (pa)
t_a	air temperature (℃)
t_{cl}	clothing surface temperature (℃)
v_{ar}	air velocity (m/s)
a	slope
b	intercept
I	segments of clothing surface temperature
J	segments of indoor temperature
k	time step
L	segments of mean radiant temperature
M	metabolic rate (W/m^2)
W	effective mechanical power (W/m^2)
z	integer variable

Abbreviations

AI	artificial intelligence
BES	building energy simulation
CNN	convolutional neural network
HVAC	heating, ventilation and air conditioning
MPC	model predictive control
PMV	predict mean vote

Subscripts

abs	absolute value
cl	clothing surface temperature
ta	indoor air temperature
tr	mean radiant temperature

1. Introduction

The building sector constitutes a significant share of worldwide energy consumption, accounting for nearly 40% of the total global usage [1]. Accordingly, this sector holds immense potential for mitigating environmental harm through emission reduction. Among the multiple energy-consuming components within a building, the heating, ventilation, and air conditioning (HVAC) system stands out due to its substantial energy footprint [2]. However, this also highlights the HVAC system's opportunity for achieving remarkable energy and cost savings. Given that people reportedly spend nearly 90% of their time indoors [3], an HVAC system must be designed and operated to ensure not only comfortable but also healthy living conditions. Therefore, energy-efficient building design necessitates a balance between energy conservation and thermal comfort [4].

Existing literature reveals numerous studies that have devised various concepts and strategies for optimising HVAC control, with the dual objective of enhancing energy efficiency and comfort [5]. Recent innovative strategies include model predictive control (MPC), adaptive, demand-driven, and comfort-based control strategies that leverage artificial intelligence (AI). The present study places particular emphasis on the comfort-based control strategy, an approach that seeks to resolve the requirements of energy efficiency and thermal comfort [6].

In traditional HVAC control methods, the air temperature is maintained within predetermined limits to deliver heating and/or cooling [7]. However, this approach of maintaining a constant indoor air temperature does not necessarily guarantee occupant comfort, given that it does not take into account the dynamic nature of factors like occupancy activity levels and internal heat gains, which can significantly affect comfort perception. While air temperature undeniably affects thermal comfort, factors such as humidity, air velocity, radiant temperature, activity, and clothing level are equally important to consider [8]. Consequently, a comfort-based control strategy seeks to automate the HVAC system to adjust in real-time according to variations in thermal comfort levels [9].

Multiple types of comfort-based control strategies have been developed, with the most commonly used being the Predict Mean Vote (PMV)-based control [12]. This control strategy dynamically adjusts indoor air temperature or humidity levels to maintain the PMV value [13]. It requires measuring occupants' comfort levels in a controlled space to facilitate the necessary adjustments. If these variables could be accurately measured in real time, it would allow for dynamic control that enhances both energy efficiency and indoor thermal comfort [1, 14]. However, current sensor technologies cannot measure personal factors, such as activity and clothing levels, which are complex variables determined by the

exchange of heat between the human body and its surroundings [15]. Given the substantial influence of clothing on comfort levels, and how adjusting clothing directly affects the heat balance [12], there is a need for an innovative method to measure and determine real-time activity levels and clothing insulation values for PMV determination in comfort-based controls.

A promising approach involves a vision-based detection method, as illustrated in Fig 1. The study will first conduct a comprehensive review of existing clothing insulation measurement methods and examine their real-time feasibility for PMV-based HVAC control. Following this, we will introduce and evaluate a real-time clothing insulation prediction method for comfort-based demand-driven system control. This method employs a computer vision and deep learning algorithms to perform detection and recognition tasks using a camera. Initial field tests in a university building case study will be conducted to assess the performance of the proposed detection method.

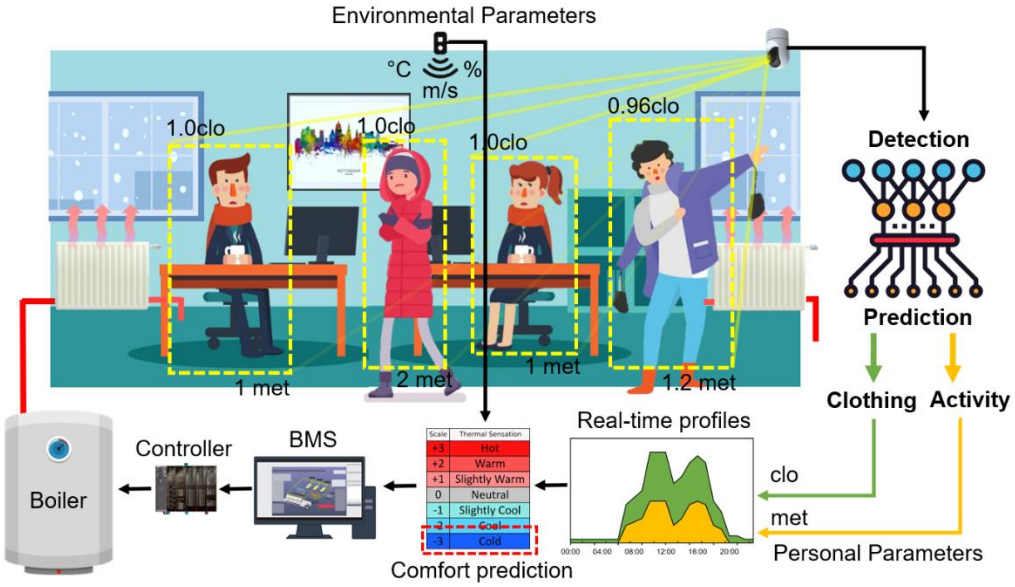

Fig. 1 A method for detecting and recognising clothing levels for indoor thermal environment control.

1.1 Novelty, research gaps and aims and objectives

Real-time and comprehensive occupancy information has been recognised as valuable in optimising HVAC, lighting, and building zone usage through demand-driven control and occupant-centric strategies [7]. Detection of occupancy-related data, including count, position, and behaviour/activity, can be achieved using various measurement techniques and sensor systems, as detailed in previous research [16]. Recently, vision-based strategies have gained significant interest due to advances in deep learning, particularly convolutional neural network (CNN) algorithms, and increased computational capabilities.

Computer vision methods have been increasingly utilised for occupancy detection tasks, successfully counting occupants in buildings [17]. However, the majority of studies in this area have primarily focused on algorithm performance, exploring methods to enhance detection accuracy and computational efficiency. Yet, there is a noticeable gap in research regarding the potential of such approaches to improve building performance [7, 18], specifically in terms of energy demand and thermal comfort. In previous investigations [7, 18], vision-based methods were applied to estimate indoor heat emissions generated by occupants during various activities and from equipment like computers. The obtained information can be leveraged to adjust the operation of heating and cooling systems, aiming to minimise unnecessary energy consumption. Furthermore, current studies often resort to simple approximate PMV models or logical algorithms for PMV-based control, finely tuning control parameters to minimise the absolute value of the PMV value [19]. This is due to the high nonlinearity of the PMV model, which presents challenges in solving for the optimal setpoint indoor temperature.

In this study, a real-time sequential order method for detecting clothing insulation was developed, serving as input data for PMV-based HVAC control (Fig 1). Additionally, the occupant's real-time activity level, another vital factor for PMV estimation, can also be predicted using the same approach [7]. This approach holds the potential to detect various objects and activities within a specific region or zone of the building, offering support for building services such as window operation and fire detection [20]. Furthermore, the proposed method presents an alternative to employing multiple individual sensors or reducing the overall number of sensors required in a building to monitor these parameters. Despite the availability of vision-based strategies for clothing level prediction, there is a scarcity of research focusing on its integration with control systems and its impact on building performance. To gain a comprehensive understanding of its capabilities, the application of this approach in real buildings is essential. Moreover, it is crucial to explore specific implementations in spaces accommodating multiple occupants, such as classrooms, libraries, malls, and recreational areas, to assess its effectiveness in diverse environments.

2. Literature review

This section provides a comprehensive review of PMV-based control strategies and clothing insulation measurements. The Predicted Mean Vote (PMV) is a critical parameter estimating the average thermal perception votes deemed acceptable by indoor occupants. A PMV value of 0 indicates a thermal neutral state, where the body's heat production equals the heat loss to the environment. Consequently, each indoor space has an optimal operating temperature corresponding to PMV=0, contingent on the occupants' clothing insulation and other pertinent parameters [24]. Notably, changes in clothing insulation, such as the

addition or removal of a garment, necessitate adjustments in the optimum indoor temperature to ensure occupants' thermal comfort while keeping other parameters constant [25, 26]. In PMV-based control, the room setpoint, including air temperature and humidity, is dynamically adjusted to achieve neutral thermal conditions, accounting for real-time environmental conditions and occupants' clothing and activity levels [9, 13, 14, 27-29]. Consequently, the HVAC system operates only when necessary, leading to energy savings [18]. Fine-grained PMV-based HVAC control has demonstrated its potential to reduce energy consumption while enhancing comfort levels [28]. However, most existing studies have employed a constant clothing insulation value in the PMV-based control strategy [9, 27, 28]. A more realistic approach was adopted by Freire et al. [13], considering different clothing indexes for day-time (0.66 clo) and night-time (0.45 clo), which accounts for clothing adjustments throughout the day.

Similarly, Zampetti et al. [27] adopted a pre-defined clothing insulation value in their PMV-based control, adhering to international standards [30] and considering the occupants' clothing during their experiments. Zhang et al. [31], on the other hand, proposed a dynamic control approach that adjusts the supply air conditions to meet thermal comfort requirements. Their model also relied on the PMV equation, assuming summer clothing and sedentary activity levels. Notably, previous studies have often employed pre-defined or precalculated values for clothing insulation, with some utilising dynamic models to predict clothing insulation based on specific parameters like outdoor and indoor temperatures [32]. However, real-time clothing measurements were not considered in these studies, creating a gap that motivates the development of real-time clothing prediction in this research, to be combined with the initial occupancy activity approach. A previous study [5] emphasised the sensitivity of energy consumption in comfort-controlled spaces to personal factors such as clothing insulation and activity level.

The thermal balance condition relies on calculating the clothing insulation, where the internal heat production in the body equals the heat loss to the environment. Clothing and boundary air insulation act as thermal resistances, preventing heat loss from the body, and the clothing thermal insulation is expressed in clo units (where 1 clo = 0.155 m^2 K/W). As mentioned earlier, the amount of clothing significantly impacts comfort levels, but adjusting clothing is another crucial factor directly affecting the heat balance [12]. Therefore, it is imperative to develop methods for determining real-time clothing insulation (and its adjustment) for accurate PMV estimation in comfort-based controls. The literature presents various approaches to assess clothing insulation, including the use of thermal manikins, field testing, and dynamic clothing insulation measurements.

Next, we evaluate pertinent studies and assess their suitability and feasibility for real-time comfort-based controls. Huang [33] employed heated manikins to calculate clothing's

thermal insulation using serial and global methods. It was observed that the serial method tends to yield higher insulation values than the global method, and the discrepancy depends on the local insulation's degree of homogeneity, a finding also corroborated by Kuklane et al. [34]. Similarly, Lee et al. [25] expanded their clothing testing to encompass 150 garments and 38 ensembles, covering both daily (garments) and seasonal (ensembles) clothing. For all tested clothing, the serial method resulted in higher insulation values than the global method. These studies underscore the complexity of clothing insulation measurement and the significance of the employed method, which can lead to overestimation or underestimation of insulation levels. Notably, these measurements were conducted in laboratory settings under controlled conditions to ensure simplicity and repeatability. Various validations against field trials conducted by several studies [25] revealed that the results were consistently lower than those obtained from human subjects for all seasonal ensembles. Although real-time measurements in practice will be based on actual human subjects, it is crucial to acknowledge that the clothing insulation data utilised in the prediction may originate from laboratory tests. Hence, when employing thermal manikin insulation values in practical scenarios, it is essential to match the surrounding conditions and clothing microclimate as closely as possible, necessitating the use of correction factors.

Advancements in image-recognition techniques have enabled the possibility of real-time estimation of clothing insulation using cameras. Li [35] proposed a computer vision model pre-trained with images and utilised the ASHRAE handbook to derive insulation values, offering a sensitive approach capable of capturing indoor occupants' clothing adjustments, making it suitable for integration with a PMV-based control strategy. Moreover, the vast repository of existing clothing insulation datasets (e.g., ISO 9920, ISO 7730, and ASHRAE 55) provides ample training values encompassing both daily and seasonal wear. Other studies have also developed real-time clothing insulation measurement methods that allow direct estimation without prior training. For instance, Lee et al. [36] employed a one-node thermoregulatory model to predict real-time clothing insulation levels, employing an infrared camera to obtain face and clothing temperatures alongside other environmental parameters like air temperature and mean radiant temperature. Lu and Hameen [37] adopted a similar model in their study to predict clothing insulation and compared it with values from ASHRAE 55 [8]. The results indicated that the estimated clothing insulation values were consistently smaller than 0.1 clo for all tested garments, aligning with ASHRAE data. It is worth noting that the one-node model used only an area-weighted average temperature for the calculation, which could be further enhanced by implementing a multi-node model, utilising all measured temperature nodes to refine clothing insulation determination. This emerging image-based approach presents promising prospects for real-

time clothing insulation estimation, advancing our capabilities in comfort-based control strategies for enhanced indoor thermal comfort and energy efficiency.

In their study, Liu et al. [38] presented a clothing insulation detection method that integrates a thermal camera and a vision-based approach. This novel method enabled the recognition of various garment types and fine distinctions in clothing insulation levels, such as distinguishing between cloth zipped or unzipped, sleeves rolled up or down, and different activities. Consequently, the proposed PMV-based control strategy can adjust HVAC operations in response to even small changes in people's clothing insulation levels. However, the evaluation of this control strategy was not conducted in their study. On the other hand, Miura et al. [39] proposed a more advanced approach, employing a robot equipped with patrolling, monitoring, and sensing technology. With the automatic measurement of skin and clothing temperatures, this method calculated clothing insulation and PMV values for different individuals, taking into account personal variations in thermal sensation. It is evident that the thermoregulatory model demonstrated excellent performance in real-time clothing insulation estimation. Nonetheless, this method requires an infrared camera, which can be costly, particularly when implemented on a large scale or in numerous building spaces. These studies showcase promising advancements in real-time clothing insulation estimation, providing valuable insights into potential applications for PMV-based control and building energy optimisation. However, further research and evaluation are necessary to fully understand the practicality and cost-effectiveness of these approaches in real-world scenarios.

2.1 Literature gap

The discussions reveal several critical research gaps that warrant further investigation. First, the accuracy and reliability of real-time clothing insulation estimation using image-recognition techniques and thermoregulatory models need thorough evaluation under diverse real-world conditions.

The majority of studies in this domain have primarily concentrated on assessing the algorithm's performance, exploring various techniques to improve detection accuracy or computational efficiency. While these efforts are valuable, there appears to be a scarcity of research on investigating the actual impact of these approaches on building performance, particularly in terms of energy demand and thermal comfort.

Additionally, the integration of such estimates into comfort-based control strategies, requires comprehensive assessment through field tests in real buildings with varied occupants, activities, clothing types and usage scenarios. The use of thermal cameras and advanced sensing technologies in real-time clothing insulation estimation may pose cost challenges, especially for large-scale implementation in multiple building spaces. Future

research should explore cost-effective alternatives and assess the scalability of these approaches for widespread adoption in different building types and sizes. While the use of thermal manikins and models provides valuable insights, it is crucial to validate the accuracy and reliability of real-time clothing insulation estimation against data obtained directly from human subjects.

Furthermore, it is crucial to explore specific implementations of real-time clothing insulation estimation and comfort-based control strategies in spaces with multiple occupancies, such as classrooms, libraries, malls, and recreational areas. These environments often exhibit diverse thermal comfort requirements due to varying occupant activities and clothing levels. Investigating the feasibility and effectiveness of the proposed approaches in such spaces can provide valuable insights into their practicality and adaptability in real-world scenarios. Evaluating the applicability of these approaches across different building types, climates, and geographical regions is essential.

3. Method

In this study, we aim to develop a real-time clothing insulation detection and prediction approach for controlling building energy systems, as illustrated in Fig 1. By utilising a Convolutional Neural Network (CNN) model deployed on a camera, the detector can gather valuable information on both occupancy and clothing insulation within a building zone. Subsequently, this information can be leveraged to optimise the operations of the heating and cooling system, with the overarching goal of achieving a comfortable indoor environment while minimising energy demand. To demonstrate the effectiveness of this approach, we implement the detector in a lecture room within a university building. We then employ Building Energy Simulation (BES), scenario-based modeling, and simulations to assess the potential impact of the proposed approach on the thermal comfort and energy performance of the building. The development and application of the proposed detection method are comprehensively discussed in the following sub-sections.

3.1 Development of deep-vision-based CLO estimation method

The adoption of deep learning methods for vision-based solutions in building applications has seen a notable increase. These methods have been specifically tailored to enhance the design and operation of building HVAC systems, with a focus on improving indoor air quality and thermal conditions. They have demonstrated applicability in diverse areas, including damage detection, fault diagnosis [40], occupancy activity recognition [41], and identification of windows and equipment [42]. Such studies underscore the potential of deep learning-based approaches in addressing various building challenges. Building on prior research [7], this study presents a vision-based approach for predicting clothing insulation, intending to incorporate it into PMV-based demand-driven HVAC control. The

initial phase of the proposed framework involved selecting and training an appropriate deep learning model to enable the detection and recognition of different clothing levels within buildings. For this study, two response categories were chosen to represent 'light' and 'heavy' clothing. The training dataset was compiled considering daily wear during winter (as shown in Table 1), with clothing insulation averages derived from specific types, including socks and shoes, as per ISO 9920 measurements under static conditions [30].

Table 1. Ensembles defined in this study

Ensembles	**Average mass (g)**	**Average I_{cl} (clo)**	**Average I_{cl} $(m^2 \cdot K \cdot W^{-1})$**
Long-sleeve shirt, T-shirt, trousers	953	0.70	0.11
Sweater, trousers	1384	1.00	0.155
Cold protective clothing with jacket, trousers	3126	2.57	0.40

The term "light" in this context denotes a clothing insulation level ranging from 0.7 to 1.0 clo, with the mass of such clothing varying between 900 to 1400 grams. Conversely, "heavy" refers to a situation where the clothing insulation level is approximately 2.5 clo, and the mass of the ensembles is around 3000 grams. To create a comprehensive dataset for each category, a total of 500 images were collected from the open-source deepfashion dataset [43], with 30% of the images reserved for model validation. Fig 2 shows the examples for training dataset. Subsequently, the selected images were appropriately labeled, setting the stage for the development and configuration of the training process for the clothing detector. The subsequent sections of this study provide a detailed account of the clothing detector's development.

Fig. 2 Training dataset example [43].

3.1.1 Training for clothing detector

In this study, MATLAB [44] served as the training platform, utilising the Deep Learning ToolboxTM, Computer Vision ToolboxTM, and Parallel Computing ToolboxTM for MATLAB. The training process was conducted on a PC equipped with an NVDIA GeForce 3080Ti Super graphics processor. To fine-tune the model for the specific task of clothing insulation prediction, GoogLeNet [45] was selected due to its ability to learn rich feature representations across a wide range of images. In comparison, three widely used pre-trained classifiers: ResNet [46], VGG19 [47], and SqueezeNet [48] were used to discover the feature extraction in clothing insulation detection. The training result of GoogleNet was showed in Fig 7. The training results for other three networks were showed in Figure A5-B7 in section B5.

Transfer learning was employed, involving the replacement of the last learnable layer and the classification layer in pre-trained networks with new layers adapted to the dataset at hand. The learning rate for the new learnable layer was set at 10, while the initial learning rate was adjusted to 0.0003. This approach allowed for efficient feature learning in the newly replaced layers while retaining the valuable features from the early pre-trained layers. Furthermore, the classification layer was replaced to accommodate the two new classes relevant to the study. Prior to training, the training images underwent pre-processing using the "imageDataAugmenter" function in MATLAB. Subsequently, transfer learning was carried out through the "trainNetwork" function. For real-time detection, YOLO [49], a pre-trained occupant detector, was implemented to identify and crop the regions occupied by individuals, which were then passed for clothing level classification (as depicted in Fig 3). The resulting clothing insulation levels for each occupant were recorded for further analysis.

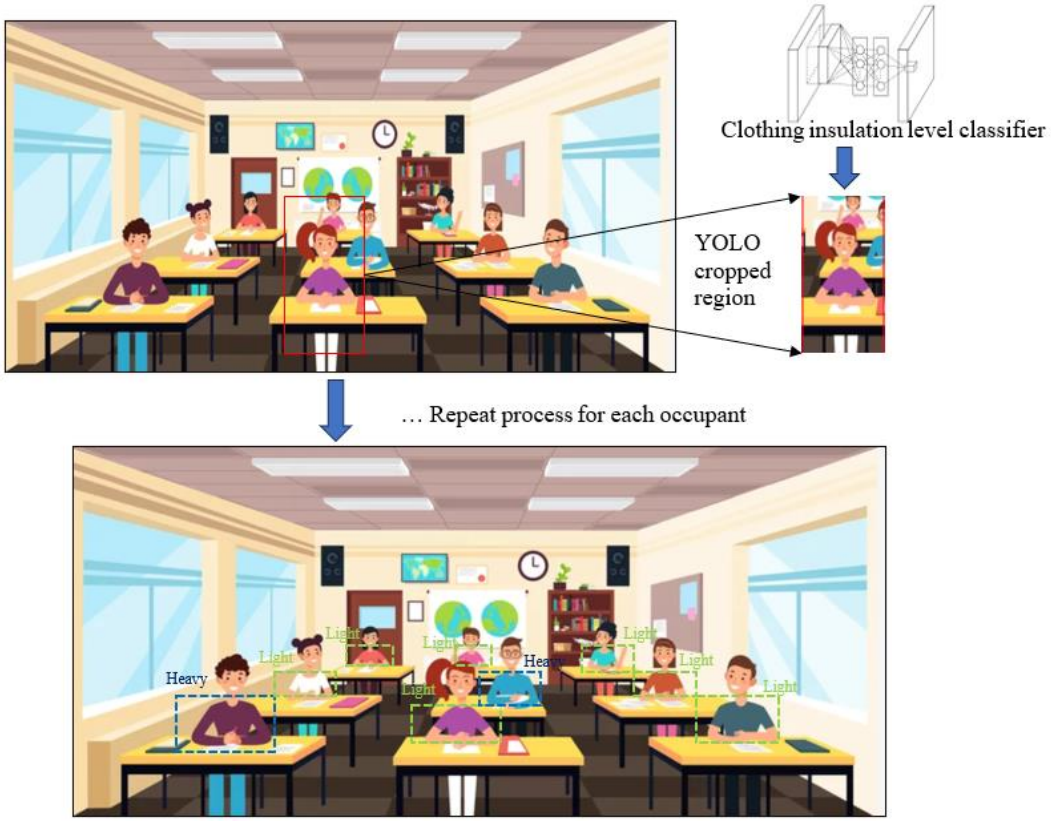

Fig. 3. 2 stage clothing insulation detection method

3.1.2 Case study building and room

In order to demonstrate the effectiveness of the proposed approach, the clothing insulation detector was implemented in a lecture room situated within one of the buildings at the University of Nottingham's main Uni Park campus, as depicted in Fig 4a. This building primarily serves as a teaching facility for architecture and engineering students, featuring various spaces for lectures, seminars, laboratories, and a café. The lecture room chosen for testing can accommodate 30-40 students and is also used as a workspace during non-lecture hours, leading to varying occupancy levels throughout the day. Heating is provided by four large radiators within the space. The room, located on the first floor, has dimensions of 36.62m^2 in area and a height of 3.52m. For the detection process, a camera with a 1080p resolution and wide-angle view was fixed on the ceiling, opposite to the side where detection was conducted (Fig 4b). Video of test 1 was recorded for evaluating proposed detector for multiple person targets. Video of test 2 was recorded for evaluating the proposed detector for clothing level changes targets. Besides, for test 1, humidity was collected by AWAIR [50], indoor temperature was measured by K-thermocouple [51], mean radiant temperature was estimated by taking average values of wall temperatures measured with IR temperature sensor [52, 53]. Those data were collected to validate estimated PMV value with real thermal sensation of indoor occupancy.

It is important to note that no images or videos were recorded during the detection process in practice. Instead, the detector solely generated profiles required for the prediction of comfort levels, ensuring privacy and data protection. To assess the performance of the vision-based clothing insulation detector, a series of tests were conducted. These tests included scenarios with multiple occupants staying in the lecture room and scenarios involving sudden changes in clothing insulation levels (i.e., taking on or off coats). Videos of the two scenarios were recorded, and the results can be viewed in video 1 and video 2, with a detailed discussion provided in Section 3. These tests served to evaluate the detector's capability in real-world conditions, validating its potential for accurately predicting clothing insulation.

(a)

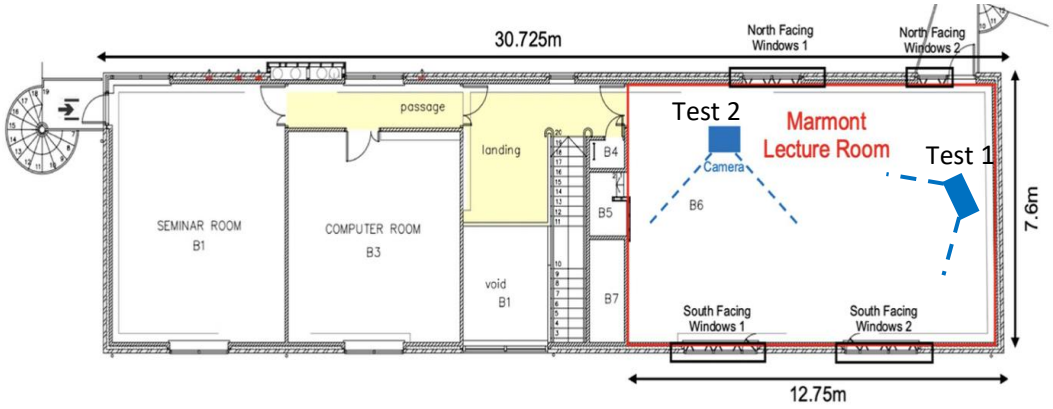

(b)

Fig. 4 (a) The case study Marmont lecture room at the University of Nottingham. (b) camera views

3.2 PMV-based control strategy simulation

The evaluation of the effect of clothing level detection and prediction on indoor thermal comfort and building energy performance was performed through the utilisation of TRNSYS software. A room model was constructed in TRNSYS by incorporating detailed material and construction information, as provided in Section B1. The lecture room under study is equipped with a central heating system comprising a boiler and radiators. The boiler supplies hot water to the radiators via a pipeline, and heating is typically required during colder months (October to May). The operational temperature setpoint for the space was set to 22 ℃ with a 2 ℃ band. To simulate real-world conditions, a one-week schedule of students attending classes during the autumn semester was collected for the case study lecture room. The lecture room is designed to accommodate up to 38 students, and their arrival and departure times were found to be highly variable (as depicted in Fig 5). Additionally, the intermittent usage of equipment and lighting, which contributes to internal heat gains, was also considered and detailed in Section B1.

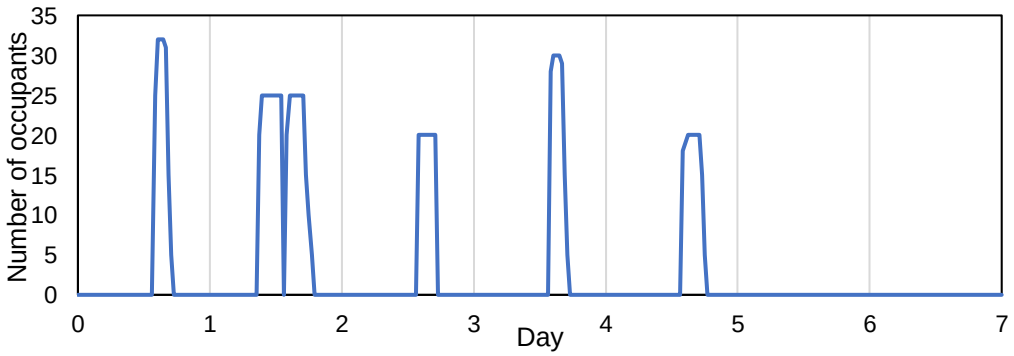

Fig. 5 Occupancy level for a typical week in the Marmont lecture room

The proposed PMV-based heating control strategy was evaluated through simulation of a building model, where the percentage of clothing insulation was varied from heavy to light, and the optimal heating system setpoint was calculated based on an average indoor clothing insulation level (as depicted in Fig 6). During the cold season, occupants entered the room wearing heavy clothing in the morning and gradually removed coats or insulated layers as time passed. To assess the performance of the control strategy, three scenarios were simulated: 10% of occupants still wearing heavy clothing, 20% with heavy clothing, and 30% with heavy clothing. These scenarios were then compared with the conventional constant setpoint strategy (i.e., 22℃). To achieve a fully real-time feedback PMV-based control strategy, MATLAB was integrated with TRNSYS. In each time step, the control strategy was calculated in MATLAB using information from TRNSYS, which included current clothing insulation levels, indoor humidity, and mean radiant temperature, all required for PMV calculation. Further details regarding the PMV model can be found in Section 3.21. Additionally, our study incorporates a control algorithm that reduces the indoor temperature setpoint to 16 degrees when the algorithm detects that there are no occupants present in the room. This ensures an energy-efficient operation of the heating system during periods of unoccupancy.

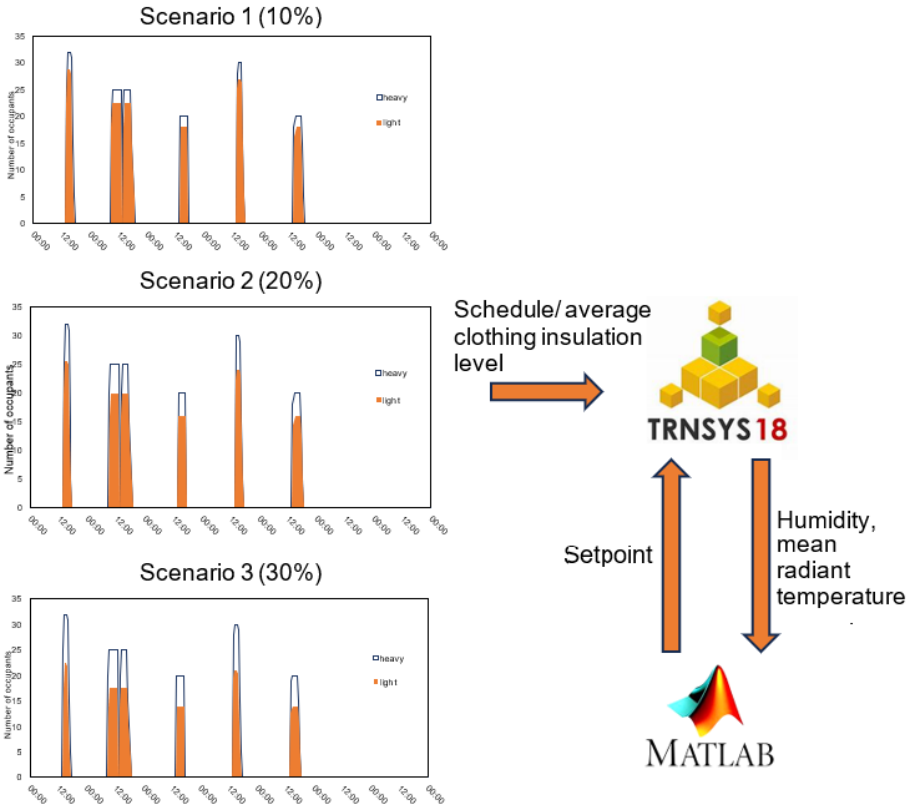

Fig. 6 Simulation scenarios for the evaluation of the PMV-based heating control strategy

3.2.1 Piecewise linearisation PMV and control algorithm

In this paper, we adopted the widely recognised Fanger's Predicted Mean Vote (PMV) model for real-time indoor comfort estimation [24]. The PMV model provides a thermal sensation index on a seven-point scale ranging from -3 (cold sensation) to +3 (hot sensation) and is determined by six environmental variables (indoor air temperature t_a, mean radiant temperature t_r, relative humidity h_{r} and air velocity v_{ar}), as well as two physical factors related to occupants, namely their clothing level and metabolic rate. The mathematical expression for PMV is given as follows:

$$PMV = [0.303 \cdot \exp(-0.036 \cdot M) + 0.028] \cdot \begin{cases} (M-W) - 3.05 \cdot 10^{-3} \cdot [5733 - 6.99 \cdot (M-W) - P_a] - 0.42[(M-W) - 58.15 \\ -1.7 \cdot 10^{-5} \cdot M \cdot (5867 - P_a) - 0.0014 \cdot M \cdot (34 - t_a) \\ -3.96 \cdot 10^{-8} \cdot f_{cl} \cdot [(t_{cl}+273)^4 - (\overline{t_r}+273)^4] - f_{cl} \cdot h_c \cdot (t_{cl} - t_a) \end{cases} \quad (1)$$

$$t_{cl} = 35.7 - 0.028 \cdot (M-W) - I_{cl} \cdot \{3.96 \cdot 10^{-8} \cdot f_{cl} \cdot [(t_{cl}+273)^4 - (\overline{t_r}+273)^4] + f_{cl} \cdot h_c \cdot (t_{cl} - t_a)\} \quad (2)$$

$$h_c = \begin{cases} 2.38 \cdot |t_{cl} - t_a|^{0.25} \; for \; 2.38 \cdot |t_{cl} - t_a|^{0.25} > 12.1\sqrt{v_{ar}} \\ 12.1 \cdot \sqrt{v_{ar}} \; for \; 2.38 \cdot |t_{cl} - t_a|^{0.25} < 12.1\sqrt{v_{ar}} \end{cases} \quad (3)$$

$$f_{cl} = \begin{cases} 1.00 + 1.290 I_{cl} & for \; I_{cl} \le 0.078 \, m^2 \cdot K/W \\ 1.05 + 0.645 I_{cl} & for \; I_{cl} > 0.078 \, m^2 \cdot K/W \end{cases} \quad (4)$$

$$P_a = h_r \cdot 6.1094 \cdot exp[(17.625 \cdot t_a)/(t_a + 243.04)] \quad (5)$$

Where, M is the metabolic rate, W is the effective mechanical power, I_{cl} is the clothing insulation, f_{cl} is the clothing surface area factor, t_a is the air temperature, $\overline{t_r}$ is the mean radiant temperature, v_{ar} is the air velocity, P_a is the water vapour partial pressure, h_c is the convective heat transfer coefficient and t_{cl} is the clothing surface temperature. To evaluate the practicality of Fanger's model, we conducted a thermal sensation questionnaire involving the individuals during the tests, comparing the calculated sensation votes from Fanger's model with the participants' actual thermal sensations. The detailed verification process is elaborated in Section B2. The results demonstrated that Fanger's model effectively predicted the occupants' real thermal sensations. However, the complexity arising from the nonlinearity of Fanger's model has hindered its practical applicability, particularly in the context of building energy optimisation control. To address this issue, our study proposes a piecewise linearisation technique [10] of Fanger's model and incorporates it into our PMV-based feedback control system. This approach aims to

enhance the practicality and usability of Fanger's model in real-world applications, particularly in the context of building energy management and control.

To address the nonlinearity of equations (1), (2), and (5), a method is proposed to divide the ranges of indoor air temperature, mean radiant temperature, and clothing surface temperature into segments, denoted as I, L, and J, respectively. This division allows for the introduction of slopes (a), intercepts (b), and an integer variable (z), which facilitate the approximation of the nonlinear terms in equations (1), (2), and (5) to linear forms:

$$(t_{cl}+273)^4-(\overline{t_r}+273)^4 = \sum_{i=1}^{I}(a_{cl,i}\cdot t_{cl,i}+b_{cl,i}\cdot z_{cl,i})-\sum_{l=1}^{L}(a_{tr,l}\cdot t_{tr,l}+b_{tr,l}\cdot z_{tr,l}) \quad (6)$$

$$p_a=\sum_{j=1}^{J}h_r(a_{ta,j}\cdot t_{a,j}+b_{ta,j}\cdot z_{ta,j}) \quad (7)$$

With the constraints for $t_{cl,i}$, $z_{cl,i}$, $t_{tr,l}$, $z_{tr,l}$, $t_{a,j}$ and $z_{ta,j}$:

$$\begin{cases}\sum_{i=1}^{I} z_{cl,i}=1\,, t_{cl}=\sum_{i=1}^{I} t_{cl,i}\\ z_{cl,i}\cdot t_{cl,i}^{min}\le t_{cl,i}\le z_{cl,i}\cdot t_{cl,i}^{max}\end{cases} \quad (8)$$

$$\begin{cases}\sum_{l=1}^{L} z_{tr,l}=1\,, t_{tr}=\sum_{l=1}^{L} t_{tr,l}\\ z_{tr,l}\cdot t_{tr,l}^{min}\le t_{tr,l}\le z_{tr,l}\cdot t_{tr,l}^{max}\end{cases} \quad (9)$$

$$\begin{cases}\sum_{j=1}^{J} z_{ta,j}=1\,, t_a=\sum_{j=1}^{J} t_{a,f}\\ z_{ta,j}\cdot t_{ta,j}^{min}\le t_{a,j}\le z_{ta,j}\cdot t_{ta,j}^{max}\end{cases} \quad (10)$$

$t_{cl,i}, t_{tr,l}$ and $t_{a,j}$ mean the i-th segment, l-th segment and j-th segment of clothing surface temperature, mean radiant temperature and indoor air temperature. $a_{cl,i}$, $a_{ta,j}$ and $b_{cl,i}b_{ta,j}$ are the slopes and intercepts of the i-th segment, l-th segment and j-th segment of clothing surface temperature, mean radiant temperature and indoor air temperature respectively. For example, the integer variable $z_{cl,i}=1$ means the clothing surface temperature is optimised in the ranges of i-th segement. In our case study, the indoor temperature during occupied periods usually ranges between 15℃ and 25℃. Te air temperature and clothing surface temperature are equally divided into two segments according to [10] and the convective heat transfer coefficient is always calculated by the second equation of eq(3). The air velocity is assumed to be a constant 0.15 m/s in the case study building [24]. Slopes and intercepts are calculated by the original PMV model from the values of two endpoints of each segment. The problem then becomes a mixed linear program problem formed with piecewise affine functions by combining eq(6-10) to eq(1)(2)(5). The optimisation was formulated in MATLAB [54] through Yalmip toolbox [55]. The Gurobi solver [56] was

chosen. For each optimisation, the measured variables through sensors and input to the optimiser are:

$$[M \quad W \quad f_{cl} \quad I_{cl} \quad h_r \quad \overline{t_r}] \tag{11}$$

With the objective function:

$$min \sum abs(PMV^k) \tag{12}$$

Subsequently, we conducted a validation of our approximate PMV model in comparison with the original PMV model, focusing on the indoor air temperature and mean radiant temperature. The results of the validation revealed that the PMV values obtained from both models exhibited very small differences, with a maximal absolute error of less than 0.024. From a practical standpoint, this level of discrepancy is considered negligible. The comprehensive validation process is elaborated in Section B3, providing robust evidence of the accuracy and reliability of our approximate PMV model in estimating thermal comfort levels based on indoor air temperature and mean radiant temperature.

3.2.2 TRNSYS modelling

In our study, we employed TRNSYS modelling to simulate the indoor response of the case study lecture room and send the measured data to the PMV-based control algorithm proposed in MATLAB (Fig 5). Within TRNSYS, Type 56 was utilised to simulate the room model, while Type 1231 was employed to simulate the radiator with a constant inlet water temperature of 65 degrees and a flow rate set at a typical rate of 15 kg/(hm^2) [54]. Weather data specific to Nottingham was generated from Meteonorm [58] and read by TRNSYS Type 109. To validate our room model, we compared the simulated data with measured data over a period of two days (2nd December - 4th December). Detailed TRNSYS model validation results can be found in section B4. At the end of each time step, TRNSYS provided the mean radiant temperature, relative air humidity, and average clothing insulation level data, which was then fed to MATLAB to obtain the setpoint temperature for the radiator system in the subsequent time step. In this study, we assumed a metabolic rate of 1.2 met and zero external work of occupancy. The control strategy was set to traditional on/off, and the results will be evaluated to assess the performance of the PMV-based feedback control strategy concerning indoor thermal comfort and building energy efficiency.

4. Results and discussion

This section presents the detection performance of our proposed method for two test videos. The detection performance was analysed for feature extraction of different networks and

concluded the characteristics of transfer learning for daily clothing insulation classification. Furthermore, scenario-analysis of real-time clothing insulation feedback for PMV-based heating system optimisation through piecewise linearisation was conducted. The comparison between PMV-based intelligent control and conventional control was presented.

4.1 Performance of detection approach

Figure 6 displays the model training process, which utilised the GPU and lasted for six complete training cycles on the entire dataset. The training was carried out with minimal total loss and a learning rate of 0.0001, indicating that the network successfully learned all the features present in the training dataset. Additionally, 30% of the dataset was reserved for validation, and the classification model achieved an average accuracy of 96% during this validation process. As a result, the classification model demonstrated its capability to detect the specific features included in the training dataset and perform accurate classification accordingly.

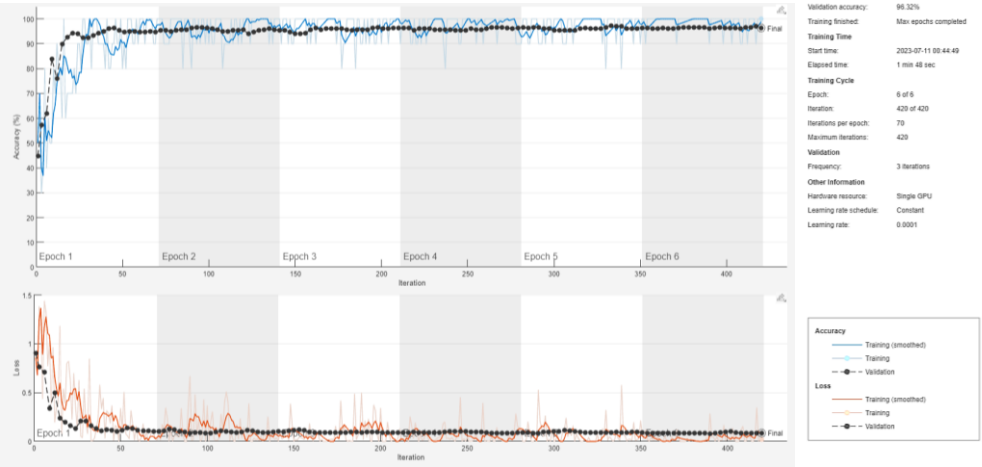

Fig. 7 Overview of the training of Googlenet

In Test 1 (Video 1) and Test 2 (Video 2), we present the video-level clothing insulation estimations for two examples. The overall detection results were further analysed using a confusion matrix and represented with statistical bars in Figure 8. The values in the confusion matrix indicate the percentage of the estimated clothing class relative to the true clothing class. Overall, the proposed method successfully estimated the video-level clothing insulation levels by capturing clothing change features (Video 2) and detecting the clothing levels of multiple people indoors (Video 1). The average estimation accuracy for clothing insulation level classification was found to be 83.99% for Video 1 and 93.20% for Video 2. Fig 9 show examples of detection frames.

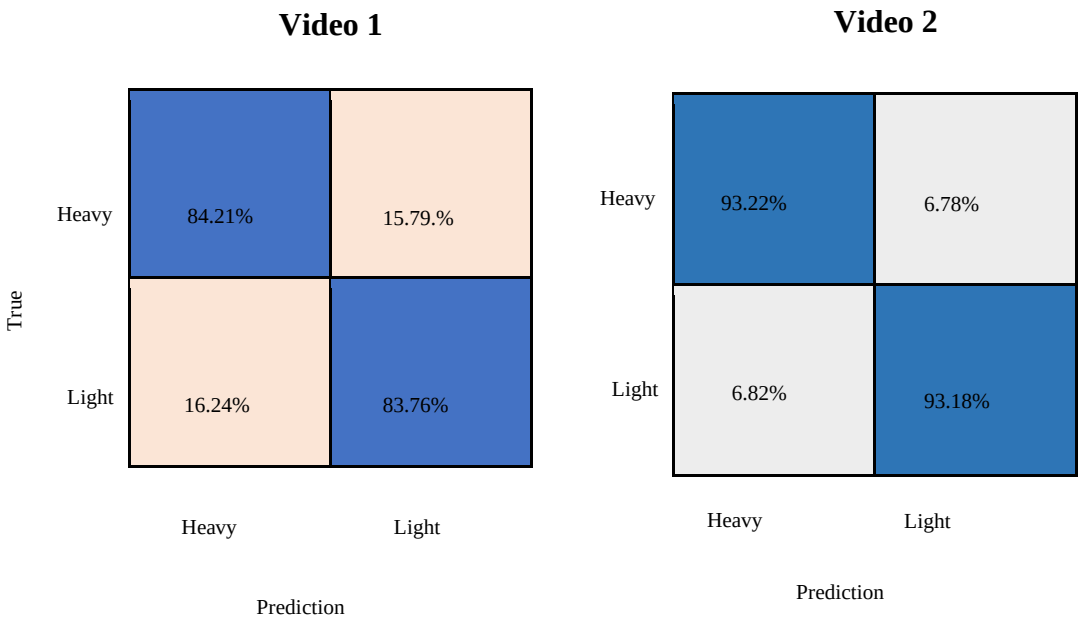

(a)

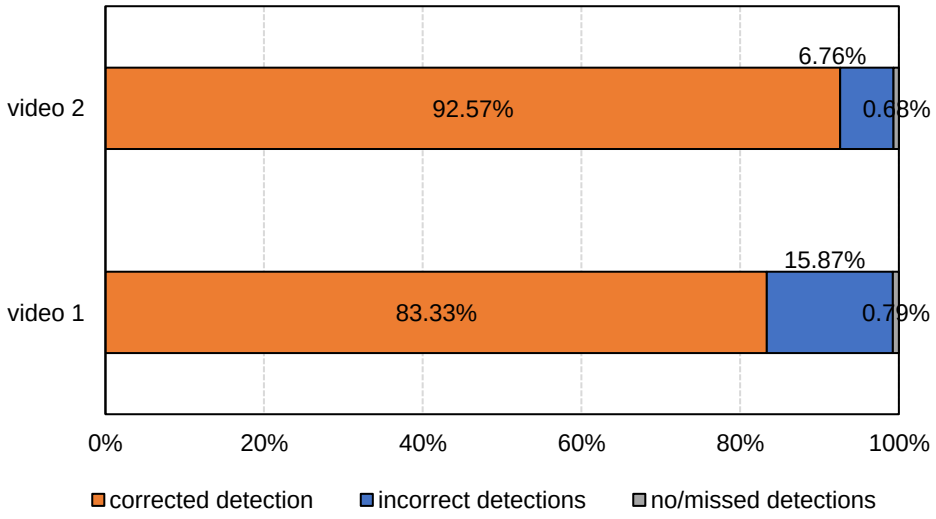

(b)

Fig. 8 Detection results presented in a (a) confusion matrix (b) statistical bar

Video 1 Example of real-time clothing detection in Test 1. ***Playable video available in the Appendix.***

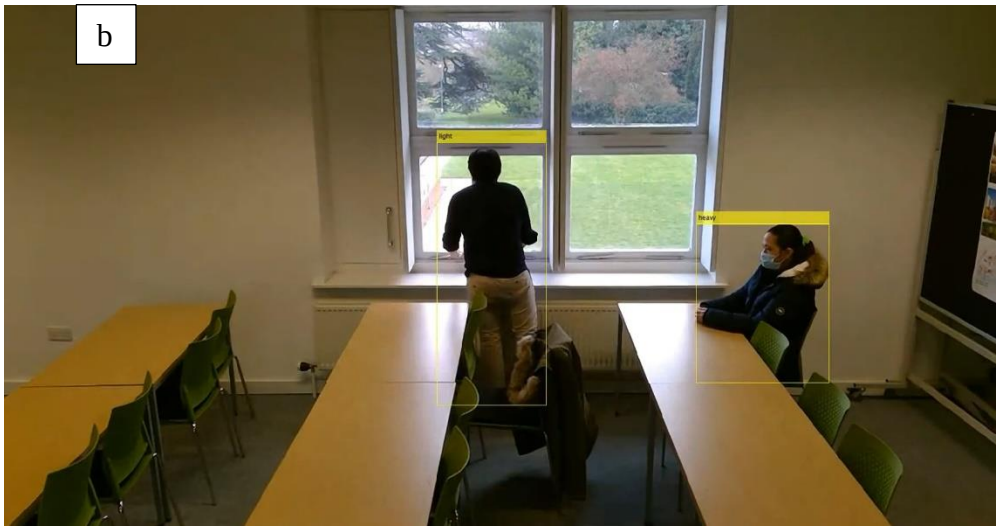

Video 2 Example of real-time clothing detection in Test 2 ***Playable video available in the Appendix.***

Fig. 9 Detection example of (a) video 1 (b) video 2

Several misclassifications were observed during the evaluation of the classifier. Notably, the classifier exhibited a tendency to incorrectly recognise heavy clothing as light clothing for individuals in Video 1 who were wearing relatively thin heavy clothing compared to other instances of heavy clothing within the camera's view. Consequently, the classifier might have identified these garments as hoodie or sweaters, as it was initially trained on features associated with light clothing. Additionally, in both videos, instances were observed where light clothing was mistakenly identified as heavy clothing, particularly under dark lighting conditions or when the entire body was not fully visible to the camera. Under dark lighting, skin areas uncovered by clothing were erroneously classified by the

classifier as being covered by cloth. Moreover, due to variations in sitting postures, air gaps were commonly present between the clothing and the body, and the volume of these air gaps depended on the individuals' postures. As a result, when the air gap was substantial, garments with relatively light insulation levels had a higher likelihood of being misclassified as heavy clothing. This observation aligns with a similar finding in the study by Choi et al. [59], where individuals wearing short clothing were mistaken for wearing long clothing when the classifier failed to recognise the naked forearm. Additionally, when there were overlapping features between the two clothing categories, the classifier also demonstrated a tendency to misclassify garments [60]. These identified challenges highlight the need for further refining the classifier's training and detection methods to address these limitations and improve accuracy.

In this study, we observed that thin heavy clothing had a high chance of being misclassified as light clothing and vice versa. For our classifier, we utilised GoogleNet [45] as a pretrained network for transfer learning, leveraging its prior training on the vast ImageNet [61] dataset, which comprises millions of photos. This choice of network allowed us to benefit from sufficient pretrained parameters, mitigating the risk of overfitting during transfer learning. Moving forward, we aim to enhance the classifier's performance by incorporating datasets related to lighting conditions and postures, thereby enabling additional feature training and activating additional network channels with relevant training information. Further evaluation involved analysing the accuracy of each detection, assessing correct, incorrect, and no/missed detections across different test segments (Fig 8b). With the help of a combined model and employing a hierarchy process, instances of missed detections were relatively rare in our study. This result attests to the feasibility and practicality of this combined approach, supporting its potential for improving clothing level classification accuracy.

Subsequently, we conducted tests to evaluate the clothing insulation estimation performance of three additional fine-tuned models, all trained on the same dataset, using test video 2 containing clothing changes and different activities. The performance of these models is presented in the form of a confusion matrix, shown in Fig 10. The training results are detailed in section B5. For transfer learning, we employed three widely used pre-trained networks: ResNet [46], VGG19 [47], and SqueezeNet [48]. The methodology and process for transfer learning are elaborated in Section 3.1.1. These tests aimed to compare the performance of multiple fine-tuned models and determine the most suitable model for accurate clothing insulation estimation in real-time applications.

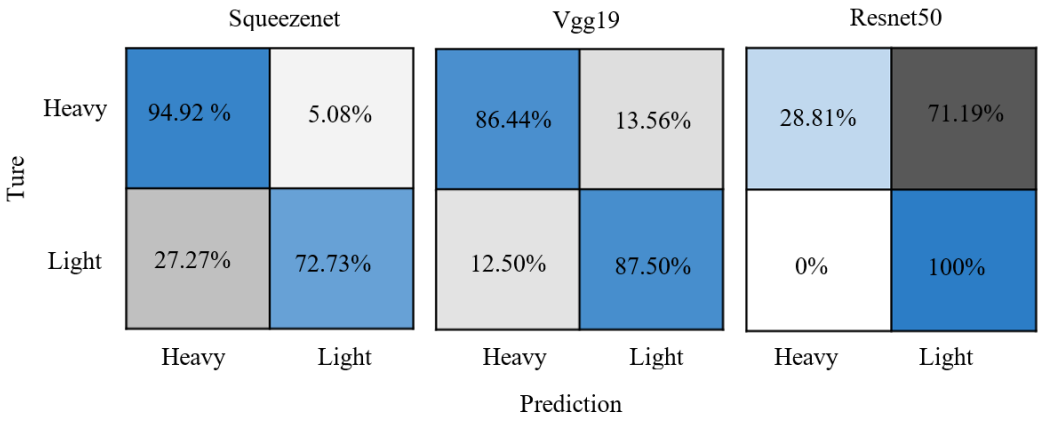

Fig. 10. Clothing insulation level estimation using the three fine-tuned models on test video 2

Overall, the ResNet50-based classifier exhibited limitations in recognising heavy clothing in our test video, despite being trained on our dataset. The primary reason for this misclassification could be attributed to the inadequate learning of relevant features from the training dataset. An example illustrating this issue is depicted in Fig 11, where individuals wearing heavy clothing were mistakenly recognised by the classifier as "light." These results highlight the need for further investigation and improvement in feature learning to enhance the accuracy of the ResNet50-based classifier in identifying heavy clothing in real-time scenarios.

Fig. 11. Example 1 of resnet50-based classifier detection

In the context of individuals sitting down, the Vgg19-based classifier displayed a tendency to misclassify people wearing heavy clothing as light clothing, particularly when the heavy clothing was relatively thin. However, the Squeezenet-based classifier exhibited greater reliability in this scenario, as depicted in Fig 12. This observation suggests that the

Squeezenet model is more effective in accurately distinguishing between heavy and light clothing when individuals are seated, making it a potentially more suitable choice for real-time clothing insulation estimation in such situations.

When people were sitting, vgg19-based classifier has chance to recognise people wear heavy clothing as light clothing, this occurs when people wear relatively thin heavy clothing. While Squeezenet-based classifier is more reliable in this case (Fig 12).

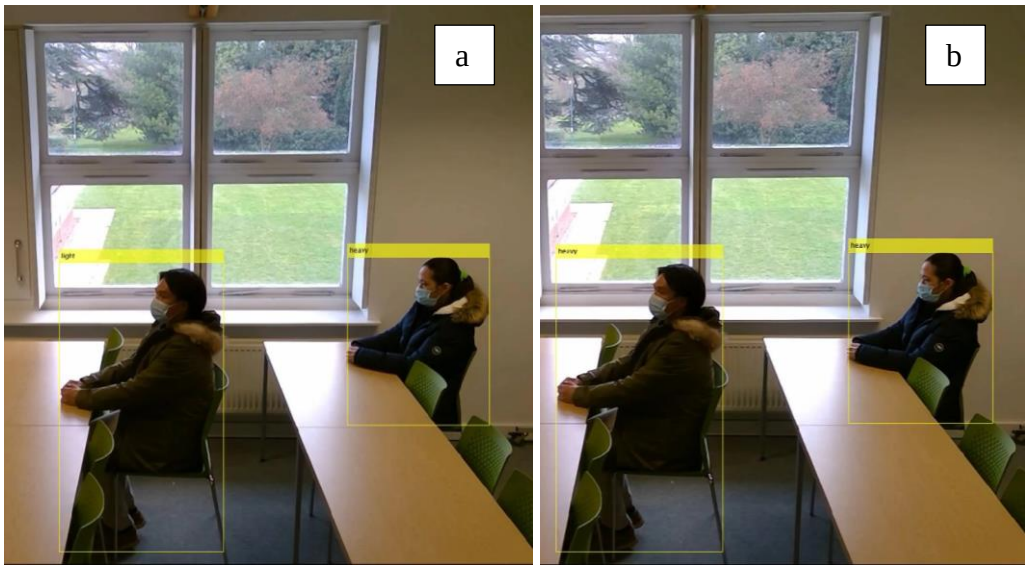

Fig. 12. Example 2 of (a) vgg19-based classifier detection (b) squeezenet-based classifier detection

While both the Squeezenet-based and Vgg19-based classifiers displayed misrecognition of light clothing as heavy clothing in instances of dark lighting or when individuals were not fully visible to the camera (Fig 13), the Squeezenet-based classifier exhibited a higher likelihood of misclassification, leading to a higher overall error rate (Fig 10). This observation suggests that the Squeezenet model may be more susceptible to inaccuracies in these challenging conditions, potentially impacting the reliability of its clothing insulation estimation compared to the Vgg19-based classifier.

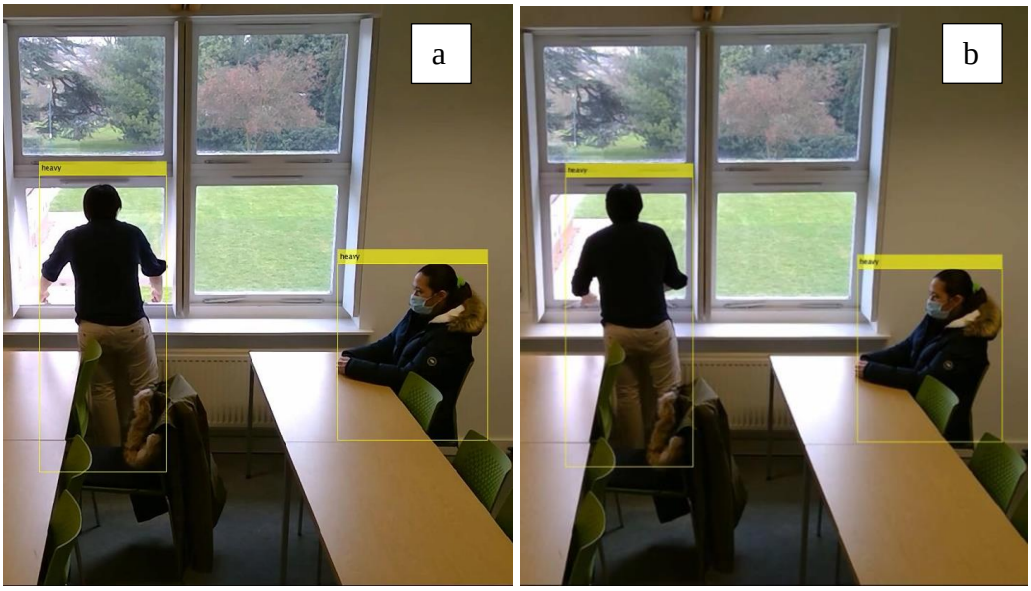

Fig. 13. Example 3 of (a) squeezenet-based classifier detection (b) vgg19-based classifier detection

In conclusion, among the three tested networks, GoogLeNet exhibited the best performance in clothing insulation detection. Squeezenet, Vgg19, and ResNet50 showed limitations in certain scenarios, including misclassifying light clothing as heavy and struggling with distinguishing clothing insulation levels in challenging situations. These findings suggest that the architecture and learned feature representations of the networks play a crucial role in their performance for clothing insulation detection. However, it is important to note that the relatively small training dataset used in this study may have limited the availability of comprehensive feature information for training, potentially leading to overfitting when applying different pre-trained networks. To address this limitation, a larger and more diverse dataset is recommended for future research, enabling the pre-trained parameters to learn distinct information from various clothing insulation levels. On a positive note, the comparison conducted in this study confirmed that pre-trained deep learning networks, such as GoogLeNet, have the capability to learn features deeply, allowing for effective transfer learning from smaller datasets and yielding satisfactory detection results even in the presence of various disturbances, such as different postures and lighting conditions, as demonstrated in our study.

4.2 Performance of PMV-based control strategy

The simulation was conducted over the course of a week, and the results are presented in Fig 8. The "reference case" corresponds to the conventional on/off control strategy, where the indoor temperature setpoints were maintained between 21 to 23 ℃. The cases labelled as "10%", "20%", and "30%" refer to scenarios where 10%, 20%, and 30% under proposed control strategy of the indoor occupants were wearing heavy clothing, respectively. In the

first phase of our study, the setpoint trajectory generated by our feedback algorithm, using a combination of TRNSYS and MATLAB simulations (Fig 14a), effectively converged the PMV to zero under the current indoor conditions, which included parameters such as mean radiant temperature, relative humidity, and average indoor clothing insulation levels. The average PMV values for the 10%, 20%, and 30% occupancy cases were found to be -0.00096, -0.00011, and 0.000758, respectively. These results validate the practicality and accuracy of our control strategy in accurately summarising measured data and precisely guiding indoor setpoints for maintaining thermal comfort. Additionally, Fig 8a indicates that clothing level significantly influences the PMV value, thereby influencing the indoor temperature setpoints and ultimately impacting building energy usage. Notably, the setpoint trajectory for the case with 10% of occupants wearing heavy clothing overlaps with the original fixed setpoint case. However, as the percentage of occupants wearing heavy clothing increases, the PMV-based strategy and the conventional strategy diverge, making it impossible for the two setpoints to converge.

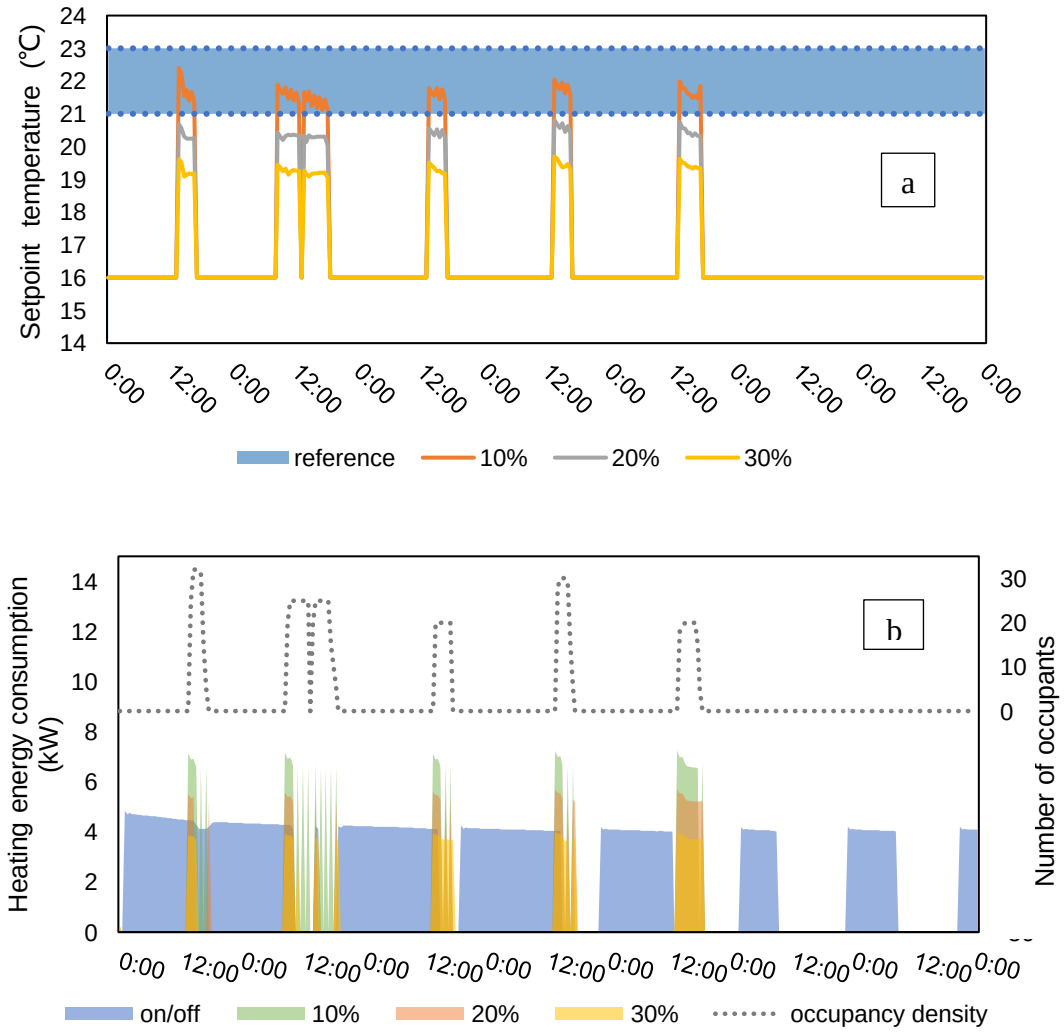

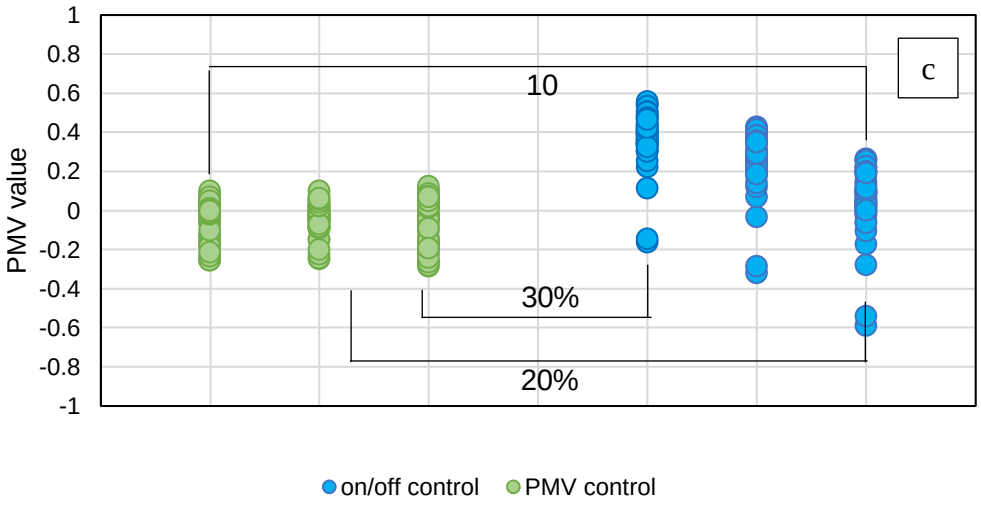

Fig. 14 (a) Generated setpoints (b) energy usage (c) indoor PMV values under different scenarios

The energy usage and indoor PMV index results are showed in Fig 8b and c. The proposed strategy shifted the energy to occupancy periods (Fig 14b). Overall, the total heating energy consumption for conventional, and proposed method at 10%, 20% and 30% cases were 465kWh, 136kWh, 91kWh and 78kWh. Since the case study room had highly variable indoor occupancy condition, by switch heating on only for periods of preheating and occupants' presents, a large portion of energy was saved compared with conventional fixed setpoint strategy, which is turning on throughout the whole week. Then, we used a flexibility factor (FF) [57] (eq 13) to indicate the increase of occupant-related energy flexibility by proposed algorithm, which describes the ability for energy shifting from non-occupancy periods to occupancy periods.

The energy usage and indoor PMV index results are presented in Fig 8b and c. The feedback control strategy effectively redistributed the energy consumption to align with the occupancy periods (Fig 14b). Specifically, the total heating energy consumption for the conventional fixed setpoint, 10%, 20%, and 30% occupancy cases were found to be 465 kWh, 136 kWh, 91 kWh, and 78 kWh, respectively. The case study room exhibited highly variable indoor occupancy conditions, and the proposed strategy switched on the heating system only during preheating periods and when occupants were present, leading to substantial energy savings compared to the conventional fixed setpoint strategy, which operates continuously throughout the entire week. To assess the increase in occupant-related energy flexibility enabled by our proposed algorithm, we employed the flexibility factor (FF) [57] (eq 13), which quantifies the ability to shift energy consumption from non-occupancy periods to occupancy periods.

$$Flexibility\ factor\ (FF) = \frac{E_{occupancy} - E_{non-occupancy}}{E_{occupancy} + E_{non-occupancy}} \quad (13)$$

$E_{occupancy}$ and $E_{non-occupancy}$ mean the energy consumption during occupancy and non-occupancy times.

The flexibility factor (FF) takes values between -1 and 1, with lower FF values indicating poorer energy efficiency resulting from occupant-centred HVAC control. A negative FF value suggests that energy is primarily consumed during non-occupancy periods. In our study, the FF values for the conventional fixed setpoint, 10%, 20%, and 30% occupancy cases were -0.87, 0.48, 0.39, and 0.49, respectively. These results demonstrate that our proposed control strategy significantly improved the energy efficiency of the HVAC system for maintaining indoor thermal comfort. Specifically, the proposed strategy effectively shifted energy consumption from non-occupancy periods to occupancy periods, leading to a considerable reduction in thermal energy usage. This finding aligns with previous studies [28, 62, 63], which have also confirmed that occupant-centred control strategies for HVAC systems can enhance energy efficiency through effective energy shifting. By precisely releasing energy based on indoor occupants' intentions and utilising indoor sensing information, control strategies can effectively reduce overall energy consumption.

Subsequently, we plotted the calculated PMV values obtained by controlling indoor temperatures under both the conventional and proposed strategies. As shown in Fig 14c, the proposed strategy successfully guided the indoor temperature towards a state of thermal neutrality, indicated by a PMV value of 0. This result confirms the feasibility of the proposed method in applying reference tracking to guide indoor temperatures towards thermal neutrality. Observing both Fig 14a and Fig 14c, it is evident that under the conventional control strategy, occupants tend to experience a sensation of being too warm, particularly in the 20% and 30% occupancy cases. However, in the 10% occupancy case, the thermal sensation is comparable between the conventional and proposed control strategies, largely due to the variation in clothing insulation levels. Similar findings have been reported in other studies as well. For instance, Xu et al. [10] found that a PMV-based indoor air temperature setpoint was higher than the conventional given range of temperature setpoints during most occupied times in cooling seasons, owing to the relatively light clothing worn by occupants in their case study. Similarly, Choi [59] demonstrated that when PMV-based setpoints closely resembled the current indoor temperature controlled by a conventional given range of setpoint strategy, occupants tended to report "no change" in thermal perception, indicating a satisfactory level of thermal comfort. Our 10% occupancy case further supports these observations.

4.3 Real-time sensing for indoor temperature setpoint control

In Fig 15a, we present an example of our proposed algorithm for determining setpoints using real-time sensing data. The algorithm begins by capturing a single frame of video through the "readFrame" function in MATLAB. Subsequently, the YOLO object detection algorithm is called to identify and crop the regions corresponding to each indoor occupant. Each cropped region is then passed through our transfer-learned network for clothing insulation level classification, yielding an average indoor clothing insulation level. Furthermore, relevant measured data, such as mean radiant temperature and relative humidity, are read by the MATLAB engine and prepared for optimal setpoint calculation. The calculation of the optimal setpoint is achieved through our proposed piecewise linearisation PMV optimisation, as shown in the example in Fig 15a which corresponds to 20.2 ℃. This process enables real-time adjustments of indoor temperature setpoints based on occupants' clothing insulation and environmental conditions, providing a personalised and energy-efficient thermal comfort experience.

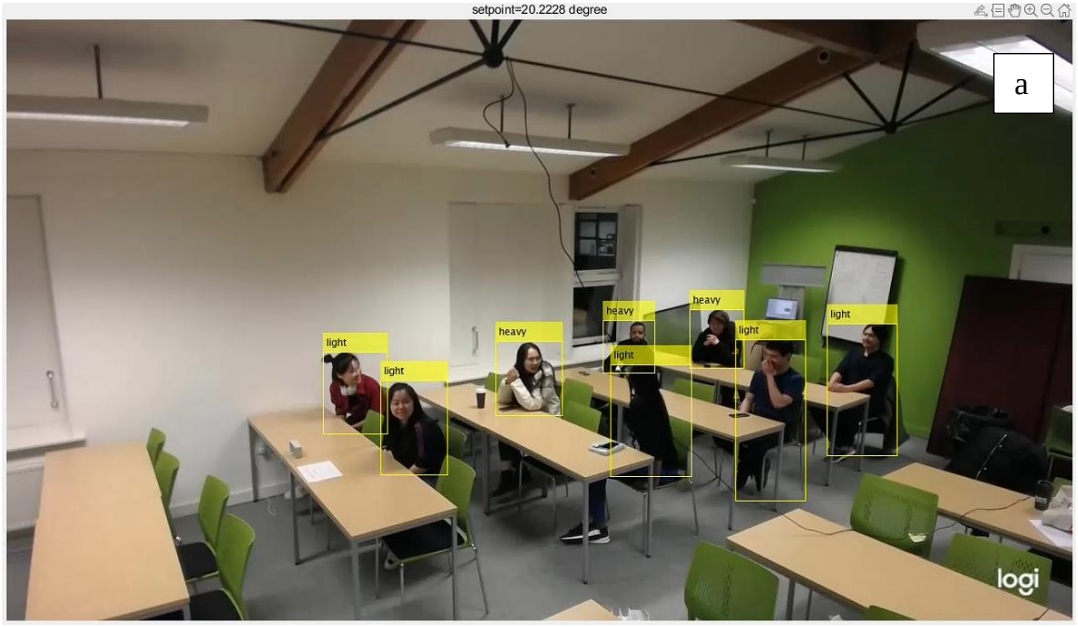

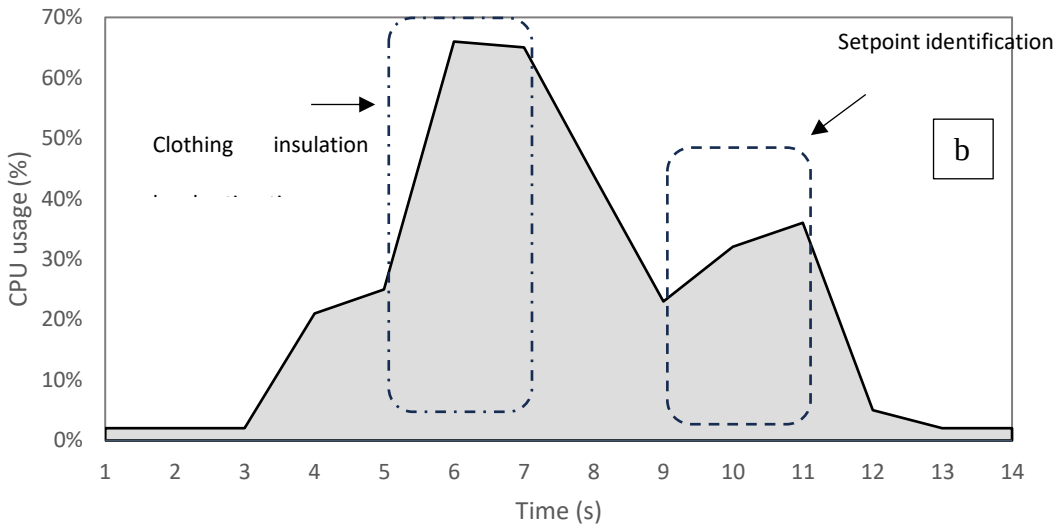

Fig. 15 (a) An example of algorithm output, along with (b) CPU usage during tasks performing.

In Fig. 15, we present the results of our algorithm's output (Fig. 15a) and the corresponding CPU usage during task execution (Fig. 15b). To assess the practicality of the proposed algorithm in real-world applications, we recorded the PC's performance during a single action. In this study, the control time interval was set to 30 minutes, and the total computation time of the algorithm remained below 10 seconds (Fig. 15b), making it suitable for implementation. The proposed algorithm is compatible with most building energy management systems, where indoor parameters typically do not change significantly within such short time intervals. As a result, the proposed control strategy can effectively fulfill the task of online control.

Notably, the CPU usage for setpoint identification is relatively low compared to the previous computer vision process (Fig. 15b). This observation confirms the lightweight nature of our optimal strategy, achieved by compressing the nonlinear problem into simple mixed-integer problems based on piecewise linearisation, rather than fine-tuning the setpoint until it reaches a zero PMV value, as commonly used in PMV-based control. Overall, the proposed strategy efficiently performs multiple tasks with lightweight CPU usage and fast response times.

The proposed strategy also allows for further intelligent sensing technique integrations, enabling the rearrangement of data allocations in the algorithm to achieve different objectives. By embracing advanced sensing technologies, our approach holds promise for enhancing building energy efficiency and thermal comfort through optimised control strategies tailored to specific requirements.

5. Conclusion and recommendations for future works

The present work employed a detection approach based on deep vision for the detection and prediction of the occupant's clothing insulation in real-time to assist in determining PMV for a comfort-based control strategy. This will help ensure adequate indoor thermal comfort conditions while minimising energy wastage to enhance the overall building performance. The deep vision method was based on a Yolo and GoogleNet algorithms which was trained with a small image dataset and implemented in videos. Experiments were conducted in a case study university building to evaluate the performance of the proposed method. During the detection, the predicted information on the occupant's clothing level was used to communicate with a PMV-based control strategy. The generated profiles were then compared with the ground truth to evaluate the accuracy and reliability of the predictions. three scenarios were evaluated; 10%, 20% and 30% indoor occupants wear heavy clothing. The initial results suggest that the detector achieved satisfactory accuracy detecting occupants wear both light and heavy clothing. Future studies should explore the impact of data curation, labelling, and training on detection performance. This includes exploring the impact of the types of detection responses selected, the types of images used, the dataset size and how the images were proposed prior to the training of the models. The detection of multiple occupancies showed the potential impact of the room conditions, such as the lighting level, camera position, and the activities carried out by the occupant. Scenario-based modelling and simulations were conducted to predict the impact of the proposed approach on a building's thermal comfort and energy performance. It was observed that the actual PMV values did not match the estimated values using the pre-defined profile. It gave insights into how the changes in clothing level could affect the occupant's thermal comfort. By applying the temperature setpoint adjustment based on PMV results, the thermal comfort within the space could be enhanced by satisfying the real-time heating demands of occupants. Meanwhile, the heating energy consumption was significantly reduced compared with the reference case.

The initial findings demonstrated that such a detection approach could provide PMV-based control strategies with real-time clothing insulation and adjustment to improve thermal comfort and address the issues faced using pre-defined values. While the capabilities of the detection method in predicting the clothing insulation level of multiple occupants performing different activities was shown, we do acknowledge that the accuracy and precision in some cases was a little low, and our biggest modification direction of this approach will be to further enhance the detection accuracy. This includes further enhancement of the image dataset, with a greater number of training images and the exploration towards developing the deep learning model further with the application of

techniques such as image segmentation to enable higher accuracy in terms of recognition for different clothing levels. The present work only evaluated two levels of clothing insulation and the use of the image segmentation approach to detect different types and levels of clothing. Further verification of such models is required to ensure such model design can provide accurate detections and become an effective solution. Further developments include a series of tests and evaluations of the application of the detector on various types of clothing levels in different indoor spaces. Furthermore, we envision that this approach can work alongside all other detection strategies that can be performed using the same camera, which can provide real-time data for the HVAC system, for example, occupancy, equipment use, and window detection. Additionally, the sub zonal control is expected to be designed for achieving thermal neutral in different locations in a room with zonal heating equipment that can be controlled separately.

Acknowledgement

We would like to acknowledge the support provided by the University of Nottingham and the Engineering and Physical Sciences Research Council (EPSRC). We also thank the volunteers who participated and supported the experiments.

Reference

1. Word Economic Forum, Why buildings are the foundation of an energy-efficient future, 2021

2. Du, Y., Zandi, H., Kotevska, O., Kurte, K., Munk, J., Amasyali, K., ... & Li, F. (2021). Intelligent multi-zone residential HVAC control strategy based on deep reinforcement learning. *Applied Energy*, *281*, 116117.

3. Wallace, L. A. (1987). *The total exposure assessment methodology (TEAM) study: Summary and analysis* (Vol. 1, pp. 966-75). Washington, DC: Office of Research and Development, US Environmental Protection Agency.

4. Wu, W., Skye, H. M., & Domanski, P. A. (2018). Selecting HVAC systems to achieve comfortable and cost-effective residential net-zero energy buildings. *Applied energy*, *212*, 577-591.

5. Du, Y., Zandi, H., Kotevska, O., Kurte, K., Munk, J., Amasyali, K., ... & Li, F. (2021). Intelligent multi-zone residential HVAC control strategy based on deep reinforcement learning. *Applied Energy*, *281*, 116117.

6. Hawila, A. A. W., Merabtine, A., Chemkhi, M., Bennacer, R., & Troussier, N. (2018). An analysis of the impact of PMV-based thermal comfort control during heating period: A case study of highly glazed room. *Journal of Building Engineering*, *20*, 353-366.

7. Tien, P. W., Wei, S., Calautit, J. K., Darkwa, J., & Wood, C. (2022). Real-time monitoring of occupancy activities and window opening within buildings using an

integrated deep learning-based approach for reducing energy demand. *Applied Energy*, *308*, 118336.

8. American Society of Heating, Refrigerating and Air-Conditioning Engineers. (2017). *Thermal Environmental Conditions for Human Occupancy: ANSI/ASHRAE Standard 55-2017 (Supersedes ANSI/ASHRAE Standard 55-2013) Includes ANSI/ASHRAE Addenda Listed in Appendix N*. Ashrae.

9. Kang, D. H., Mo, P. H., Choi, D. H., Song, S. Y., Yeo, M. S., & Kim, K. W. (2010). Effect of MRT variation on the energy consumption in a PMV-controlled office. *Building and Environment*, *45*(9), 1914-1922.

10. Xu, Z., Hu, G., Spanos, C. J., & Schiavon, S. (2017). PMV-based event-triggered mechanism for building energy management under uncertainties. *Energy and Buildings*, *152*, 73-85.

11. Ferreira, P. M., Ruano, A. E., Silva, S., & Conceicao, E. Z. E. (2012). Neural networks based predictive control for thermal comfort and energy savings in public buildings. *Energy and buildings*, *55*, 238-251.

12. ASHRAE, A. (2013). Standard 55-2013, Therm. *Environ. Cond. Hum. Occup*.

13. Freire, R. Z., Oliveira, G. H., & Mendes, N. (2008). Predictive controllers for thermal comfort optimisation and energy savings. *Energy and buildings*, *40*(7), 1353-1365.

14. Hwang, R. L., & Shu, S. Y. (2011). Building envelope regulations on thermal comfort in glass facade buildings and energy-saving potential for PMV-based comfort control. *Building and Environment*, *46*(4), 824-834.

15. Iso, B. S. E. N. (2009). Ergonomics of the thermal environment—Estimation of thermal insulation and water vapor resistance of a clothing ensemble (ISO 9920: 2007, Corrected version 2008-11-01). *Management*.

16. Labeodan, T., Zeiler, W., Boxem, G., & Zhao, Y. (2015). Occupancy measurement in commercial office buildings for demand-driven control applications—A survey and detection system evaluation. *Energy and Buildings*, *93*, 303-314.

17. Choi, H., Um, C. Y., Kang, K., Kim, H., & Kim, T. (2021). Review of vision-based occupant information sensing systems for occupant-centric control. *Building and Environment*, *203*, 108064.

18. Wei, S., Tien, P. W., Calautit, J. K., Wu, Y., & Boukhanouf, R. (2020). Vision-based detection and prediction of equipment heat gains in commercial office buildings using a deep learning method. *Applied Energy*, *277*, 115506.

19. H. Kim, H. Kang, H. Choi, D. Jung, and T. Hong, "Human-building interaction for indoor environmental control: Evolution of technology and future prospects," *Automation in construction*, vol. 152, p. 104938, 2023, doi: 10.1016/j.autcon.2023.104938.

20. Pincott, J., Tien, P. W., Wei, S., & Kaiser Calautit, J. (2022). Development and evaluation of a vision-based transfer learning approach for indoor fire and smoke detection. *Building Services Engineering Research and Technology*, 01436244221089445.
21. Yamaguchi, K., Hadi Kiapour, M., & Berg, T. L. (2013). Paper doll parsing: Retrieving similar styles to parse clothing items. In *Proceedings of the IEEE international conference on computer vision* (pp. 3519-3526).
22. Liu, Z., Luo, P., Qiu, S., Wang, X., & Tang, X. (2016). Deepfashion: Powering robust clothes recognition and retrieval with rich annotations. In *Proceedings of the IEEE conference on computer vision and pattern recognition* (pp. 1096-1104).
23. Inoue, N., Simo-Serra, E., Yamasaki, T., & Ishikawa, H. (2017). Multi-label fashion image classification with minimal human supervision. In *Proceedings of the IEEE International Conference on Computer Vision Workshops* (pp. 2261-2267).
24. ISO, "7730: Ergonomics of the thermal environment Analytical determination and interpretation of thermal comfort using calculation of the PMV and PPD indices and local thermal comfort criteria," *Management,* vol. 3, no. 605, p. e615, 2005.
25. Lee, J. Y., Ko, E. S., Lee, H. H., Kim, J. Y., & Choi, J. W. (2011). Validation of clothing insulation estimated by global and serial methods. *International Journal of Clothing Science and Technology*.
26. A. V. M. Oliveira, A. R. Gaspar, and D. A. Quintela, "Measurements of clothing insulation with a thermal manikin operating under the thermal comfort regulation mode: comparative analysis of the calculation methods," *European journal of applied physiology,* vol. 104, no. 4, pp. 679-688, 2008, doi: 10.1007/s00421-008-0824-5.
27. Zampetti, L., Arnesano, M., & Revel, G. M. (2018). Experimental testing of a system for the energy-efficient sub-zonal heating management in indoor environments based on PMV. *Energy and Buildings*, *166*, 229-238.
28. Wu, J., Li, X., Lin, Y., Yan, Y., & Tu, J. (2020). A PMV-based HVAC control strategy for office rooms subjected to solar radiation. *Building and Environment*, *177*, 106863.
29. E. Z. E. Conceição, J. M. M. Gomes, and A. E. Ruano, "Application of HVAC Systems with Control Based on PMV Index in University Buildings with Complex Topology," *IFAC PapersOnLine*, vol. 51, no. 10, pp. 20-25, 2018, doi: 10.1016/j.ifacol.2018.06.230.
30. A. AC08013703, *Ergonomics of the thermal environment-Estimation of thermal insulation and water vapour resistance of a clothing ensemble*. ISO, 2008.
31. Zhang, S., Cheng, Y., Fang, Z., & Lin, Z. (2018). Dynamic control of room air temperature for stratum ventilation based on heat removal efficiency: Method and experimental validations. *Building and Environment*, *140*, 107-118.

32. Schiavon, S., & Lee, K. H. (2013). Dynamic predictive clothing insulation models based on outdoor air and indoor operative temperatures. *Building and Environment*, *59*, 250-260.

33. Huang, J. (2008). Calculation of thermal insulation of clothing from mannequin test. *Measurement Techniques*, *51*(4), 428-435.

34. Kuklane, K., Gao, C., Wang, F., & Holmér, I. (2012). Parallel and serial methods of calculating thermal insulation in European manikin standards. *International journal of occupational safety and ergonomics*, *18*(2), 171-179.

35. Li, Y., De La Ree, J., & Gong, Y. (2018, October). The smart thermostat of HVAC systems based on PMV-PPD model for energy efficiency and demand response. In *2018 2nd IEEE Conference on Energy Internet and Energy System Integration (EI2)* (pp. 1-6). IEEE.

36. Lee, K., Choi, H., Kim, H., Kim, D. D., & Kim, T. (2020). Assessment of a real-time prediction method for high clothing thermal insulation using a thermoregulation model and an infrared camera. *Atmosphere*, *11*(1), 106.

37. Lu, S., & Cochran Hameen, E. (2018). Integrated IR Vision Sensor for Online Clothing Insulation Measurement.

38. Liu, J., Foged, I. W., & Moeslund, T. B. (2021). Automatic estimation of clothing insulation rate and metabolic rate for dynamic thermal comfort assessment. *Pattern Analysis and Applications*, 1-16.

39. Miura, J., Demura, M., Nishi, K., & Oishi, S. (2020). Thermal comfort measurement using thermal-depth images for robotic monitoring. *Pattern Recognition Letters*, *137*, 108-113.

40. Guo, Y., Tan, Z., Chen, H., Li, G., Wang, J., Huang, R., ... & Ahmad, T. (2018). Deep learning-based fault diagnosis of variable refrigerant flow air-conditioning system for building energy saving. *Applied Energy*, *225*, 732-745.

41. Tien, P. W., Wei, S., Calautit, J. K., Darkwa, J., & Wood, C. (2021). Occupancy heat gain detection and prediction using deep learning approach for reducing building energy demand. *Journal of Sustainable Development of Energy, Water and Environment Systems*, *9*(3), 1-31.

42. Wei, S., Tien, P. W., Wu, Y., & Calautit, J. K. (2021). The impact of deep learning–based equipment usage detection on building energy demand estimation. *Building Services Engineering Research and Technology*, *42*(5), 545-557.

43. Z. Liu, P. Luo, S. Qiu, X. Wang, and X. Tang, "Deepfashion: Powering robust clothes recognition and retrieval with rich annotations," in *Proceedings of the IEEE conference on computer vision and pattern recognition*, 2016, pp. 1096-1104.

44. S. Matlab, "Matlab," *The MathWorks, Natick, MA*, 2012.

45. C. Szegedy *et al.*, "Going deeper with convolutions," in *Proceedings of the IEEE conference on computer vision and pattern recognition*, 2015, pp. 1-9.
46. K. He, X. Zhang, S. Ren, and J. Sun, "Deep residual learning for image recognition," in *Proceedings of the IEEE conference on computer vision and pattern recognition*, 2016, pp. 770-778.
47. K. Simonyan and A. Zisserman, "Very deep convolutional networks for large-scale image recognition," *arXiv preprint arXiv:1409.1556,* 2014.
48. F. N. Iandola, S. Han, M. W. Moskewicz, K. Ashraf, W. J. Dally, and K. Keutzer, "SqueezeNet: AlexNet-level accuracy with 50x fewer parameters and< 0.5 MB model size," *arXiv preprint arXiv:1602.07360,* 201
49. MathWorks. "Pretrained YOLO v4 Network for Object detection." https://uk.mathworks.com/matlabcentral/fileexchange/107969-computer-vision-toolbox-model-for-yolo-v4-object-detection?s_tid=srchtitle_pretrained%20yolo%20v4_1 (accessed 1st July, 2023).
50. Demanega, I., Mujan, I., Singer, B. C., Anđelković, A. S., Babich, F., & Licina, D. (2021). Performance assessment of low-cost environmental monitors and single sensors under variable indoor air quality and thermal conditions. *Building and Environment*, *187*, 107415.
51. PICO Technology. "calibration certificates for thermocouple loggers." https://www.picotech.com/accessories/data-logger-calibration/calibration-thermocouple-loggers (accessed 11th Dec, 2022).
52. AC08013621, A. (Ed.). (1998). *Ergonomics of the thermal environment-Instruments for measuring physical quantities*. ISO.
53. Kang, E., Lee, R., Yoon, J., Cho, H., & Kim, D. (2023). Uncertainty Assessment of Mean Radiant Temperature Estimation for Indoor Thermal Comfort Based on Clustering Analysis of Reduced-Input Surfaces. *Buildings*, *13*(2), 342.
54. L. Ljung, "System identification toolbox," *The Matlab user's guide,* 2014.
55. J. Lofberg, "YALMIP: A toolbox for modeling and optimization in MATLAB," in *2004 IEEE international conference on robotics and automation (IEEE Cat. No. 04CH37508)*, 2004: IEEE, pp. 284-289.
56. B. Bixby, "The gurobi optimiser," *Transp. Re-search Part B,* vol. 41, no. 2, pp. 159-178, 2007.
57. M. Hu, F. Xiao, J. B. Jørgensen, and R. Li, "Price-responsive model predictive control of floor heating systems for demand response using building thermal mass," *Applied thermal engineering,* vol. 153, pp. 316-329, 2019, doi: 10.1016/j.applthermaleng.2019.02.107.

58. J. Remund, S. Müller, M. Schmutz, and P. Graf, "Meteonorm version 8," *METEOTEST (www. meteotest. com),* 2020.
59. Choi, H., Jeong, B., Lee, J., Na, H., Kang, K., & Kim, T. (2022). Deep-vision-based metabolic rate and clothing insulation estimation for occupant-centric control. Building and Environment, 221, 109345.
60. H. Choi, H. Na, T. Kim, and T. Kim, "Vision-based estimation of clothing insulation for building control: A case study of residential buildings," *Building and environment,* vol. 202, p. 108036, 2021, doi: 10.1016/j.buildenv.2021.108036.
61. J. Deng, W. Dong, R. Socher, L.-J. Li, K. Li, and L. Fei-Fei, "Imagenet: A large-scale hierarchical image database," in *2009 IEEE conference on computer vision and pattern recognition*, 2009: Ieee, pp. 248-255.
62. J. Ren, J. Liu, S. Zhou, M. K. Kim, and J. Miao, "Developing a collaborative control strategy of a combined radiant floor cooling and ventilation system: A PMV-based model," *Journal of Building Engineering,* vol. 54, p. 104648, 2022, doi: 10.1016/j.jobe.2022.104648.
63. J. Park, H. Choi, D. Kim, and T. Kim, "Development of novel PMV-based HVAC control strategies using a mean radiant temperature prediction model by machine learning in Kuwaiti climate," *Building and environment,* vol. 206, p. 108357, 2021, doi: 10.1016/j.buildenv.2021.108357.
64. Chartered Institution of Building Services Engineer (CIBSE), 2015. Environmental Design: CIBSE Guide, A; CIBSE: London, UK.

Appendix

B1. Material and construction information of case study room

The lecture room under study has specific dimensions, measuring 12.75 meters in length and 7.6 meters in width, with variable heights ranging from 2.71 meters to 4.26 meters. The room features windows on both the south-east and north-west facing walls, with window-to-wall ratios of 0.22 and 0.08, respectively. To create an accurate representation of the actual structure, the construction of the room was based on real-world materials. Table B1 provides a comprehensive list of the materials used, arranged in the order from the outside to the inside of the room. Additionally, Table 2 presents the properties and overall U-values of the walls, roof, and floor. The room was constructed using lightweight materials, while the U-value for the windows was assumed to be 1.1 W/m^2K.

Table B.1 Properties of materials in the case study room

	Material	Conductivity (w/m K)	Density (kg/m^3)	Specific heat (J/kg K)	Overall U-value (W/m^2 K)
Wall	100mm brick	0.84	1700	800	1.133
	100mm insulation	0.2	1000	1700	
	100mm concrete	1.13	2000	1000	
	225mm mild steel	45	7800	480	
Roof	0.9mm aluminum sheet	230	2700	880	0.259
	25mm Plywood	0.15	700	1420	
	150mm Softwood rafters	0.047	250	1300	
	67mm insulation	0.2	1000	1700	
Floor	95mm sand/cement	0.72	1860	840	2.301
	150mm concrete	1.13	2000	1000	
	heating pipes	30 pipes			

The estimation of internal heat gains attributed to occupants in the lecture room was conducted in accordance with the guidelines outlined in CIBSE Guide A [60]. For each occupant, the convective and radiative gains were calculated to be 46 W and 69 W, respectively. Furthermore, it was assumed that LED luminaires were installed, with each light having a maximum power consumption of 10 W, contributing to 30% of the total radiative gains. Similarly, the electric equipment was assumed to consume a maximum of 10 W per piece, with 20% of the generated heat being radiated. The usage patterns of both lighting and equipment were visually presented in Fig B1, offering a comprehensive

representation of their respective contributions to the internal heat gains within the lecture room.

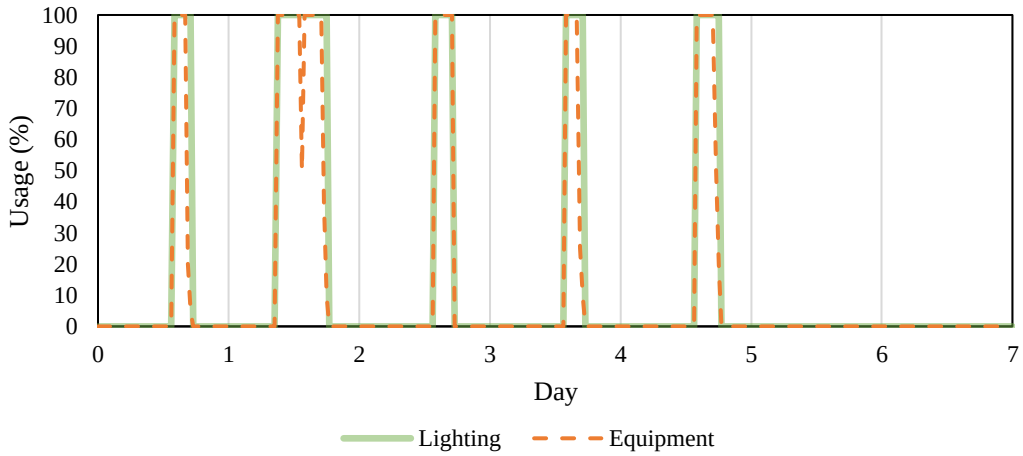

Fig B.1 Lighting and equipment usage

B2. Thermal sensation verification of applied Fanger's PMV model

In order to validate the optimal indoor temperature setpoints derived from Fanger's PMV model, a comparison was performed during the test periods for each data collection time, encompassing a total of 10 individuals. The calculated PMV values, obtained through inserting the optimal setpoints back into the original PMV model, were then assessed against the occupants' thermal sensations, as presented in Table B2. Additionally, a questionnaire was utilised to gather the occupants' intentions for the setpoints.

Table B.2. Data collected from 10 subjects

	Person 1	Person 2	Person 3	Person 4	Person 5	Person 6	Person 7	Person 8	Person 9	Person 10
Gender	Female	Female	Female	Female	Male	Male	Male	Male	Female	Female
Activity	Sitting	Sitting	Sitting	Sitting	Sitting	Sitting	Sitting	Sitting	Standing	Walking
Clothing level	Light	Light	Light	Heavy	Light	Heavy	Light	Heavy	Heavy	Heavy

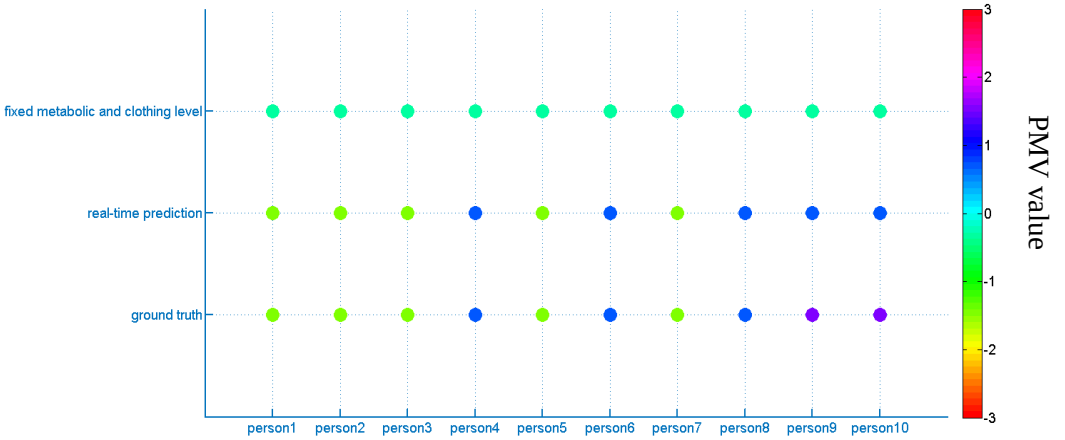

Fig B.2 PMV values obtained from different methods

The validation of the PMV prediction based on real-time observations is depicted in Fig B2. The fixed values of clothing insulation (Icl) and metabolic rate (M) were utilised in accordance with Table B3 and Fig B1. Remarkably, the subjects were consistently regarded as neutral according to the PMV predictions, implying that the indoor microclimate should remain unchanged. However, the actual sensations reported by the subjects during data collection suggested that the indoor temperature should be either increased or decreased. For instance, subjects wearing light clothing in a room with a temperature of 19.9°C felt slightly cool, which aligns with the calculated results. The Fanger's model predicted dynamic changes in thermal sensations from slightly cool to slightly warm with varying levels of clothing insulation and activity among the subjects. Overall, 8 out of 10 (80%) thermal sensations predicted by the proposed method were found to be in agreement with the real sensations reported by the subjects. This comparison highlights the practicality and effectiveness of Fanger's method in accurately predicting thermal comfort levels.

Table B.3. thermal sensation verification

	Person 1	Person 2	Person 3	Person 4	Person 5	Person 6	Person 7	Person 8	Person 9	Person 10
Ground truth	slightly cool	slightly cool	slightly cool	slightly warm	slightly cool	slightly warm	slightly cool	slightly warm	warm	warm
Prediction	slightly cool	slightly cool	slightly cool	slightly warm	slightly cool	slightly warm	slightly cool	slightly warm	slightly warm	slightly warm

Fixed Icl and M	neutral	neutral	neutral	neutral	neutral	neutral	neutral	neutral	neutral	neutral

B3. Validation of linearized PMV model

The validity of the approximate PMV model is assessed by comparing it with the original PMV model concerning the indoor air temperature and mean radiant temperature, as illustrated in Figure B3. The primary reason for this validation is that the main piecewise linearization is applied to the indoor temperature, which subsequently allows us to infer the clothing surface temperature. The temperature ranges considered for both air temperature and mean radiant temperature are set from 15 to 25℃ to align with the environmental conditions of the test room in this study. The results obtained from the comparison are presented in the figures below. Notably, it is observed that the difference between the PMV values obtained by the two models is exceedingly small, with a maximum absolute error of less than 0.024. This level of discrepancy is considered negligible from a practical perspective, confirming the accuracy and reliability of the approximate PMV model in estimating thermal comfort levels based on indoor air temperature and mean radiant temperature.

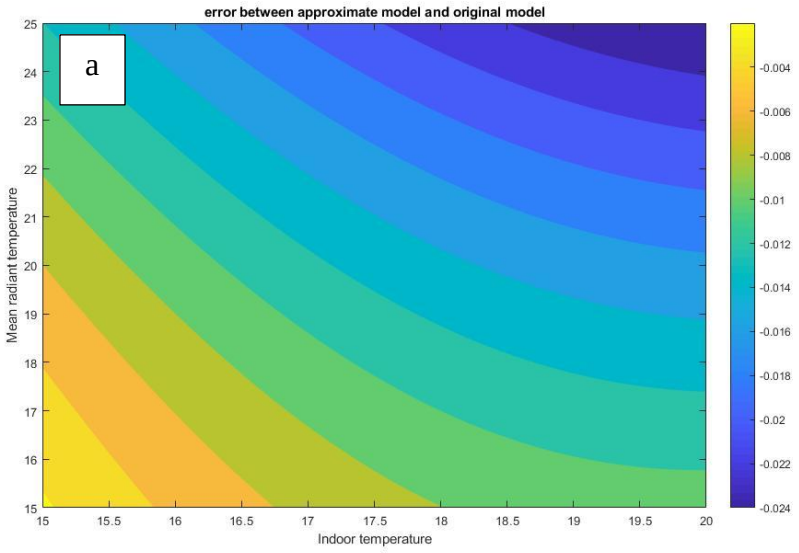

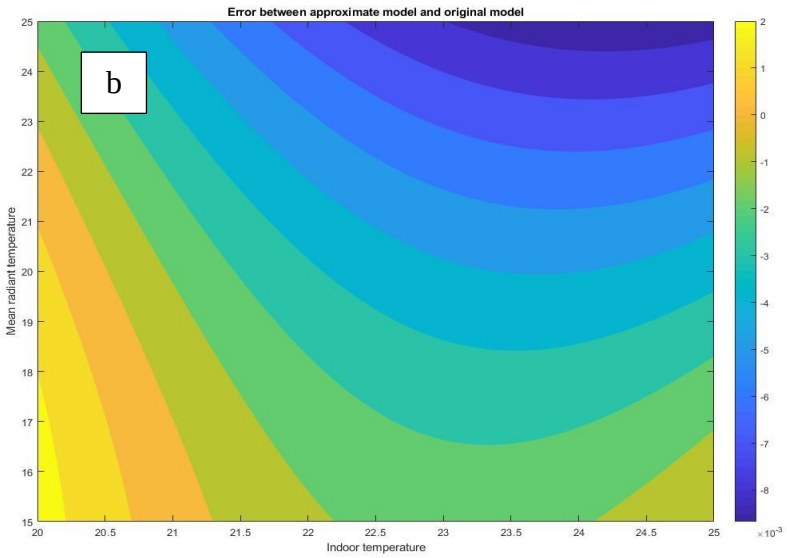

Fig B. 3 Validation of PMV values of (a) 15 to 20 ℃ (b) 20 to 25 ℃

B4. TRNSYS model validation of case study room

To establish the validity of the TRNSYS model, we conducted a thorough comparison with the measured indoor temperature data collected over a two-day period (2nd December - 4th December) in the case study room. Following the disconnection of the heating system on the preceding Friday night, indoor temperature measurements were taken at five-minute intervals using a K-type thermocouple and a data logger TC-08 thermocouple data logger, boasting an accuracy of ±0.5 °C [48]. The outcomes of this validation process are illustrated in Figure B4, which highlights the excellent agreement between the simulated and measured data. The cross-validation root mean square error (CVRMSE) of 0.0052 further substantiates the model's ability to accurately predict indoor temperature dynamics, underscoring its reliability for subsequent analyses and predictions.

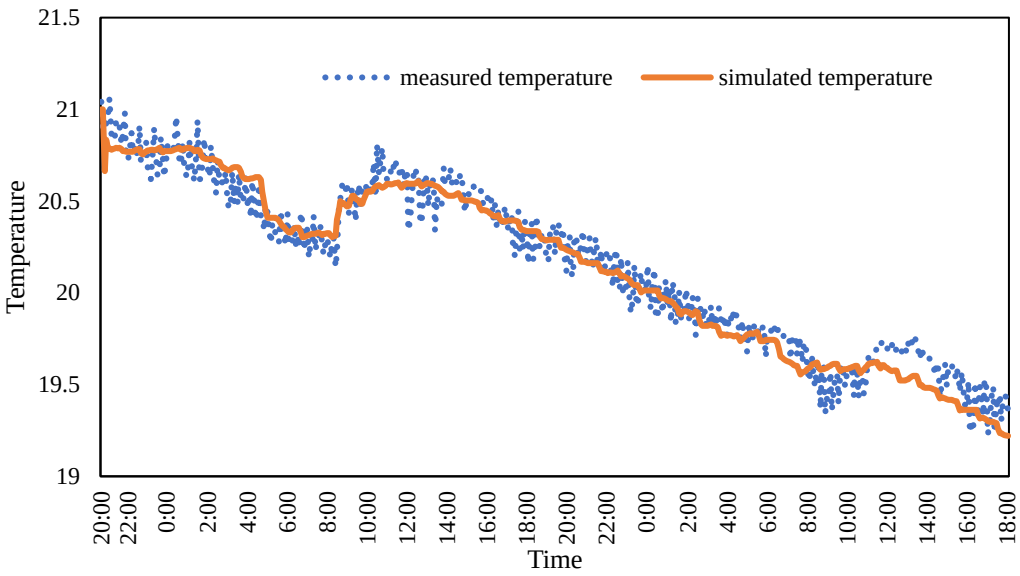

Fig B. 4 Measured and simulated indoor temperature

B5. Training results for Resnet 50, Vgg19 and Squeezenet

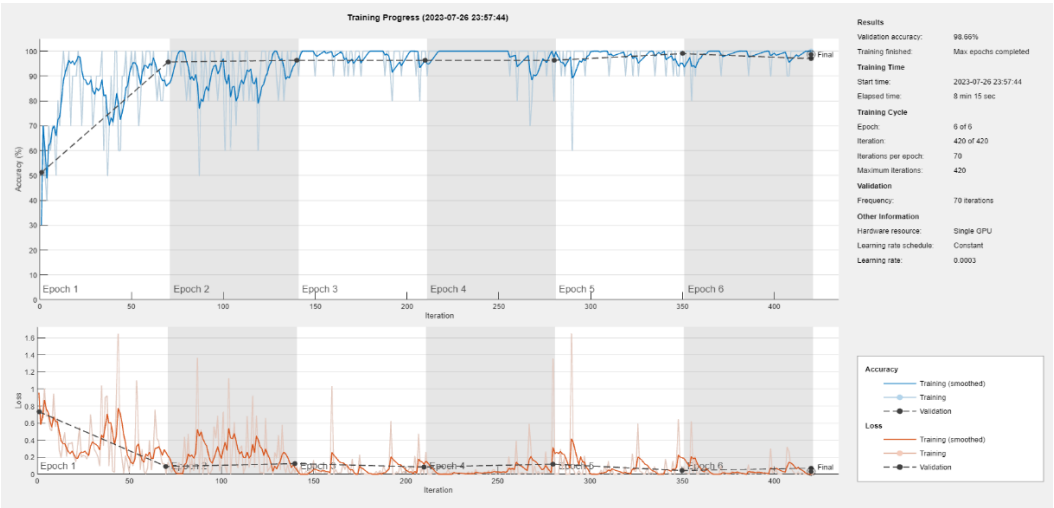

Fig B5. Training results of Resnet50

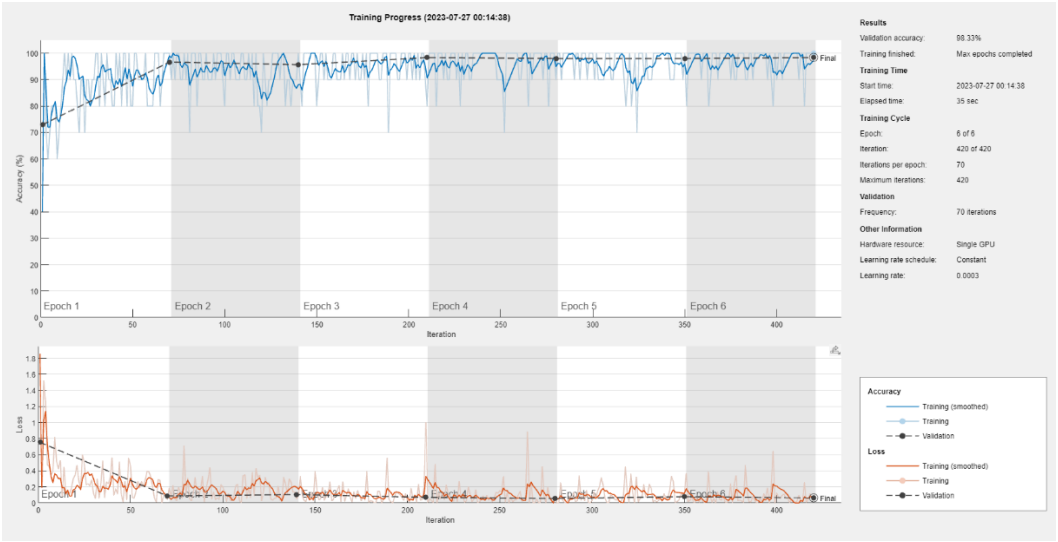

Fig B6. Training results of Squeezenet

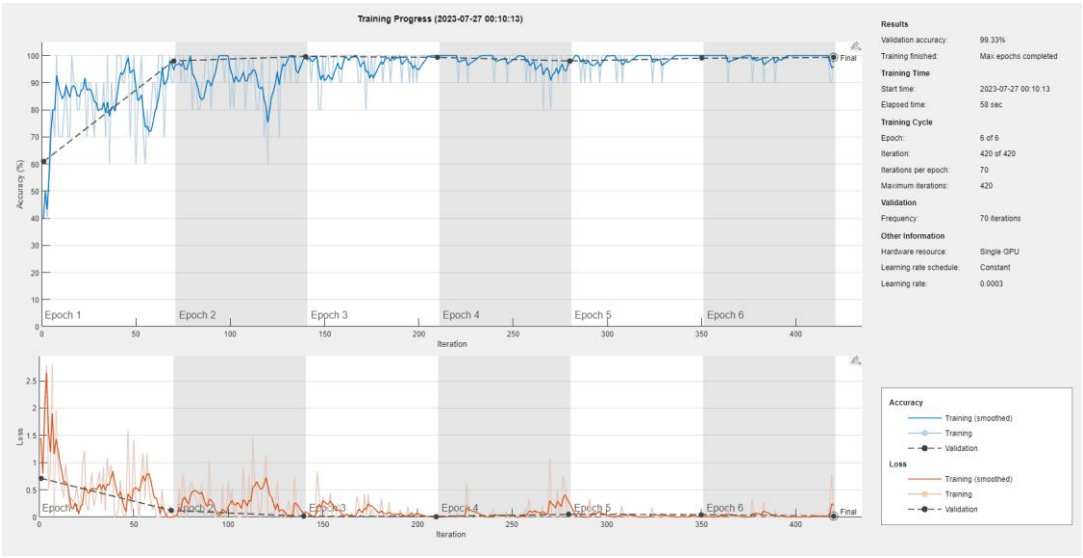

Fig B7. Training results of Vgg19

Reference

[1] J. Mouli-Castillo, N. Heinemann, and K. Edlmann, "Mapping geological hydrogen storage capacity and regional heating demands: An applied UK case study," *Applied energy,* vol. 283, p. 116348, 2021, doi: 10.1016/j.apenergy.2020.116348.

[2] D. Williams, L. Elghali, R. Wheeler, and C. France, "Climate change influence on building lifecycle greenhouse gas emissions: Case study of a UK mixed-use development," *Energy and Buildings,* vol. 48, pp. 112-126, 2012.

[3] M. J. Hannon, "Raising the temperature of the UK heat pump market: Learning lessons from Finland," *Energy Policy,* vol. 85, pp. 369-375, 2015.

[4] A. N. Ayoub, A. Gaigneux, N. Le Brun, S. Acha, and N. Shah, "The development of a low-carbon roadmap investment strategy to reach Science Based Targets for commercial organisations with multi-site properties," *Building and environment,* vol. 186, p. 107311, 2020, doi: 10.1016/j.buildenv.2020.107311.

[5] L. Xu, F. Guo, P.-J. Hoes, X. Yang, and J. L. M. Hensen, "Investigating energy performance of large-scale seasonal storage in the district heating system of chifeng city: Measurements and model-based analysis of operation strategies," *Energy and buildings,* vol. 247, p. 111113, 2021, doi: 10.1016/j.enbuild.2021.111113.

[6] R. Pereira, J. Figueiredo, R. Melicio, V. M. F. Mendes, J. Martins, and J. C. Quadrado, "Consumer energy management system with integration of smart meters," *Energy reports,* vol. 1, no. C, pp. 22-29, 2015, doi: 10.1016/j.egyr.2014.10.001.

[7] M. H. Rehmani, M. Reisslein, A. Rachedi, M. Erol-Kantarci, and M. Radenkovic, "Integrating Renewable Energy Resources Into the Smart Grid: Recent Developments in Information and Communication Technologies," *IEEE transactions on industrial informatics,* vol. 14, no. 7, pp. 2814-2825, 2018, doi: 10.1109/tii.2018.2819169.

[8] Y. W. Law, H. R. Pota, J. Jin, Z. Man, and M. Palaniswami, "Control and Communication Techniques for the Smart Grid: An Energy Efficiency Perspective," *IFAC Proceedings Volumes,* vol. 47, no. 3, pp. 987-998, 2014, doi: 10.3182/20140824-6-ZA-1003.01736.

[9] M. S. Thomas and J. D. McDonald, "Energy management systems (EMS) for control centres," 1 ed: CRC Press, 2015, pp. 177-214.

[10] E. Vaahedi, "Energy Management Systems," 1 ed. Hoboken, NJ: Hoboken, NJ: Wiley, 2014, pp. 161-175.

[11] X. Xue, S. Wang, Y. Sun, and F. Xiao, "An interactive building power demand management strategy for facilitating smart grid optimization," *Applied energy,* vol. 116, pp. 297-310, 2014, doi: 10.1016/j.apenergy.2013.11.064.

[12] P. Faria and Z. Vale, "Demand response in electrical energy supply: An optimal real time pricing approach," *Energy (Oxford),* vol. 36, no. 8, pp. 5374-5384, 2011, doi: 10.1016/j.energy.2011.06.049.

[13] A. Arteconi, N. J. Hewitt, and F. Polonara, "State of the art of thermal storage for demand-side management," *Applied energy,* vol. 93, pp. 371-389, 2012, doi: 10.1016/j.apenergy.2011.12.045.

[14] G. Happle, J. A. Fonseca, and A. Schlueter, "Impacts of diversity in commercial building occupancy profiles on district energy demand and supply," *Applied energy,* vol. 277, p. 115594, 2020, doi: 10.1016/j.apenergy.2020.115594.

[15] Y. Kim and L. K. Norford, "Optimal use of thermal energy storage resources in commercial buildings through price-based demand response considering distribution network operation," *Applied energy,* vol. 193, pp. 308-324, 2017, doi: 10.1016/j.apenergy.2017.02.046.

[16] L. Navarro *et al.*, "Thermal energy storage in building integrated thermal systems: A review. Part 1. active storage systems," *Renewable energy,* vol. 88, pp. 526-547, 2016, doi: 10.1016/j.renene.2015.11.040.
[17] M. Hu, F. Xiao, J. B. Jørgensen, and R. Li, "Price-responsive model predictive control of floor heating systems for demand response using building thermal mass," *Applied thermal engineering,* vol. 153, pp. 316-329, 2019, doi: 10.1016/j.applthermaleng.2019.02.107.
[18] G. Reynders, J. Diriken, and D. Saelens, "Generic characterization method for energy flexibility: Applied to structural thermal storage in residential buildings," *Applied energy,* vol. 198, pp. 192-202, 2017, doi: 10.1016/j.apenergy.2017.04.061.
[19] G. Reynders, T. Nuytten, and D. Saelens, "Potential of structural thermal mass for demand-side management in dwellings," *Building and environment,* vol. 64, pp. 187-199, 2013, doi: 10.1016/j.buildenv.2013.03.010.
[20] W. J. N. Turner, I. S. Walker, and J. Roux, "Peak load reductions: Electric load shifting with mechanical pre-cooling of residential buildings with low thermal mass," *Energy (Oxford),* vol. 82, pp. 1057-1067, 2015, doi: 10.1016/j.energy.2015.02.011.
[21] R. A. Kishore, M. V. A. Bianchi, C. Booten, J. Vidal, and R. Jackson, "Modulating thermal load through lightweight residential building walls using thermal energy storage and controlled precooling strategy," *Applied thermal engineering,* vol. 180, p. 115870, 2020, doi: 10.1016/j.applthermaleng.2020.115870.
[22] R. A. Kishore, M. V. A. Bianchi, C. Booten, J. Vidal, and R. Jackson, "Enhancing building energy performance by effectively using phase change material and dynamic insulation in walls," *Applied energy,* vol. 283, p. 116306, 2021, doi: 10.1016/j.apenergy.2020.116306.
[23] A. Jayalath, L. Aye, P. Mendis, and T. Ngo, "Effects of phase change material roof layers on thermal performance of a residential building in Melbourne and Sydney," *Energy and buildings,* vol. 121, pp. 152-158, 2016, doi: 10.1016/j.enbuild.2016.04.007.
[24] Y. Xia, M. Zhu, A. Jiang, J. Wang, X. Bai, and S. Deng, "Model predictive control of indoor thermal environment conditioned by a direct expansion air conditioning system," *Building simulation,* vol. 16, no. 3, pp. 357-378, 2023, doi: 10.1007/s12273-022-0949-1.
[25] K. Zhang and M. Kummert, "Evaluating the impact of thermostat control strategies on the energy flexibility of residential buildings for space heating," *Building simulation,* vol. 14, no. 5, pp. 1439-1452, 2021, doi: 10.1007/s12273-020-0751-x.
[26] R. Tang, C. Fan, F. Zeng, and W. Feng, "Data-driven model predictive control for power demand management and fast demand response of commercial buildings using support vector regression," *Building simulation,* vol. 15, no. 3, pp. 317-331, 2022, doi: 10.1007/s12273-021-0811-x.
[27] S. Yang *et al.*, "Model predictive control for integrated control of air-conditioning and mechanical ventilation, lighting and shading systems," *Applied energy,* vol. 297, p. 117112, 2021, doi: 10.1016/j.apenergy.2021.117112.
[28] J. Jeoung, S. Jung, T. Hong, and J.-K. Choi, "Blockchain-based IoT system for personalised indoor temperature control," *Automation in construction,* vol. 140, p. 104339, 2022, doi: 10.1016/j.autcon.2022.104339.
[29] J.-S. Chou and N.-T. Ngo, "Smart grid data analytics framework for increasing energy savings in residential buildings," *Automation in construction,* vol. 72, pp. 247-257, 2016, doi: 10.1016/j.autcon.2016.01.002.
[30] X. Huang, Y. Liu, L. Huang, E. Onstein, and C. Merschbrock, "BIM and IoT data fusion: The data process model perspective," *Automation in construction,* vol. 149, p. 104792, 2023, doi: 10.1016/j.autcon.2023.104792.

[31] T. Thi Kim Tuoi, N. Van Toan, and T. Ono, "Self-powered wireless sensing system driven by daily ambient temperature energy harvesting," *Applied energy,* vol. 311, p. 118679, 2022, doi: 10.1016/j.apenergy.2022.118679.

[32] I. Baskar and M. Chellapandian, "Experimental and finite element analysis on the developed real-time form stable PCM based roof system for thermal energy storage applications," *Energy and buildings,* vol. 276, p. 112514, 2022, doi: 10.1016/j.enbuild.2022.112514.

[33] Han, H. J., Jeon, Y. I., Lim, S. H., Kim, W. W., & Chen, K. (2010). New developments in illumination, heating and cooling technologies for energy-efficient buildings. *Energy (Oxford)*, *35*(6), 2647–2653. https://doi.org/10.1016/j.energy.2009.05.020

[34] Kaska, O., & Yumrutas, R. (2008). Comparison of experimental and theoretical results for the transient heat flow through multilayer walls and flat roofs. *Energy (Oxford)*, *33*(12), 1816–1823. https://doi.org/10.1016/j.energy.2008.07.016

[35] Heier, J., Bales, C., & Martin, V. (2015). Combining thermal energy storage with buildings – a review. Renewable & Sustainable Energy Reviews, 42, 1305–1325. https://doi.org/10.1016/j.rser.2014.11.031

[36] Navarro, L., de Gracia, A., Colclough, S., Browne, M., McCormack, S. J., Griffiths, P., & Cabeza, L. F. (2016). Thermal energy storage in building integrated thermal systems: A review. Part 1. active storage systems. Renewable Energy, 88, 526–547. https://doi.org/10.1016/j.renene.2015.11.040

[37] Parameshwaran R, Kalaiselvam S, Harikrishnan S, Elayaperumal A. Sustainable thermal energy storage technologies for buildings: a review. Renew Sust Energ Rev 2012;16:2394–433.

[38] Zhu N, Ma Z, Wang S. Dynamic characteristics and energy performance of buildings using phase change materials: a review. Energ Convers Manage 2009;50:3169–81.

[39] EFFLOCOM. "Energy efficiency and load curve impacts of commercial development in competitive markets: basis for demand response." https://www.sintef.no/globalassets/project/efflocom/efflocom-report-no.-1-basis-for-load-management1.pdf (accessed 25 November, 2020).

[40] J. Guerrero, D. Gebbran, S. Mhanna, A. C. Chapman, and G. Verbič, "Towards a transactive energy system for integration of distributed energy resources: Home energy management, distributed optimal power flow, and peer-to-peer energy trading," *Renewable & sustainable energy reviews,* vol. 132, p. 110000, 2020, doi: 10.1016/j.rser.2020.110000.

[41] S. Al-Hallaj, S. Khateeb, A. Aljehani, and M. Pintar, "Thermal energy storage for smart grid applications," vol. 1924, ed, 2018.

[42] T. Boßmann and E. J. Eser, "Model-based assessment of demand-response measures—A comprehensive literature review," *Renewable & sustainable energy reviews,* vol. 57, pp. 1637-1656, 2016, doi: 10.1016/j.rser.2015.12.031.

[43] Y. Chen, P. Xu, J. Gu, F. Schmidt, and W. Li, "Measures to improve energy demand flexibility in buildings for demand response (DR): A review," *Energy and buildings,* vol. 177, pp. 125-139, 2018, doi: 10.1016/j.enbuild.2018.08.003.

[44] S. Ashok, "Peak-load management in steel plants," *Applied energy,* vol. 83, no. 5, pp. 413-424, 2006, doi: 10.1016/j.apenergy.2005.05.002.

[45] D. Papadaskalopoulos, G. Strbac, P. Mancarella, M. Aunedi, and V. Stanojevic, "Decentralized Participation of Flexible Demand in Electricity Markets-Part II: Application With Electric Vehicles and Heat Pump Systems," *IEEE transactions on power systems,* vol. 28, no. 4, pp. 3667-3674, 2013, doi: 10.1109/TPWRS.2013.2245687.

[46] S. Ashok and R. Banerjee, "Optimal cool storage capacity for load management," *Energy (Oxford),* vol. 28, no. 2, pp. 115-126, 2003, doi: 10.1016/S0360-5442(02)00109-3.
[47] S. Chua-Liang and D. Kirschen, "Quantifying the Effect of Demand Response on Electricity Markets," *IEEE transactions on power systems,* vol. 24, no. 3, pp. 1199-1207, 2009, doi: 10.1109/TPWRS.2009.2023259.
[48] S. Feuerriegel and D. Neumann, "Measuring the financial impact of demand response for electricity retailers," *Energy policy,* vol. 65, pp. 359-368, 2014, doi: 10.1016/j.enpol.2013.10.012.
[49] C. De Jonghe, B. F. Hobbs, and R. Belmans, "Optimal Generation Mix With Short-Term Demand Response and Wind Penetration," *IEEE transactions on power systems,* vol. 27, no. 2, pp. 830-839, 2012, doi: 10.1109/TPWRS.2011.2174257.
[50] D. Wang, S. Parkinson, W. Miao, H. Jia, C. Crawford, and N. Djilali, "Hierarchical market integration of responsive loads as spinning reserve," *Applied energy,* vol. 104, pp. 229-238, 2013, doi: 10.1016/j.apenergy.2012.10.054.
[51] P. Finn, C. Fitzpatrick, and D. Connolly, "Demand side management of electric car charging: Benefits for consumer and grid," *Energy (Oxford),* vol. 42, no. 1, pp. 358-363, 2012, doi: 10.1016/j.energy.2012.03.042.
[52] J. Chen, F. N. Lee, A. M. Breipohl, and R. Adapa, "Scheduling direct load control to minimise system operational cost," *IEEE transactions on power systems,* vol. 10, no. 4, p. 1994, 1995.
[53] M. Nikzad, B. Mozafari, M. Bashirvand, S. Solaymani, and A. M. Ranjbar, "Designing time-of-use program based on stochastic security constrained unit commitment considering reliability index," *Energy (Oxford),* vol. 41, no. 1, pp. 541-548, 2012, doi: 10.1016/j.energy.2012.02.015.
[54] H. Falsafi, A. Zakariazadeh, and S. Jadid, "The role of demand response in single and multi-objective wind-thermal generation scheduling: A stochastic programming," *Energy (Oxford),* vol. 64, pp. 853-867, 2014, doi: 10.1016/j.energy.2013.10.034.
[55] H. Zhong *et al.*, "Integrated dispatch of generation and load: A pathway towards smart grids," *Electric power systems research,* vol. 120, pp. 206-213, 2015, doi: 10.1016/j.epsr.2014.04.005.
[56] M. Tanaka, "Real-time pricing with ramping costs: A new approach to managing a steep change in electricity demand," *Energy policy,* vol. 34, no. 18, pp. 3634-3643, 2006, doi: 10.1016/j.enpol.2005.07.012.
[57] A. Keane *et al.*, "Demand side resource operation on the Irish power system with high wind power penetration," *Energy policy,* vol. 39, no. 5, pp. 2925-2934, 2011, doi: 10.1016/j.enpol.2011.02.071.
[58] P. S. Moura and A. T. de Almeida, "Multi-objective optimization of a mixed renewable system with demand-side management," *Renewable & sustainable energy reviews,* vol. 14, no. 5, pp. 1461-1468, 2010, doi: 10.1016/j.rser.2010.01.004.
[59] R. Sioshansi, "Evaluating the Impacts of Real-Time Pricing on the Cost and Value of Wind Generation," *IEEE transactions on power systems,* vol. 25, no. 2, pp. 741-748, 2010, doi: 10.1109/TPWRS.2009.2032552.
[60] D. Pengwei and L. Ning, "Appliance Commitment for Household Load Scheduling," *IEEE transactions on smart grid,* vol. 2, no. 2, pp. 411-419, 2011, doi: 10.1109/TSG.2011.2140344.
[61] A. Asadinejad and K. Tomsovic, "Optimal use of incentive and price based demand response to reduce costs and price volatility," *Electric power systems research,* vol. 144, no. C, pp. 215-223, 2017, doi: 10.1016/j.epsr.2016.12.012.

[62] M. H. Albadi and E. F. El-Saadany, "A summary of demand response in electricity markets," *Electric power systems research,* vol. 78, no. 11, pp. 1989-1996, 2008, doi: 10.1016/j.epsr.2008.04.002.
[63] J. Le Dréau and P. Heiselberg, "Energy flexibility of residential buildings using short term heat storage in the thermal mass," *Energy (Oxford),* vol. 111, pp. 991-1002, 2016, doi: 10.1016/j.energy.2016.05.076.
[64] H. Johra, P. Heiselberg, and J. L. Dréau, "Influence of envelope, structural thermal mass and indoor content on the building heating energy flexibility," *Energy and buildings,* vol. 183, pp. 325-339, 2019, doi: 10.1016/j.enbuild.2018.11.012.
[65] L. Navarro *et al.*, "Thermal energy storage in building integrated thermal systems: A review. Part 2. Integration as passive system," *Renewable energy,* vol. 85, pp. 1334-1356, 2016, doi: 10.1016/j.renene.2015.06.064.
[66] L. Zhu, R. Hurt, D. Correia, and R. Boehm, "Detailed energy saving performance analyses on thermal mass walls demonstrated in a zero energy house," *Energy and buildings,* vol. 41, no. 3, pp. 303-310, 2009, doi: 10.1016/j.enbuild.2008.10.003.
[67] T. Başaran, "Thermal Analysis of the Domed Vernacular Houses of Harran, Turkey," *Indoor + built environment,* vol. 20, no. 5, pp. 543-554, 2011, doi: 10.1177/1420326x11411237.
[68] D. M. Ogoli, "Predicting indoor temperatures in closed buildings with high thermal mass," *Energy and buildings,* vol. 35, no. 9, pp. 851-862, 2003, doi: 10.1016/S0378-7788(02)00246-3.
[69] K. Ip and A. Miller, "Thermal behaviour of an earth-sheltered autonomous building – The Brighton Earthship," *Renewable energy,* vol. 34, no. 9, pp. 2037-2043, 2009, doi: 10.1016/j.renene.2009.02.006.
[70] J. Sánchez Ramos, M. Pavón Moreno, M. Guerrero Delgado, S. Álvarez Domínguez, and L. F. Cabeza, "Potential of energy flexible buildings: Evaluation of DSM strategies using building thermal mass," *Energy and buildings,* vol. 203, p. 109442, 2019, doi: 10.1016/j.enbuild.2019.109442.
[71] L. A. Hurtado, J. D. Rhodes, P. H. Nguyen, I. G. Kamphuis, and M. E. Webber, "Quantifying demand flexibility based on structural thermal storage and comfort management of non-residential buildings: A comparison between hot and cold climate zones," *Applied energy,* vol. 195, pp. 1047-1054, 2017, doi: 10.1016/j.apenergy.2017.03.004.
[72] K. Gi, F. Sano, A. Hayashi, T. Tomoda, and K. Akimoto, "A global analysis of residential heating and cooling service demand and cost-effective energy consumption under different climate change scenarios up to 2050," *Mitigation and adaptation strategies for global change,* vol. 23, no. 1, pp. 51-79, 2016, doi: 10.1007/s11027-016-9728-6.
[73] IEA, *Transition to Sustainable Buildings [electronic resource]: Strategies and Opportunities to 2050 / IEA* (Transition to Sustainable Buildings). Paris: Paris : IEA, 2013.
[74] Y. Cao, J. Du, and E. Soleymanzadeh, "Model predictive control of commercial buildings in demand response programs in the presence of thermal storage," *Journal of cleaner production,* vol. 218, pp. 315-327, 2019, doi: 10.1016/j.jclepro.2019.01.266.
[75] J. Ma, J. Qin, T. Salsbury, and P. Xu, "Demand reduction in building energy systems based on economic model predictive control," *Chemical engineering science,* vol. 67, no. 1, pp. 92-100, 2012, doi: 10.1016/j.ces.2011.07.052.
[76] M. D. Knudsen, L. Georges, K. S. Skeie, and S. Petersen, "Experimental test of a black-box economic model predictive control for residential space heating," *Applied energy,* vol. 298, p. 117227, 2021, doi: 10.1016/j.apenergy.2021.117227.
[77] J. Široký, F. Oldewurtel, J. Cigler, and S. Prívara, " ," *Applied energy,* vol. 88, no. 9, pp. 3079-3087, 2011, doi: 10.1016/j.apenergy.2011.03.009.

[78] E. Khanmirza, A. Esmaeilzadeh, and A. H. D. Markazi, "Design and experimental evaluation of model predictive control vs. intelligent methods for domestic heating systems," *Energy and buildings,* vol. 150, pp. 52-70, 2017, doi: 10.1016/j.enbuild.2017.05.074.
[79] J. B. Rawlings, N. R. Patel, M. J. Risbeck, C. T. Maravelias, M. J. Wenzel, and R. D. Turney, "Economic MPC and real-time decision making with application to large-scale HVAC energy systems," *Computers & chemical engineering,* vol. 114, pp. 89-98, 2018, doi: 10.1016/j.compchemeng.2017.10.038.
[80] D. Sturzenegger, D. Gyalistras, M. Morari, and R. S. Smith, "Model Predictive Climate Control of a Swiss Office Building: Implementation, Results, and Cost-Benefit Analysis," *IEEE transactions on control systems technology,* vol. 24, no. 1, pp. 1-12, 2016, doi: 10.1109/TCST.2015.2415411.
[81] T. Yang, A. Bandyopadhyay, Z. O'Neill, J. Wen, and B. Dong, "From occupants to occupants: A review of the occupant information understanding for building HVAC occupant-centric control," *Building simulation,* vol. 15, no. 6, pp. 913-932, 2022, doi: 10.1007/s12273-021-0861-0.
[82] W. Zhang, Y. Wu, and J. K. Calautit, "A review on occupancy prediction through machine learning for enhancing energy efficiency, air quality and thermal comfort in the built environment," *Renewable & sustainable energy reviews,* vol. 167, p. 112704, 2022, doi: 10.1016/j.rser.2022.112704.
[83] B. Zhou *et al.*, "Smart home energy management systems: Concept, configurations, and scheduling strategies," *Renewable & sustainable energy reviews,* vol. 61, pp. 30-40, 2016, doi: 10.1016/j.rser.2016.03.047.
[84] P. W. Tien, S. Wei, J. K. Calautit, J. Darkwa, and C. Wood, "Real-time monitoring of occupancy activities and window opening within buildings using an integrated deep learning-based approach for reducing energy demand," *Applied energy,* vol. 308, p. 118336, 2022, doi: 10.1016/j.apenergy.2021.118336.
[85] F. Oldewurtel, D. Sturzenegger, G. Andersson, M. Morari, and R. S. Smith, "Towards a standardized building assessment for demand response," ed: IEEE, 2013, pp. 7083-7088.
[86] M. Yudong, J. Matusko, and F. Borrelli, "Stochastic Model Predictive Control for Building HVAC Systems: Complexity and Conservatism," *IEEE transactions on control systems technology,* vol. 23, no. 1, pp. 101-116, 2015, doi: 10.1109/TCST.2014.2313736.
[87] M. B. Rasheed *et al.*, "Priority and delay constrained demand side management in real-time price environment with renewable energy source," *International journal of energy research,* vol. 40, no. 14, pp. 2002-2021, 2016, doi: 10.1002/er.3588.
[88] R. A. Verzijlbergh, L. J. De Vries, and Z. Lukszo, "Renewable Energy Sources and Responsive Demand. Do We Need Congestion Management in the Distribution Grid?," *IEEE transactions on power systems,* vol. 29, no. 5, pp. 2119-2128, 2014, doi: 10.1109/TPWRS.2014.2300941.
[89] S. Chapaloglou *et al.*, "Microgrid energy management strategies assessment through coupled thermal-electric considerations," *Energy conversion and management,* vol. 228, p. 113711, 2021, doi: 10.1016/j.enconman.2020.113711.
[90] N. Khordehgah, A. Żabnieńska-Góra, and H. Jouhara, "Energy Performance Analysis of a PV/T System Coupled with Domestic Hot Water System," *ChemEngineering,* vol. 4, no. 2, p. 22, 2020, doi: 10.3390/chemengineering4020022.
[91] T. Kemmler and B. Thomas, "Design of Heat-Pump Systems for Single- and Multi-Family Houses using a Heuristic Scheduling for the Optimization of PV Self-Consumption," *Energies (Basel),* vol. 13, no. 5, p. 1118, 2020, doi: 10.3390/en13051118.
[92] A. Toradmal, T. Kemmler, and B. Thomas, "Boosting the share of onsite PV-electricity utilization by optimised scheduling of a heat pump using buildings

thermal inertia," *Applied thermal engineering,* vol. 137, pp. 248-258, 2018, doi: 10.1016/j.applthermaleng.2018.03.052.
[93] L. Langer and T. Volling, "An optimal home energy management system for modulating heat pumps and photovoltaic systems," *Applied energy,* vol. 278, p. 115661, 2020, doi: 10.1016/j.apenergy.2020.115661.
[94] A. de Gracia, J. Tarragona, A. Crespo, and C. Fernández, "Smart control of dynamic phase change material wall system," *Applied energy,* vol. 279, p. 115807, 2020, doi: 10.1016/j.apenergy.2020.115807.
[95] F. Guo, J. Zhang, M. Shan, and X. Yang, "Analysis on the optimum matching of collector and storage size of solar water heating systems in building space heating applications," *Building simulation,* vol. 11, no. 3, pp. 549-560, 2018, doi: 10.1007/s12273-018-0429-9.
[96] J. Tarragona, C. Fernández, and A. de Gracia, "Model predictive control applied to a heating system with PV panels and thermal energy storage," *Energy (Oxford),* vol. 197, p. 117229, 2020, doi: 10.1016/j.energy.2020.117229.
[97] M. H. Benzaama, S. Menhoudj, M. C. Lekhal, A. Mokhtari, and S. Attia, "Multi-objective optimisation of a seasonal solar thermal energy storage system combined with an earth – Air heat exchanger for net zero energy building," *Solar energy,* vol. 220, no. 2021, pp. 901-913, 2021, doi: 10.1016/j.solener.2021.03.070.
[98] Z. Wei and J. Calautit, "Predictive control of low-temperature heating system with passive thermal mass energy storage and photovoltaic system: Impact of occupancy patterns and climate change," *Energy (Oxford),* vol. 269, p. 126791, 2023, doi: 10.1016/j.energy.2023.126791.
[99] M. Khodabakhshian, L. Feng, S. Börjesson, O. Lindgärde, and J. Wikander, "Reducing auxiliary energy consumption of heavy trucks by onboard prediction and real-time optimization," *Applied energy,* vol. 188, pp. 652-671, 2017, doi: 10.1016/j.apenergy.2016.11.118.
[100] S. Yang, H. Oliver Gao, and F. You, "Model predictive control in phase-change-material-wallboard-enhanced building energy management considering electricity price dynamics," *Applied energy,* vol. 326, p. 120023, 2022, doi: 10.1016/j.apenergy.2022.120023.
[101] H. Wang, W. Lu, Z. Wu, and G. Zhang, "Parametric analysis of applying PCM wallboards for energy saving in high-rise lightweight buildings in Shanghai," *Renewable energy,* vol. 145, pp. 52-64, 2020, doi: 10.1016/j.renene.2019.05.124.
[102] Y. Qu, D. Zhou, F. Xue, and L. Cui, "Multi-factor analysis on thermal comfort and energy saving potential for PCM-integrated buildings in summer," *Energy and buildings,* vol. 241, p. 110966, 2021, doi: 10.1016/j.enbuild.2021.110966.
[103] S. Wijesuriya, C. Booten, M. V. A. Bianchi, and R. A. Kishore, "Building energy efficiency and load flexibility optimization using phase change materials under futuristic grid scenario," *Journal of cleaner production,* vol. 339, p. 130561, 2022, doi: 10.1016/j.jclepro.2022.130561.
[104] T. Weber and G. Jóhannesson, "An optimised RC-network for thermally activated building components," *Building and environment,* vol. 40, no. 1, pp. 1-14, 2005, doi: 10.1016/j.buildenv.2004.04.012.
[105] G. Zhou and J. He, "Thermal performance of a radiant floor heating system with different heat storage materials and heating pipes," *Applied energy,* vol. 138, pp. 648-660, 2015, doi: 10.1016/j.apenergy.2014.10.058.
[106] Chen, Q., Li, N., & Feng, W. (2021). Model predictive control optimization for rapid response and energy efficiency based on the state-space model of a radiant floor heating system. Energy and Buildings, 238, 110832. https://doi.org/10.1016/j.enbuild.2021.110832
[107] Joe, J., & Karava, P. (2019). A model predictive control strategy to optimise the performance of radiant floor heating and cooling systems in office

buildings. Applied Energy, 245, 65–77. https://doi.org/10.1016/j.apenergy.2019.03.209
[108] A. Fredriksson, A. A. Sezer, V. Angelakis, and D. Gundlegård, "Construction related urban disturbances: Identification and linking with an IoT-model," *Automation in construction,* vol. 134, p. 104038, 2022, doi: 10.1016/j.autcon.2021.104038.
[109] S. Acha, G. Vieira, M. Bird, and N. Shah, "Modelling UK electricity regional costs for commercial buildings," *Energy and buildings,* vol. 271, p. 112301, 2022, doi: 10.1016/j.enbuild.2022.112301.
[110] W. Li, H. Li, and S. Wang, "An event-driven multi-agent based distributed optimal control strategy for HVAC systems in IoT-enabled smart buildings," *Automation in construction,* vol. 132, p. 103919, 2021, doi: 10.1016/j.autcon.2021.103919.
[111] T. Jafarinejad, A. Erfani, A. Fathi, and M. B. Shafii, "Bi-level energy-efficient occupancy profile optimization integrated with demand-driven control strategy: University building energy saving," *Sustainable cities and society,* vol. 48, p. 101539, 2019, doi: 10.1016/j.scs.2019.101539.
[112] S. Salimi and A. Hammad, "Critical review and research roadmap of office building energy management based on occupancy monitoring," *Energy and buildings,* vol. 182, pp. 214-241, 2019, doi: 10.1016/j.enbuild.2018.10.007.
[113] J. P. Torreglosa, P. García, L. M. Fernández, and F. Jurado, "Energy dispatching based on predictive controller of an off-grid wind turbine/photovoltaic/hydrogen/battery hybrid system," *Renewable energy,* vol. 74, pp. 326-336, 2015, doi: 10.1016/j.renene.2014.08.010.
[114] L. Bartolucci, S. Cordiner, V. Mulone, V. Rocco, and J. L. Rossi, "Renewable source penetration and microgrids: Effects of MILP – Based control strategies," *Energy (Oxford),* vol. 152, pp. 416-426, 2018, doi: 10.1016/j.energy.2018.03.145.
[115] F. Bünning *et al.*, "Physics-informed linear regression is competitive with two Machine Learning methods in residential building MPC," *Applied energy,* vol. 310, p. 118491, 2022, doi: 10.1016/j.apenergy.2021.118491.
[116] A. Martín-Garín, J. A. Millán-García, A. Baïri, J. Millán-Medel, and J. M. Sala-Lizarraga, "Environmental monitoring system based on an Open Source Platform and the Internet of Things for a building energy retrofit," *Automation in construction,* vol. 87, pp. 201-214, 2018, doi: 10.1016/j.autcon.2017.12.017.
[117] S. Li, J. Joe, J. Hu, and P. Karava, "System identification and model-predictive control of office buildings with integrated photovoltaic-thermal collectors, radiant floor heating and active thermal storage," *Solar energy,* vol. 113, pp. 139-157, 2015, doi: 10.1016/j.solener.2014.11.024.
[118] D. Simon, "Kalman filtering," *Embedded systems programming,* vol. 14, no. 6, pp. 72-79, 2001.
[119] L. Ljung, "System identification toolbox," *The Matlab user's guide,* 2014.
[120] B. Bixby, "The gurobi optimiser," *Transp. Re-search Part B,* vol. 41, no. 2, pp. 159-178, 2007.
[121] S. Klein *et al.*, "TRNSYS 18: A Transient System Simulation Program, Solar Energy Laboratory, University of Wisconsin, Madison, USA," ed, 2017.
[122] X. F. Zheng, Y. S. Hsu, A. V. Pasos, L. Smith, and C. J. Wood, "A progressive comparison of the novel pulse and conventional steady state methods of measuring the airtightness of buildings," *Energy and buildings,* vol. 261, p. 111983, 2022, doi: 10.1016/j.enbuild.2022.111983.
[123] Ecowitt. "ECOWITT GW1100 Mannual." https://www.manualslib.com/manual/2311383/Ecowitt-Gw1100.html (accessed Nov 13th, 2022).
[124] A. Barbón, J. A. Fernández-Rubiera, L. Martínez-Valledor, A. Pérez-Fernández, and L. Bayón, "Design and construction of a solar tracking system for small-scale

linear Fresnel reflector with three movements," *Applied energy,* vol. 285, p. 116477, 2021, doi: 10.1016/j.apenergy.2021.116477.
[125] E. A. Abioye, M. S. Z. Abidin, M. N. Aman, M. S. A. Mahmud, and S. Buyamin, "A model predictive controller for precision irrigation using discrete lagurre networks," *Computers and electronics in agriculture,* vol. 181, p. 105953, 2021, doi: 10.1016/j.compag.2020.105953.
[126] M. integrated. "Technical data." https://datasheets.maximintegrated.com/en/ds/MAX6675.pdf . (accessed 21st Dec, 2022).
[127] R. Ahmed *et al.*, "Computer vision and photosensor based hybrid control strategy for a two-axis solar tracker - Daylighting application," *Solar energy,* vol. 224, pp. 175-183, 2021, doi: 10.1016/j.solener.2021.05.077.
[128] S. Matlab, "Matlab," *The MathWorks, Natick, MA,* 2012.
[129] K. Benjamin, Z. Luo, and X. Wang, "Crowdsourcing Urban Air Temperature Data for Estimating Urban Heat Island and Building Heating/Cooling Load in London," *Energies (Basel),* vol. 14, no. 16, p. 5208, 2021, doi: 10.3390/en14165208.
[130] I. Livada, A. Pyrgou, S. Haddad, M. Sadeghi, and M. Santamouris, "Recent Climatic Trends and Analysis of Monthly Heating and Cooling Degree Hours in Sydney," *Climate (Basel),* vol. 9, no. 7, p. 114, 2021, doi: 10.3390/cli9070114.
[131] J. Yu, L. Tian, C. Yang, X. Xu, and J. Wang, "Optimum insulation thickness of residential roof with respect to solar-air degree-hours in hot summer and cold winter zone of china," *Energy and buildings,* vol. 43, no. 9, pp. 2304-2313, 2011, doi: 10.1016/j.enbuild.2011.05.012.
[132] K. Papakostas and N. Kyriakis, "Heating and cooling degree-hours for Athens and Thessaloniki, Greece," *Renewable energy,* vol. 30, no. 12, pp. 1873-1880, 2005, doi: 10.1016/j.renene.2004.12.002.
[133] Ministry of Housing Communities & Local Government, "English Housing Survey 2019 to 2020: headline report ", ed. London, 2020.
[134] J. Remund, S. Müller, M. Schmutz, and P. Graf, "Meteonorm version 8," *METEOTEST (www. meteotest. com),* 2020.
[135] A. M. Thomson *et al.*, "RCP4.5: a pathway for stabilization of radiative forcing by 2100," *Climatic change,* vol. 109, no. 1-2, pp. 77-94, 2011, doi: 10.1007/s10584-011-0151-4.
[136] R. Hou *et al.*, "Assessing of impact climate parameters on the gap between hydropower supply and electricity demand by RCPs scenarios and optimised ANN by the improved Pathfinder (IPF) algorithm," *Energy (Oxford),* vol. 237, p. 121621, 2021, doi: 10.1016/j.energy.2021.121621.
[137] E. Marshall, J. K. Steinberger, V. Dupont, and T. J. Foxon, "Combining energy efficiency measure approaches and occupancy patterns in building modelling in the UK residential context," *Energy and buildings,* vol. 111, pp. 98-108, 2016, doi: 10.1016/j.enbuild.2015.11.039.
[138] K. Butcher and B. Craig, *CIBSE guide: A Environmental design*. Cibse, 2016.
[139] R. Dott, M. Y. Haller, J. Ruschenburg, F. Ochs, and J. Bony, "The reference framework for system simulations of the IEA SHC Task 44/HPP Annex 38 Part B: buildings and space heat load," *International Energy Agency,* 2013.
[140] R. Simson, J. Kurnitski, and M. Maivel, "Summer thermal comfort: compliance assessment and overheating prevention in new apartment buildings in Estonia," *Journal of Building Performance Simulation,* vol. 10, no. 4, pp. 378-391, 2017.
[141] O. B. Kazanci, M. Shukuya, and B. W. Olesen, "Exergy performance of different space heating systems: A theoretical study," *Building and environment,* vol. 99, pp. 119-129, 2016, doi: 10.1016/j.buildenv.2016.01.025.
[142] H. Cao and Q. Liao, "The application of air source heat pump assisting solar low-temperature floor heating system in the construction of new countryside," 2011: IEEE, pp. 571-574, doi: 10.1109/ICAE.2011.5943862.

[143] H. Ma, C. Li, W. Lu, Z. Zhang, S. Yu, and N. Du, "Investigation on a solar-groundwater heat pump unit associated with radiant floor heating," *Renewable & sustainable energy reviews,* vol. 75, pp. 972-977, 2017, doi: 10.1016/j.rser.2016.11.077.
[144] Nord Pool. "Day-ahead Prices in UK." https://www.nordpoolgroup.com/Market-data1/GB/Auction-prices/ (accessed 15th Nov, 2022).
[145] J. Prasanth Ram and N. Rajasekar, "A Novel Flower Pollination Based Global Maximum Power Point Method for Solar Maximum Power Point Tracking," *IEEE transactions on power electronics,* vol. 32, no. 11, pp. 8486-8499, 2017, doi: 10.1109/TPEL.2016.2645449.
[146] S. Lu, Y. Zhao, K. Fang, Y. Li, and P. Sun, "Establishment and experimental verification of TRNSYS model for PCM floor coupled with solar water heating system," *Energy and buildings,* vol. 140, pp. 245-260, 2017, doi: 10.1016/j.enbuild.2017.02.018.
[147] J. Kensby, A. Trüschel, and J.-O. Dalenbäck, "Potential of residential buildings as thermal energy storage in district heating systems – Results from a pilot test," *Applied energy,* vol. 137, pp. 773-781, 2015, doi: 10.1016/j.apenergy.2014.07.026.
[148] M. Krajčík and O. Šikula, "Heat storage efficiency and effective thermal output: Indicators of thermal response and output of radiant heating and cooling systems," *Energy and buildings,* vol. 229, p. 1, 2020, doi: 10.1016/j.enbuild.2020.110524.
[149] S. Firląg and B. Zawada, "Impacts of airflows, internal heat and moisture gains on accuracy of modeling energy consumption and indoor parameters in passive building," *Energy and buildings,* vol. 64, pp. 372-383, 2013, doi: 10.1016/j.enbuild.2013.04.024.
[150] E. Ampatzi and I. Knight, "Modelling the effect of realistic domestic energy demand profiles and internal gains on the predicted performance of solar thermal systems," *Energy and buildings,* vol. 55, pp. 285-298, 2012, doi: 10.1016/j.enbuild.2012.08.031.
[151] H. Lund and G. Salgi, "The role of compressed air energy storage (CAES) in future sustainable energy systems," *Energy conversion and management,* vol. 50, no. 5, pp. 1172-1179, 2009, doi: 10.1016/j.enconman.2009.01.032.
[152] J. Sardi, N. Mithulananthan, and D. Q. Hung, "Strategic allocation of community energy storage in a residential system with rooftop PV units," *Applied energy,* vol. 206, pp. 159-171, 2017, doi: 10.1016/j.apenergy.2017.08.186.
[153] M. Chesser, J. Hanly, D. Cassells, and N. Apergis, "The positive feedback cycle in the electricity market: Residential solar PV adoption, electricity demand and prices," *Energy policy,* vol. 122, pp. 36-44, 2018, doi: 10.1016/j.enpol.2018.07.032.
[154] J. P. Ríos-Ocampo, S. Arango-Aramburo, and E. R. Larsen, "Renewable energy penetration and energy security in electricity markets," *International journal of energy research,* vol. 45, no. 12, pp. 17767-17783, 2021, doi: 10.1002/er.6897.
[155] H. Okuyama and Y. Onishi, "System parameter identification theory and uncertainty analysis methods for multi-zone building heat transfer and infiltration," *Building and environment,* vol. 54, pp. 39-52, 2012, doi: 10.1016/j.buildenv.2012.02.002.
[156] A. Kokate and M. Wagh, "Experimental Analysis of Performance Ratio of Solar Rooftop Photovoltaic System (SRTPV) for Various Roof Orientation and Tilt," *Journal of Physics: Conference Series,* vol. 1172, no. 1, p. 12067, 2019, doi: 10.1088/1742-6596/1172/1/012067.
[157] J. Lofberg, "YALMIP: A toolbox for modeling and optimization in MATLAB," in *2004 IEEE international conference on robotics and automation (IEEE Cat. No. 04CH37508)*, 2004: IEEE, pp. 284-289.

[158] P. Technology. "calibration certificates for thermocouple loggers." https://www.picotech.com/accessories/data-logger-calibration/calibration-thermocouple-loggers (accessed 11th Dec, 2022).
[159] S. Yang, M. P. Wan, W. Chen, B. F. Ng, and D. Zhai, "An adaptive robust model predictive control for indoor climate optimization and uncertainties handling in buildings," *Building and environment,* vol. 163, p. 106326, 2019, doi: 10.1016/j.buildenv.2019.106326.
[160] U. MET Office. "Nottingham weather forecast." https://www.metoffice.gov.uk/weather/forecast/gcrjm8jf7#?date=2023-07-01 (accessed 19th Dec, 2022).
[161] L. Sharmila, U. Sakthi, A. Geethanjali, and S. Sagadevan, "Regular expression based pattern matching for gene expression data to identify the abnormality gnome," in *2017 Second International Conference on Recent Trends and Challenges in Computational Models (ICRTCCM)*, 2017: IEEE, pp. 301-305.
[162] M. Ahmad, A. Bontemps, H. Sallée, and D. Quenard, "Thermal testing and numerical simulation of a prototype cell using light wallboards coupling vacuum isolation panels and phase change material," *Energy and buildings,* vol. 38, no. 6, pp. 673-681, 2006, doi: 10.1016/j.enbuild.2005.11.002.
[163] S. O. Weber, M. Oei, M. Linder, M. Böhm, P. Leistner, and O. Sawodny, "Model predictive approaches for cost-efficient building climate control with seasonal energy storage," *Energy and buildings,* vol. 270, p. 112285, 2022, doi: 10.1016/j.enbuild.2022.112285.
[164] A. Jáñez Morán, P. Profaizer, M. Herrando Zapater, M. Andérez Valdavida, and I. Zabalza Bribián, "Information and Communications Technologies (ICTs) for energy efficiency in buildings: Review and analysis of results from EU pilot projects," *Energy and buildings,* vol. 127, pp. 128-137, 2016, doi: 10.1016/j.enbuild.2016.05.064.
[165] Z. Wang *et al.*, "Thermal storage performance of building envelopes for nearly-zero energy buildings during cooling season in Western China: An experimental study," *Building and environment,* vol. 194, p. 107709, 2021, doi: 10.1016/j.buildenv.2021.107709.
[166] H. Golmohamadi, K. Guldstrand Larsen, P. Gjøl Jensen, and I. Riaz Hasrat, "Optimization of power-to-heat flexibility for residential buildings in response to day-ahead electricity price," Energy and buildings, vol. 232, p. 110665, 2021, doi: 10.1016/j.enbuild.2020.110665.
[167] S. Yu, S.-G. Jeong, O. Chung, and S. Kim, "Bio-based PCM/carbon nanomaterials composites with enhanced thermal conductivity," Solar Energy Materials and Solar Cells, vol. 120, pp. 549-554, 2014
[168] Sherman, M. H. (1987). Estimation of infiltration from leakage and climate indicators. Energy and buildings, 10(1), 81-86.
[169] Sari, A. (2016). Thermal energy storage characteristics of bentonite-based composite PCMs with enhanced thermal conductivity as novel thermal storage building materials. Energy Conversion and Management, 117, 132–141. https://doi.org/10.1016/j.enconman.2016.02.078
[170] Kenisarin, M., & Mahkamov, K. (2007). Solar energy storage using phase change materials. Renewable & Sustainable Energy Reviews, 11(9), 1913–1965. https://doi.org/10.1016/j.rser.2006.05.005
[171] Omara, A. A., Abuelnuor, A. A., Mohammed, A. O., Sirelkhatim, O. M., & Suleman, A. A. (2018, August). An experimental study on using polyethylene glycol (PEG) 600 as phase change material for thermal comfort and energy saving in buildings. In 2018 international conference on computer, control, electrical, and electronics engineering (ICCCEEE) (pp. 1-5). IEEE.
[172] J. Noel, Y. Jannot, C. Métivier, and N. R. Sgreva, "Thermal characterization of polyethylene glycol 600 in liquid and solid phase and across the phase transition," Thermochimica acta, vol. 716, p. 179326, 2022, doi: 10.1016/j.tca.2022.179326.

[173] Kiliccote, S., Piette, M. A., & Hansen, D. (2006). Advanced Controls and Communications for Demand Response and Energy Efficiency in Commercial Buildings.
[174] Yu, Z., Haghighat, F., Fung, B. C. M., & Yoshino, H. (2010). A decision tree method for building energy demand modeling. Energy and Buildings, 42(10), 1637–1646. https://doi.org/10.1016/j.enbuild.2010.04.006
[175] Petrollese, M., Valverde, L., Cocco, D., Cau, G., & Guerra, J. (2016). Real-time integration of optimal generation scheduling with MPC for the energy management of a renewable hydrogen-based microgrid. Applied Energy, 166, 96–106. https://doi.org/10.1016/j.apenergy.2016.01.014
[176] Carli, R., Cavone, G., Ben Othman, S., & Dotoli, M. (2020). IoT Based Architecture for Model Predictive Control of HVAC Systems in Smart Buildings. Sensors (Basel, Switzerland), 20(3), 781. https://doi.org/10.3390/s20030781
[177] Serra, J., Pubill, D., Antonopoulos, A., & Verikoukis, C. (2014). Smart HVAC Control in IoT: Energy Consumption Minimization with User Comfort Constraints. TheScientificWorld, 2014, 161874–11. https://doi.org/10.1155/2014/161874
[178] Wu, F., Rüdiger, C., & Yuce, M. R. (2017). Real-Time Performance of a Self-Powered Environmental IoT Sensor Network System. Sensors (Basel, Switzerland), 17(2), 282–282. https://doi.org/10.3390/s17020282